Drosophila Indirect Flight Muscles as a model system for the study of human thin filament myopathies.

Maria Sevdali

University of York
Department of Biology
October 2009

THESIS CONTAINS

VIDEO

CD

DVD

TAPE CASSETTE

Abstract

Human thin filament myopathies are a group of skeletal muscle diseases caused by mutations in thin filament protein genes. Over 170 mutations within the human skeletal α-actin gene, *ACTA1*, cause congenital actin myopathies (CAM). These are dominant, often lethal mutations resulting in death at birth or shortly after. Several mutations have been identified in the genes encoding for Troponin I and Troponin T proteins, which cause arthrogryposis. The aim of this work was to see if the *Drosophila* Indirect Flight Muscles can be used as a genetic model system, with which to study the *ACTA1* and arthrogryposis disorders and understand their aetiology.

Six different mutations in the *Drosophila Act88F* gene, G15R, I136M, D154N, V163L, V163M and D292V, homologous to the human CAM actin mutations were transgenically expressed in *Drosophila* Indirect Flight Muscles (IFM) as wild type heterozygotes. All the mutants were dominant and with some myofibrillar defects similar to those seen in humans. Certain mutations resulted in intranuclear rods, similar to those found in humans and split Z-discs. The mutations varied in severity and matched that of the human mutations. An extra copy of wild type actin rescued the phenotype of all the heterozygote mutants, suggesting that upregulation of expression of the wild type actin gene might be a future prospect for therapy.

Atypically, flies heterozygous for the R372H *Act88F* mutation complete normal IFM myogenesis and young flies can fly, but later become flightless and by day 7 show the *Drosophila* equivalent of the human nemaline phenotype. Electron microscopy revealed progressive loss of muscle structure. From the ultrastructure, the phenotypic requirement for muscle usage and the known α-actinin binding sites on the actin monomer, the R372H mutation is proposed to reduce the strength of F-actin/α-actinin binding, leading to muscle damage during use and breakdown of muscle structure. Binding studies confirmed a 13-fold reduction in α-actinin binding for R372H actin.

The *GAL4/UAS* system was employed for the study of arthrogryposis mutations. The wild-type TnT and TnI IFM isoforms were transgenically expressed to rescue the TnT and TnI IFM nulls, respectively. Only the TnI null was rescued. The TnI arthrogryposis mutants were transgenically expressed and resulted in hypercontracted muscles.

Contents

Figure contents

Chapter 1: Introduction

Chapter 2: Materials and Methods

Chapter 3: Characterization of transgenic lines of mutant Act88F carrying human nemaline phenotypes

Chapter 4: Use of genetic approaches to understand the NM phenotypes

Chapter 5: The *Act88F*^{R372H} mutation: a progressive nemaline myopathy model

Chapter 6: *Drosophila* IFM as a model system for studying distal arthrogryposes

Chapter 7: General Discussion

Table contents

Chapter 5: The *Act88F*^{R372H} mutation: a progressive nemaline myopathy model

Chapter 6: *Drosophila* IFM as a model system for studying arthrogryposes

Appendix I – Primers

Movie contents

Preface

Give me a lever long enough, a fulcrum strong enough
and I will move the earth

Archimedes (287 BC - 212 BC)

Acknowledgements

I first wish to thank Professor John Sparrow for the opportunity of undertaking my PhD which, after a painstaking period, provided me with results that surpassed my most far-reaching initial expectations and through which I came to realize my deep love for this beautiful and wondrous species of flies. I want to wholeheartedly thank him for his guidance, inspiration, support and encouragement throughout these years.

I am thankful to Prof. Belinda Bullard for sharing her antibodies and scientific discussions all these years. I am also grateful to my training committee for their great support, advice and useful ideas. I am especially indebted to Daniela Barilà whose friendship and assistance I value. I would like to thank Dr. Bogdan Iorga for making my stay in Cologne a memorably pleasurable experience and Dr. Michelle Peckham for the technical advice and useful discussions. I would like to express my deep gratitude to Dr Teresa Jagla who performed the embryo microinjections of all my constructs. I would also like to thank Meg Stark and other staff of the Technology Facility for their expertise and advice.

I want like to sincerely thank Helen and Nikos for awesome legal mind. My family, Christina, Sophie and Thanassi for their peerless skills and for supporting my mother and me for all these years. I also want to thank Ms Despina and Ms Danai for their care, words of wisdom and incredible cooking. Eleni Kourtidou for always making sure I can fly home!

I am deeply indebted to Daniel for his tremendous encouragement and love. Thank you Anja Katzemich, Ari Franco and Zac Orfanos for making my time in the lab an unforgettable experience and Emmanuele Severi for your thoughtfulness and valuable advice.

Lastly I would like to thank my mother for her love and for inspiring me every day.

This work was funded by MYORES

Author's Declaration

I declare that the work presented in this thesis is my own, except where it is acknowledged in the text or figures.

None of this work has been submitted for a previous degree.

Chapter 1: Introduction

1.1 Muscle disease

Over the past decade, there has been an increase in awareness of the mechanisms of cardiac and skeletal muscle diseases. Mutations in a large number of protein components of the sarcomere, the functional unit of skeletal and cardiac muscle, have been discovered to cause a range of muscle disorders (reviewed in Laing and Nowak, 2005; Tajsharghi, 2008). Since the early 1990s, mutations in genes coding for skeletal muscle thin filament proteins have been identified that are associated with various clinical symptoms and result in specific structural changes within the sarcomere (Sung *et al.*, 2003; Goebel, 2007; Laing *et al.*, 2009). Many thin filament diseases present themselves at birth (congenital myopathies), hence it is not possible to follow the development of the disease. Currently our understanding regarding the pathobiology of the gene defects remains limited, despite some of these proteins being studied for decades. A greater understanding of how the presence of the mutated proteins in the patient's muscle is leading to weakness and disease is needed.

1.1.1 Thin filament myopathies

1.1.1.1 *ACTA1* congenital myopathies

Actin forms the core of the thin filament of the sarcomere where it interacts with a plethora of proteins and produces the force for muscle contraction (Craig and Padron, 2004). Six actin isoforms exist in humans, which show 90 % similarity at the amino acid level (Sheterline *et al.*, 1998). Cardiac α-actin (*ACTC1*) is the principal actin isoform expressed in skeletal muscle during gestation (Ilkovski *et al.*, 2005). By 25-27 weeks pre-parturition skeletal muscle α-actin (*ACTA1*) becomes the dominant and permanent isoform in human adult muscle (Ilkovski *et al.*, 2005).

By 2009, more than 170 different mutations in the human *ACTA1* gene have been reported that cause congenital myopathies (reviewed in Laing *et al.*, 2009). These are a group of skeletal muscle disorders characterized by generalized muscle weakness (Sparrow *et al.*, 2003). They are often clinically severe with most patients dying at birth or shortly after (Romero and Fardeau, 1996). Most are dominant *de novo* mutations (Laing *et al.*, 2009). The prevalence of *ACTA1* congenital myopathies is 1 in 500,000 live births (Wallgren-Pettersson, 1990; North *et al.*, 2008).

Clinicians have divided the *ACTA1* disorders into six subtypes depending on the age of the disease onset and severity: adult onset, mild, typical, intermediate, severe and other forms (Wallgren-Pettersson, 1999). The severe subtype is presented at birth or even in utero, where patients show no spontaneous movement and require mechanical ventilation (Lammens *et al.*, 1997). These patients typically do not survive more than a few weeks. Survival to birth may be because the predominant actin isoform of foetal skeletal muscle is cardiac actin.

Five distinct overlapping (Jungbluth *et al.*, 2001; Schroder *et al.*, 2004) pathological phenotypes are caused by mutations in the *ACTA1* gene in humans (Figure 1.1): (a) actin filament aggregate myopathy, (b) intranuclear rod myopathy, (c) nemaline myopathy (Nowak *et al.*, 1999; Sparrow *et al.*, 2003), (d) congenital fibre type disproportion and (e) myopathy with core-like areas. Appearance of any of these features in a muscle biopsy is an indicator of an *ACTA1* mutation. Other common pathological features are fiber atrophy and/or hypotrophy.

Of the five histopathologies, nemaline rod myopathy is the most common phenotype (Figure 1.1 C). The term nemaline was applied because of the thread-like appearance of the rods (nema means thread in Greek) (Shy *et al.*, 1963; Wallgren-Petterson, 1999, North *et al.*, 2007). NM is genetically heterogeneous, with disease-causing mutations identified in different genes coding the thin filament proteins α-skeletal actin (ACTA1) (Jungbluth *et al.*, 2001; Nowak *et al.*, 1999), α-tropomyosin (TM3) (Durling *et al.*, 2002; Laing *et al.*, 1995; Tan *et al.*, 1999; Wattanasirichaigoon *et al.*, 2002), β-tropomyosin (TM2) (Donner *et al.*, 2002), Troponin-T (TNNT1) (Johnston *et al.*, 2000) and nebulin (NEB) (Pelin *et al.*, 1999; Sewry *et al.*, 2001). *ACTA1* mutations cause 20 % to 30 % of all known NM cases after mutations in nebulin, which make it the second most common cause of NM (Laing *et al.*, 2009). *ACTA1* mutations causing NM are mostly severe with early death (Agrawal *et al.*, 2004; Wallgren-Petterson *et al.*, 2004).

Clinicians diagnose human nemaline myopathy by muscle biopsies and Gomori trichrome staining (Engel and Cunningham 1963; Nienhuis *et al.*, 1967), which contrasts the dark blue nemaline rods against the pale blue fibres. The nemaline rods are

also visible in electron micrographs as electron dense bodies (Figure 1.1 C). Nemaline rods show the same appearance independent of age or severity (Shimomura and Nonaka, 1989) and the phenotype is already apparent at birth in most patients. Patients diagnosed with NM can present muscle weakness before nemaline rods are visible (Tajsharghi *et al.*, 2007; North *et al*, 1999). This suggests that the nemaline rods may be a secondary symptom of the disease and not be directly responsible for the skeletal muscle weakness (Michele and Metzger, 2000). Another symptom is signs of type I muscle fibre atrophy. The decrease in size could also suggest an abortive regenerative response (Sanoudou *et al.*, 2003). Each cell is unable to produce the same absolute force as a wild-type one resulting in an abortive partly muscle weakness in NM.

The less frequent intranuclear rod myopathy (IR) is characterized by filamentous actin rod inclusions in the fibre nuclei (Figure 1.1 D) and is often associated with a severe clinical phenotype (Hutchinson *et al.*, 2006; Kaimaktchiev *et al.*, 2006). Mutations that cause intranuclear rod myopathy have been identified on 12 amino acid residues, leading to 13 *ACTA1* changes. Eight of these residues cluster between residues 139-165, possibly a hot spot for this disorder (Laing *et al.*, 2009).

The also infrequent actin filament aggregate myopathy (AM) is characterized by large accumulations of filamentous actin in the muscle fibres (Figure 1.1 A, B) and is often associated with severe disease. Ten different mutations have been identified that cause AM. A hot spot for mutations associated with this disorder has been identified between residues 144 and 165. All known mutations associated with actin filament aggregate myopathy and intranuclear rod myopathy have implicated *ACTA1* (Nowak *et al.*, 1999; Sparrow *et al.*, 2003; Laing and Nowak, 2005; Hutchinson *et al.*, 2006).

Congenital fibre type disproportion (CFTD) is characterized by an early onset, nonprogressive muscle weakness caused where the type 1 muscle fibres are at least 12 % smaller compared to the type 2 fibres (Figure 1.1 E) (Laing *et al.*, 2004). Eight mutations in the *ACTA1* gene have been identified that cause CFTD and cluster on one area on the actin monomer, suggesting the involvement with a specific actin interaction partner (Laing *et al.*, 2009). Mutations in *TPM3* and selenoprotein N1 have been identified to also cause CFTD (Clarke *et al.*, 2006).

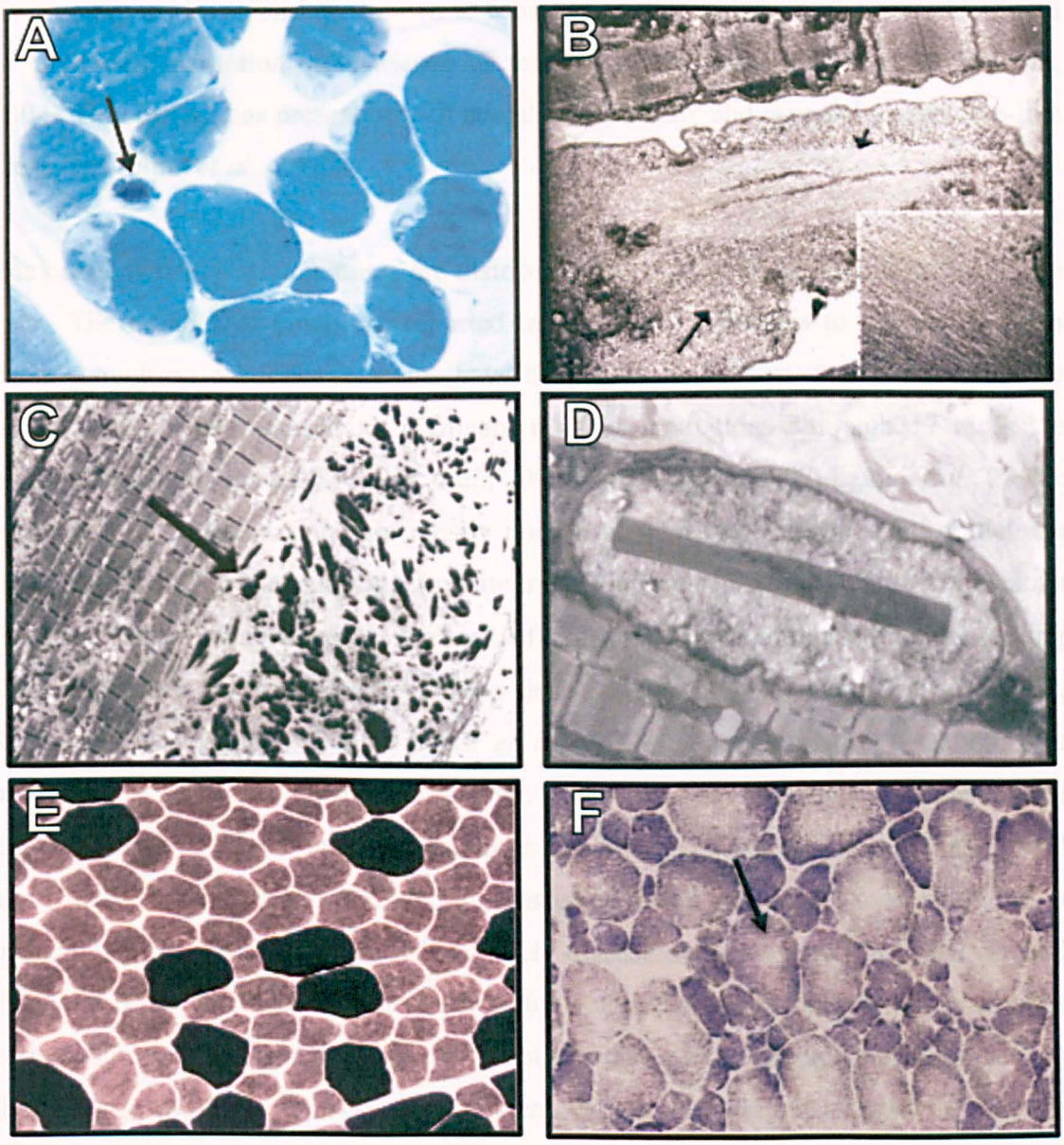

Figure 1.1. Microscopic images of the different histopathologies caused by the *ACTA1* mutations. (A) Actin filament aggregate myopathy (AM), light microscopy of transverse muscle section (Gomori trichrome stain), accumulated actin filaments are stained darker than the pale blue myofibrils (arrow). **(B)** Electron microscopy (EM) of AM, accumulation of filamentous actin inclusions within areas devoid of sarcomeres (arrows, enlarged in inset). **(C)** EM of nemaline myopathy, accumulations of nemaline bodies in the sarcoplasm (arrow). **(D)** EM of intranuclear rod myopathy, an actin rod within the muscle nucleus. **(E)** Congenital fiber type disproportion, light microscopy showing small (pale) type 1 and larger (dark) type 2 muscle fibers, respectively. **(F)** Core myopathy, light microscopy of core-like areas (arrow) (reduced nicotinamide adenine dinucleotide staining). Images reproduced from Sparrow *et al.*, 2003 and Laing *et al.*, 2009.

Two mutations in *ACTA1* are known to cause myopathy with core-like areas identified by myofibril disruption and absence of mitochondria (Figure 1.1 F) (Kaindl *et al.*, 2004). One patient has presented both nemaline myopathy and myopathy with core-like areas (Jungbluth *et al.*, 2001).

The congenital *ACTA1* mutations are distributed throughout all six coding exons of the gene. The number of mutations reported in each exon correlates to the size of each exon, though no particular hotspots have been identified. Most *ACTA1* cases are *de novo*, isolated cases caused by dominant missense mutations although 17 recessive cases have been reported (Sparrow *et al.*, 2003; Nowak *et al.*, 2007; Laing *et al.*, 2009). Recessive *ACTA1* mutations are mostly nonsense, frameshift or splice-site mutations that are predicted to prematurely terminate translation, or cause omission of entire exons from the mRNA. These result in a lack of skeletal α-actin protein. Patients carrying these mutations survive by upregulating their cardiac *ACTC1* gene (Sparrow *et al.*, 2003; Agrawal *et al.*, 2004; Nowak *et al.*, 2007). Four missense mutations are associated with recessive disease (H73D, L94P, E259V, M299K) and have been hypothesized to be functional null mutations (Sparrow *et al.*, 2003), two of which (L94P and E259V) have been demonstrated in transfected fibroblast cultures to be so (Costa *et al.*, 2004). All patients with recessive *ACTA1* disease therefore lack functional skeletal muscle α-actin. The heterozygous carriers for a nonsense mutation (parents or siblings of patients with recessive mutations) do not display any disease symptoms suggesting that a single wild type actin copy is sufficient for normal muscle development, function and subsequent maintenance throughout life (Sparrow *et al.*, 2003).

As the recessive *ACTA1* mutations produce null alleles, the dominancy of the non-recessive mutations must not be due to insufficient wild type actin levels but caused by the interference with wild type actin function. That is, the mutant actin monomer interacts with the wild-type actin, incorporates into polymerized filamentous actin and interferes with the function, assembly, and stability of the thin filaments. As actin has numerous interacting partners the dominant *ACTA1* mutations may disrupt any of the skeletal muscle α-actin normal functions. Hitherto, the experimental evidence shows that different monomer or polymer actin properties are affected by the different dominant *ACTA1* mutations (Hennessey *et al.*, 1992). However, no apparent correlations between the functions affected, the location of the mutations within known

actin-binding sites to other proteins or actin itself and the five histopathological phenotypes have as yet been found (reviewed by Sparrow *et al.*, 2003; Feng and Marston 2009).

1.1.1.2 Arthrogryposis

Arthrogryposes are a group of complex, rare human congenital disorders characterized by permanent non-progressive joint contractures (joint fixation caused by atrophy and shortening of muscle fibres or loss of normal elasticity of skin) that affect limb function (Figure 1.2) (Bamshad *et al.,* 1996a;b). The precise course of the distal arthrogryposes (DA) malformations is unclear. It has been proposed that decreased fetal movement may lead to contractures at birth via the accumulation of additional connective tissue around the joints (Hall, 1997). The reduced movement could be due to muscular or neuronal disorders, connective tissue abnormalities or problems within the uterus (Hall e*t al.*, 1982; Hall, 1997; Gordon, 1998).

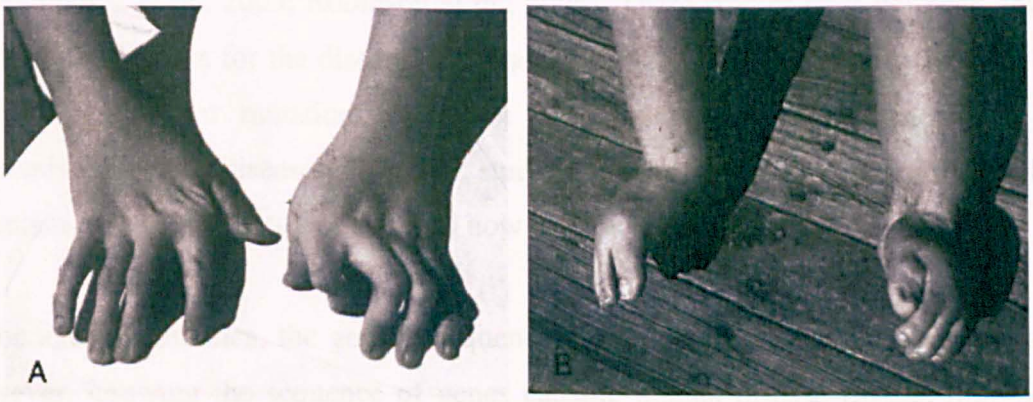

Figure 1.2. Typical malformations observed at the distal ends in patients with DA2B. (A) Hands showing camptodactyly and ulnar deviation. **(B)** Feet characterized by camptodactyly. Images reproduced from Sung *et al*, 2003.

Two types of arthrogryposis have been identified which are caused by mutations in thin filament proteins. These are Distal arthrogryposis type 1 (DA1) and Distal arthrogryposis type 2B (DA2B, also called DA2A) (Bamshad *et al.*, 1996a;b). The first is caused by mutations in the tropomyosin gene (*TPM2*) and the latter by mutations in the skeletal troponin I (*TNNI2*) and troponin T (*TNNT3*) genes that are specific to fast-twitch myofibres (Sung *et al.*, 2003). Unlike NM, DA is not accompanied by muscle wasting (Bealls, 2005). Consequently, the thin filament protein mutation-induced

muscle weakness stems from other phenomena likely associated with altered regulation of muscle contraction.

1.2 Model organisms of human muscle disease

Currently there are no known therapeutic treatments to alleviate or cure the symptoms of *ACTA1* associated congenital myopathies or arthrogryposis. Several experimental model systems for *ACTA1* associated congenital myopathies exist where the majority of 22 different congenital myopathy mutant *ACTA1* genes have been expressed *in vitro*, or examined in cultured fibroblasts, myocytes and myotubes. These showed a variety of defects, including the inability of the actin to fold (two mutants), or formation of aggregates *in vivo* (Costa *et al.*, 2004; Domazetovska *et al.*, 2007a;b; Ilkovski *et al.*, 2004). Although these studies have been able to reproduce the sarcoplasmic and nuclear actin aggregations they have not furthered our understanding as to how these phenotypes form or how the *ACTA1* associated congenital myopathies are caused. Four arthrogryposis mutants have been studied in ATPase assays or tropomyosin binding assays (Wang *et al.*, 2005; Robinson *et al.*, 2006). These studies have not been able to offer an explanation for the disease. The use of a solely *in vitro* or *in vivo* approach to study thin filament mutations does not offer a complete understanding of the mechanism for these diseases. However, studying a mutation in the context of the whole organism may help to better understand how it leads to disease.

In the age of genomics, the genetic sequences of entire organisms are now available. However, knowing the sequence of genes causing human disease reveals little about their normal function. Legal and ethical arguments justify the experimentation on other organisms in order to investigate both normal and abnormal functions, and to improve the duration and quality of life of people. The human muscle is inaccessible during foetal development, which argues the case for experimentation on other organisms. The European Union has funded MYORES, a large research network on 'Multi-organismic approaches to muscle development and disease' to research human muscle disease. Model organisms currently being used to study these diseases include mice, the zebrafish *Danio rerio* the nematode *Caenorhabditis elegans* and the fruit fly *Drosophila melanogaster*. The literature demonstrates the importance of these model genetic organisms in the study of human skeletal myopathies as their use has increased in the last 20 years (reviewed in Bedell *et al.*, 1997; Sparrow *et al.*, 2008).

1.2.1 Model genetic organisms – mice, zebrafish, nematodes

Human skeletal myopathies have been studied in mice, zebrafish and nematode animal models. The reasoning for using these model organisms to study human skeletal myopathies is because they contain striated muscle groups conserved to humans (reviewed in Bedell *et al.*, 1997; Lecroisey *et al.*, 2007, Sparrow *et al.*, 2008). The genome sequences of these organisms are known and have been catalogued in the Mouse Genome Database (http://informatics.jax.org/), the Zebrafish Information Service (http://zfin.org/) and Wormbase (http://www.wormbase.org/). These databases facilitate the search for human disease gene homologues in these organisms and allow the comparison of sequences and selection of specific sequence changes for the ready creation of transgenic human disease animals. Information on the organisms' biology, genetics, transgenic stock collections and bibliography are also available in these databases.

A valuable genetic model organism of a human disease should be able to offer: cheap maintenance and grow in large numbers; have fast generation times; an annotated genome sequence; a well understood biology and genetics; information shared resources; transgenesis tools and contain the genes of interest to a high sequence identity to its human counterparts. Ideally a perfect genetic model organism would cover all these points but this is not possible. Though each organism has its own advantages and limitations as models for human muscle diseases.

Mice have generally been the animal of choice for studying human disease as they are more homologous anatomically and physiologically to humans than zebrafish or invertebrates. Most murine genes have functional counterparts in humans. Mutations that cause diseases in humans often cause similar diseases in mice. Compared to most mammals, mice are easy to maintain and have a short breeding cycle (~2 months). Well known genetics and transgenesis systems are available in mice for the creation of disease models (reviewed in Bedell *et al.*, 1997a).

Zebrafish has emerged as human disease model due to its high similarity in the developmental gene pathways and regulatory mechanisms to humans. Its organs are more homologous to those of humans than invertebrates and myogenesis proceeds in waves similar to those in mammals (Barbazuk *et al.*, 2000; Postlethwait *et al.*, 2000; Liu

et al., 2002; Lieschke and Currie, 2007). Although the facilities required for culturing fish are more costly to maintain than for invertebrate models, sperm can be stored frozen which allows many different mutations and transgenic lines to be kept for long periods at low cost. Further advantages include good transgenesis tools, external fertilisation, which facilitates genetic and cellular manipulation, rapid development, a 3 month generation time (Kimmel *et al.*, 1989), high fecundity and the embryos are transparent, which allows muscle defects to be easily identified using microscopy.

Although the nematode physiology is very distant from that of humans, sequencing of the *C. elegans* genome (*C. elegans* Sequencing Consortium, 1998) revealed that more than 50 % of human genes have homologues in the nematode. Growing nematodes is easy and cheap on *Escherichia coli* spread Petri plates. As the female worm is a self-fertilizing hermaphrodite, homozygotes are readily produced without the need to mate. Genetic crosses are easily made and different mutant lines can be stored by freezing. Worms can be grown in large numbers, which allows the recovery of primary mutations and screening for secondary mutations in other genes that either reduce the severity of the primary mutation or enhance it. The body wall muscles have been the target of most genetic studies (Wood, 1988). These muscles are prominent and as the organism is small and translucent they can be readily visualized by microscopy of the whole organism.

The ability to manipulate the genetics of these organisms has founded their potential in understanding muscle development and human muscle disease mutations. Point mutations in these organisms can be introduced by irradiation or feeding with chemical mutagens (ENU mutagen) (Russell *et al.*, 1979; Wood, 1988; McArdle *et al.*, 1998; Paton *et al.*, 2001). Transgenesis methods are available for introducing foreign DNA with homologues of human disease genes in nematodes (reviewed in Rieckher *et al.*, 2009) zebrafish (Raz *et al.*, 1998; Weinberg, 1998) and mice (Hogan *et al.*, 1994) by embryo microinjection. Retroviral systems can be employed for insertional mutagenesis in zebrafish (Gaiano *et al.*, 1996; Amsterdam *et al.*, 1999; Golling *et al.*, 2002; Sivasubbu *et al.*, 2007). Some human skeletal myopathies are caused due to the lack of protein synthesis. Gene knockouts in mice are achieved using the Cre/*Lox*P site-specific recombination system (Chambers, 1994) and in nematodes using RNA interference

(RNAi) (http://www.wormbook.org/). In zebrafish, morpholino antisense RNA oligonucleotides are used to block mRNA transcription (Nasevicius and Ekker, 2000).

1.2.1.1 Model organism studies of human muscular disease

Use of these animals has allowed the generation of several models of human skeletal muscle diseases to be studied. The most extensively studied skeletal myopathy among mice, zebrafish and nematodes is Duchenne Muscular Dystrophy (reviewed in Sparrow *et al.*, 2008), a disease caused by mutations in the human dystrophin gene resulting in progressive muscle degeneration and death. Several dystrophin mutants exist in zebrafish that result in lack of the protein (Hoffman *et al.*, 1987 Guyon *et al.*, 2007; Kunkel *et al.*, 2006). A zebrafish dystrophy model reveals that that dystrophin is required for the formation of stable muscle attachments (Bassett *et al.*, 2003; Guyon *et al.*, 2007).

Mutations inactivating the *C. elegans dys-1* gene alone cause only mild muscle degeneration (Bessou *et al.*, 1998; Gieseler *et al.*, 1999). However, when the *dys-1* mutation is combined with another mutation, *hlh-1* (MyoD homologue) (Chen *et al.*, 1994), it results in a progressive muscular dystrophy (Gieseler *et al.*, 2000). *C. elegans* screens have identified the molecules serotonin and prednisone as possible drugs to alleviate the symptoms of dystrophin mutations (Bessou *et al.*, 1998; Gaud *et al.*, 2004; Carre-Pierrat *et al.*, 2006).

In mice the Dmd^{mdx} model that results in loss of dystrophin has been used extensively to study the disease but it presents only a mild phenotype possibly due to muscle regeneration effects (Collins *et al.*, 2003).

1.2.1.2 Limitations

These model genetic organisms are not perfect. The generation of transgenic mice is time consuming and expensive compared to nematodes and zebrafish. It is also nontrivial to misexpress transgenes in regulated, temporal and tissue specific manners (Bedell *et al.*, 1997a; b). As mammals, mice develop *in utero*, which makes the study of muscle diseases that manifest during early stages of development difficult.

When working with a model system for human muscle disease one problem is that the animal is unlikely to recapitulate the human disease well enough. In contrast to mammals and zebrafish, the nematode muscle lacks both an adaptive immune response and regenerative capacity in response to dysfunction. This is a disadvantage, as the model system cannot fully mimic a muscle disease. However, this can also be an advantage as it allows investigation of the molecular mechanisms of the disease without complications from immune or repair responses.

While zebrafish muscle shares closer homologies to humans than nematodes, processing and screening large numbers of animals for muscle mutations and for chemicals that suppress a disease phenotype is slow and labour intensive. As RNAi approaches are not yet possible in zebrafish, the effects of gene knockdowns cannot be examined across the whole transcriptome. Furthermore, the zebrafish genome underwent a duplication event after the mammalian and fish lineages diverged (Amores *et al.*, 1998; Postlethwait *et al.*, 1998). Hence, there is polyploidy for specific genes, making the study of a particular gene in zebrafish more complicated compared to invertebrates, where occasions nematodes and flies often possess a single gene isoform of a human disease homologue in a tissue or in the whole organism. The single dystrophin genes present in nematodes and flies (Roberts and Bobrow, 1998; Greener and Roberts, 2000; Grisoni *et al.*, 2002) simplify the study of muscular dystrophy compared to zebrafish, which contain 29 orthologues for human dystrophin (Steffen *et al.*, 2007).

The study of an individual animal model for a human disease may be limited in the amount that can be learnt but from multiple animal models one can appreciate different aspects of the human disease and even screen and test potential therapeutic agents at low cost and reduced ethical impact. *Drosophila melanogaster* has presented itself as an additional model organism for the study of human muscle disease.

1.3 *Drosophila* as a model animal for the study of human disease genes

With the completion of the *Drosophila* genome sequence (Adams *et al.*, 2000), a cross-genomic analysis was conducted of all human disease genes known to have at least one mutant allele listed in the Online Mendelian Inheritance in Man (OMIM). Using Homophila (http://homophila.sdsc.edu) of the current 3714 human disease genes (defined by matches with expectation values, E-value $\leq 10^{-10}$), 657 genes (E-value $\leq 10^{-100}$) are estimated to have sufficiently well conserved homologues that could be analyzed in Drosophila. Many of the genetic pathways that are involved in basic developmental mechanisms in vertebrates and invertebrates have remained intact during evolution. Thus insights gained from studies in *Drosophila* can be applied in vertebrate systems. As most human disease genes have counterparts in the *Drosophila* genome and many of these are involved in cancer, neuromuscular disorders, immunological disorders, as well as heart disease (Bier 2005, Vidal and Cagan, 2006) the fly is becoming increasingly popular for studying the molecular mechanisms of human disease. A rapidly expanding collection of mutations exists in many homologues of human disease genes (Rubin *et al.*, 2000).

For such a small organism, flies are equipped with several attractive features that make them a valuable experimental genetic model system. They are inexpensive to maintain, with a rapid breeding time (~ 12 days) and the capacity to generate a large number of individuals from a single cross. The fly genome is well annotated and consists of just four chromosomes. A general fly resource, Flybase (http://flybase.bio.indiana.edu), is available where a complete breakdown of the biology and genome of *Drosophila* as well as links to other sources can be found. The fly has a well-defined musculature that can be readily examined by light and fluorescent microscopy. The organism is accessible during all stages of muscle development and many specimens can be rapidly screened. In addition there is considerable information known about the details of myogenesis in flies (reviewed in Sparrow *et al.*, 2008).

1.3.1 Genetic tools

The strength of *Drosophila* as a genetic model system relies on its plethora of available genetic tools. A very important genetic tool specific to *Drosophila*, balancer chromosomes, are small genomic pieces that during meiosis prevent recombination between homologous chromosomes. These allow lethal mutations and deletions to be studied and be maintained indefinitely. Mutants have been produced in flies for the study of genetics, development, behaviour etc. for nearly a century (reviewed in Bökel *et al.*, 2008). Early studies relied on spontaneous mutagenesis. The traditional way for obtaining mutants was to feed flies a mutagen most commonly ethyl-methane sulphonate, EMS or to subject them to irradiation (Mogami and Hotta, 1981, Deak *et al.*, 1982). But in the last half-century *Drosophila* geneticists have mutagenized flies and 'screened' for mutations with specific phenotypes.

1.3.1.1 Transgenesis methods in Drosophila

The efficient and reliable transgenesis system for gene manipulation has released *Drosophila*'s potential to study human diseases (reviewed in Venken and Bellen, 2007). Transgenic constructs can be readily introduced in flies to misexpress genes of interest in a spatially and temporally specific manner. The recent generation of nearly 19000 P-element and piggyBac insertions covering the *Drosophila* genome allowed the screening of the entire genome for loss of function alleles, a feature not yet applicable to any other species (Parks *et al.*, 2004; Thibault *et al.*, 2004). If the disease causing protein has a dominant effect it is possible to overexpress the associated gene in a wild-type fly background.

Transgenic manipulation of *Drosophila* has enabled the study of specific mutations. Transposon-based transgenesis techniques exploit native P-elements called transposons that mobilise autonomously within the fly genome (Castro and Carareto, 2004). P-elements encode for a transposase that recognises a 31-base pair inverse terminal repeat at the transposon's 5' end and an 11-basepair subterminal inverted repeat at the 3' end (Figure 1.3 A). These repeats are important for transposition to occur by the transposase (Beall and Rio, 1997).

For P-element mediated transgenesis, a vector containing the transposon's ends, the sequence of interest and a marker (usually red eyes) (Karess and Rubin, 1984) is coinjected with a helper plasmid that carries the gene for the transposase or with the enzyme itself (Kaufman and Rio, 1991; Rubin and Spradling, 1982; Spradling and Rubin, 1982) (Figure 1.3 B). Separation of the transposase from the transposon allows the regulated mobilisation of genes into the genome.

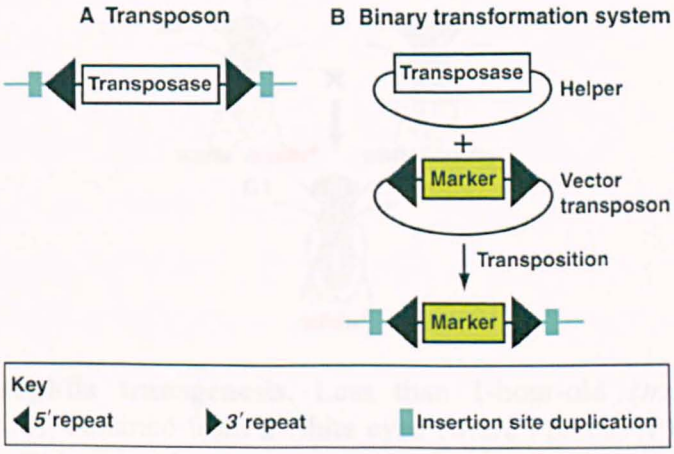

Figure 1.3. Transposon transformation system. (A) Transposons consist of two inverted terminal repeats that flank an open reading frame encoding a transposase. **(B)** The helper plasmid carrying the transposase and a vector plasmid carrying the transposon and a marker are cotransformed. Transposition results in the duplication of the insertion site and is recognized by the marker. Image reproduced from Venken and Bellen, 2007.

When P-elements carrying constructs of interest are microinjected into the syncytial blastoderm of *Drosophila* along with a source of transposase, the transgenes become integrated only in the genome of the germ line cells (Figure 1.4) (Laski *et al.*, 1986). The transgene will be stably inherited to the progeny from these individuals (Rubin and Spradling, 1982). Transgene integration is identified by selecting for the marker. This way entire genes can be introduced for 'rescue' experiments, *in vitro* mutagenized genes and promoter-reporter fusions for *in vivo* gene expression studies (see section 1.4). P-elements can also be used to knockout gene expression by transposing into genes and disrupting their function.

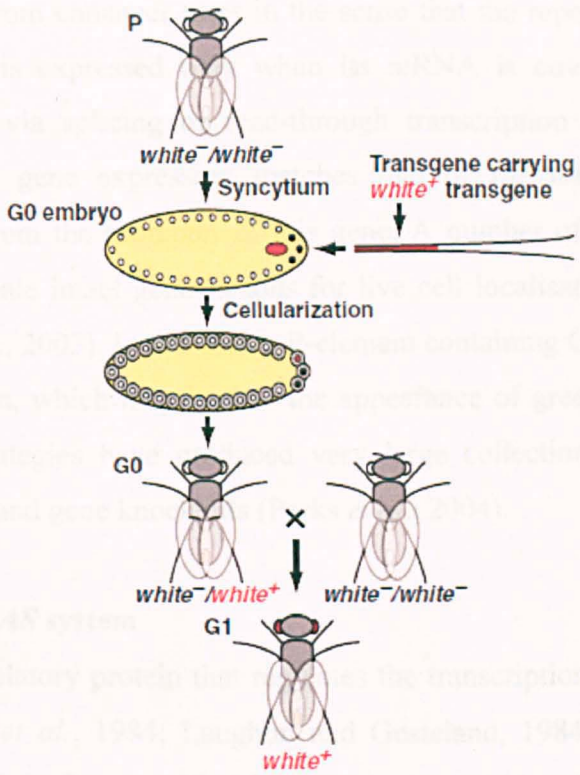

Figure 1.4. Drosophila transgenesis. Less than 1-hour-old *Drosophila* embryos (generation zero, G0), obtained from a white eyed (*white*$^-$) parent (P) are injected with transgenic DNA carrying a red eye marker (*white*$^+$). Rapid nuclear divisions create a syncytium. Transgenic DNA is integrated into the germ cells (red pole cell) and becomes transmitted from G0 generation to the next (G1 progeny). Integration of transgenic DNA is identified using the *white*$^+$ marker. When integrated in a *white*$^-$ strain, this transgene gives transgenic flies a darker eye colour. Image reproduced from Venken and Bellen, 2007.

1.3.1.2 Enhancer and protein trapping

Enhancer and protein trapping strategies using transposons are widely used in *Drosophila* for identifying and studying the function of new genes on the basis of their expression pattern (Bellen *et al.*, 1989; Bier *et al.*, 1989; Wilson *et al.*, 1989). For enhancer (promoter) trapping a P-element transposon carrying a reporter gene (e.g. *GAL4*, *GFP*, *lacZ*) linked to a weak promoter can be mobilised randomly into the genome to a large number of chromosomal locations. P-element constructs have a preference for inserting into the 5' regulatory region of functional transcription units (Spradling *et al.*, 1995). Thus integration near a gene enhancer may activate the transcription of the weak promoter and express the reporter under the control of that enhancer. If on the other hand the construct integrates into a gene, the trap may disrupt gene function.

Protein traps differ from enhancer traps in the sense that the reporter sequence lacks a promoter, hence, it is expressed only when its mRNA is covalently ligated to an endogenous mRNA via splicing or read-through transcription (Lukacsovich *et al.*, 2001). The reporter gene expression matches that of the trapped gene since its transcription starts from the promoter of this gene. A number of GFP traps exist that were designed to create intact gene fusions for live cell localisation studies (Morin *et al.*, 2001; Clyne *et al.*, 2003). In this case a P-element containing GFP as an exon inserts into a genomic intron, which may lead to the appearance of green fluorescent tissues. Altogether these strategies have produced very large collections of enhancer traps, expression reporters and gene knockouts (Parks *et al.*, 2004).

1.3.1.3 The *GAL4/UAS* system

GAL4 is a yeast regulatory protein that regulates the transcription of genes induced by galactose (Laughon *et al.*, 1984; Laughon and Gesteland, 1984). In the presence of galactose, *GAL4* binds to four specific 17-base pair sites within a DNA sequence termed the Upstream Activating Sequence (*UAS*) and activates transcription of the galactose genes located downstream of *UAS* (Guarente *et al.*, 1982; Bram and Kornberg, 1985; Giniger *et al.*, 1985). The activity of *GAL4* is not restricted to yeast but it can function in a variety of biological systems to activate transcription from the *UAS* element (Kakidani and Ptashne, 1988; Ma *et al.*, 2003; Webster *et al.*, 1988).

The *GAL4/UAS* system has been used very successfully and widely in *Drosophila* to express genes and study their roles during development (Brand and Perrimon, 1993; Duffy, 2002). The system consists of two elements: a *GAL4* 'driver' and a *GAL4*-responsive *UAS* line (Figure 1.5). The driver line uses an enhancer or the promoter of a gene with known expression pattern (regulatory element) cloned upstream of the *GAL4* coding sequence, which allows *GAL4* expression in a spatially and temporally controlled manner. The flies expressing *GAL4* alone rarely show abnormalities associated to this event probably due to the absence of targets for *GAL4* in the *Drosophila* genome. A pan-muscle driver, *dmef2-GAL4*, exists but several tissue-specific drivers are also available.

The responder line bears the sequence of the target gene cloned downstream of multiple binding sites (*UAS*). In the absence of *GAL4* the target gene remains transcriptionally

silent. Mating of the driver and the responder lines results in progeny bearing both the responder and the driver transgenes simultaneously. In these flies, the GAL4 protein binds to the *UAS* sequence and activates transcription of the responder gene only in the cells/tissues expressing *GAL4*. The pattern of expression of the reporter gene is therefore the same as that of the *GAL4* driver. Maintaining the responder and driver as separate parental lines allows 1) the propagation of flies bearing transgenes encoding lethal alleles or toxic products that only become active in the offspring of crosses between the responder line and the *GAL4* driver and 2) the ready 'mix and match' of driver and responder produced by different investigators.

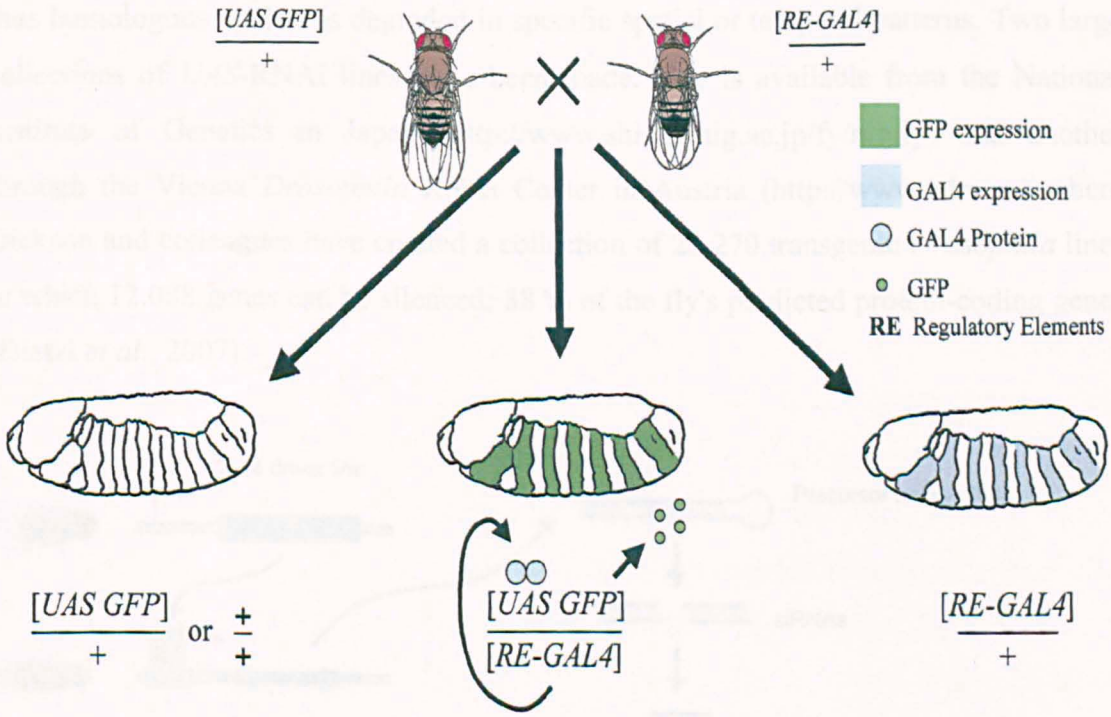

Figure 1.5. The *GAL4-UAS* system in *Drosophila*. The driver line carrying a tissue specific promoter upstream of the *GAL4* coding sequence and the responder line carrying a gene (*GFP* in this case) are crossed. In the progeny the fly that carries both the *GAL4* and the *UAS-GFP* the GAL4 will bind to the *UAS* sequences and activate transcription of the downstream *GFP* gene. In the flies carrying the *GAL4* insert alone there is no *GFP* gene to be activated. Likewise in flies carrying the *UAS-GFP* insert there is no *GAL4* to activate its transcription and therefore there is no *GFP* expression. Image reproduced from Duffy, 2002.

An increasingly common approach used to study gene function and development in *Drosophila* is RNAi interference (RNAi). The *GAL4/UAS* system is used to express a transgenic RNAi construct that forms a double stranded hairpin RNA (dsRNA) capable of degrading or suppressing translation of homologous mRNAs. The dsRNA is cleaved into 25 base pair fragments (Fire *et al.*, 1998; Hammond *et al.*, 2000), which then act as a 'degradation template' for the target mRNA (Yang *et al.*, 2000). In *Drosophila* the method involves expressing the gene fragments in an inverted repeat (IR) separated by an intron (Figure 1.6) (Lee and Carthew, 2003). The complementarity of the inverted repeats results in the expression of an RNAi hairpin loop, which activates the long dsRNA pathway. The dsRNA to target the gene of interest is cloned downstream of the UAS sequence. Expression of the dsRNA is achieved by using specific GAL4 drivers thus homologous mRNA is degraded in specific spatial or temporal patterns. Two large collections of *UAS*-RNAi lines have been made. One is available from the National Institute of Genetics in Japan (http://www.shigen.nig.ac.jp/fy/nigfly) and another through the Vienna *Drosophila* RNAi Center in Austria (http://www.vdrc.at.) where Dickson and colleagues have created a collection of 22,270 transgenic *Drosophila* lines in which 12,088 genes can be silenced; 88 % of the fly's predicted protein-coding genes (Dietzl *et al.*, 2007).

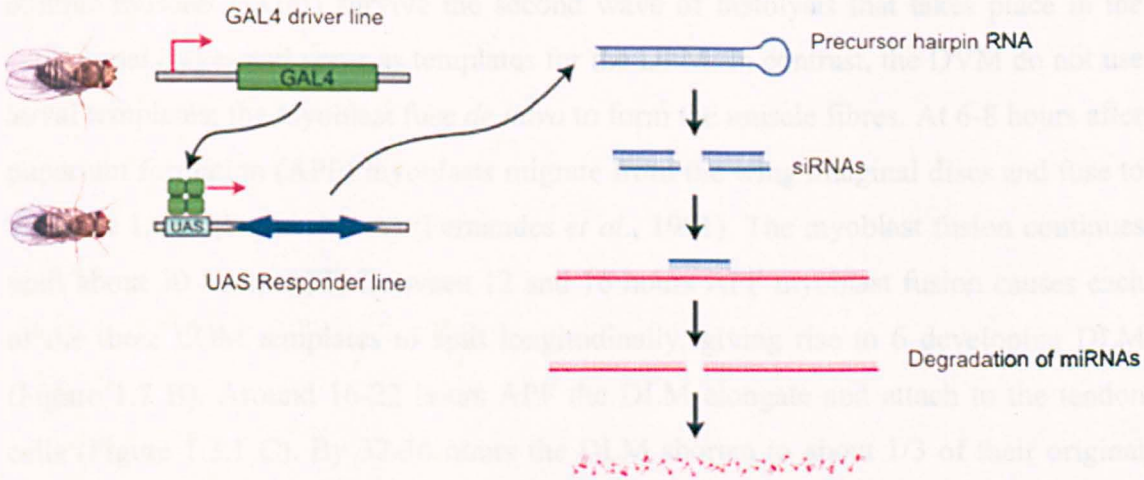

Figure 1.6. dsRNA in *Drosophila*. The responder line bears the *GAL4* binding site upstream of a gene cloned as an inverted repeat (IR) and when crossed with a tissue specific *GAL4* driver results in expression of the IR. The IR are separated by a functional intron which becomes spliced out leaving a long dsRNA molecule that will be processed into small interfering RNAs (siRNAs) which will eventually trigger the homologous mRNA degradation. Image modified from the Vienna stock centre website (http://www.vdrc.at).

1.3.2 *Drosophila* Indirect Flight Muscles as a model to study mutations in muscle proteins

Drosophila studies of human skeletal myopathies have concentrated in the larval muscles or in the adult Indirect Flight Muscles (IFM) (Calado *et al.* 2000, Abu-Baker *et al.*, 2003; Grumbling and Strelets, 2006, de Haro *et al.*, 2006; Rajendra *et al.*, 2007; Garcia-Lopez *et al.*, 2008). The latter are located in the fly's thorax and are responsible for powering flight. They are a suitable model for studying human skeletal myopathies as they are the only fibrillar type of muscle found in flies (Josephson, 2006) that its structure resembles human skeletal muscle. Furthermore, they occupy the majority of the thorax hence they can be easily accessed by microdissection for analysis.

1.3.2.1 IFM development

Drosophila undergoes myogenesis twice; once during embryonic development to generate the larval musculature and again during the pupal development to form the muscles of the adult fly (Bate, 1993). The IFM are split into two groups, the dorso-ventral (DVMs) and the dorsal-longitudinal (DLMs). These muscles originate from a subset of myoblasts of the wing imaginal discs, which differentiates during larval and pupal stages (Fernandes *et al.*, 1991; Bate, 1993, Farrell *et al.*, 1996). Three larval oblique muscles (LOM) survive the second wave of histolysis that takes place in the early pupal stages and serve as templates for the DLM. In contrast, the DVM do not use larval templates; the myoblast fuse *de novo* to form the muscle fibres. At 6-8 hours after puparium formation (APF) myoblasts migrate from the wing imaginal discs and fuse to the three LOM (Figure 1.7 A) (Fernandes *et al.*, 1991). The myoblast fusion continues until about 30 hours APF. Between 12 and 16 hours APF myoblast fusion causes each of the three LOM templates to split longitudinally, giving rise to 6 developing DLM (Figure 1.7 B). Around 16-22 hours APF the DLM elongate and attach to the tendon cells (Figure 1.3.1 C). By 32-36 hours the DLM shorten to about 1/3 of their original length and the tendon cells elongate (Figure 1.7 D). The DLM start elongating again between 42-44 hours APF whereas the tendon cells retract towards the cuticle (Figure 1.7 E). Between 46-48 hours APF myofibrillogenesis initiates (Figure 1.7 F) and the myofibrils continue to grow in length and thickness until they become mature myofibrils (Fernandes *et al.*, 1991; Reedy and Beall, 1993).

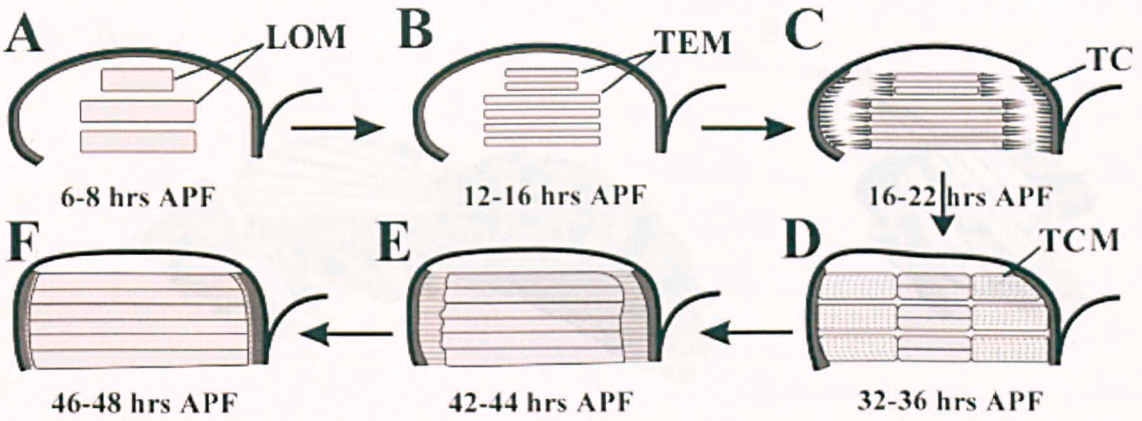

Figure 1.7. IFM development. (A) At 6-8 hours APF myoblasts fuse to the remnants of the larval oblique muscles (LOM). (B) Myoblast fusion causes the three LOM which have escaped histolysis and serve as templates (TEM) for the DLM to split around 12-16 hours APF. (C) By 16-22 hours APF myoblast fusion causes the IFM to lengthen and attach to the tendon cells (TC). (D) Around 32-36 hours APF the DLM shorten at about 1/3 of their length whereas the tendon cells elongate. (E) By 42 hours APF myofibrillogenesis is initiated, the muscles increase in length and size and the region of tendon and muscle processes (TCM) retracts. (F) At 46 hours APF functional myofibres have formed which continue to grow until they reach their final size. Image taken from Nongthomba *et al.*, 2003, not to scale.

1.3.2.2 IFM of *Drosophila melanogaster*

The IFM are so-called because they are not attached directly to the wings; instead they induce wing movement by distorting the fly's thorax. The position of the DLMs and DVMs is shown in Figure 1.8 A. Jumping of the fly is caused by contraction of the tergal depressor of the trochanter (TDT), which is another thoracic muscle. When it contracts (shortens) it lengthens and stretches the DLM oriented perpendicular to it (Figure 1.8 C). The DLM responds to stretch with a delayed rise in active tension (stretch activation response) causing it to contract (Figure 1.8 C). This causes a reciprocal delayed stretch activation of contraction in the DVM. As the two sets of muscles alternately contract, the thorax oscillates rapidly; causing deformation of the wing hinges that make the wings beat at the resonant frequency of the flight system. Stretch activation is essential to sustain flight in small insects (Drosophila beats its wings for flight at 200 Hz) (Molloy *et al.*, 1987). When the wings beat at frequencies well above the firing capability of the motorneurons the contractions of the IFM are not coincident with motorneuron firing and Ca^{2+} activation and consequently these muscles are called asynchronous.

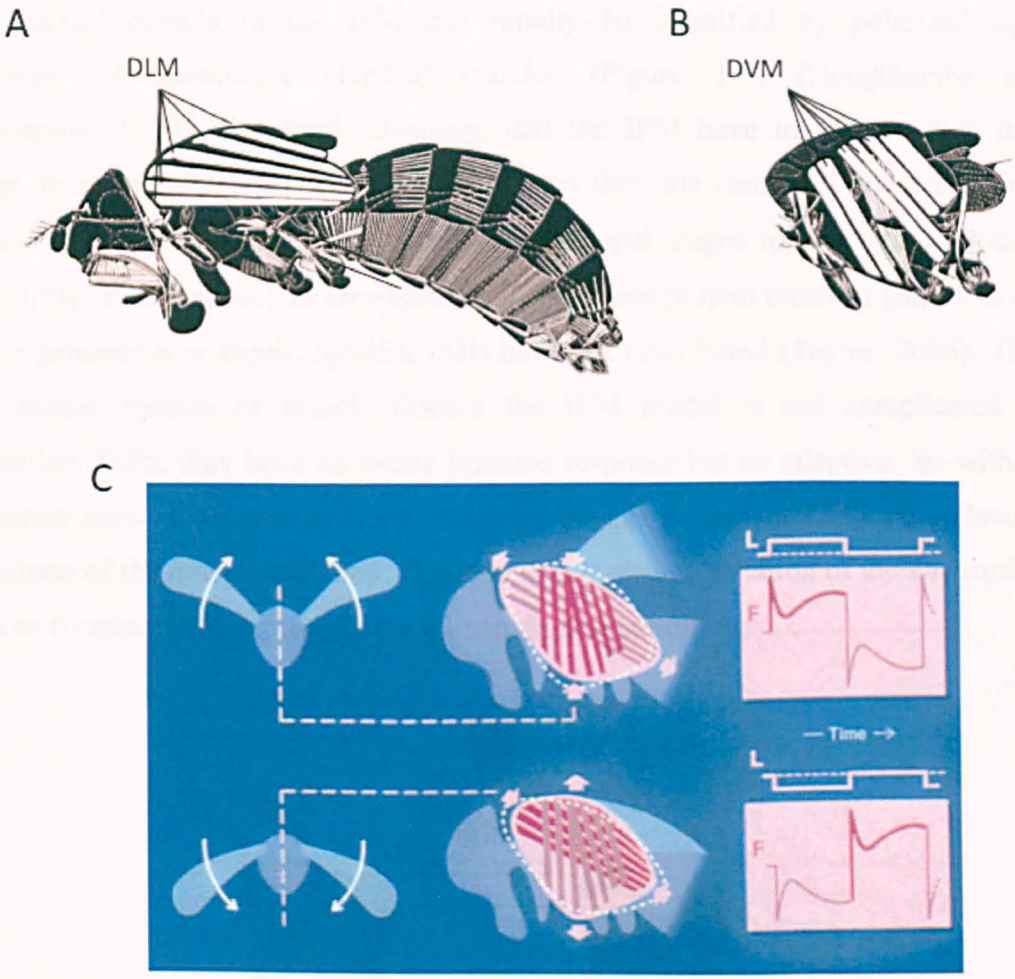

Figure 1.8. The indirect flight muscles of Drosophila *melanogaster*. Each hemithorax contains a set of **(A)** dorso-longitudinal (DLMs) and **(B)** dorso-ventral (DVMs) muscles. **(C)** During flight contraction of opposing muscles deforms the thorax resulting in wing movement. Images A and B reproduced from Demerec, 1950 and C from Vigoreaux, 2001.

1.3.2.3 The IFM as a model to study muscle mutations

Five important features of the IFM identify them as an excellent model for studying the effects of transgenes on muscle development. First, they are dispensable for viability (Bernstein *et al.,* 1993). Second, correct assembly and structure maintenance of muscle fibres are vital requirements for successful muscle function. So any mutation or silencing of an IFM specific gene that has an effect on muscle structure can be easily screened by a flightless phenotype. Some flightless mutants are also easily identifiable from the permanent atypical position of their wings beside their bodies when not flying in contrast to wild type flies (Kronert *et al*, 1999; Spradling *et al*., 1999). In mutants resulting in hypercontraction of the IFM, the wings are held permanently in a vertical position hence allowing easy identification of such mutants (Nongthomba *et al*., 2003).

Morphological defects in the IFM can rapidly be identified by polarized light microscopy of chemically clarified cuticles (Figure 1.9) (Nongthomba and Ramachandra, 1999). The third advantage that the IFM have to offer is that they develop over 4 days (Reedy and Beall, 1993) so that one can study the effect of a transgene throughout muscle development, from pupal stages to adult flies. Fourth, there is little or no evidence in *Drosophila* for sarcomere protein turnover (Smith *et al.*, 1970), regeneration or repair. Satellite cells have not been found (Taylor, 2006). Thus unlike mouse models of muscle disease the IFM model is not complicated by regeneration. Fifth, they have an innate immune response but no adaptive. So without the complications of repair or immune responses one can investigate the basic molecular mechanisms of the muscle mutation. However this is also a limitation of the *Drosophila* system as it cannot fully reproduce the human disease condition.

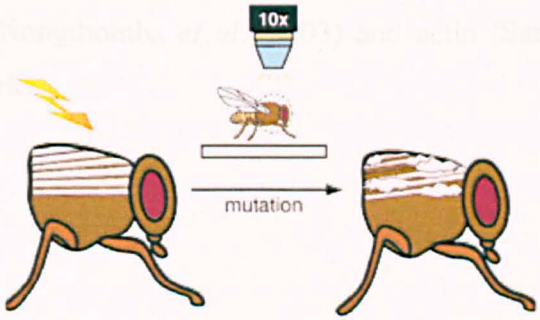

Figure 1.9. Mutagenized flies with defects in the IFM can be visualized using light microscopy. Image reproduced from Vigoreaux *et al.*, 2001.

Drosophila IFM have a long history of being used successfully to investigate the effects of mutations in actin and other sarcomeric proteins on muscle function (O'Donnell and Bernstein, 1988; Drummond *et al.*, 1990; Bernstein *et al.*, 1993; Molloy *et al.*, 1993; Nongthomba *et al.*, 2004). The availability of IFM-specific null mutants for the muscle proteins; myosin heavy chain (Mhc^7), actin (KM88), tropomyosin (Ifm(3)3Tm2), Troponin I (up^1) and Troponin T (hdp^3) (Bernstein *et al.*, 1993) has allowed the study of transgenic mutations for these genes in a wild type null background. Genetic deficiencies also permit the study of dosage requirements for IFM function (Bernstein *et al.*, 1993; Kreuz *et al.*, 1996; Vigoreaux *et al.*, 1998).

1.3.2.4 Dissection of genetic interactions in the IFM

The IFM is a very good system for identification of protein interactions using genetic approaches. Two fly strains each carrying a mutation in a different gene can be mated to generate progeny that are heterozygous for both mutations (Kronert *et al.*, 1999; Prado *et al.*, 1995). A genetic interaction is evident if the phenotype of the progeny is different from that of either parent (e.g. flightless progeny from two flighted parents) or if the progeny exhibits an otherwise recessive phenotype. Such genetic interactions may indicate that the mutations affect an interaction between two proteins that are in direct contact, function in the same pathway or are components of the same protein complex. An example is suppressor mutations, like those that have been identified for the hypercontraction phenotype of the IFM troponin mutant hdp^2 that autodestructs the muscles (Figure 1.10). Suppressor mutations for hdp^2 are located in genes encoding troponin I (Prado *et al.*, 1995), tropomyosin (Naimi *et al.*, 2001), myosin heavy chain (Kronert *et al.*, 1999; Nongthomba *et al.*, 2003) and actin (Sarah Haigh, PhD thesis, 2003, University of York)

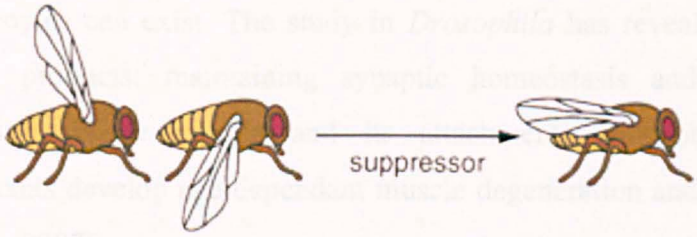

Figure 1.10. Genetic approaches to isolate mutations that affect the IFM. Flightless mutants exhibit abnormal wing position. The effects of a mutation can be reverted using intergenic or intragenic mutations. Image reproduced from Vigoreaux *et al.*, 2001.

1.4 *Drosophila* models of human skeletal myopathies

Hitherto there have been relatively few studies in *Drosophila* aimed at understanding human muscle diseases (reviewed in Sevdali and Sparrow, in preparation). The *Drosophila* models of the different myopathies, which do exist reproduce the human phenotype to different extents and have made some significant contributions towards our understanding of the molecular basis of the diseases. The skeletal myopathies have been modelled in both the larval muscles and in the IFM of the adult.

1.4.1 Duchenne muscular dystrophy

Duchenne muscular dystrophy is caused by mutations in genes of the Dystrophin (Dys)-Dystroglycan (Dg) complex (DGC) expressed in skeletal muscle cells (Hoffman *et al.*, 1987). Domains known to mediate the interactions between members of the DGC are highly conserved between humans and flies, suggesting that the structure of the DGC is identical (Greener and Roberts, 2000). Similar to vertebrates, the dystrophin products are expressed in a tissue specific manner (Neuman *et al.*, 2001; 2005; Dekkers *et al.*, 2004; Van der Plas *et al.*, 2006; Shcherbata *et al.*, 2007). Flies are a desirable system for the study of this disease because they express a single dystrophin gene (Greener and Roberts, 2000) ad thus reduces the genetic complexity found in vertebrate systems where multiple copies can exist. The study in *Drosophila* has revealed two roles for dystrophin gene products: maintaining synaptic homeostasis and preserving the structural stability of the muscle and its attachment. Drosophila dystrophyn-dystroglycan mutants develop age-dependant muscle degeneration and mobility defects (Shcherbata *et al.*, 2007).

1.4.2 Barth syndrome

Barth syndrome (BTHS) is an X-linked disease where patients present with cardiomyopathy and skeletal muscle weakness (Barth *et al.*, 1999). The disease is caused by mutations in tafazzin (Bione *et al.*, 1996), a phospholipid acyltransferase (Neuwald, 1997). Patients with BTHS display mitochondrial abnormalities (Barth *et al.*, 1993; Vreken *et al.*, 2000; Schlame *et al.*, 2000; Bissler *et. al.*, 2002; Schlame *et al.*, 2002; Valianpour *et al.*, 2002). Hitherto yeast, fibroblasts and lymphoblasts have been used to study BTHS, but the inability to replicate the tissue pathology of the disease is a major limitation of these models (Gu *et al.*, 2004; Vreken *et al.*, 2000; Xu *et al.*, 2003). *Drosophila* expresses several tafazzin isoforms (Grumbling and Strelets, 2006) and as

IFM have abundant mitochondria flies have emerged as an attractive experimental system for BTHS research. In tafazzin-deficient flies, total cardiolipin levels were reduced by 80%, the main cardiolipin species was absent similar to BTHS patients (Grumbling and Strelets, 2006) and displayed flight defects with reduced locomotor activity. Their IFM showed mitochondrial abnormalities, mostly in the cristae membranes which displayed hyperdense aberrant phenotypes such as swirls, curls and rings (Grumbling and Strelets, 2006).

1.4.3 Spinal muscular atrophy

Spinal muscular atrophy (SMA) is a genetic disorder associated with recessive loss-of function mutations in the human survival motor neurons 1 gene (*SMN1*) (Lefebvre *et al.*, 1995). The most severe form is the most common and patients die within 2 years of birth (Ogino and Wilson, 2004; Monani 2005). The disease is characterized by loss of motor neurons and progressive muscular atrophy in the limps and trunk (Ogino and Wilson, 2004). In a *Drosophila* model of SMA, hypomorphic Smn^{E33} mutants reduce dSMN levels in adult thorax, are unable to fly or jump and exhibit severe neuromuscular defects (Rajendra *et al.*, 2007). The *Smn* mutant myofibres fail to form thin filaments resembling the IFM-specific actin *Act88F* null mutants. SMA patients have also been shown to exhibit myofibrillar and sarcomeric abnormalities (Szliwowski and Drochmans, 1975; Braun *et al.*, 1995). The most surprising finding was that in wild type flies dSMN colocalized with sarcomeric actin and α-actinin in the IFM myofibrils revealing for the first time that SMN is a sarcomeric protein. Although it is not currently known whether the phenotype observed in the Smn^{E33} hypomorphs is due to reduced dSMN levels or the motoneurons or a combination of the two, there is a promising future for examining myogenesis and motoneuron development during pupal stages.

1.4.4 Oculopharyngeal muscular dystrophy

Oculopharyngeal muscular dystrophy (OPMD) is an adult-onset syndrome characterized by progressive muscle degeneration that is caused by short GCG repeat expansions of an N-terminal polyalanine tract within the nuclear poly(A)-binding protein 1 (PABPN1) (Brais *et al.*, 1998). A coiled-coil N-terminal domain is responsible for stimulation of poly(A) polymerase (Kerwitz *et al.*, 2003), whereas a central RNA-binding domain and an arginine-rich COOH-terminal domain are involved in binding [illegible] tail (Kuhn *et al.*, 2003). Mutant PABPN1 aggregates as intranuclear

inclusions. A *Drosophila* model of OPMD exists where mutant PABPN1 is expressed specifically in the musculature (Chartier *et al*, 2006). The wing position of the mutant flies was normal at day 1 but by day 2 they displayed abnormal wing phenotypes, were flightless and displayed nuclear PABPN1 inclusions (Calado *et al.*, 2000; Abu-Baker *et al.*, 2003) demonstrating that the disease is also progressive in *Drosophila.* Flies where the alanine extension is deleted (PABPN1-ΔA) did not display inclusions. Expression of PABPN1-17A with a deletion of the RNA-binding (PABPN1-17A-ΔRRM) domain did not cause muscle defects or in abnormal intranuclear accumulation. This suggests that the RNA-binding domain is required for the OPMD phenotype.

The modeling of different skeletal muscle diseases in *Drosophila* is possible and has already contributed significantly to the understanding of these skeletal muscle diseases. Clearly *Drosophila* IFM are developing as a useful genetic model for a range of muscular diseases. Modelling of thin filament skeletal myopathies (including the nemaline *ACTA1* myopathies and arthrogryposis) has not as yet been reported.

1.4.5 *Drosophila* IFM: a model for thin filament myopathies

Drosophila expresses a single actin isoform, *ACT88F*, which encodes all of the sarcomeric actin present in the IFM (Fyrberg *et al.*, 1983; Ball *et al.*, 1987) and is highly homologous (~ 93 % homology) to the human α-skeletal actin (Figure 1.11) (Hanauer *et al.*, 1983). Hence it is possible to introduce mutations in the *Act88F* gene that are homologous to the human *ACTA1* nemaline myopathy mutations. Initial studies (Sarah Haigh, 2003, PhD thesis, University of York) showed that genomic mutations in the IFM-specific *ACT88F* gene at specific residues (A13V, R256C, G268D, R372H) associated in humans with NM (A138P, R256H/L, G268R/C, R372H) are dominant flightless and cause variable sarcomere lengths and in the zebra body phenotype which is also found in human patients and is thought to be the beginning of nemaline rods. Three of these *ACT88F* mutants do not make sarcomeres during early myogenesis and the flies cannot fly. However the $ACT88F^{R372H}$ mutant has normal myogenesis and the pupae show normal myofibrils, but adults develop the nemaline phenotype clearly demonstrating two pathways to the 'nemaline' phenotypes.

```
Act88F          -DDDAGALVIDNGSGMCKAGFAGDDAPRAVFPSIVGRPRHQGVMVGMGQKDSYVGDEAQS 59
Acta1           DEDETTALVCDNGSGLVKAGFAGDDAPRAVFPSIVGRPRHQGVMVGMGQKDSYVGDEAQS 60
                 :*:: *** *****: ******************************************

Act88F          KRGILTLKYPIEHGIITNWDDMEKIWHHTFYNELRVAPEEHPVLLTEAPLNPKANREKMT 119
Acta1           KRGILTLKYPIEHGIITNWDDMEKIWHHTFYNELRVAPEEHPTLLTEAPLNPKANREKMT 120
                ******************************************.*****************

Act88F          QIMFETFNSPAMYVAIQAVLSLYASGRTTGIVLDSGDGVSHTVPIYEGFALPHAILRLDL 179
Acta1           QIMFETFNVPAMYVAIQAVLSLYASGRTTGIVLDSGDGVTHNVPIYEGYALPHAIMRLDL 180
                ******** ******************************:*.******:******:****

Act88F          AGRDLTDYLMKILTERGYSFTTTAEREIVRDIKEKLCYVALDFEQEMATAAASTSLEKSY 239
Acta1           AGRDLTDYLMKILTERGYSFVTTAEREIVRDIKEKLCYVALDFENEMATAASSSSLEK-- 238
                ********************.**********************:******:*:****

Act88F          ELPDGQVITIGNERFRCPEALFQPSFLGMESCGIHETVYNSIMKCDVDIRKDLYANSVLS 299
Acta1           ------------------------------------------------------------MS 240
                                                                          :*

Act88F          GGTTMYPGIADRMQKEITALAPSTIKIKIIAPPERKYSVWIGGSILASLSTFQQMWISKQ 359
Acta1           GGTTMYPGIADRMQKEITALAPSTMKIKIIAPPERKYSVWIGGSILASLSTFQQMWITKQ 300
                ************************:********************************:**

Act88F          EYDESGPGIVHRKCF 374
Acta1           EYDEAGPSIVHRKCF 315
                ****:**.*******
```

Figure 1.11. Alignment of human ACTA1 and *Drosophila* ACT88F protein sequences. The sequences of the two proteins show 93% homology. The annotation symbol for *Acta1* is X56644.2 (release 27) and for *Act88F* NP_524367.1. Note: '*' indicates that the residues in that column are identical in all sequences in the alignment, ':' indicates that conserved substitutions have been observed, '.' indicates that semi-conserved substitutions are observed.

All four reported TnI mutations responsible for Distal Arthrogryposes cause increased contractility (Sung *et al.*, 2003; Robinson *et al.*, 2006) and are hence likely to cause muscle hypercontraction *in vivo*. TnI mutations in *Drosophila* IFM have also been identified that cause muscle hypercontraction (Deak 1977; Deak *et al.*, 1982; Beall and Fyrberg 1991; Barbas *et al.*, 1993, Nongthomba *et al.*, 2004). In the IFM TnI and TnT nulls exist which can be used to study arthrogryposis mutants using transgenesis.

Nemaline myopathy and arthrogryposis are both diseases caused by mutations in sarcomeric thin filament proteins. The organisation of the thin filament will now be discussed.

1.5 Organisation of skeletal muscle

Skeletal muscle is made up of multinucleated cells called muscle fibres (or myofibres) that are aligned parallel to each other. Each myofibre contains multiple contractile protein assemblies called myofibrils (Figure 1.12). Mitochondria are located between the myofibrils and nuclei are found in the periphery of the cytoplasm (Figure 1.12).

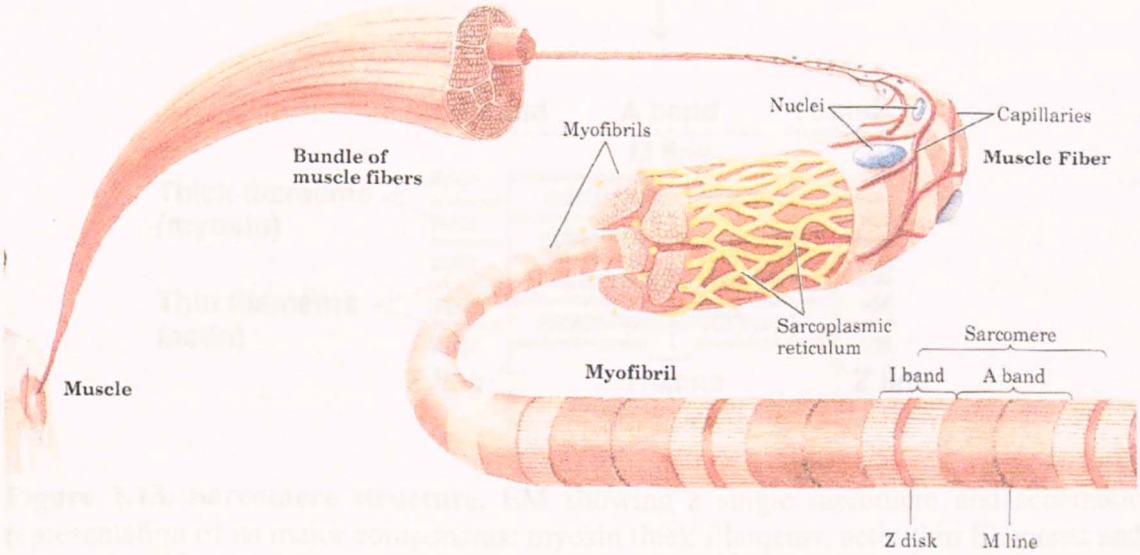

Figure 1.12. Muscle organisation. Skeletal muscle is composed of muscles fibres, which in turn consist of myofibrils, nuclei located in the periphery of the muscle fibre shown in blue. Myofibrils consist of repeating units called sarcomeres that power muscle contraction. Image reproduced from Lehninger *et al.* 2000.

Each myofibril is a long array of by specialized and highly ordered repeating contractile units, the sarcomeres (Figure 1.13). The sarcomere is composed of myosin-based thick and actin-based thin filaments arranged parallel to each other in a lattice. Longitudinal sections of electron micrographs from muscle fibres show an electron dense area called the Z-disc, which demarcates each sarcomere and anchors actin thin filaments from adjacent sarcomeres. The actin thin filaments extend from the Z-discs across a lighter area termed the I-band followed by a darker area termed the A-band. Myosin thick filaments project from the M-line, extend through the H-zone and interdigitate with actin thin filaments across the A-band. Sarcomere passive stiffness is maintained by a third filament system whereby a long modular protein, titin, connects the thick filaments to the Z-disc (Granzier and Labeit, 2007).

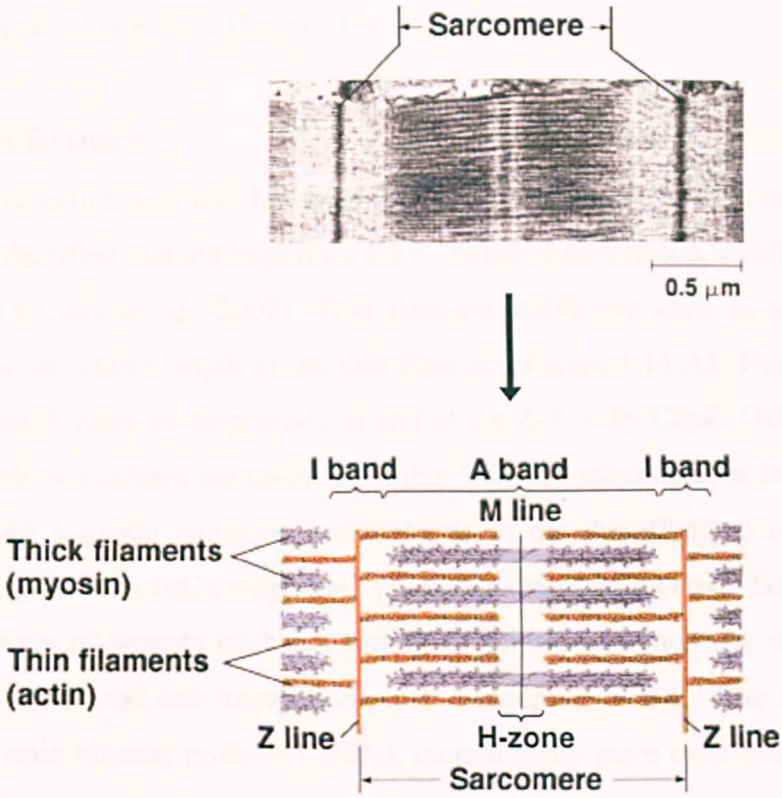

Figure 1.13. Sarcomere structure. EM showing a single sarcomere and schematic representation of its major components: myosin thick filaments, actin thin filaments and Z-discs. Image reproduced from http://themedicalbiochemistrypage.org/muscle.html.

1.5.1 Thick filament- Myosin

Myosin, a large multidomain protein (520 kDa) is the major component of the thick filaments (reviewed in Geeves and Holmes, 2005). Myosin acts as a molecular motor that converts the chemical energy of ATP hydrolysis into mechanical force (Ruppel and Spudich, 1996). Muscle myosin is composed of two heavy chain (MHC) (~ 220 kDa) subunits and two pairs of light chain (MLC) (~ 20 kDa) subunits. The MHC and two light chains from a globular, NH_2-terminal head domain, which contains the binding sites for actin and nucleotides and exhibits the motor function (Rayment *et al.*, 1993; Milligan *et al.*, 1996). Myosin heads are excluded in the sarcomere H-zone. The COOH-terminal regions of the MHC associate to form an α-helical coiled-coil dimer rod, which subsequently polymerize to form thick filaments (Squire and Vibert, 1987; Ruppel and Spudich, 1996). Contraction of muscle is the result of cyclic interactions between the globular heads of the myosin molecules, also known as cross-bridges, and the actin filaments. Myosin powers muscle contraction by hydrolysis of ATP, an interaction with the actin thin filaments and a large conformational change. This mechanism undergoes a number of cycles to drive muscle contraction (Geeves and Holmes, 2005). As a result, each end of the thick filament 'pulls' the thin filaments with

which it interacts toward the H-zone (Figure 1.13).

1.5.2 Thin filament

The major constituent of the thin filament is actin, although numerous others proteins have been identified that are important for its length maintenance, stability and function (reviewed in Clark *et al.*, 2002). Thin filament stabilizers such as tropomyosin and nebulin span the entire length of the thin filament (Figure 1.14 A). The thin filament is capped at the A-band by tropomodulin and at the Z-disc by CapZ. Other thin filament proteins such as α-actinin are involved in thin filament attachment at the Z-disc (Figure 1.14 A). The troponin complex, which binds to the thin filament consists of three subunits: troponin C (TnC), troponin I (TnI) and troponin T (TnT). Each thin filament strand consists of repeats each containing seven actin monomers, one tropomyosin coiled coil dimer and one troponin complex (Figure 1.14 B). These represent only a handful of actin binding proteins (ABPs), though many more exist but are not relevant to this thesis.

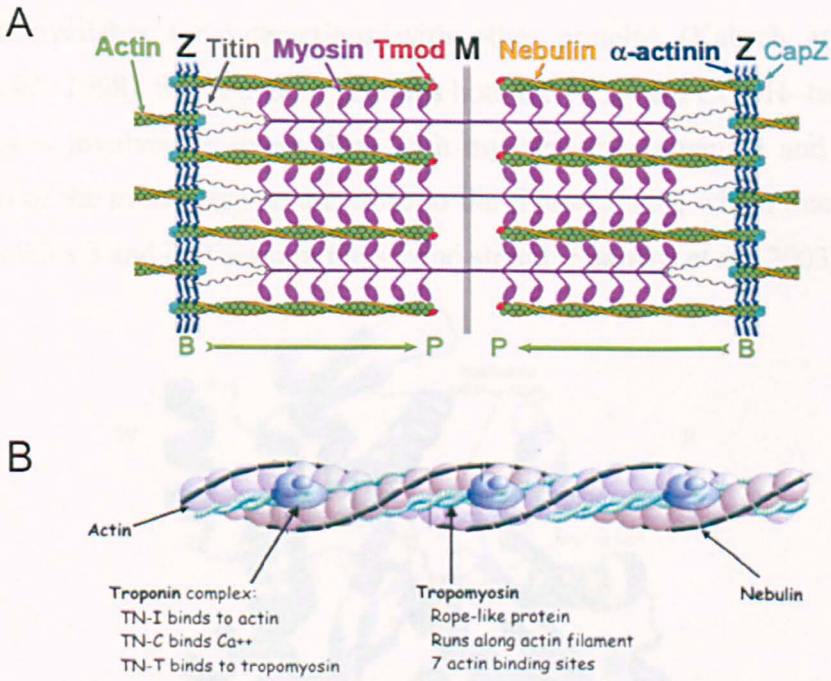

Figure 1.14. Thin filament organisation in striated muscle. (A) Schematic representation of sarcomere showing the actin thin filaments (green), titin (grey), myosin thick filaments (purple), tropomodulin (red), nebulin (yellow), CapZ (cyan), α-actinin (blue) are indicated. Z: Z-disc, M: M-line, B: barbed end and P: pointed end. Image reproduced from Littlefield and Fowler, 2008. **(B)** Actin monomers shown in light purple, the troponin complex of TnI, TnT and TnC shown in darker purple, tropomyosin dimers in light blue and nebulin in black. Image reproduced from Laing and Nowak, 2005.

1.5.2.1 Actin

Actin is the second most abundant sarcomeric protein (20 % in muscle). Actins are a highly conserved protein family, at the amino acid level human skeletal muscle α-actin shares 100 % homology with mouse skeletal muscle α-actin and 87 % homology with rice cytoskeletal actin (Sheterline *et al.*, 1998). Thus most residues in skeletal muscle α-actin may be classified as highly conserved, and any amino acid change is likely to be disease causing. It is a single 375 amino acid polypeptide chain (MW ~ 42 kDa) that binds to both adenosine nucleotide (ATP or ADP) and a divalent cation (usually magnesium or calcium) (reviewed in Sheterline *et al.*, 1998). It exists in two forms, monomeric G-actin and polymeric filamentous F-actin, which is a linear chain of actin monomers (Holmes *et al.*, 1990). The monomer is divided into two domains (inner and outer) by a cleft, which forms the binding site for ATP in G-actin (ADP in F-actin) and the divalent ion (Figure 1.15) (Kabsch *et al.*, 1990; Otterbein *et al.*, 2001). The domains are connected together by two polypeptide chains known as the 'hinge', which allows domain movement (Sparrow *et al.*, 2003). The small domain of the monomer consists of subdomains 1 and 2 that are located on the outer surface of the actin filament, which are exposed and available for interactions with other proteins (Kabsch *et al.*, 1990; Sheterline *et al.*, 1998). Subdomain 1 contains both the NH_2- and COOH- termini of the molecule and is involved in interactions with myosin. Subdomains 3 and 4 form the large domain of the monomer and are close to the filament axis, which interacts across to the subdomains 3 and 4 of actin in the second strand (Sparrow *et al.*, 2003).

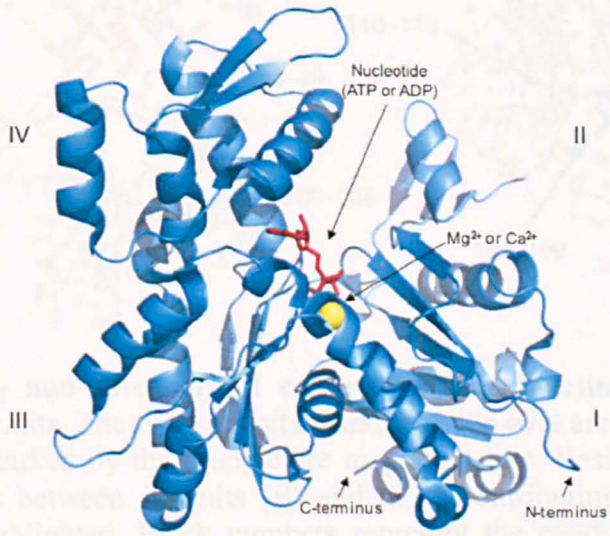

Figure 1.15. G-actin structure. Cartoon of G-actin bound to ATP and Ca^{2+}, depicting the four actin subdomains (I, II, III, IV), the nucleotide and divalent ion binding sites and the NH_2- and COOH-termini. PDB file 2hf4, image was produced in PYMOL.

In vitro, actin is monomeric under low ionic strength conditions (0.2 mM Ca^{2+} or 0.05 mM Mg^{2+}). Elevating the ionic strength to physiological conditions (2 mM $MgCl_2$ and 100 mM KCl), in neutral or slightly acidic pH causes monomeric G-actin to polymerize into F-actin filaments (Sheterline *et al.*, 1998). The process is reversible upon lowering the ionic strength. F-actin filaments are polarized, right-handed, double-helical polymers composed of 370 subunits per µm with one twist of the double helix every 36 nm (Figure 1.16 A) (Hanson and Lowy, 1964; Sparrow et al., 2003). This polarity was first identified in electron micrographs of myosin S1 fragment decorated actin filaments, which appeared as a thread of arrowheads repeating every 36 nm. One end of the filament became known as the barbed end (attached to the Z-disc) and the other as the pointed end (at the end of the A-band). In the F-actin helix, each actin contacts four other actins, the preceding and following actin on the same filament and two actins across on the other filament (Figure 1.16). Residues facilitating the intra-strand contacts between subunits and those contributing to the inter-strand contacts are highlighted in Figures 1.16 B and C, respectively.

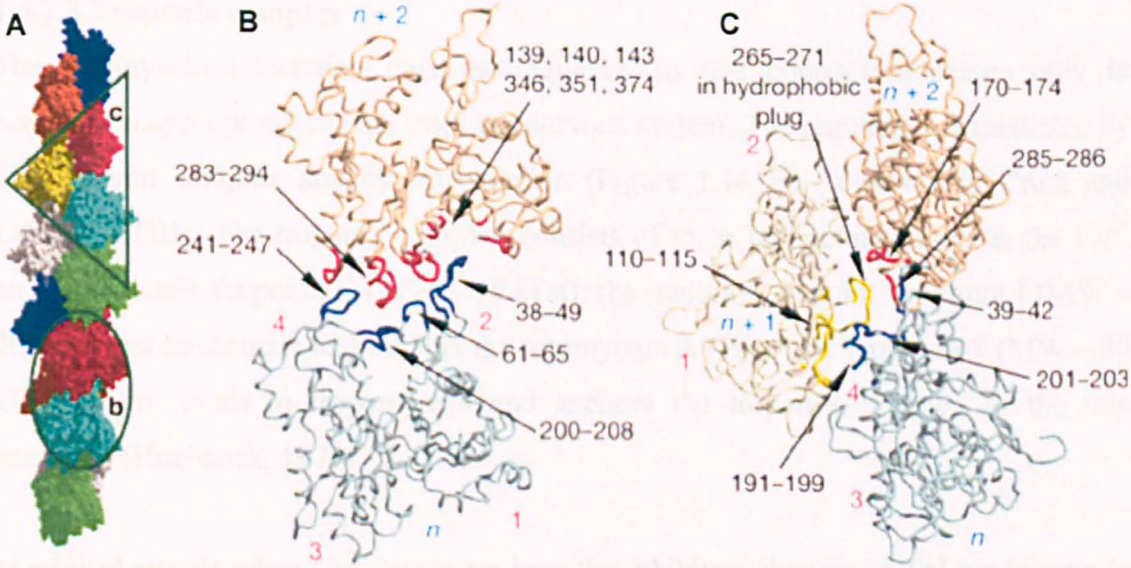

Figure 1.16. Intra- and inter-strand contacts within F-actin. (A) F-actin helix composed of 13 subunits. The two subunits marked by the oval are magnified in b, and the three subunits marked by the triangle are magnified in c. Residues facilitating the intra-strand contacts between subunits **(B)** and those contributing to the inter-strand contacts **(C)** are highlighted. Black numbers represent the residue numbers and red numbers represent subdomain numbers; n, n + 1 and n + 2 are subunit numbers. Image reproduced from Oda *et al.*, 2009.

1.5.2.2. Tropomyosin

Tropomyosins (MW ~ 37 kDa) are constructed of two α-helices arranged into a coiled-coil structure. They bind as a dimer along the sides adjacent to the thin filaments in a head-to-tail manner (Figure 1.14 A, B), with an overlap of 8-11 amino acids (Wegner, 1979). Depending on the isoform, six to seven (in muscle) actin monomers may be spanned by a tropomyosin molecule (Perry, 2001). Tropomyosin interacts with tropomodulin to stabilize the thin filament by slowing its polymerisation and depolymerisation from the pointed ends (Broschat *et al.*, 1989; Broschat, 1990; Sung and Lin, 1994; Vera *et al.*, 2000; Greenfield and Fowler, 2002). Tropomyosin binding protects the thin filament against severing and depolymerisation from cofilin (Des Marais *et al.*, 2005; Nishida *et al.*, 1985; Ono and Ono, 2002), DNaseI (Hitchcock *et al.*, 1976) and gelsolin (Fujime and Ishiwata, 1971; Ishikawa *et al.*, 1989). The *Drosophila* Tm isoforms are encoded by two genes *Tm1* and *Tm2*. The *Tm1* gene encodes two additional Tm IFM specific isoforms, *TnH33* and *TnH34*, which contain a 200 amino acid long proline and alanine rich extension (KarliK and Fyrberg, 1986; Bullard *et al.*, 1988; Barbas *et al.*, 1991; Beall and Fyrberg, 1991).

1.5.2.3 Troponin complex

The actomyosin interaction must be regulated so that contraction occurs only in response to appropriate signals from the nervous system. The regulation is mediated by the troponin complex and by tropomyosin (Figure 1.14 B) (reviewed in Craig and Lehman, 2001). The troponin complex consists of three interacting subunits, the Ca^{2+} binding subunit Troponin C (MW ~ 18 kDa); the inhibitory subunit Troponin I (MW ~ 20 kDa) that binds actin and inhibits the actomyosin ATPase and Troponin T (MW ~ 30 kDa), which binds to tropomyosin and anchors the troponin complex to the thin filaments (Hitchcock, 1975).

In relaxed muscle when Ca^{2+} levels are low, the inhibitory domain of TnI binds actin in such a way that tropomyosin sterically blocks the myosin head-binding sites on the outer domain of the thin filaments. Upon Ca^{2+} binding to TnC, the affinity of the inhibitory region of TnI becomes stronger for TnC than for actin (Potter and Gergely, 1974). This results in conformational changes in the troponin complex which allows tropomyosin to shift its position to expose the weak myosin-binding sites on actin, thereby allowing cross-bridges to form (Huxley 1972; Parry and Squire, 1973; Lehman

et al. 1994, 1995; Tobacman, 1996; McKillop and Geeves, 1993; Vibert *et al.*, 1997). Myosin binding activates the myosin ATPase and causes further translocation of tropomyosin on actin filaments allowing strong, force-generating interactions between actin and myosin (Craig and Lehman, 2001).

1.5.2.4 Nebulin

Nebulin is a 600-900 kDa actin-binding protein found only in vertebrate sarcomeres (Wang and Williamson, 1980). A single nebulin molecule spans the entire length of the thin filament (Figure 1.14 A) hence nebulin is thought to be a ruler of thin filament lenghts (Littlefield and Fowler, 1998; McElhinny *et al.*, 2003). Its NH_2-terminus interacts with tropomodulin whereas its COOH-terminus extends into the Z-disc (Nave *et al.* 1990; McElhinny *et al.*, 2001). The closest homologue found in Drosophila is Lasp, which is characterized by actin-binding nebulin repeats (Chen *et al.*, 1993, Suyama *et al.*, 2009).

1.5.2.5 Tropomodulin

Tropomodulins (Tmods) (MW ~ 40 kDa) are a conserved family of actin and tropomyosin binding proteins that are associated stoichiometrically with thin filament pointed ends in all vertebrate, worm and fly striated muscles (Figure 1.14 A) (reviewed in Fowler, 1997; Fischer and Fowler, 2003). Unlike actin cytoskeletal structures in nonmuscle cells where barbed ends are the predominant assembly ends (Pollard *et al.*, 2000), muscle cells actin dynamics predominates at the thin filament pointed ends (Littlefield and Fowler, 2008). A substantial body of data demonstrates that thin filament lengths are controlled by inhibition of actin assembly at pointed ends by Tmods (Gregorio and Fowler, 1995). This is achieved by two distinct regions within the Tmod protein sequence; (1) an actin capping NH_2-terminal region which binds to two tropomyosin molecules (Vera *et al.*, 2000; Kostyukova *et al.*, 2006) and (2) a second COOH-terminal actin-binding site, which may cap two actin monomers (Gregorio *et al.*, 1995; Fowler *et al.*, 2003; Wear *et al.*, 2003). Binding to tropomyosin is required in order to achieve high affinity pointed end capping (K_d < 1nM) (Weber, 1994).

1.5.3 The Z-disc

The Z-disc is an electron dense structure that represents the lateral borders of the sarcomeres in striated muscle (reviewed in Clark *et al.*, 2002). It stabilizes the filament lattices of adjacent sarcomeres thus ensuring that active and passive tensions are transmitted along the sarcomeres. It consists of numerous proteins that anchor both the thin and thick filaments to the Z-disc (Frank *et al.*, 2006). Thin filaments from adjacent sarcomeres overlap and terminate within the Z-disc where they are anchored by the capping protein CapZ, α-actinin and nebulin, other proteins are also present (reviewed in Clark *et al.*, 2002). A large modular protein, titin, connects the thick filaments to the Z-disc (reviewed in Clark *et al.*, 2002). In *Drosophila*, there is no titin homologue but the function of titin is divided between projectin and sallimus (Burkart *et al.* 2007).

1.5.3.1 Capping protein (CapZ)

Capping protein is a heterodimeric protein consisting of α and β subunits. It was named capping protein because of its ability to inhibit growth of the actin filament at the barbed end (Isenberg *et al.*, 1980). The sarcomeric isoform of capping protein, CapZ, is localized at the Z-disc in muscle (Figure 1.14 A) (Casella *et al.*, 1987), probably through an interaction with α-actinin and another thin filament protein, nebulin, at the Z-disc (Figure 1.17 A) (Papa *et al.*, 1999; Pappas *et al.*, 2008). CapZ binds to the barbed end of the thin filament with a high affinity ($K_d \approx 1$ nM) and a 1:1 stoichiometry (Caldwell *et al.*, 1989; Schafer *et al.*, 1993; Wear *et al.*, 2003) thus preventing both the addition and loss of actin monomers at the fast growing end (Isenberg *et al.*, 1980). The α and β subunits have very similar secondary structures despite their complete lack of sequence similarity (Wear *et al.*, 2003). Capping protein binding to actin is mediated via the COOH-terminal extensions of the α and β subunits. In the crystal structure the COOH-terminal end of the α subunit forms an amphipathic helix, which is folded down on the surface of the protein. The COOH-terminal end of the β subunit is also an amphipathic helix, but longer than in its CPα counterpart and protrudes from the rest of the structure via a long loop (Narita *et al.*, 2006) to caps the thin filaments in a 'tentacular' mechanism (Figure 1.17 B) (Yamashita *et al.*, 2003).

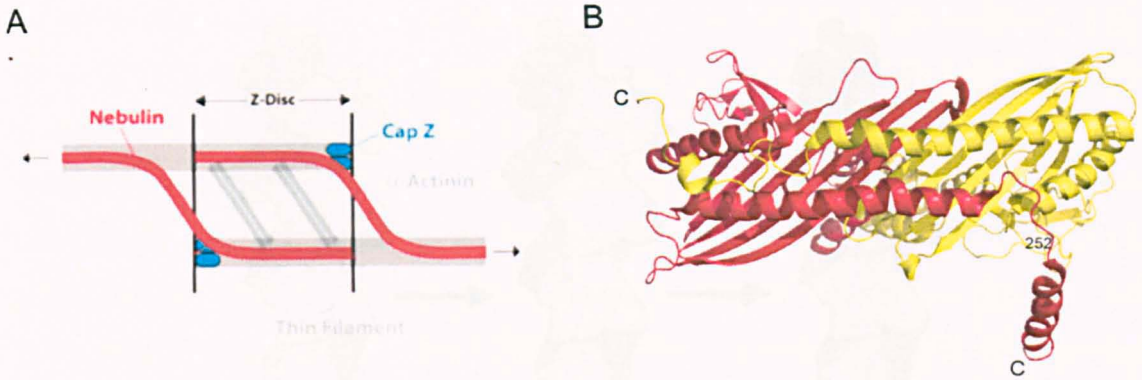

Figure 1.17. Actin-CapZ interaction. (A) Model of the architecture of CapZ, nebulin and α-actinin at the Z-disc. The CapZ heterodimer is shown in blue circles, the α-actinin homodimers in vertical grey bars and nebulin in red. Diagram reproduced from Pappas *et al.*, 2003. **(B)** Crystal structure of the CapZ heterodimer, the CPα subunit is shown in yellow, and the CPβ subunit in red, the first residue (252) of the disordered region is indicated. Picture reproduced from Wear *et al.*, 2003.

The X-ray crystal structure of CP has inspired a model where the COOH-terminal 30 amino acids of the α and β subunits are mobile extensions ('tentacles') responsible for high affinity binding to and capping of the F-actin barbed end (Yamashita *et al.*, 2003). The proposed mechanism for the binding of CP to the thin filament barbed end involves two steps. First, basic residues on the α-tentacle interact with the acidic residues of the end actin protomers on the actin filament. The freely mobile β-tentacle binds to the hydrophobic cleft between subdomain 1 and 3 of the end actin protomer (Figure 1.18). The flexibility of the CapZ extensions probably acts to uncap the actin filament for incorporation of exogenous actin at the barbed end without disrupting the sarcomeric structure (Littlefield *et al.*, 2001).

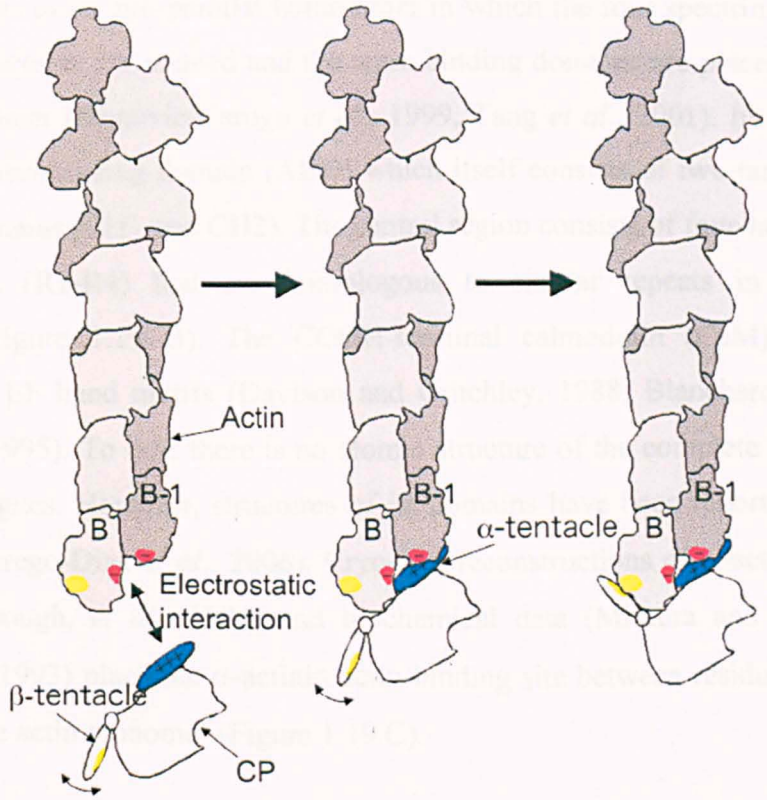

Figure 1.18. CapZ binding to the barbed end of the thin filament. The monomers of the actin filament are shown in grey and the CapZ heterodimer in white. Acidic residues (red) of the end actin protomers B and B-1 on the barbed end of the filament attract basic residues (blue) on the CP α-tentacle. The hydrophobic surface (yellow) of the flexible β tentacle (indicated) binds to the hydrophobic cleft (yellow) on the terminal protomer, B thereby stabilizing the binding. Picture reproduced from Narita *et al.*, 2006.

1.5.3.2 α-Actinin

α-Actinin (MW ~ 97 kDa) is found in both muscle and non-muscle cells at points where F-actin filaments are anchored within a variety of intracellular structures. It belongs to a highly conserved family of actin-binding proteins, the spectrin superfamily that contains spectrin, utrophin and dystrophin (Blanchard *et al.*, 1989; Pascual *et al.*, 1997). α-Actinin cross-links anti-parallel actin filaments (Luther, 2000) found in the Z-disc of striated muscle (Figure 1.14 A) (Sorimachi *et al.*, 1997; Young *et al.*, 1998; Young and Gautel, 2000), smooth muscle and in stress fibres of non-muscle cells (Blanchard *et al.*, 1989). Actin thin filaments of adjacent sarcomeres overlap and terminate within the Z-disc where they are linked by transversely oriented α-actinin molecules that form ladder-like structures with the thin filaments (Figure 1.19 A) (Meyer and Aebi, 1990; Vigoreaux 1994).

α-Actinin exists as an anti-parallel homodimer in which the four spectrin repeats of the anti-parallel partners are aligned and the actin-binding domains are placed at both ends of the homodimer (Djinovic-Carugo *et al.*, 1999, Tang *et al.*, 2001). Its NH_2-terminus contains an actin-binding domain (ABD) which itself consists of two-tandem calponin homology domains (CH1 and CH2). The central region consists of four-tandem spectrin 3-helix-motifs (R1-R4) that are homologous to similar repeats in spectrin and dystrophin (Figure 1.19 B). The COOH-terminal calmodulin (CaM)-like domain, contains four EF hand motifs (Davison and Critchley, 1988; Blanchard *et al.*, 1989; Trave *et al.*, 1995). To date there is no atomic structure of the complete protein or any of its homologues. However, structures of its domains have been reported (Franzot *et al.*, 2005; Borrego-Diaz *et al.*, 2006). Cryo-EM reconstructions of α-actinin decorated F-actin (McGough, *et al.*, 1994) and biochemical data (Mimura and Asano, 1987; Lebart *et al.*, 1993) place the α-actinin actin-binding site between residues 83-117 and 350-372 of the actin monomer (Figure 1.19 C).

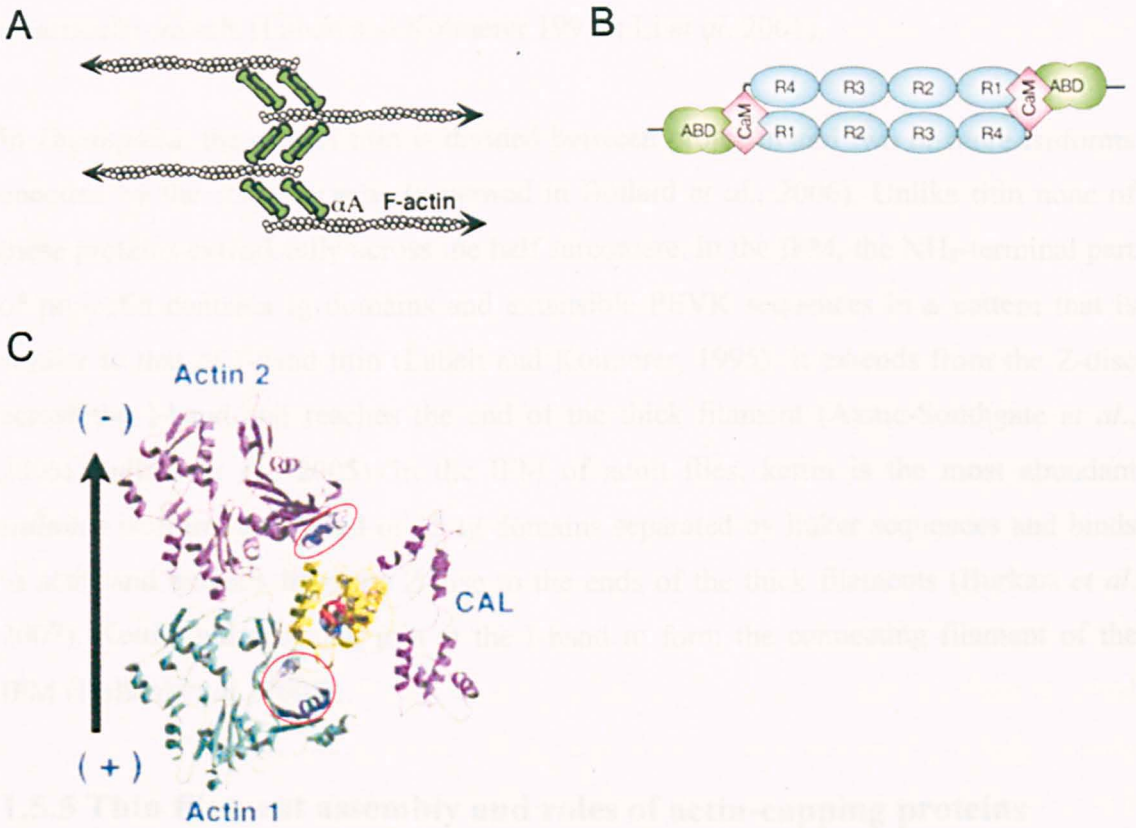

Figure 1.19. Structures of α-actinin and the thin filament. (A) At the Z-discs α-actinin (αA) homodimers (green) form cross-bridges with actin filaments (other proteins that are not shown here are also involved). Image reproduced from Djinovic-Carugo *et al.,* 1999. **(B)** The domain architecture of α-actinin: actin binding domain (ABD) (green), CaM-like domains (pink) and R1–R4 domains (light blue). Image reproduced from Janmey and Lindberg, 2004. **(C)** Two actin monomers along the thin filament shown in cyan (actin 1) and pink (actin 2) and α-actinin. On the α-actinin structure the actin binding domain is shown in yellow and the calponin homology domain (CAL) in magenta. Red circles highlight the α-actinin binding sites on actin. Image reproduced from Tang *et al.*, 2001.

1.5.4 Connecting filaments

During muscle contraction to prevent the sarcomere from overstretching or shortening too much a third filament called the connecting filament, provides an elastic structure that is adaptive to the force applied. In vertebrate muscles passive elasticity of a stretched muscle fibre is achieved by titin, a giant modular protein (MW ~ 3.7 MDa) (reviewed in Granzier and Labeit, 2005). The NH_2-terminal ends of titin, from adjacent sarcomeres, overlap in the Z-disc, and the molecule reaches across half the sarcomere to the M-line thereby forming a third filament system (Figure 1.14 A). The region of titin that spans the I-band is composed of immunoglobulin-like (Ig) repeats and PEVK sequences that can be extended a variable amount, depending on the isoform present in

a particular muscle (Labeit and Kolmerer 1995b; Li *et al.* 2001).

In *Drosophila*, the role of titin is divided between projectin and two or more isoforms encoded by the *sallimus* gene (reviewed in Bullard *et al.*, 2006). Unlike titin none of these proteins extend fully across the half sarcomere. In the IFM, the NH_2-terminal part of projectin contains Ig domains and extensible PEVK sequences in a pattern that is similar to that of I-band titin (Labeit and Kolmerer, 1995). It extends from the Z-disc across the I-band and reaches the end of the thick filament (Ayme-Southgate *et al.*, 2005; Bullard *et al.*, 2005). In the IFM of adult flies, kettin is the most abundant *sallimus* isoform, composed of 35 Ig domains separated by linker sequences and binds to actin and extends from the Z-disc to the ends of the thick filaments (Burkart *et al.* 2007). Kettin and projectin join at the I-band to form the connecting filament of the IFM (Bullard *et al.*, 2005).

1.5.5 Thin filament assembly and roles of actin-capping proteins

1.5.5.1 Actin polymerization *in vitro*

The nucleotide-binding site of G-actin is almost exclusively associated with ATP *in vivo.* Assembly of G-actin to F-actin is accompanied by hydrolysis of ATP to ADP and the release of inorganic phosphate. Hydrolysis of the bound ATP of newly added actin subunits is carried through three sequential steps: first it is converted to ADP.Pi, followed by the release of Pi and a conformation change in the actin filament (Carlier and Pantaloni, 1986; Carlier *et al.*, 1987; Melki *et al.*, 1996; Fujiwara *et al.*, 2007). Dissociated ADP-actin subunits exchange their bound ADP for ATP in solution (Neidl and Engel, 1979), a process that is accelerated by profilin (discussed in section 1.5.5.2).

Polymerization of G-actin monomers into F-actin filaments proceeds in three sequential phases: an initial nucleation phase, followed by an almost linear elongation phase and a steady-state phase (reviewed by Pollard, 1990; Carlier, 1991; Estes, 1992). The nucleation phase is characterized by the formation of a small oligomer called a nucleus. Kinetic analysis and structural considerations suggest that nuclei consist of just three actin molecules. After a significant number of nuclei have been formed, rapid subunit addition ensues. *In vitro* the polymerization progresses into the elongation phase during which the relationship of total polymer versus time is approximately linear. As F-actin filaments grow the concentration of free G-actin decreases until equilibrium between

the monomeric and polymeric actin has been reached. This concentration of free monomers in equilibrium with a population of actin filaments is referred to as the *Critical concentration, Cc.* Above this value, a solution of G-actin will polymerize; below this value a solution of F-actin will depolymerise. Association and dissociation of monomers normally occurs at either end of the filament, but association predominantly occurs at the barbed end and dissociation at the pointed end (Carlier *et al.*, 1987 Pollard, 1986). Under physiological conditions the *Cc* at the barbed end is about 0.1 μM and at the pointed end *Cc* is about 0.7 μM (Rickard and Sheterline, 1986). Solvent conditions influence the *Cc* e.g. in the presence phalloidin, the initial nucleation phase of ATP-G-actin shortens, and the elongation phase is accelerated by a factor of 2 (Dancker *et al.*, 1975).

The slower rate of addition at the pointed end allows for ATP hydrolysis of the terminal monomer (Coué and Korn, 1986). Thus the pointed end has an ADP-bound actin terminal monomer and the barbed end an ATP-bound actin monomer. Since the two ends share the same monomer pool in order to achieve equilibrium there will be a loss of monomers from the pointed ends and gain from the barbed end. Hence, assembled ATP monomers move progressively along the filament from the barbed end (the end associated with Z-discs) of the sarcomere, toward the free pointed end of the filament (located in the middle of the sarcomere) to be released as ADP monomers (Wegner, 1976). The continual flux of actin subunits (< 1 subunit per second) from the pointed to the barbed end of the filament results in unidirectional growth of the actin filament (Oosawa, 1972; Wegner, 1976).

The length of actin filaments is not an inherent property, as in *in vivo* and *in vitro* studies, actin subunits assemble to different polymer lengths (Oosawa, 1970; Pollard and Borisy, 2003). Since the ~1 μm lengths of the mature striated muscle thin filaments are extremely precise, they must be regulated by actin binding proteins (ABPs). Within cells thin filament dynamics are modulated by over 70 classes of ABPs (reviewed in Pollard *et al.*, 2000; Dos Remedios *et al.*, 2001). Some ABPs bind to G-actin and maintain the monomer pool (profilin, cofilin). Others sever filaments thus creating ends for addition of actin subunits (gelsolin). Some associate with the barbed or pointed end and inhibit the assembly/disassembly process (CapZ, tropomodulin). Alternatively some

nucleate new filaments (formin). The role of certain ABPs relevant to this thesis will be discussed.

1.5.5.2 Profilin

Profilins are a family of small cytoplasmic proteins (14-17 kDa) that sequester monomeric actin and function in processes related to F-actin nucleation and polymerization (Witke, 2004). Profilin binds to subdomains 1 and 3 of actin in a 1:1 complex (Mockrin *et al.*, 1980; Schutt *et al.*, 1993). It acts as nucleotide exchange factor for actin with a higher affinity for ATP-bound G-actin than for ADP-bound G-actin (Stossel *et al.*, 1985; Pollard and Cooper, 1984; Goldschmidt-Clermont *et al.*, 1991). When profilin binds to G-actin it forms a less compact structure (Schutt *et al.*, 1993), hence facilitating nucleotide exchange, which generates polymerization-competent ATP-G-actin (Gieselmann *et al.*, 1995; Perelroizen *et al.*, 1995). Profilin binding to actin monomers inhibits nucleation and elongation of pointed ends but not elongation of barbed ends (Korenbaum *et al.*, 1998). Hence, profilin has two functions related to actin. Alone it inhibits actin polymerization by sequestering free G-actin (Tobacman *et al.*, 1982; 1983) and can also promote nucleotide exchange of ADP-bound G-actin to ATP-bound G-actin. Binding of profilin to actin monomers prevents spontaneous nucleation of actin filaments (Pollard and Cooper, 1984) without affecting elongation of existing filaments (Tilney *et al.*, 1983; Pollard and Cooper, 1984).

1.5.5.3 Capping proteins and their function in thin filament assembly

There is increasingly strong evidence that actin thin filaments in muscle cells elongate from their pointed ends (reviewed in Littlefield and Fowler, 2008). Thin filament lengths are controlled by inhibition of actin assembly at pointed ends by tropomodulins (Littlefield and Fowler, 2008). In *Drosophila* thin filaments elongate from their pointed ends and are capped by the *Drosophila* tropomodulin homologue *sanpodo* (Mardahl-Dumensil and Fowler, 2001). At their barbed ends actin thin filaments are capped by CapZ (Fowler, 1996). Inhibition of thin filament capping by CapZ in chicken skeletal myotubes led to impairment in myofibril assembly but had little effect on thin filaments of mature myofibrils (Schafer *et al.*, 1995). This suggested that that barbed end polymerization does not modulate thin filament lengths (Schafer *et al.*, 1995). Instead, the role of CapZ may be to organize actin filaments at the Z-discs during early stages of myofibrillogenesis (Fowler, 1996). The degree of thin filament overlap at the Z-disc is

most likely to have a physiological significance as Z-disc width is related to the speed of muscle shortening. For example, fast and slow twitch fibres have narrow and wide Z-discs respectively (Rowe, 1973; Vigoreaux, 1994). Z-disc width can vary from ~ 160 nm in cardiac muscle (Goldstein *et al.*, 1979) to ~ 30 nm in fish skeletal muscle (Franzini-Armstrong, 1973). The widths of Z-discs from human biopsies in nemaline myopathy cases can however be greater than 1 μm (Morris *et al.*, 1990).

The role of barbed/pointed end capping proteins, severing and sequestering actin proteins is pivotal as thin filament reassembly takes place during development of human skeletal muscle when the cardiac *ACTC1* actin isoform is replaced by the skeletal actin isoform *ACTA1* pre-parturition (Ilkovski et al., 2005). Unregulated thin filament elongation from the barbed and/or pointed end due to the *ACTA1* mutations may be one of the causes of nemaline rod formation. Nemaline bodies are penetrated by thin filaments and their ultrastructure resembles Z-disc lattice pattern (Luther and Squire, 2002). They can often be seen to have structural continuity with the Z-discs hence, they are considered to derive from lateral expansion of the Z-disc (Engel and Gomez, 1967; Yamaguchi *et al.*, 1982; Morris *et al.*, 1990).

1.6 General Aims

More than 170 different mutations within the *ACTA1* gene in humans are associated with nemaline myopathy, intranuclear rod myopathy, actin filament aggregate myopathy, myopathy with core-like areas and congenital fibre type disproportion (reviewed in Laing *et al.,* 2009; Feng and Marston, 2009). Five mutations in the TnT and TnI genes are responsible distal arthrogryposis. Most of the mutations in both *ACTA1* congenital myopathies and arthrogryposis are typically missense mutations causing the change of a single amino acid in the thin filament proteins. This raises the question of the mechanisms by which such minor changes result in contractile dysfunctions.

The general aim of this project was to investigate if *Drosophila* IFM can be used as a model genetic system that recapitulates the different phenotypes associated with *ACTA1* congenital myopathies and arthrogryposes causing mutations. The approach was to create *Act88F* transgenic flies carrying *ACTA1* homologous mutations that each results in a variety of the human histopathologies. Also, UAS-TnI and UAS-TnT transgenic flies were created carrying the different arthrogryposis mutations. If *Drosophila* IFM could successfully reproduce some of the phenotypes observed in human patients the next aim was to understand how the mutations in the thin filament proteins result in sarcomeric disease. The outcome of this work will not only provide insights into the mechanisms of the disease but it should also contribute into the better understanding of muscle thin filament assembly and maintenance.

1.6.1 Objectives

1) To choose mutations that cause a complete range of *ACTA1* myopathies and introduce these mutations into the *Act88F* gene.

2) To express these mutations transgenically to determine whether *Drosophila* IFM can be used as a model system to study nemaline myopathy.

3) To follow the development of the nemaline phenotype in the $Act88F^{R372H}$ mutant by examining changes in the structure and function of the IFM.

4) To isolate ACT88F^{R372H} actin to determine why this mutation causes the nemaline phenotype through biophysical techniques.

5) To make and express *UAS* constructs carrying the *Drosophila* wild type TnI and TnT IFM-specific isoforms, with a muscle-specific GAL4 driver line so as to rescue the IFM *TnT* (*up*^{1}) and *TnI* (*hdp*^{3}) null mutants.

6) To make and express *UAS* constructs of the IFM-specific TnI and TnT isoforms carrying arthrogryposis mutations, so as to determine whether *Drosophila* IFM can be used as a model to study arthrogryposis. A truncated TnT was also expressed to investigate the role of the protein's COOH-terminus.

Chapter 2: Materials and Methods

2.1 Fly experiments

2.1.1 Fly stocks

Genotypes and source of origin of the fly stocks used in this project are summarized in Table 2.1

Table 2.1. Fly stocks used in this work

Line	Genotype	Source
Canton-S	Wild type	Bloomington stock centre
Texas	Wild type	Bloomington stock centre
UH3-GAL4	*w*[*], P{GawB}-UH3	Dr. Upendra Nongthomba
dmef2-GAL4	*y*[1] *w*[*]; P{w(+mC)=GAL4-Mef2.R}3	Dr Frank Schnorrer
UAS-GFP-Act88F$^+$	*w*[*]; P{ w(+mC)=UASp-GFP, Act88F }1-2	Bloomington stock centre (9254), Röper *et al.*, 2005
UAS-GFP-Act88F$^+$	*w*[*]; P{w(+mC)=UASp-GFP, Act88F }15-1	Bloomington stock centre (9253), Röper *et al.*, 2005
2B/Cyo	*y w*; su-hdp^2 (2B)/ *CyO, y*$^+$	Nongthomba *et al.*, 2003
up^{101}	*f up*^{101}	Prof. John Sparrow
hdp^2	*f hdp*^{2}	Prof. John Sparrow
Multiple balancer	*y w; CyO/If; MKRS/ TM6b, Tb, Hu*	Dr. Sean Sweeney
Δ2-3	*y w; CyO/Sp*; Δ2-3, *Dr/ TM6b, Tb, Hu*	Prof. John Sparrow
FM7	*FM7, y w B/* Df(1)C49	Prof. John Sparrow
UAS-dsRNAi[cpb]	*y w;* P{UASp- dsRNAi[cpb]}	Vienna Drosophila RNAi Center (9299)

2.1.2 Fly stock maintenance

Fly stocks were grown in plastic vials containing standard yeast-sugar medium at 25 °C in a controlled temperature room apart from the *dmef2-GAL4* experiments which were first grown at an 18 °C room and larvae were subsequently moved to the 25 °C room.

2.1.3 Fly manipulation and setting up crosses

Flies were anesthetized using di-ethyl ether or CO_2 and manipulated under a dissection microscope. To set up crosses male and virgin female flies for the correct genotype were put in the same vial.

2.1.4 P-element mobilisation

Mobilisation of a P-element containing the *Act88F*^{R372H} transgene was achieved by crossing the *Act88F*^{R372H} mutant line to an active transposase coding line (Δ2-3) (Figure 2.1 A). Flies carrying both the *Act88F*^{R372H} P-element marked with *ry*$^{+}$ (red eyes) and the Δ2-3 active transposase coding line were recovered (Figure 2.1 B). P-element transposition occurs in the germ line of these individuals. These flies were then crossed to another line (*TM3*, *Ser*, *ry*) maintaining the *ry* (brown eyes) background to be able to recognize the ones carrying the *Act88F*^{R372H} P-element, which has a *ry*$^{+}$ marker (Figure 2.1 B). Flies from the offspring were selected for the red eyes (*ry*$^{+}$) and the *Ser* marker. These were crossed to the *Act88F*^{KM88} null line (*ry*^{506}, *e*^{s}) (Figure 2.1 C). Flies from the offspring were selected against the third chromosome where the *Act88F*^{R372H} was originally inserted that still had red eyes (*ry*$^{+}$), the *Ser* marker, KM88 and darker cuticle pigmentation due to *e*^{s} (Figure 2.1 D).

2.1.5 Pupal aging

For the pupal aging experiments pre-pupae, identifiable by their white coloured cuticle and the appearance of spiracles were collected. The pre-pupal stage is regarded as time 0 hours after puparium formation (APF). If pupae at that stage are kept at 25 °C, eclosion takes place between 96 hours and 104 hours APF. When 0 h old pre-pupae were identified, the spot of the vial where they were positioned was circled with a permanent pen and the vial was placed in a 25 °C incubator until the pupae developed to the desired age.

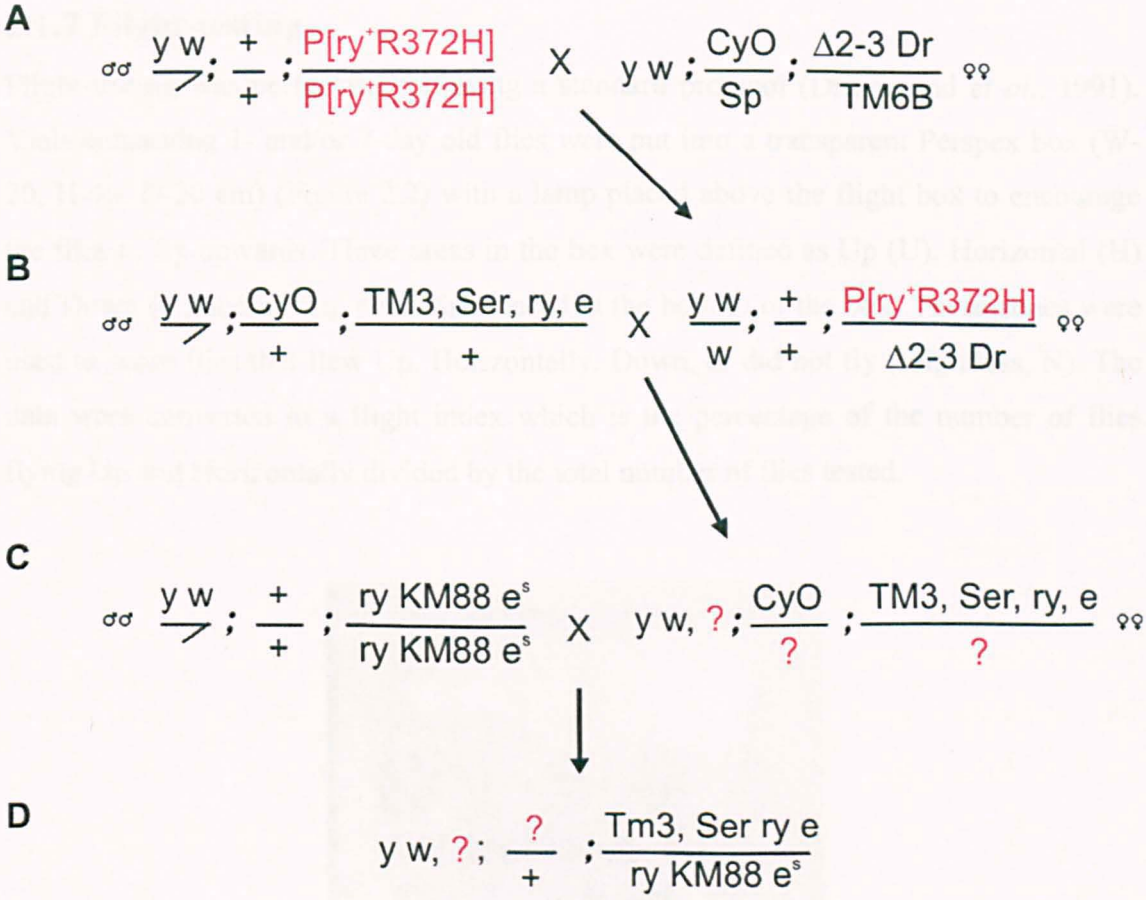

Figure 2.1. Mobilisation of the P-element in the *Act88F*^{R372H} line. '+' indicates wild type alleles, '♂' male and '♀' for female flies.

2.1.6 Petri plate confinement

Small round Petri dishes were filled with standard yeast-sugar medium to within 2 mm of the bottom of the rim, which allowed enough space for the flies to walk but not jump. Flies that had just emerged from their pupal case had their wings clipped with a pair of microsurgical scissors and were aged in these petri-plates at 25 °C to be subsequently used for immunofluorescence.

2.1.7 Flight-testing

Flight-testing was performed following a standard protocol (Drummond *et al.*, 1991). Vials containing 1- and/or 7-day old flies were put into a transparent Perspex box (W-20, H-40, D-20 cm) (Figure 2.2) with a lamp placed above the flight box to encourage the flies to fly upwards. Three areas in the box were defined as Up (U), Horizontal (H) and Down (D) and a 9 cm petri dish placed at the bottom of the box. These zones were used to score flies that flew Up, Horizontally, Down, or did not fly (Flightless, N). The data were converted to a flight index which is the percentage of the number of flies flying Up and Horizontally divided by the total number of flies tested.

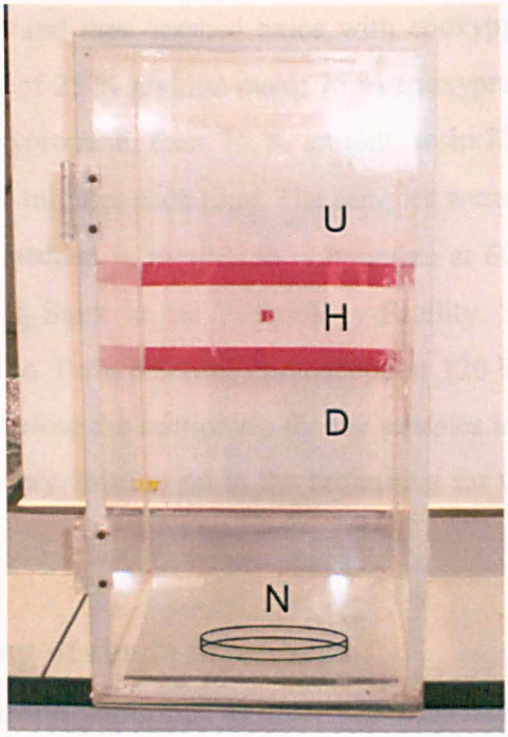

Figure 2.2. Flight-testing box. Up (U), Horizontally (H), Down (D), or didn't fly (Flightless, N) according to the areas defined by the red lines and the petri dish at the bottom of the box.

2.2 Microscopy of the IFM

2.2.1 Transmission Electron Microscopy

Electron microscopy of IFMs was performed as described elsewhere (Kronert *et al.*, 1995). Briefly, fly thoraces were bisected in dissection buffer [100 mM sucrose, 100 mM sodium phosphate buffer pH 7.2, 2 mM EGTA (Ethylene glycol tetraacetic acid)], followed by overnight fixation in primary fixative (4 % paraformaldehyde, 2 % glutaraldehyde, 100 mM sucrose, 100 mM NaPi buffer pH 7.2, 2 mM EGTA) at 4°C. Fixed samples were washed 3 times in 100 mM sodium phosphate buffer pH 7.2, followed by secondary fixation in 1 % 100 mM OsO_4 and then washed again 3 times in 100 mM NaPi buffer pH 7.2. Samples were dehydrated using an alcohol series (25%, 50 %, 75 %, 90 %, 100 %) and then washed twice with epoxypropane. The IFMs were infiltrated with a mixture of 25 % araldite resin: 75 % epoxypropane, followed by 50% araldite resin: 50% epoxypropane, then 75 % araldite resin:25 % epoxypropane, and finally 100 % resin for 30 minutes each time. The samples were placed in resin at 37 °C for 2 hours and then embedded in moulds to polymerize at 60 °C for 48 hours. Thin sections were cut by Meg Stark in the Technology Facility. Sections were examined using a FEI Tecnai 12 Bio Twin electron microscope at 120 kV. The procedure was carried by myself up to before the sectioning for the samples in Chapter 5 and by Meg Stark from after the primary fixation up to the sectioning for the samples presented in Chapters 3 and 4.

2.2.2 Immunostaining of single myofibrils

Immunostaining of IFMs was performed as described elsewhere (Kulke *et al.*, 2001). In brief, fly head and abdomen were removed, thoraces were dissected in York modified glycerol solution [0.1 M NaCl, 20 mM NaPi pH 7.2, 5 mM, 2 mM $MgCl_2$, 2 mM ethylene glycol tetraacetic acid (EGTA), 50 % glycerol, 0.5 % Triton X-100 and complete protease inhibitor cocktail-Roche] (Peckham *et al.*, 1990). Half thoraces were left overnight at -20°C in rigor solution. The next day glycerol was washed out (3x) using rigor buffer without glycerol, and with rigor buffer without glycerol or Triton X-100 (3x). The half thoraces were then placed in relaxing solution [0.1M NaCl, 20 mM NaPi, 6 mM $MgCl_2$, 5 mM ATP (Adenosine-5'-triphosphate), 2 mM EGTA, 90 mM KPr and complete protease inhibitor cocktail-Roche] followed by 15 minutes into blocking solution (relaxing solution containing 1 % BSA). The thoraces were then

incubated with primary antibody (diluted in relaxing solution) for 60 minutes, then washed thrice with relaxing solution and incubated with the secondary antibody (diluted in relaxing solution) for another 60 minutes. TRITC-phalloidin (1:1000) was used in first and second antibody incubations to stain the actin thin filaments and to also prevent them from depolymerising. After the incubation with the secondary antibody thoraces were washed thrice with relaxing solution and the IFMs were removed from the cuticle and teased on a microscope slide in relaxing solution to fray apart the myofibrils. The myofibrils were then fixed in relaxing solution containing 2% paraformaldehyde for 10 minutes and distilled H_2O was used to wash the fixed myofibrils. A drop of Prolong Antifade (Invitrogen Molecular Probes) mountant was then added; a coverslip was placed over the sample and allowed it to set for a few hours. Imaging was carried out using confocal microscopy with a 60x lens objective, in a Zeiss LSM 510 META microscope with LSM imaging software. 3D reconstructions of Z-stacks were created using Volocity LE 3D imaging software. The antibodies used for this procedure and for the procedure in section 2.2.3 during this project are summarized in Table 2.2.

2.2.3 Dissection of adult and pupal thoraces

To dissect the IFM, flies were anaesthetized using ether and placed on a card. The head and abdomen were removed using forceps and the fly thorax was cut in half along the longitudinal axis using a pair of microsurgical scissors (Fine Science Tools) while submerged in an appropriate solution. Using a pair of sharp tungsten needles the IFM were removed from the cuticle and transferred to the appropriate buffer at -20 °C until use (never longer than 5 days). For isolation of IFM for immunostaining thoraces were dissected in 4 % paraformaldehyde and left for 30 minutes.

To isolate the IFM from pupae, a glass slide with double sticky tape was used to hold pupae of the desired age in order to remove the pupal cases. Pupae were then transferred on a Sylgard plate (Dow Corning silicone elastomere kit) lying on their dorsal side where entomology needles were used to pin them through their heads. After submersion in 4 % paraformaldehyde, a small incision was made in the posterior end of the pupa followed by a second incision along the longitudinal axis, which exposed the IFM.

2.2.4 Immunostaining of half thoraces

Both adult half thoraces and IFM from pupae were washed 3 times with relaxing solution and left for 1 hour in rigor solution, followed by 15 minutes into relaxing solution. The samples were incubated with primary antibody (diluted in relaxing solution) overnight on a shaker at 4 °C, then washed thrice with relaxing solution and incubated with the secondary antibody (diluted in relaxing solution) for 5 hours on a shaker at room temperature. TRITC-phalloidin (1:1000) was used in the first and second antibody incubations to prevent thin filaments from depolymerising. When staining for nuclei the DAPI (4,6-diamino-2-phenylindole) stain was used at 1 μg/ml, during the last 15 minutes of the secondary antibody incubation. After the secondary antibody and DAPI incubation, thoraces were washed thrice with relaxing solution and the IFMs were removed from the cuticle and placed on a microscopy slide in a drop of relaxing solution. A drop of Prolong antifade was then added and a coverslip was placed over the sample. Confocal imaging was carried out using a Zeiss LSM 510 META microscope with LSM imaging software. Deconvolution imaging was carried out using an Olympus fluorescence microscope and Softworx software (Deltavision, USA).

Table 2.2. Antibodies used for immunostaining of single myofibrils and half thoraces

Antibodies	Description	Source	Dilution
Anti-α-actinin	Anti-α-actinin monoclonal antibody developed in rat	Prof. Belinda Bullard	1:50
Anti-GFP	Anti-GFP IgG polyclonal antibody (whole molecule) developed in rabbit	abcam ab290	1:100
Anti-Kettin	Monoclonal antibody to KIg16 (Ig number 16 in kettin) developed in rat	Prof. Belinda Bullard	1:100
Anti-Myosin	Anti-Myosin monoclonal antibody developed in rat	Prof. Belinda Bullard	1:50
Anti-Obscurin	Anti-Obscurin polyclonal antibody developed in rabbit	Prof. Belinda Bullard	1:100
Anti-Tropomodulin	Anti-Tropomodulin polyclonal antibody developed in rat	Prof. Velia Fowler	1:50
Anti-Tropomyosin	Anti-Tropomyosin monoclonal antibody developed in rat	Prof. Belinda Bullard	1:50
Anti-Z210 (zetalin)	Anti-Zetalin monoclonal antibody developed in mouse	Dr. Judith Saide	1:50
Anti-rat-FITC	Anti-rat IgG (whole molecule) FITC-conjugate developed in goat	Sigma Aldrich/F- 6258	1:500
Anti-rabbit-FITC	Anti-rabbit IgG (whole molecule) FITC-conjugate developed in goat against purified rabbit IgG	Sigma Aldrich/F-9887	1:500
Anti-rat-Cy5	Anti-Rat Cy5-conjugate AffiniPure $F(ab')_2$ Fragment IgG (H+L) developed in goat (minimum crossreaction to Human, Bovine, Horse Serum Proteins)	Jackson Immunoresearch// 112-176-062	1:500
Anti-mouse-FITC	Anti-mouse IgG (whole molecule) FITC-conjugate developed in goat against purified mouse IgG	Sigma Aldrich/F-0257	1:500

2.2.5 Polarized light microscopy

Polarized light microscopy was performed as described elsewhere (Nongthomba and Ramachndra, 1999). Briefly, etherised flies were placed on their back on a microscope slide in a drop of 50 % ethanol and were submerged into liquid nitrogen. A razor blade was used to bisect the flies along the longitudinal axis. The samples were then dehydrated using an alcohol series (50 %, 70 %, 80 %, 90 %, 100 % one hour each) and were left overnight in methyl salicylate. The head, legs and abdomen from each half fly were removed; thoraces were placed on a microscope slide, mounted in DPX mountant (Sigma-Aldrich) and a cover slip was placed over the sample that was left to set. Samples were examined on a Nikon inverted Eclipse T2000-U microscope fitted with a conventional Nikon 35 mm photographic camera. Photographic film was developed in a regular photo-shop to obtain digital images. A representative image from several pictures obtained for each genotype is shown.

2.2.6 Brightfield and fluorescent microscopy of whole organisms

Brightfield and fluorescent pictures of whole pupae and anesthetized adult flies that were positioned on a microscope slide, were taken using a Zeiss AxioCam MRc5 digital camera fitted to a Zeiss Stereo Lumar V12 microscope.

2.3 Molecular Biology

2.3.1 Media and bacterial strains

E. coli cultures were either grown in autoclaved Luria-Bertani (LB) broth (1 % Bacto-tryptone, 0.5 % Bacto-yeast extract, 10 g/L NaCl) or plated on autoclaved LB-agar. Antibiotic selection was performed by use of ampicillin (amp) (100 μg/ml), and chloramphenicol (chl) (34 μg/ml) where indicated (Melford). The bacterial strains used in this project are listed in Table 2.3.

2.3.2 Preparation of chemically competent *E. coli* cells

Competent cells were prepared from 35 ml *E. coli* cultures that had reached an OD_{600nm} of ~0.3-0.6. Cells were harvested by centrifugation, washed in 20 ml of ice-cold 20 mM Tris-HCl, 50 mM $CaCl_2$, pH 8.0 and left on ice for 1 hour. Cells were harvested again by centrifugation and resuspended in 2 ml of ice-cold 20 mM Tris-HCl, 50 mM $CaCl_2$, 20% w/v glycerol pH 8.0. Aliquots of 100 μl were made and stored at -80 °C.

Table 2.3. Bacterial strains used in this project.

Strain	Uses
DH5α (F⁻ φ80*lac*ZΔM15 Δ(*lac*ZYA-*arg*F)U169 *rec*A1 *end*A1 *hsd*R17(rk⁻, mk⁺) *pho*A *sup*E44 *thi*-1 *gyr*A96 *rel*A1 λ⁻)	Competent cells used for transformation of plasmids generated by ligation or whole plasmid mutagenesis (< 10 kb). Cells were also used for the preparation of plasmid DNA for sequencing and transformation into the pET15b expression strain.
BL21(DE3) pLysS (F^-, *omp*T, *hsd*S_B (r_B^-, m_B^-), *dcm*, *gal*, λ(DE3), pLysS, Cm^r)	Competent cells used for induced protein expression from recombinant plasmids under the regulation of a T7 promoter. Protein expression was controlled by isopropyl-β-D-thiogalactopyranoside (IPTG)
XL10-GOLD ultracompetent cells (Stratagene 200314): Tet^r *Δ(mcrA)183 Δ(mcrCB-hsdSMR-mrr)173 endA1 supE44 thi-1 recA1 gyrA96 relA1 lac* Hte [F' *proAB lacI*^{q}*ZΔM15 Tn10* (Tet^r) Amy Cam^r]^a	Ultracompetent cells used for transformation of >12 kb plasmids made by whole plasmid mutagenesis or ligation.

2.3.3 Transformation of competent *E. coli* cells

Approximately 50 ng plasmid DNA was added to 100 µl DH5α or BL21(DE3)pLysS competent cells and incubated on ice for 30 minutes. The cells were heat shocked at 42 °C for 90 seconds, followed by a 5 minute incubation on ice. Next 400 µl of pre-warmed LB were added and cells were left to incubate at 37 °C for 1 hour. After this step cells were plated onto pre-warmed LB-agar plates (containing the correct antibiotic) and incubated overnight at 37°C. When XL10-GOLD ultracompetent cells were used, 45 µl of cells were incubated on ice for 10 minutes, heat-shocked at 42 °C for 60 seconds, followed by a three minute incubation on ice and treated as described above for DH5α/BL21(DE3)pLysS cells.

2.3.4 Preparation of glycerol stocks

200 µl of overnight culture was added to 800 µl of autoclaved glycerol and the mixture was stored at -80 °C in 2 ml screw cap polypropylene tubes.

2.3.5 Plasmid DNA extraction

Plasmids were isolated using the Qiagen Mini and Maxi prep kits as per manufacturer's instructions.

2.3.6 Restriction digests

1 µg of DNA was digested with 5-10U of the appropriate restriction enzymes purchased from New England Biolabs (NEB). Using the appropriate buffer (and BSA if needed), reactions were performed at a 20 µl scale at 37 °C for 2 hours. Agarose gel electrophoresis (see section 2.3.14) was performed on the digested PCR products and linerarised vectors, which were extracted using the QIAquick Gel Extraction Kit (Qiagen) as per manufacturer's instructions.

2.3.7 Ligation reactions

Ligation reactions of double stranded DNA were performed using the T4 DNA ligase and the 10 x T4 ligase buffer (Promega). An excess of PCR product was mixed with linerarised vector and incubated for 3 hours at room temperature before transformation in competent DH5α cells as described above.

2.3.8 DNA Primers

DNA primers were synthesised by Sigma Genosys (Sigma-Aldrich). A full list of the primers used for whole plasmid mutagenesis is listed in Table 1 of the Appendix. The rest are indicated in the relevant sections of Materials and Methods or relevant Results Chapters.

2.3.9 Cloning of the IFM-specific *TnI* gene coding sequence

2.3.9.1 RNA extraction from *Drosophila* IFM

The IFM of wild-type 96 hour APF old pupae were dissected in 70 % ethanol and RNA was isolated using the QIAgen RNeasy mini kit as per manufacturer's instructions.

2.3.9.2 Synthesis of the first strand cDNA

The RNA was reversed transcribed into cDNA using the Stratagene Stratascript First-Strand synthesis kit. Briefly 15 µl of the RNA was mixed with 1 µl of oligo dT primer (0.5 µg/µl), 0.8 µl of dNTP mix and 2 µl of 10 x AffinityScript RT buffer. The mixture was incubated at 65 °C for 5 minutes and the reaction was subsequently cooled to room temperature for 10 minutes to allow the primers to anneal to the RNA. 2 µl of the 10 x AffinityScript RT buffer , 0.8 µl of dNTP mix , 0.5 µl of RNase Block Ribonuclease Inhibitor (40U/µl) and 1 µl of AffinityScript Multiple Temperature RT were mixed and incubated at 55 °C in a thermal block for an hour before terminating the reaction by incubation at 70 °C for 15 minutes.

2.3.9.3 Amplification of the coding sequence

The primers used to amplify the *TnI* gene from the IFM cDNA created an *Eco*R I restriction site before the 5' end and a *Kpn* I restriction site on the 3' end (see Table 1 of the Appendix). The PCR conditions are shown in Table 2.4.

Table 2.4. The PCR conditions used to isolate the *TnI* gene coding sequence from the cDNA.

Number of Cycles	Temperature	Time
1	98 °C	1 seconds
16	98 °C	30 seconds
	72 °C	1 minute
	72 °C	2 minutes
1	72 °C	5 minutes
	4 °C	∞

2.3.9.4 Subcloning of *TnI* gene coding sequence and site-directed whole plasmid PCR mutagenesis

The *TnI* gene coding sequence was then digested, gel-purified and ligated to the digested TA vector. Site-directed whole plasmid mutagenesis was performed to create four TnI mutant plasmids each carrying a different single point mutation. The primers used to perform the site-directed PCR mutagenesis reactions are shown in Table 1 of the Appendix and the PCR conditions in Table 2.5. The wild type *TnI* gene coding sequence and those carrying the K245@, V256G, ΔK257 and ΔE258 mutations were excised from the TA vector and ligated into the pP[UAST] vector to create the pP[*UAST-TnI*], pP[*UAST-TnI*$^{K245@}$], pP[*UAST-TnI*^{V256G}], pP[*UAST-TnI*$^{\Delta K257}$] and pP[*UAST-TnI*$^{\Delta E258}$] plasmids all of which were used to transform XL10-GOLD ultracompetent cells.

Table 2.5. The site-directed PCR mutagenesis conditions used for creating the *TnI* mutants.

Number of Cycles	Temperature	Time
1	95 °C	1 seconds
16	95 °C	50 seconds
	60 °C	50 seconds
	68 °C	4.5 minutes
1	68 °C	7 minutes
	4 °C	∞

2.3.10 Site-directed whole plasmid PCR mutagenesis of *TnT* gene coding sequence and subcloning

The IFM-specific *TnT* gene coding sequence carried in a TA cloning vector (Bangalore Genei) was a kind gift from Dr Upendra Nongthomba (Indian Institute of Science, Bangalore). Site-directed whole plasmid mutagenesis was then performed to create two *TnT* mutant plasmids each carrying a different single point mutation. The primers used to perform the site-directed PCR mutagenesis reactions are shown in Table 1 of the Appendix and the PCR conditions were the same as for the *TnI* gene coding sequence. The wild-type *TnT* gene coding sequence as well as those carrying the K43H and E314@ mutations were excised from the TA vector and ligated into the pP[UAST] vector to create the pP[*UAST-TnT*], pP[*UAST-TnT*^{K43H}] and pP[*UAST-TnT*$^{E314@}$] plasmids all of which were used to transform XL10-GOLD ultracompetent cells.

2.3.11 Subcloning of the α-actinin actin binding domain (ABD) gene coding sequence of *Gallus gallus*

The *α-actinin ABD* gene coding sequence (1-807 bp) of *Gallus gallus* in the pMW172 expression vector (Way *et al.*, 1992) was a kind gift from Dr Steve Winder (University of Sheffield). Whole plasmid PCR site directed mutagenesis was performed to create the α-actinin ABD S103C mutant (reaction conditions Table 2.6 and mutagenesis primers listed in Table 1 of the Appendix). Stratagene XL10-GOLD ultracompetent cells were transformed with the mutagenized plasmid.

Table 2.6. Whole plasmid PCR site directed mutagenesis conditions for creating the α-actinin ABD S103C mutant.

Number of Cycles	Temperature	Time
1	95 °C	1 minute
16	95 °C	50 seconds
	60 °C	50 seconds
	68 °C	7 minutes
1	72 °C	7 minutes
	4 °C	∞

PCR was performed to introduce the *Nde* I and *Xho* I restriction sites, at the N and C terminus respectively, of the α-actinin ABD gene coding sequence in the S103C mutant as well as for the wild type. In addition a Factor Xa cleavage site was introduced at the 5' - end of the gene, which leaves a blunt end after cleavage (primers are listed in Table 1 of the Appendix). The wild type and mutant α-actinin ABD gene coding sequences were subsequently digested and cloned to a pre-digested pET15b His tag vector (Novagen, cat nbr. 69661-3). The PCR conditions for isolation of the gene coding sequence are shown in Table 2.7.

Table 2.7. The PCR conditions for isolation of the α-actinin ABD gene coding sequence from the pMW172 vector.

Number of Cycles	Temperature	Time
1	95 °C	2 minute
30	95 °C	30 seconds
	60 °C	30 seconds
	72 °C	1 minutes
1	72 °C	10 minutes
	4 °C	∞

2.3.12 Construction of *pW8Act88F* plasmid and site-directed whole plasmid PCR mutagenesis

The p*P{W8, w*$^{+mW.hs}$ *Act88F*$^{+}$*}* plasmid was a gift from Vikash Kumar, who constructed this plasmid by subcloning a 4.0 kb SalI fragment of the *Act88F* gene taken from the pUC9*Act88F* plasmid (Drummond *et al.*, 1990) into the p*P{W8, w*$^{+mW.hs}$*}* plasmid, a *Drosophila* P-element vector for germline trangenesis (Klemenz *et al.*, 1987), between two *Xho* I restriction sites. Whole plasmid site directed mutagenesis was performed on this plasmid to create all the *Act88F* mutants during this project. The PCR conditions are shown in Table 2.8 and the primers in Table 1 of the Appendix. The mutagenized plasmids were used to transform XL10-GOLD ultracompetent cells and were subsequently sequenced.

Table 2.8. The PCR site directed mutagenesis conditions for creating all the *Act88F* mutants.

Number of Cycles	Temperature	Time
1	95 °C	1 seconds
16	95 °C	50 seconds
	55 °C	50 seconds
	68 °C	17 minutes
1	68 °C	7 minutes
	4 °C	∞

2.3.13 Site directed mutagenesis of whole plasmids

Whole plasmid mutagenesis was performed to create point mutations and deletions of single residues. The QuikChange® Site-Directed Mutagenesis kit (Stratagene) protocol was used. The protocol required the use of complementary mutagenic primers which had a melting temperature (T_m) greater than 78 °C. In certain cases this was not possible and therefore all primers were designed to have a T_m greater than 70 °C. The T_m was calculated using the following formula;

$$T_m = 81.5 + (0.41 \times (\%)GC) - (675/N) - (\%)MM$$

where (%) GC is the percent of G and C bases content in the primer, N is the number of bases in the primer and (%) MM is the mismatch percentage of the primer with complementary region of the template. Whole plasmid mutagenesis was performed

using a total reaction volume of 50 µl. The PCR reaction mixture is listed in Table 2.9. A negative control was performed where no *PfuUltra* II Phusion was added. Following the PCR reaction, treatment with *DpnI* enzyme was performed in order to digest the methylated parental DNA strands at 37 °C for 1 hour. The *DpnI* enzyme was deactivated at 80 °C for 20 minutes.

Table 2.9. A typical whole plasmid mutagenesis PCR reaction mixture.

Component	Volume
Autoclaved Milli-Q water	37 µl
10× *PfuUltra* II Phusion Polymerase Reaction Buffer	5 µl
QuickSolution	3 µl
dNTPs (10 mM stock)	1 µl
Plasmid template dsDNA (50 ng/µl)	1 µl
Forward primer (125 ng/µl)	1 µl
Reverse primer (125 ng/µl)	1 µl
PfuUltra II Phusion Polymerase (2.5 U/µl)	1 µl

2.3.14 DNA agarose gel electrophoresis

1 % w/v agarose gels were prepared using 89 mM Tris-Borate pH 8.3 with 2 mM EDTA (TBE). 5 µl of SYBR® Safe 10000× concentrate (Invitrogen) was added per 50 ml of gel. Agarose gels were run in 1 x TBE at a constant voltage of 120 V using the Mini-Sub Cell GT system (BioRad) and imaged using Gene Genius bioimaging gel documentation system (Syngene).

2.3.15 DNA quantification

DNA concentration was measured at 260 nm using an ND-1000 spectrophotometer (NanoDrop).

2.3.16 Sequencing

DNA sequencing reactions were out-sourced (Cogenics) and performed on an ABI 3730xl Platform (Applied Biosciences). The universal primers T7F and T7R were used for sequencing pET based plasmids and self-designed primers for sequencing plasmids containing the *Act88F*, *α-actinin ABD*, *TnI*, and *TnT* genes.

2.4 Biochemical techniques

2.4.1 1D SDS gels

To examine the protein contents of intact IFM, dissections were carried out in PBS (phosphate buffered saline), which was subsequently removed by a 1 minute 13000 rpm spin on a microcentrifuge. Then 1x sample buffer [312.5 mM Tris-HCl pH 6.8, 10 % SDS (Sodium dodecyl sulfate), 0.5% bromophenol blue, 50% glycerol] was added to the pellet and samples were boiled for 3 minutes at 90 °C. When examining the protein contents of skinned myofibrils the IFM were dissected in rigor solution (section 2.2.2) and were kept at -20 °C overnight. The following day glycerol was washed out three times using rigor buffer without glycerol, and three times with rigor buffer without glycerol and Triton X-100. Subsequently the muscles were homogenized in 1x sample buffer and boiled for 3 minutes at 90 °C. All samples were stored at -20 °C until ready to load on the gels. Proteins were separated in 10 % SDS gels (37.5 acrylamide: 1 bisacrylamide ratio) using the Mini-protean 3 electrophoresis system (BioRad) unless stated otherwise. The protein samples were run at a constant voltage (200 V) in Tris-glycine running buffer containing 25 mM Tris base, 0.1% SDS and 200 mM glycine until the dye front had reached the bottom of the gel. Gels were stained with Coomassie blue (10 % acetic acid, 0.1 % Coomassie brilliant blue-R, 40% methanol) for 20 minutes. A 10 % acetic acid solution was used to destain the gels which were imaged using the Gene Genius bioimaging gel system (Syngene).

2.4.2 Actin purification from *Drosophila* IFM

The actin purification method has been described in Razzaq *et al.*, 1999. Briefly, the IFM from 120 flies were dissected in rigor buffer and centrifuged. The IFM pellet was then homogenized on ice using a sealed glass pipette in high salt buffer [1 M KCl, 10 mM NaPi, 20 mM KPi pH 7.0, 4 mM dithiothreitol (DTT), 1 mM EGTA, 4 mM $MgCl_2$, 1/500 v/v phenylmethylsulphonyl fluoride (PMSF)]. The pellet was washed twice with 500 µl of ddH_2O, followed by one wash with 50% acetone and one wash with 100 % acetone. The pellet was air-dried for 1 hour before actin was extracted from the muscles with three consecutive incubations of 45 µl low salt actin extraction buffer (2 mM Tris pH 8.0, 0.2 mM $CaCl_2$, 0.2 mM ATP, 1 mM DTT) 1 hour long each and this was repeated 3 times. The samples were spun after each extraction and the supernatants were combined and transferred to a Beckman 7x20 polycarbonate centrifuge tube and 1/10th

volume of 10x polymerization buffer (50 mM Tris pH 8.0, 500 mM KCl, 20 mM $MgCl_2$, 10 mM ATP) was added to the supernatant and actin was allowed to polymerize for 2 hours at room temperature. When actin was going to be subsequently used in fluorescent anisotropy measurements 30 pmol phalloidin was also added at this step. Then KCl was added to a final concentration of 850 mM and was left to incubate for 5 minutes. The actin filaments were then spun at 100.000 rpm for 15 min, at 4 °C in a TL-100 centrifuge using the TLA-100 rotor. The supernatant was removed and the pellet was gently dissolved using previously filtered F-buffer. Protein concentration was measured using a Nanodrop.

2.4.3 α-Actinin overexpression and purification

pET15B α-actinin ABD plasmids were transformed into BL21(DE3) pLysS cells for expression. Single colonies were picked for overnight 60 ml starter cultures. A 1:1000 dilution of a 60 ml overnight culture was used to inoculate 6 x 0.8 L media, and cultures were grown on an Innova 2300 platform shaker (New Brunswick Scientific) at 37 °C. When an OD_{600} of 0.5-0.6 was reached protein expression was induced with a final concentration of 1 mM IPTG (isopropyl-beta-D-thiogalactopyranoside) (Melford). Cells were grown for 4 hours on the orbital shaker at 37 °C before harvesting in a Sorval centrifuge (SLC-6000 rotor for 12 minutes, 4000 rpm, 4 °C). The pellets were combined and resuspended in approximately 35 ml binding buffer (20 mM Tris pH 7.5, 500 mM NaCl, 5 mM imidazole) containing 5 mM $MgCl_2$, 1.4 mg DNAse I, 60 mg lysozyme, 1 mM PMSF and 4 complete protease inhibitor tablets were added. Cells were lysed by sonication on ice twice using a Sonicator 3000 with a $^3/_8$ inch stud probe (Misonix) with 50×3 seconds pulses at 70 W and a 7 second spacing between pulses. Lysed cells were then left for 15 minutes at room temperature and were subsequently centrifuged (SS34 rotor for 30 minutes at 17000 rpm, at 4 °C) to remove the cell debris. The supernatant was filtered prior to purification using a 0.22 μm filter (Millipore).

All solutions, protein samples and ddH_2O were filtered prior to all chromatography steps. The cell extract was loaded onto a 10 ml nickel column previously equilibrated with binding buffer at a flow rate of 2 ml/min. 5 column volumes (c.v.) of nickel sulphate was used to charge the resin (His Bind Resin, Novagen). Excess nickel sulphate was removed by passing 5 c.v. of binding buffer. Protein loading was monitored by UV absorbance at 280 nm on an Äkta Prime purifier (GE Healthcare).

Binding buffer was passed through the column to elute the unbound proteins until the UV signal had returned to A280 nm ~ 0. The α-actinin ABD was eluted from the column using an imidazole gradient over 90 ml (5 mM to 400 mM). The peaks were analyzed by 12% SDS gels and the α-actinin ABD containing fractions were pooled and dialysed overnight against 50 mM Tris pH 7.5, 200 mM NaCl, 5 mM EDTA buffer at 4 °C using a 3500 molecular weight cut-off dialysis tube (Spectrum).

The protein was further purified by size exclusion chromatography using a Hiload 26/60 Superdex 75 pg column (GE Healthcare). The column was equilibrated with 50 mM Tris-HCl, 250 mM NaCl, pH 7.5 prior to injecting 10 ml of protein. The protein was eluted at 3 ml/min flow rate and was monitored by the absorbance at 280 nm. All elution peaks were analysed by a 12 % SDS gel. The α-actinin ABD containing fractions were pooled and dialysed overnight at 4 °C using a 3500 molecular weight cut-off dialysis tube against 20 mM Tris pH 8.0, 100 mM NaCl, 2 mM $CaCl_2$ buffer for cleavage of the His tag.

2.4.4 Factor Xa His tag cleavage

The His tag was cleaved using Factor Xa protease (Sigma Aldrich F9302) according to the manufacturer's instructions for 7 hours at room temperature and the reaction was stopped using 1 mM PMSF. Subsequently the protein was dialyzed overnight in binding buffer and was purified using a 1 ml Nickel column pre-equilibrated with binding buffer. Cleaved α-actinin ABD eluted in the flow through. A sample of the α-actinin ABD containing fraction was analyzed by a 12% SDS gel and the remainder was dialysed overnight against 50 mM Tris pH 7.5, 200 mM NaCl, 5 mM EDTA buffer at 4 °C using a 3500 molecular weight cut-off dialysis tube. Cleaved protein mass was confirmed by a 20 % SDS gel and electrospray ionisation mass spectrometry (section 2.4.12).

2.4.5 Protein estimation

A Biophotometer (Eppendorf) was used to measure protein concentrations by the absorbance at 280 nm. The following formula was used to calculate the theoretical molar absorbance coefficient (ε_{280nm}) for cleaved α-actinin ABD:

$$\varepsilon_{280nm} = (N_{cys} \times \varepsilon_{280nm\ of\ cys}) + (N_{tyr} \times \varepsilon_{280nm\ of\ tyr}) + (N_{trp} \times \varepsilon_{280nm\ of\ trp})$$

where N is the number of amino acids (cys, cysteine; tyr, tyrosine; trp, tryptophan) and ε_{280nm} is the molar absorption coefficient for the amino acids (125 M^{-1} cm^{-1}, 1490 M^{-1} cm^{-1} and 5500 M^{-1} cm^{-1} respectively). Based on the above equation the predicted molar extinction coefficient for α-actinin is 45045 M^{-1} cm^{-1}. The Beer-Lambeth law was used to calculate the protein concentration:

$$c = A / d \cdot \varepsilon$$

Where c is the protein concentration (mol L^{-1}), A the A280 absorbance, d the length of wavelength path (cm) and ε the molar extinction coefficient (M^{-1} cm^{-1}).

2.4.6 Protein labelling

Cleaved α-actinin ABD was dialyzed overnight at 4 °C against 2 M sucrose, 50 mM MOPS pH 7.0, 200 mM NaCl. The dialysed protein was reduced with 3-fold excess DTT for 1 hour at room temperature. A 20-fold excess of 5-carboxyfluorescein (FAM, C1359 Invitrogen) fluorophore was added; the tube was wrapped in foil and was kept at 37 °C for 10 minutes. Excess fluorophore was quenched with 35 mM DTT. A small sample was taken for electrospray ionisation mass spectrometry (see section 2.4.12) and the remnants of the protein was dialyzed overnight in F-buffer (50mM NaCl, 1 mM $MgCl_2$ and 20mM Tris pH 7.0) at 4 °C. Small aliquots of labelled α-actinin ABD were snap-frozen in liquid nitrogen and stored at -80 °C.

2.4.7 Electrospray Ionisation Mass Spectrometry (ESI-MS)

Protein samples were concentrated to 50 μM and ESI-MS analysis was performed on an ABI Qstar tandem mass spectrometer by Berni Strongitharm in the University of York Technology Facility. The observed molecular weight of wild type α-actinin with and without the His tag was shown to be 33616.3 Da and 30866 Da, respectively.

2.4.8 Matrix-Assisted Laser Desorption Ionisation – Time Of Flight mass spectrometry (MALDI-TOF MS)

10 μl of protein sample was loaded and run on a 10 % 1-D SDS gel. The gel was stained with Coomassie blue solution (section 2.4.1) and the appropriate band was excised and

stored in ddH_2O. The samples were analysed by MALDI-TOF MS by the University of York Technology Facility in the Biology Department (Adam Dowle).

2.4.9 Sedimentation assays

The interaction of α-actinin with wild type and mutant actin was estimated by sedimenting α-actinin with F-actin. G-actin extracted from the IFM was mixed with α-actinin in F-buffer (section 2.4.6) to give a constant actin concentration of 3 μM whereas the α-actinin concentration was 7.2 μM in 100 μl reaction volume. After incubating for 1 hour at 25 °C, samples were centrifuged at 40.000 rpm for 40 min, at 4 °C in a TL-100 centrifuge with a TLA-100 rotor. Control samples of α-actinin were centrifuged without actin. After the centrifugation 30 μl of 1x sample buffer were added to the pellet and 200 μl of 2x sample buffer were added to the supernatant. Supernatants and pellets were denatured at 90 °C for 3 minutes and analyzed on a 10 % 1-D SDS gel; all sample volumes were loaded using a Hamilton syringe for high accuracy.

2.4.10 Fluorescence anisotropy

Fluorescence anisotropy measurements were used to study the binding of fluorescently labelled α-actinin ABD to F-actin.

Fluorescence anisotropy parameters:

- Black 96 well plate (FluoroNunc)
- Temperature = 24 °C
- Plate reader with polarisers (BMG Labtech POLARstar OPTIMA):
  Excitation = 490 nm
  Emission = 520 nm
- FAM: Excitation = 492 nm
  Emission = 512-520 nm

Labelled α-actinin ABD (prepared as described in section 2.4.10) was used at a constant concentration of 4 nM and was diluted to this concentration by F-buffer (section 2.4.6). F-actin (prepared as described in section 2.4.3) was titrated at concentrations between 0.025 μM to 4.6 μM in the case of wild type actin and 6.2 μM for the R372H actin. After each aliquot of F-actin was added, the plate was shaken for 10 seconds, given two minutes to equilibrate and the anisotropy was measured 25 times and averaged.

Absorption and emission spectra of the labelled α-actinin ABD were measured pre- and post- titration to confirm no quenching of the fluorophore by F-actin was occurring. Data were fitted with equations derived in Appendix III. Graphs were plotted using SigmaPlot v11.

2.5 Single myofibril mechanical experiments

The single myofibril mechanical experiments were done in collaboration with Dr B. Iorga and Prof G. Pfitzer (University of Köen). Single myofibrils and chemical solutions were prepared by myself. Dr. B. Iorga performed the single myofibril stretching experiments and analyzed the force transients. Video analysis was also carried out by Dr. Iorga because the file format (NAF) was only readable on a computer from their laboratory.

2.5.1 Myofibrillar preparation

Half thoraces from 10 newly emerged flies were dissected and skinned in rigor solution (Section 2.2.2). Half thoraces were left overnight at -20 °C. The next day fly thoraces were washed three times using rigor buffer without glycerol, and three times with rigor buffer without glycerol or Triton X-100. The half thoraces were then washed in degassed relaxing solution [0.1 M NaCl, 20 mM NaPi pH 7.2, 90 mM KPr, 6 mM $MgCl_2$, 2 mM DTT, 5 mM ATP, 5 mM EGTA, 30 mM BDM (2,3-butane- dione 2-monoxime), complete protease inhibitor cocktail-Roche]. The muscles were dissected in the relaxing solution and teased with needles to produce single myofibrils.

2.5.2 Apparatus and experiments

The setup for single myofibril force measurements was previously described (Stehle *et al.*, 2002a, 2002b). Single myofibrils were attached in relaxing solution to a glue-coated length-driving tungsten stiff needle at one end and to the coated tip of an atomic force cantilever (AFC) at the other end (Figure 2.3). Both the length-driving tungsten stiff needle and the AFC were previously coated with a mixture of 50 % flowable silicon (Dow Corning 3140, Dow Corning Corp., Midland, MI) and pyroxylin in 2 % amyl acetate. The chamber was washed with 100 % EtOH so as to create an electrical charge which later helped with sedimentation of the myofibrils to the bottom of the chamber. A 100 μl drop of freshly prepared single myofibrils was placed in the chamber and left for

one and a half hour to allow the myofibrils to sediment. Following this the chamber was filled with 10 ml of filtered degassed relaxing solution. After sedimentation, to remove debris (e.g. myofibril aggregates) the chamber was washed with degassed relaxing solution. Myofibrils between 100-150 μm long were only used for the measurements, which were performed at 15 °C.

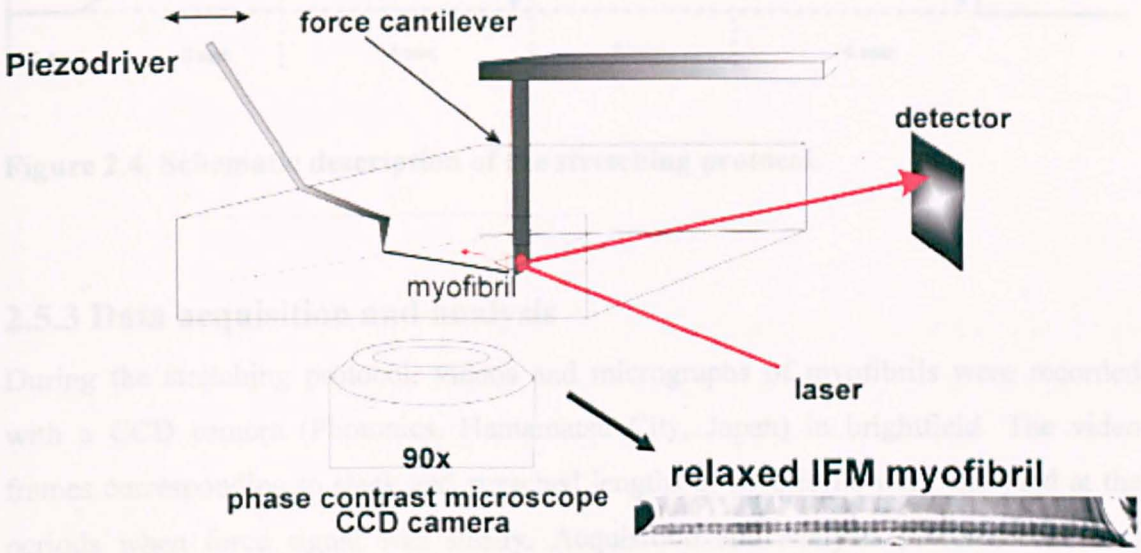

Figure 2.3. Schematic representation of the apparatus used for stretching single myofibrils. Inside the chamber a myofibril is attached on one end to the length-driving tungsten stiff needle attached to a piezodriver and to the AFC at the other end. A laser beam hits on a mirror positioned at the back of the AFC, and becomes redirected to a photo detector to measure movement of the AFC (calibrated to measure force). A phase contrast microscope charge-coupled device (CCD) camera positioned below the chamber is used to record brightfield microphotographs and videos. Diagram reproduced from an image provided by Dr. Stehle.

Passive force responsiveness was recorded in successive stretch protocols applied to fully relaxed single myofibrils. Figure 2.4 highlights the stretching protocol. The mounted myofibrils was stretched over a 3 seconds ramp (1st ramp) so that its length increased by 2 %, subsequently maintained at steady stretch for 4 seconds during which time the force (F1) was measured. Next the myofibril was imposed to a higher stretch over a 3 seconds ramp (2nd ramp) so that its length increased to 4%, maintained at steady stretch for 4 seconds during which the force (F2) was measured. Finally the myofibril was released to zero passive force and was then ready for another round of stretching from 3 % - 6 %, followed by a third stretch of 4 % - 8 % of its slack sarcomere length.

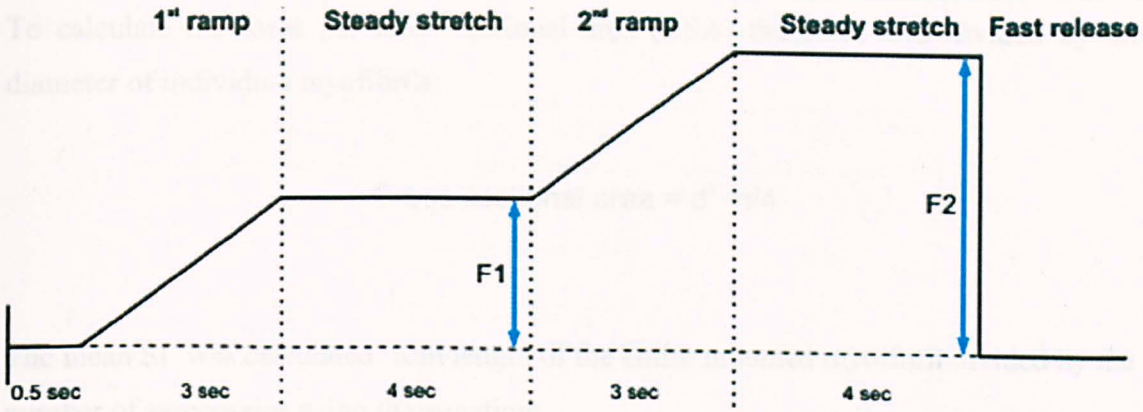

Figure 2.4. Schematic description of the stretching protocol.

2.5.3 Data acquisition and analysis

During the stretching protocol, videos and micrographs of myofibrils were recorded with a CCD camera (Photonics, Hamamatsu City, Japan) in brightfield. The video frames corresponding to slack and stretched lengths of myofibrils were analyzed at the periods when force signal was steady. Acquisition and analysis of force data was performed with custom-written programs in LabView 5.0 (National Instruments, Austin, TX). Video images were quantitatively analyzed by selecting a rectangular region of interest and integrating pixel intensities to an intensity profile in Aqua Cosmos 1.3.0.1 (Photonics, Hamamatsu City, Japan). Mean sarcomere length (SL) values were then determined from the profiles using the LabView built-in files.

2.5.4 Calculations

Explanations and values of the symbols used in the equations are summarized in Table 2.10. Total slack myofibril length l_0 (μm) was measured before and after stretching the myofibrils, to compute the change in myofibril length Δl_0 (μm).

The equation used in order to calculate the voltage to be applied on a myofibril with l_0 length in order to achieve an x % stretch:

$$V = \frac{x}{100} \cdot l_0(\mu m)$$

To calculate the force per cross sectional area (CSA) the force was divided by the diameter of individual myofibrils:

$$\text{Cross sectional area} = d^2 \cdot \pi/4$$

The mean SL was calculated from length of the entire mounted myofibril divided by the number of sarcomeres using the equation:

$$SL = \frac{\text{MF length}(\mu m) \cdot \text{Pixel}}{\text{Number of sarcomeres}}$$

The incorporation of the pixels in the equation was necessary to calibrate the image before taking myofibril length measurements. Length position of the needle coupled with a DAQ-board interfaced piezodriver and the force signal detection and acquisition are described elsewhere (Stehle *et al.*, 2002a, 2002b). Briefly, to calibrate the AFC a direct mechanical contact between the length-driving tungsten stiff needle and the AFC was imposed and a displacement of the AFC tip by $\Delta l_0 = 300$ nm was imposed and the detected ΔV at the photodetector due to this applied mechanical displacement was obtained. This process was repeated thrice and an average ΔV was computed. With the spring constant for cantilever (c) from the AFC data sheet and these values (Δl, ΔV) the calibration factor of the AFC was computed using the equation:

$$\text{Calibration factor} = \frac{c\left(\frac{nN}{\mu m}\right) \cdot \Delta l\,(nm)}{\Delta V calib(V)}$$

Force (F) values in the experiments were calculated by:

$$F = \text{calibration factor} \cdot \Delta V$$

Table 2.10. Explanation and values of symbols that were used in equations.

Symbol	Representation	Value
c	Spring for cantilever	μN/μm
CSA	Cross sectional area	μm^2
d	Myofibril diameter	μm
Δl_0	Difference in myofibril length	μm
ΔV	Average voltage	V
F	Force applied on myofibril	$nN/\mu m^2$
l_0	Total slack myofibril length	μm
MF	Myofibril	
SL	Mean sarcomere length	μm

2.6 Generation of transgenic lines

The DNA constructs created to generate the transgenic flies for this project were microinjected by Dr. Teresa Jagla (MYORES Injection Platform, Clermont Ferrant, France). The wild-type UAS-TnI construct was microinjected at York using the protocols described below.

2.6.1 Nucleic acid preparation

A protocol for P-element mediated transformation described by Rubin and Spradling (1982) was followed. Briefly, 5 μg of the transposase-carrying pπΔ2-3 plasmid were mixed with 20 μg of pP[*UAS-TnI*] plasmid DNA. The two-plasmid mixture was precipitated with 3M NaOAc-EtOH and then redissolved to a final concentration of 1 μg/μl using Spradling injection buffer (5 mM KCl, 0.1 mM NaH_2PO_4 pH 6.8). The plasmid mixture was then spun on a benchtop centrifuge for 10 minutes and loaded into needles pulled from borosilicate capillaries.

2.6.2 Egg preparation

Flies from the w^{118} strain were left in a cage with an apple juice-agar plate (5 % sugar, 2 % agar and apple juice) and fresh yeast paste at 21°C. Eggs laid during 50 minutes were collected with a paintbrush, previously washed with distilled water, and spread on

double-sided sticky tape placed on a glass slide. A second glass slide equipped with non-toxic double-sided sticky tape on which copper wire was stuck lengthwise was used to sandwich the embryos and pulled apart causing the chorions of the eggs to split. The eggs were then lined up with their posterior ends just overhanging a small strip of double sticky tape on a coverslip.

2.6.3 Embryo microinjections

Lined-up embryos were covered in oxygen permeable halocarbon oil (kind gift from Dr. Sweene) to prevent them from drying out and were placed on a glass slide that was pre-positioned on the stage of a light microscope. The DNA fitted to a glass needle was attached to a micromanipulator. The posterior end of the embryos was gently pierced with the needle and pressure was applied to the air-fitted syringe to inject the DNA. Between injection rounds the needle was kept dipped in the halocarbon oil to avoid drying of the DNA solution. Each embryo coverslip was treated within 10 minutes.

2.6.4 Manipulation post-injection

The embryo-containing coverslip was then placed on an agar-apple juice plate, with fresh yeast paste, and kept in a moist container at 25 °C. Hatched larvae were transferred to a standard yeast-sugar vial and eclosed adults were individually crossed to w^{118} flies. The progeny of this cross was screened for successfully transformed w^+ eyed flies and maintained by selection for w^+.

2.6.5 Determining the insertion chromosome

Transformed male flies (red eyed) were individually crossed with *y w; +; TM6B/TM3* female flies. If all female flies in the progeny were w^+ (red eyed) then it meant that the insertion was in the first chromosome and the *FM7c* balancer was used to balance those lines (Figure 2.5.1 A). If male flies in the progeny were a mixture of *w* (white eyed) and w^+ (red eyed) then it meant that the insertion was either in the second or third chromosome. Those flies were first crossed again to *y w; +; TM6B/TM3* and if in the progeny flies identified were w^+ (red eyed) and *TM6B/TM3* it meant that the insertion was in the second chromosome. Those lines were balanced with *CyO*, y^+ (Figure 2.6.1 B). If on the other hand the progeny were all *w* (white eyed) it meant that the insertions were in the third chromosome and those lines were balanced with either the *TM6B* or *TM3* balancers (Figure 2.6 C).

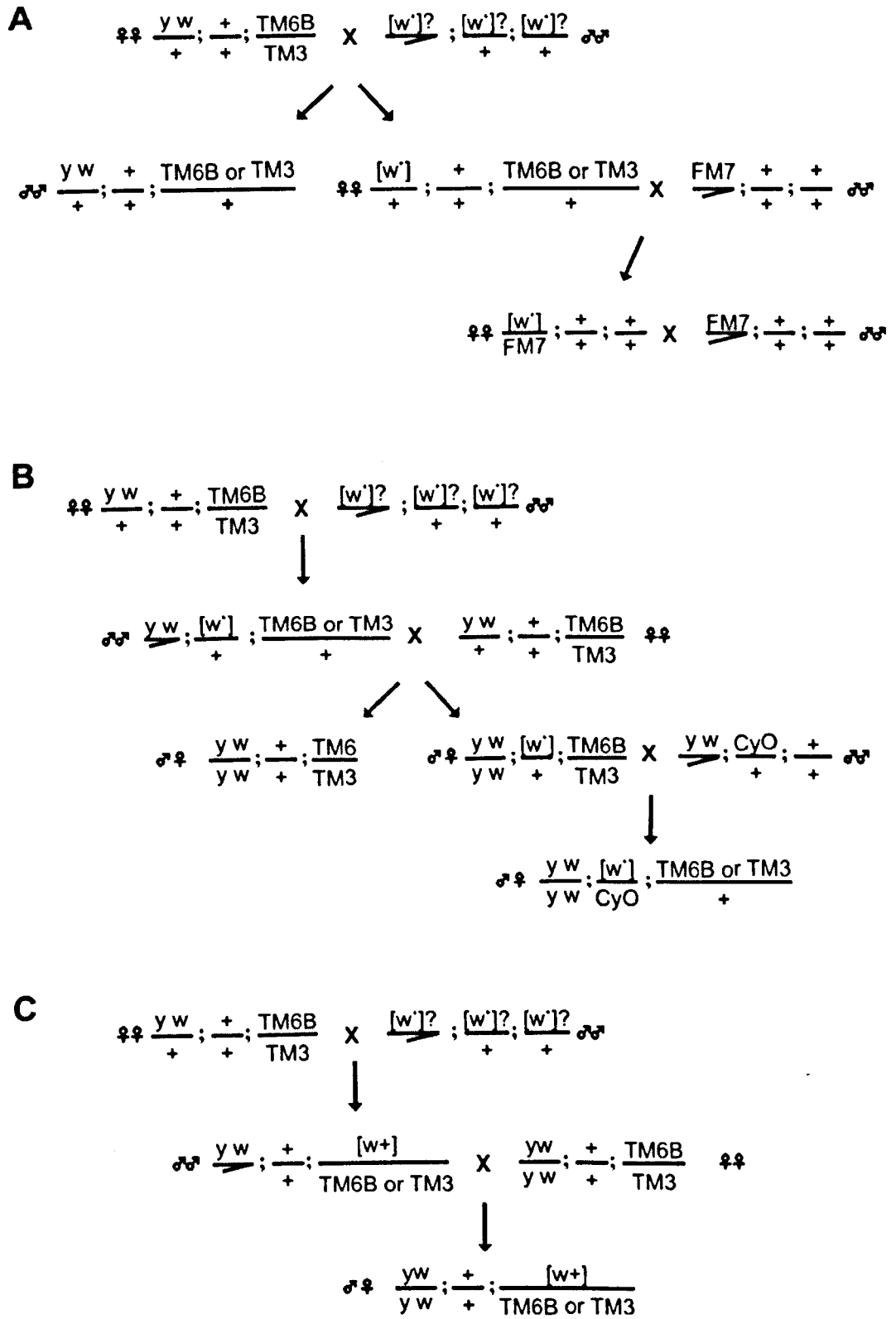

Figure 2.5. Mating scheme to identify the P-element insertion site. Genetic crosses to obtain stable lines for inserts in the first **(A)**, second **(B)** and third **(C)** chromosomes. [w+] for the insert, '+' for wild type alleles, '♂' for male and '♀' for female flies.

2.6.6 Inserting the *Act88F*$^{[mutation]}$ transformants in the correct genetic background

The wild type *Act88F* gene is on the third chromosome hence amongst the different *Act88F*$^{[mutation]}$ lines that were obtained the ones selected for further analysis were in the first or second chromosome. Each *Act88F*$^{[mutation]}$ line was studied as wild-type heterozygote or homozygote by eliminating one or two wild type *Act88F* copies respectively. In order to achieve this the third chromosome wild type *Act88F* gene was exchanged with the amorphic *Act88F*^{KM88} allele. The mating schemes for obtaining stable *Act88F*$^{[mutation]}$ lines are described in Figure 2.6. One red star indicates *Act88F*$^{[mutation]}$/+ heterozygotes and two red stars indicate *Act88F*$^{[mutation]}$/*Act88F*$^{[mutation]}$ homozygotes.

2.6.7 Inserting the *UAS-TnI*$^{[mutation]}$ and *UAS-TnT*$^{[mutation]}$ transformants in the correct genetic background

The TnT (*up*^{1}) and TnI (*hdp*^{3}) null mutations, both *w*, are in the first chromosome. The *UAS-TnI*$^{+}$, *UAS-TnI*$^{[mutation]}$, *UAS-TnT*$^{+}$ and *UAS-TnT*$^{[mutation]}$ insertions (w^{+}) are in the second or third chromosome. The *UAS-TnI* lines (w^{+}) were crossed with the *y w hdp*^{3}/*FM7c* line so as to be studied in a *TnI* null background. Similarly all the *UAS-TnT* lines (w^{+}) were crossed with the *y w up*^{1}/*FM7c* line so as to be studied in a *TnT* null background (Figure 2.7 A). The mating scheme for lines carrying the insert on the second chromosome is shown in Figure 2.8 A. The mating scheme for the lines carrying the insert on the third chromosome was the same as that for the *dmef2-GAL4* driver (Figure 2.8 B). The progeny that was crossed later to the *GAL4* driver is pointed by a single red star.

The *dmef2-GAL4* driver (third chromosomal) was used to express the *UAS-TnI*$^{+}$, *UAS-TnI*$^{[mutation]}$, *UAS-TnT*$^{+}$ and *UAS-TnT*$^{[mutation]}$ constructs; and it had to be inserted in a *TnI* or *TnT* null background (Figure 2.7 B). The progeny that was crossed later to the UAS constructs is pointed by two red stars. Flies from A and B with one and two red stars, respectively were mated (Figure 2.7 B) and the progeny that was used for further analysis is pointed by the three red stars.

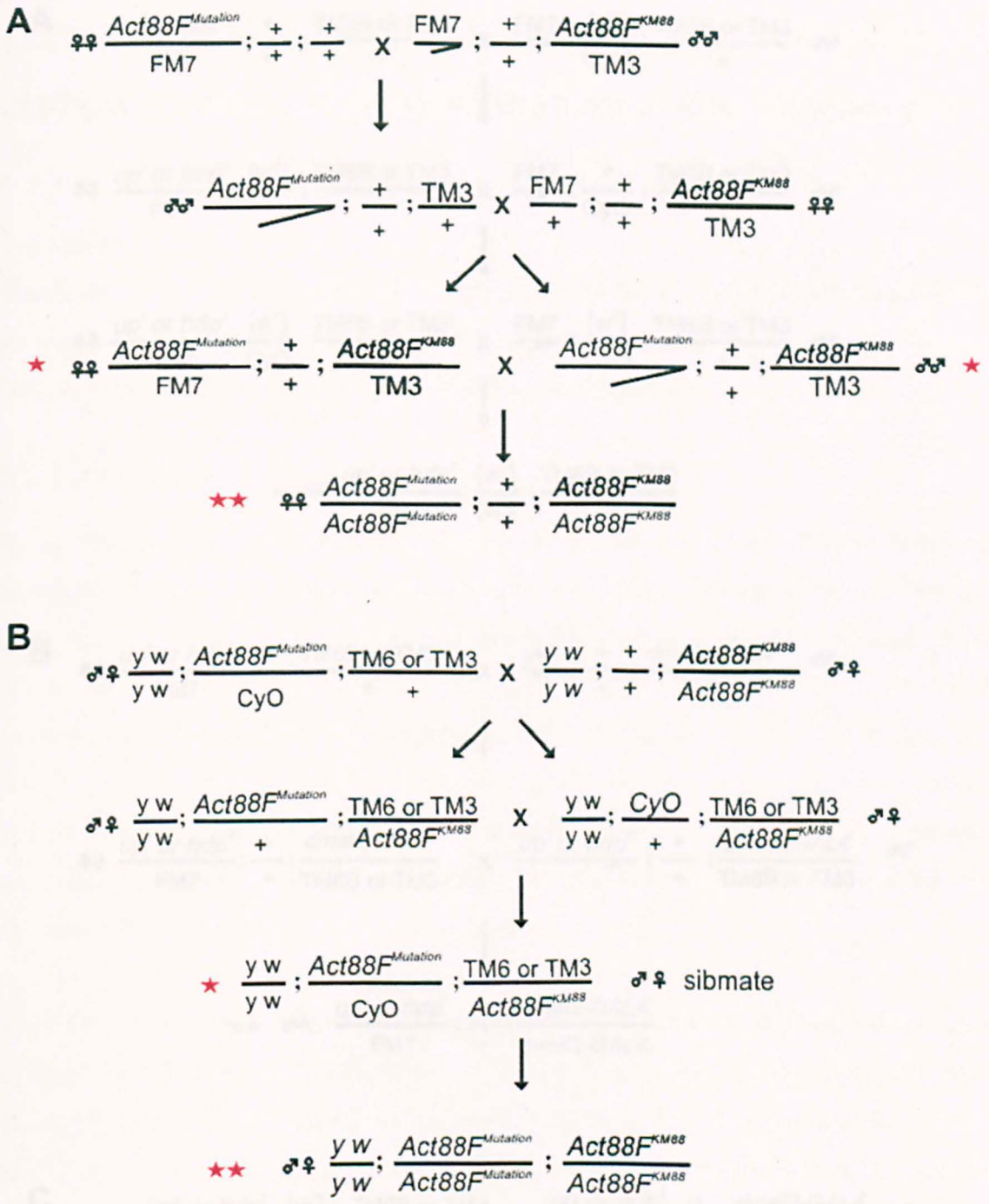

Figure 2.6. Mating scheme for obtaining stable heterozygous and homozygous *Act88F[mutation]* lines. The position of the *Act88F*^{KM88} allele is in the third chromosome. Transformants for the *Act88F[mutation]* insert in the first **(A)** and second **(B)** chromosome were inserted in a wild type heterozygote or in a homozygote background. Wild type heterozygotes for the insert *Act88F[mutation]* or *Act88F[mutation]* homozygotes are designated by one and two red stars respectively. '+' indicates wild type alleles, '♂' male and '♀' female flies.

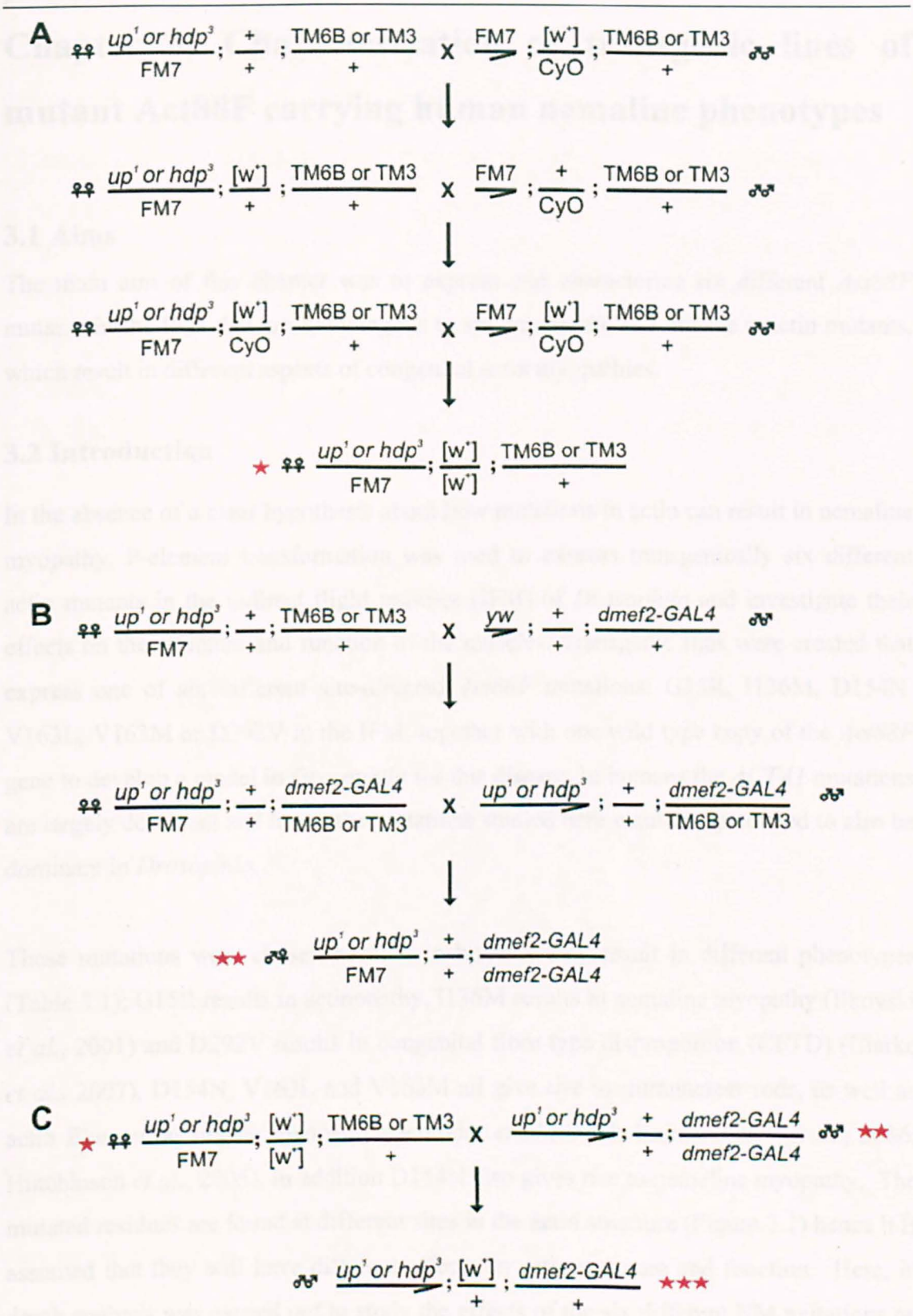

Figure 2.7. Mating scheme for obtaining lines expressing *UAS-TnI or UAS-TnT* and *dmef2-GAL4* in wild type *TnI* and *TnT* null backgrounds, respectively. Genetic crosses to obtain *UAS-TnI* (w^+), *UAS-TnT* (w^+) lines (single star) **(A)** and *dmef2-GAL4* (two stars) lines **(B)** in up^1 or hdp^3 backgrounds. **(C)** Progeny from A (single star) and B (two stars) were mated to obtain progeny with a single insertion for a UAS construct and the GAL4 driver (three stars). [w+] indicates the insert, '+' wild type alleles, '♂' male and '♀' female flies.

Chapter 3: Characterization of transgenic lines of mutant Act88F carrying human nemaline phenotypes

3.1 Aims

The main aim of this chapter was to express and characterize six different *Act88F* mutants in the IFM that are homologous to six human skeletal muscle α-actin mutants, which result in different aspects of congenital actin myopathies.

3.2 Introduction

In the absence of a clear hypothesis about how mutations in actin can result in nemaline myopathy, P-element transformation was used to express transgenically six different actin mutants in the indirect flight muscles (IFM) of *Drosophila* and investigate their effects on the structure and function of the muscles. Transgenic flies were created that express one of six different site-directed *Act88F* mutations: G15R, I136M, D154N, V163L, V163M or D292V in the IFM, together with one wild type copy of the *Act88F* gene to develop a model in *Drosophila* for this disease. In humans the *ACTA1* mutations are largely dominant and hence the mutations studied here would be predicted to also be dominant in *Drosophila.*

These mutations were chosen because in humans they result in different phenotypes (Table 3.1); G15R results in actinopathy, I136M results in nemaline myopathy (Ilkovski *et al.*, 2001) and D292V results in congenital fibre type disproportion (CFTD) (Clarke *et al.*, 2007). D154N, V163L and V163M all give rise to intranuclear rods, as well as actin filament aggregate myopathy (Schroder *et al.*, 2004; Kaimaktchiev *et al.*, 2006; Hutchinson *et al.*, 2005). In addition D154N also gives rise to nemaline myopathy. The mutated residues are found at different sites in the actin structure (Figure 3.1) hence it is assumed that they will have different effects on actin structure and function. Here, in depth analysis was carried out to study the effects of the six different NM mutations on muscle structure and function by flight testing, electron microscopy, immunostaining and protein analysis of the isolated muscles. Moreover, apart from studying the mutations in a heterozygous state, *Drosophila* genetics enables one to easily study them in a homozygous state in wild type *Act88F* null background so as to understand how muscle structure is affected when composed solely of mutant actin.

Table 3.1 List of the nemaline myopathy actin mutants. Actin filament aggregate myopathy (AM), congenital fibre type disproportion (CFTD), intranuclear rods (IR), nemaline myopathy (NM) and sarcoplasmic rods (SR).

Mutation	Phenotype	NM classification	References
G15R	AM, NM	Nemaline	Goebel *et al.*, 1997a
I136M	mild NM	Typical nemaline	Ilkovski *et al.*, 2001
D154N	AM, IR, NM	Severe nemaline	Schroder *et al.*, 2004
V163L	AM, IR, sparse SR	Severe nemaline	Weeks *et al.*, 2003; Kaimaktchiev *et al.*, 2006
V163M	AM, IR, sparse SR	Typical nemaline	Hutchinson *et al.*, 2005
D292V	CFTD	Severe nemaline	Clarke *et al.*, 2007

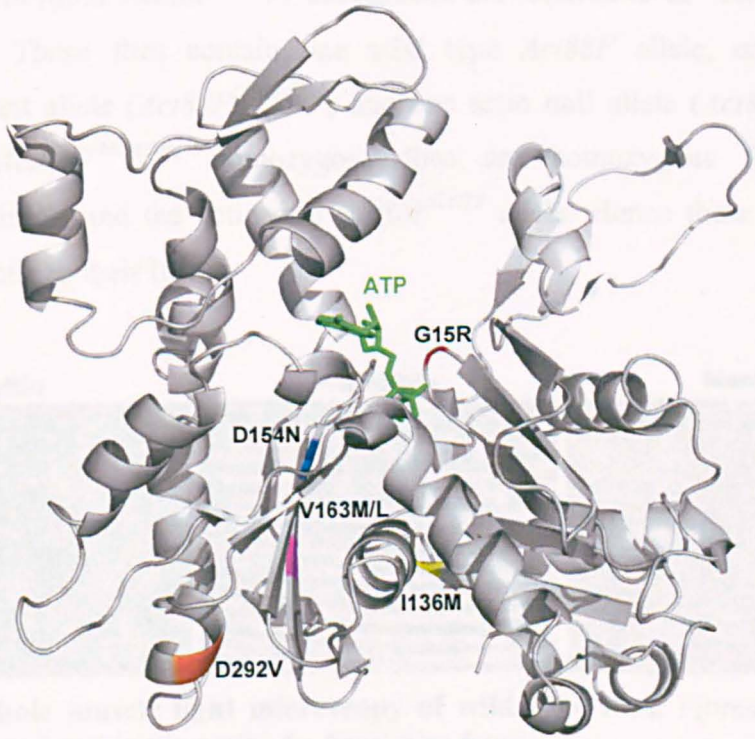

Figure 3.1. Cartoon of the ATP-bound G-actin highlighting the position of the six *Act88F* mutations. The ATP is shown in green sticks, the mutations G15R, I136M, D154N, V163L/M and D292V are shown in red, yellow, blue, magenta and orange, respectively. The image was created using PYMOL and PDB file 1ATN (the same pdb structure is used for all the G-actin images in Chapters 3,4 and 5).

The IFM are an excellent model to study the effect of mutations on sarcomere structure. The wild type flies have very regular Z-discs and fixed sarcomere length of about 3.2 μm (Reedy and Beall, 1993) (Figures 3.2; 3.3) allowing to easily identify structural defects caused by mutations in sarcomeric proteins. Each *Act88F* mutation was

introduced in a heterozygous or homozygous actin null background using the *Act88F*^{KM88} actin null line (Hiromi and Hotta, 1985). Wild type heterozygous flies for the *Act88F*^{KM88} actin null produce > 85 % actin compared to wild type flies (Prof. John Sparrow unpublished results). The *Act88F*^{KM88}/+ mutants are flightless and display myofibril fraying. The thin filaments appear detached or torn from the Z-discs (Figure 3.3 top black arrowhead) and in some cases gaps in the filament lattice can be seen (Figure 3.3 bottom black arrow head). The Z-discs appear bent at their ends and the M-lines are not always apparent across the entire width of the sarcomere. Since there are no significant sarcomeric defects, the *Act88F*^{KM88}/+ heterozygous flies provide a suitable genetic background to study *Act88F* mutants and their dominant effects on muscle structure and function. In Chapters 3, 4 and 5, lines containing one transgenic insert in a heterozygous *Act88F*^{KM88}/+ background are referred to as '*Act88F*$^{[Mutation]}$/+ heterozygotes'. These flies contain one wild type *Act88F* allele, one functional transgenic mutant allele (*Act88F*$^{[Mutation]}$) and one actin null allele (*Act88F*^{KM88}). The *Act88F*$^{[Mutation]}$/*Act88F*$^{[Mutation]}$ homozygous flies are homozygous for both the *Act88F*$^{[Mutation]}$ insert and the actin null *Act88F*^{KM88} allele. Hence these flies express solely mutant actin in their IFM.

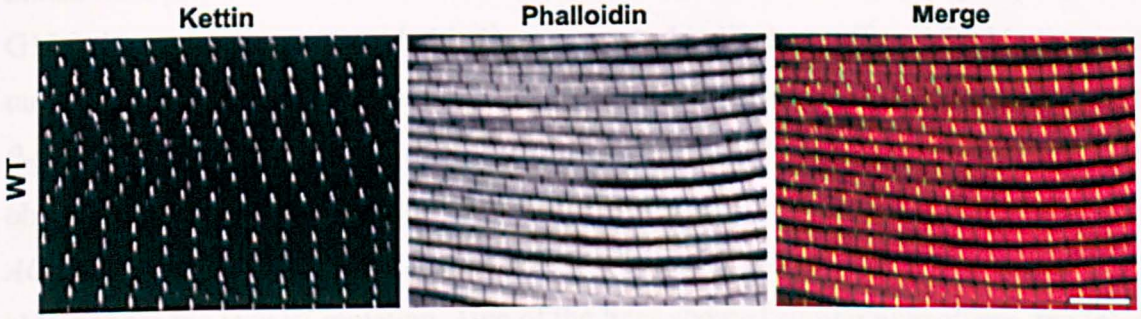

Figure 3.2. Whole muscle light microscopy of wild type flies. Fibres were stained with phalloidin and anti-kettin antibody. Scale bar: 5 μm.

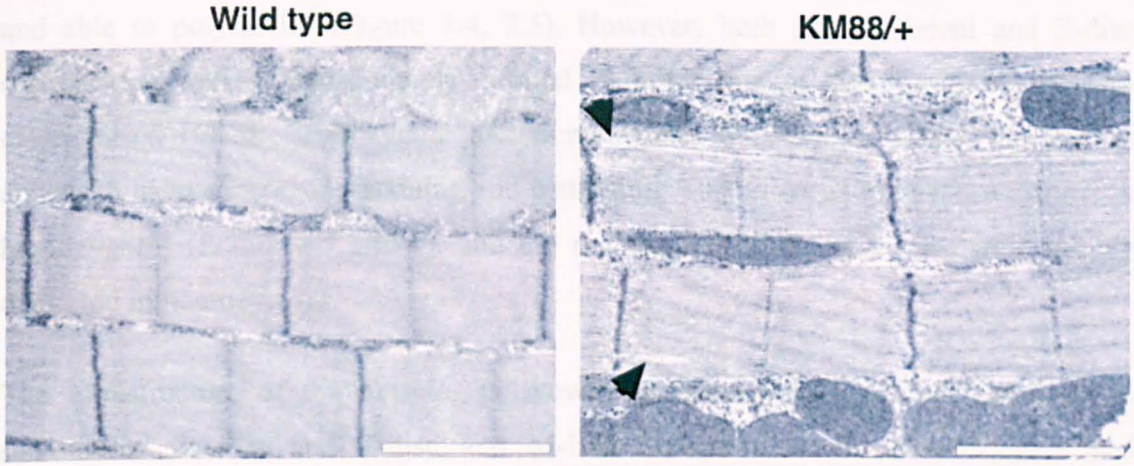

Figure 3.3. TEM of wild type and Act88F^{KM88}/+ heterozygous flies. Arrowheads highlight areas with significant sarcomere damage as demonstrated by gaps in the filament lattice. Scale bars: 2 μm.

3.3 CFTD and nemaline rod producing mutants - G15R, I136M, D292V

The mild I136M *ACTA1* mutation causes typical nemaline myopathy with nemaline bodies (Ilovski *et al.*, 2001). It was chosen to see if it also results in a milder phenotype in *Drosophila* IFM than the other mutants. A single line was obtained for the I136M mutation. The G15R *ACTA1* mutation causes congenital nemaline myopathy; residue G15 is located in the nucleotide-binding pocket and is likely to affect ATP-binding and turnover (Sparrow *et al.*, 2003) as it takes part in a β-hairpin and directly contacts the β-phosphate of the adenine nucleotide (Kabsch *et al.*, 1990). A total of three lines were obtained for the G15R mutation all of which showed the same phenotype. The third *ACTA1* mutation D292V results in CFTD (Laing *et al.*, 2004). Three lines were obtained for the D292V mutation. Two of the lines showed similar phenotypes, the third line was not analyzed. Whole muscle staining was performed to obtain an overview of the structural integrity for the whole muscle fibre. The muscles were studied at the ultrastructural level by electron microscopy. However not all the characteristics and abnormalities observed for each mutant could be captured in a single EM image. Hence some of them are being described in the text but not shown.

Immunostaining of the indirect flight muscle for the Z-line protein kettin and staining for actin using fluorescent phalloidin showed a range of muscle fibre disruption for the different mutations (Figure 3.4, 3.5). In all cases, there was positive phalloidin staining for actin filaments even in homozygote mutants, suggesting that the actin is produced

and able to polymerise (Figure 3.4, 3.5). However, both actin filament and Z-disc organisation varied from almost normal (I136M mutant heterozygote) to very disorganised (G15R heterozygote and homozygote mutants). In G15R the Z-lines appear to have an irregular staining and patterning. This effect is even more distinct in homozygotes (Figure 3.5 arrow), and the regular actin staining is also more highly disrupted in homozygotes.

The ultrastructure of the muscle, as shown by electron microscopy, demonstrates sarcomeric disorder and Z-disc and M-line disruption in the heterozygous and homozygous G15R mutants (Figure 3.6). Pieces of Z-discs stacked parallel to each other otherwise known as zebra bodies (Yamaguchi *et al.*, 1982; Morris *et al.*, 1990; Luther and Squire, 2002) were also found in both heterozygotes and homozygotes G15R mutants (Figure 3.6 arrowhead). The zebra bodies caused by the G15R mutation were very frequent, long (laterally) and spanning the whole of the myofibre. There is myofibrillar branching, and areas of broken/disorganised thick and thin filaments (not captured in Figure 3.6).

In the mildest mutation, I136M, the myofibrils appeared almost normal in heterozygotes but in homozygotes the myofibrils had a wavy appearance and others were found to be disordered. In agreement with the immunostaining for the heterozygote I136M, by EM the myofibrils looked relatively normal, but some actin filaments are not well organised into muscle sarcomeres and appear to lie outside the myofibril and/or join up with adjacent myofibrils (Figure 3.6 arrow). This is reminiscent of actin filament aggregate myopathy in humans where actin filaments are found that are not organised into myofibrils at all next to areas of normal sarcomeres. Small and infrequent zebra bodies (Figure 3.6 arrowheads) as well as Z-disc and M-line disruption can also be seen in both heterozygote and homozygote I136M mutants. In the homozygous state the I136M mutation displays the same characteristics at the ultrastructural level but the muscle appears more disrupted and the myofibrils are not as tightly packed.

In D292V whole muscle staining, disrupted myofibrils were present but many myofibrils look relatively normal in both heterozygote and homozygote mutants (Figure 3.4, 3.5). By EM Z-disc and M-line abnormalities can be seen as well as zebra bodies (Figure 3.6 arrowhead). Aberrant structure of myofibrils and areas of broken/disorganised thick and thin filaments can also be observed. The myofibrils of the

Act88F^{D292V}/+ heterozygotes seem to vary in size with some being half the size of others. The decrease in size can also be seen when comparing the myofibril shown for the *Act88F*^{D292V}/+ heterozygote in Figure 3.6 to that of the wild type in Figure 3.3. This is least pronounced in the D292V homozygotes, which display Z-disc or M-line shifting (only shown for the M-line).

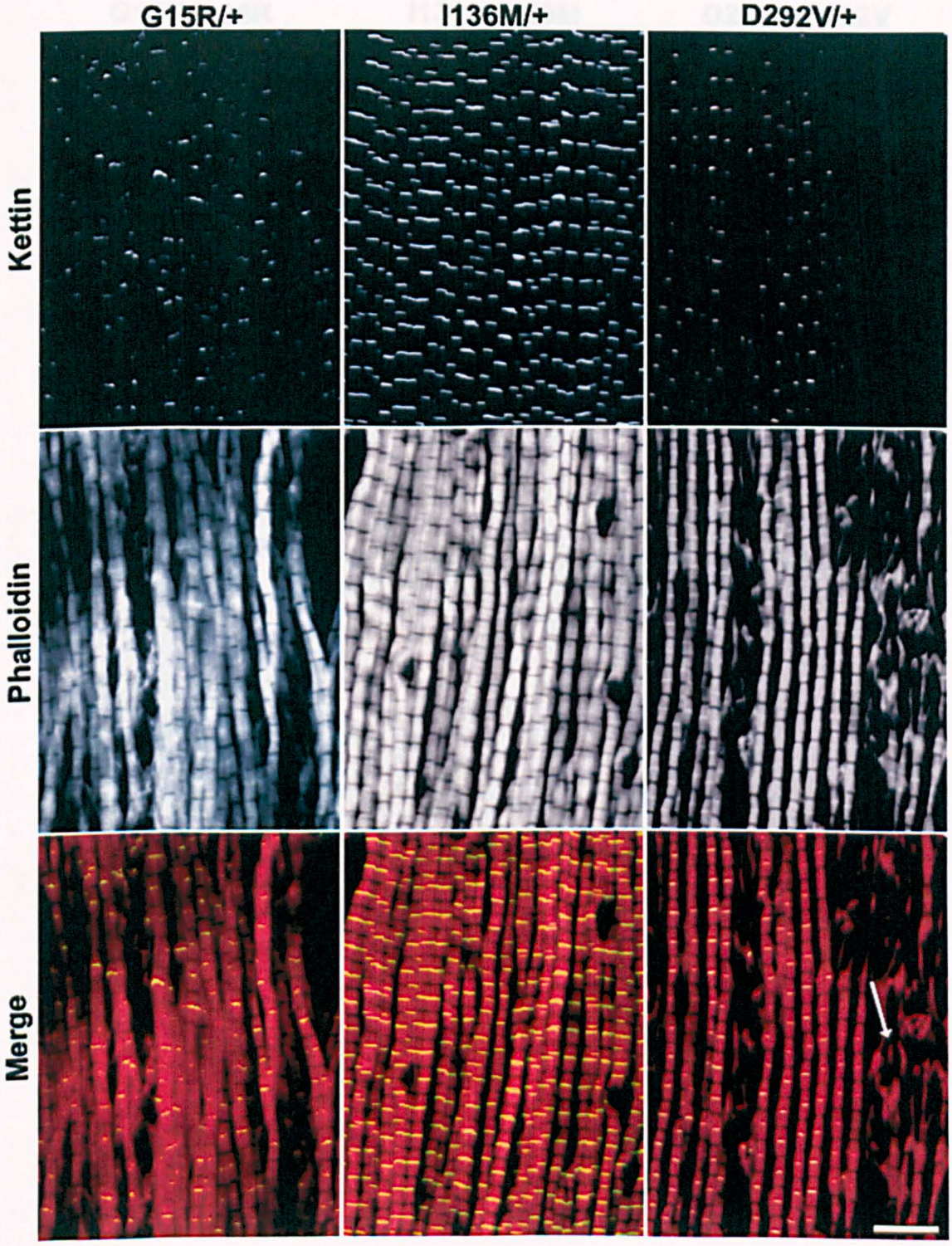

Figure 3.4. Whole muscle light microscopy of mild nemaline myopathy mutants. *Act88F*^{G15R}, *Act88F*^{I136M} and *Act88F*^{D292V} heterozygotes were stained with phalloidin and anti-kettin antibody. Arrows indicate disorganised thin filaments. Scale bar: 5 μm.

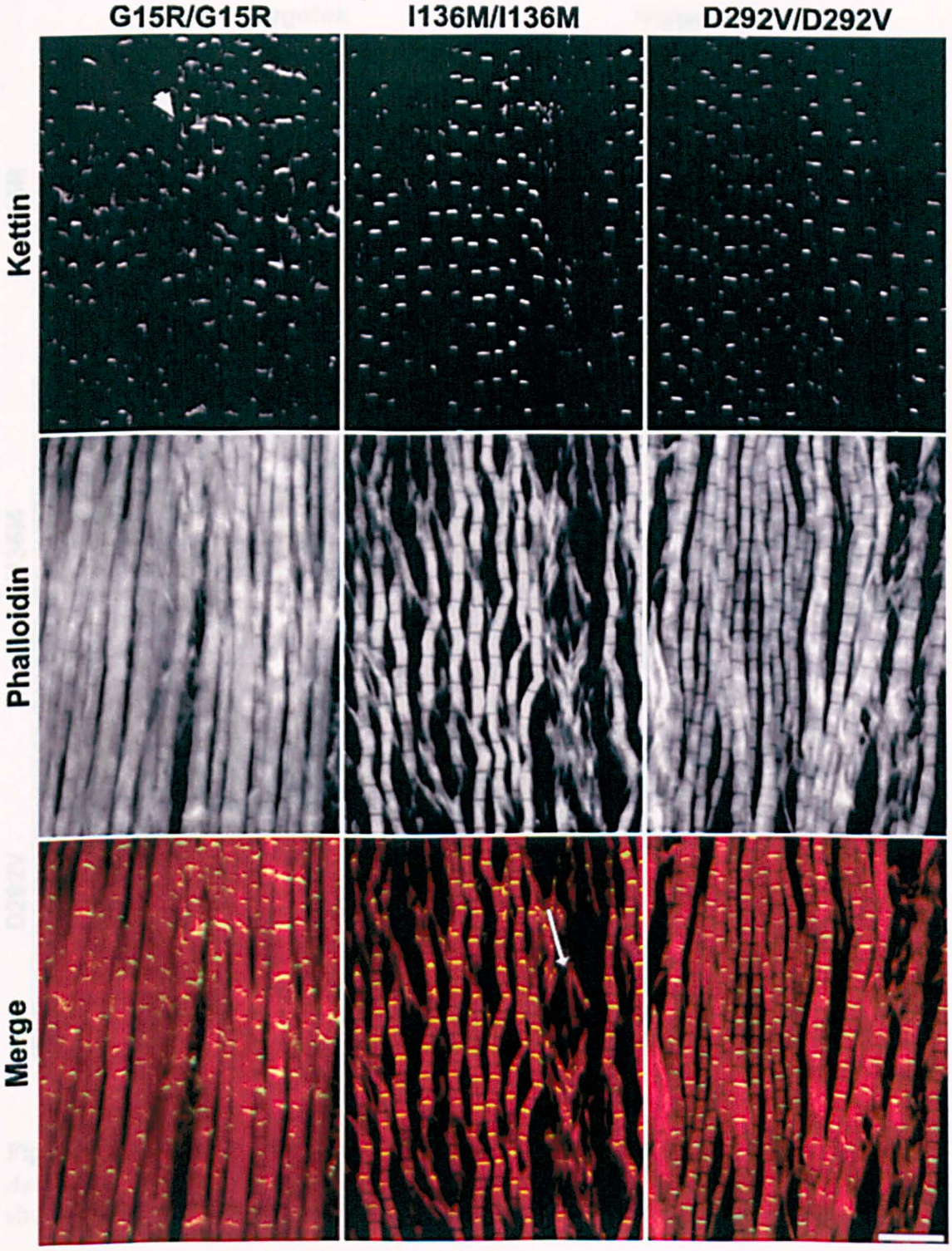

Figure 3.5. Whole muscle light microscopy of mild nemaline myopathy mutants. *Act88F*^{G15R}, *Act88F*^{I136M} and *Act88F*^{D292V} homozygotes were stained with phalloidin and anti-kettin antibody. Disorganised thin filaments are indicated by arrows and aberrant Z-discs by arrowhead. Scale bar: 5 µm.

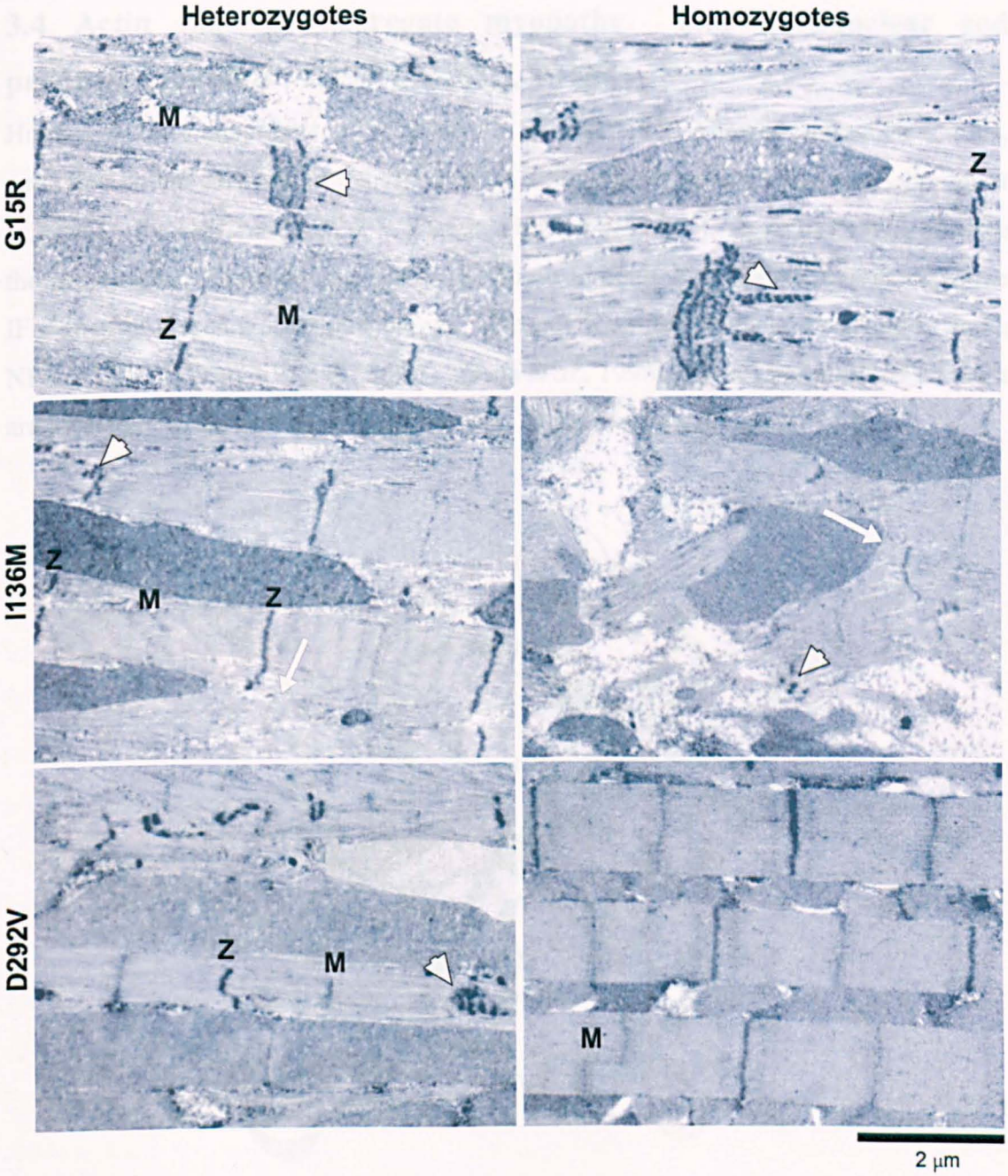

Figure 3.6. TEM images of nemaline myopathy mutants. Longitudinal sections of *Act88F*^{G15R}, *Act88F*^{I136M} and *Act88F*^{D292V} heterozygotes and homozygotes. White arrows show myofibril branching. White arrowheads show zebra bodies. Z: Z-line, M:M-line.

3.4 Actin filament aggregate myopathy and intranuclear rod producing mutants - D154N, V163L, V163M

Human *ACTA1* mutations of residues D154 and V163 showed intranuclear rods, nemaline bodies and accumulations of actin filaments in patient biopsies (Schroder *et al.*, 2004; Hutchinson *et al.*, 2005; Kaimaktchiev *et al.*, 2006). These mutations produce the more rare NM phenotypes and were chosen to determine if when expressed in the IFM they produced similar phenotypes. Two nuclear export signals are found in actin; NES1 (170-181) and NES2 (211-222) (Wada *et al.*, 1998). The D154 and V163 residues are located near the first nuclear actin export signal of actin (Figure 3.7).

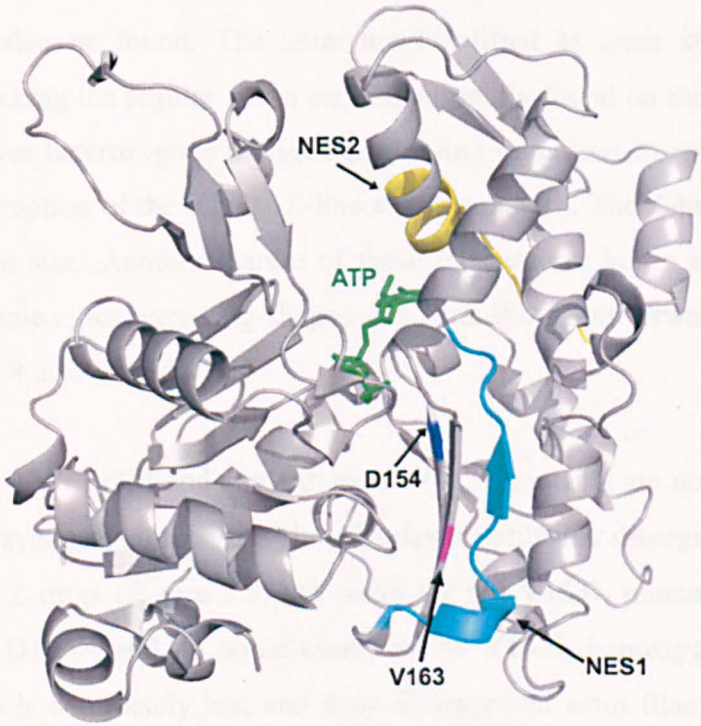

Figure 3.7. Cartoon of ATP-bound G-actin showing the proximity of residues D154 and V163 to nuclear export signals 1 and 2. ATP shown in stick (green); NES1 in cyan, NES2 in yellow, D154 and V163 residues are shown in blue and magenta, respectively. Image produced using PYMOL.

Two transgenic lines were obtained for the D154N mutation only one of which was analyzed as the second line contained the *Act88F*^{D154N} insert on the third chromosome. Three lines were obtained for the V163L mutation, two of which showed the same sarcomeric phenotypes and disarray, but one displayed the intranuclear actin rods at a higher frequency than the other. The third line was not analyzed as the *Act88F*^{V163L} insert was in the third chromosome. Also three lines were obtained for the V163M

mutation, which showed the same phenotypes in two of the lines analyzed. The third line was not studied as the *Act88F*^{V163M} insert was too found in the third chromosome. Studying the *Act88F*$^{[mutation]}$ transgenes in a homozygous state requires that they are expressed in an *Act88F* null background. As both the *Act88F*^{KM88} actin null and wild type *Act88F* genes are located on the third chromosome, studying lines carrying the *Act88F*$^{[mutation]}$ inserts on the same chromosome would not have been possible.

Immunostaining and phalloidin staining of whole muscle fibres showed that the D154N, V163L and V163M mutations resulted in greater myofibrillar disarray compared to the nemaline rod and CFTD causing mutants discussed in Section 3.3. In the muscle fibres of the D154N, V163L and V163M mutants sarcomeres are formed but areas devoid of sarcomeres can also be found. The latter are identified as areas stained solely by phalloidin and lacking the regular kettin staining normally found on the Z-discs (Figure 3.8, 3.9). Moreover heterozygous transgenics carrying mutations in residues D154 and V163 display disruption of the regular Z-line staining pattern. The Z-lines are irregular, bent and differ in size. Another feature of these muscles are kettin and actin stained rods, which in some cases were ring-shaped and from this point forward will be called Z-rings (Figure 3.8 arrow head).

As homozygotes the V163M and some in cases V163L mutants are not much different from their heterozygous counterparts. They display myofibrillar disorganization with Z-disc defects and Z-rings (Figure 3.9, the result for the V163L mutant is not shown). However in the D154N and, in some cases, in the V163L homozygotes the regular myofibril pattern is completely lost and only disorganised actin filaments are present (Figure 3.9). In those muscles no Z-disc or sarcomeric pattern can be observed. The kettin staining for these mutants is grainy and no specific pattern can be identified (Figure 3.9).

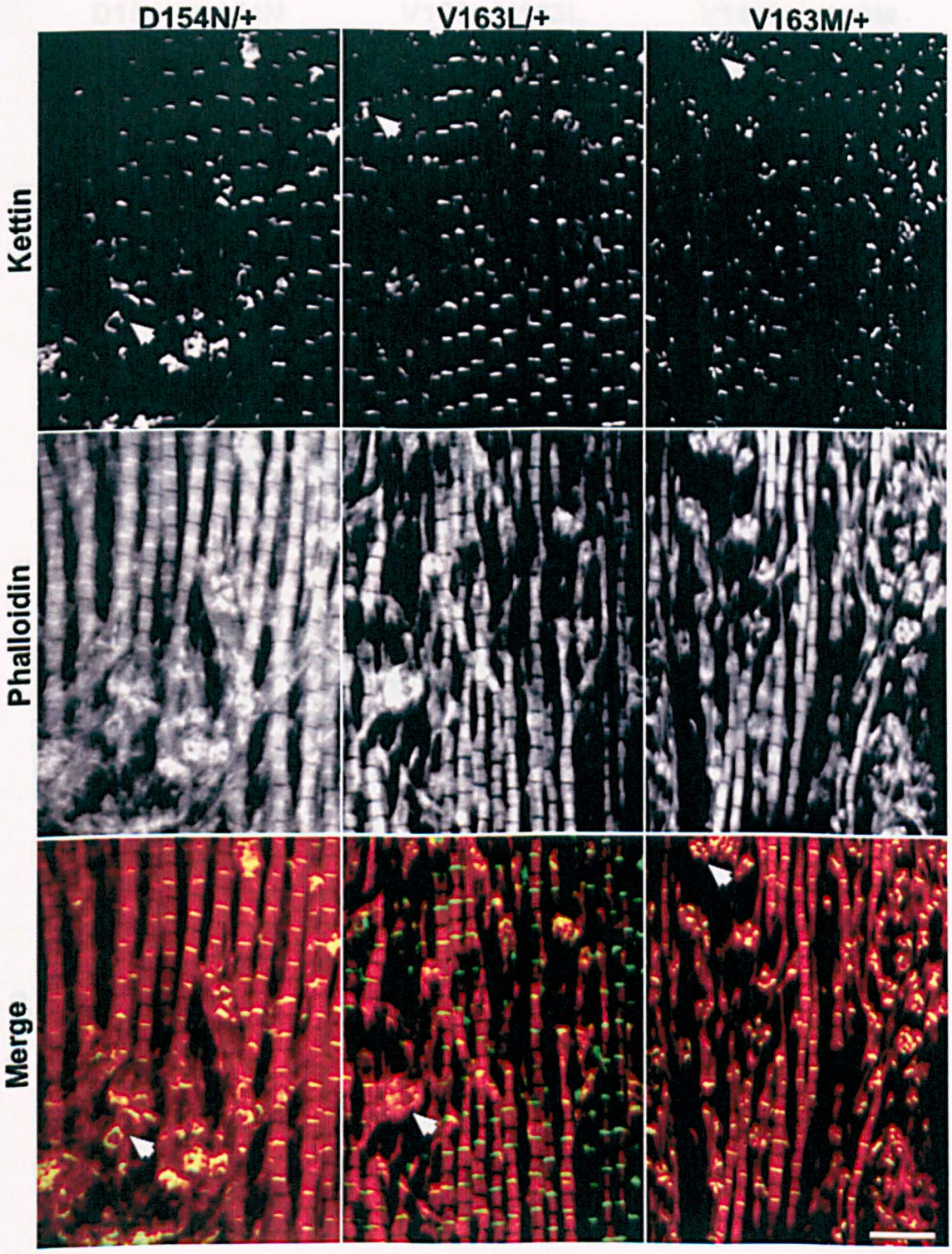

Figure 3.8. Whole muscle light microscopy of intranuclear rod-linked mutants. IFM from *Act88F*^{D154N}, *Act88F*^{V163L} and *Act88F*^{V163M} heterozygotes stained with phalloidin and anti-kettin antibody. Arrowheads show Z-rings. Scale bar: 5 μm.

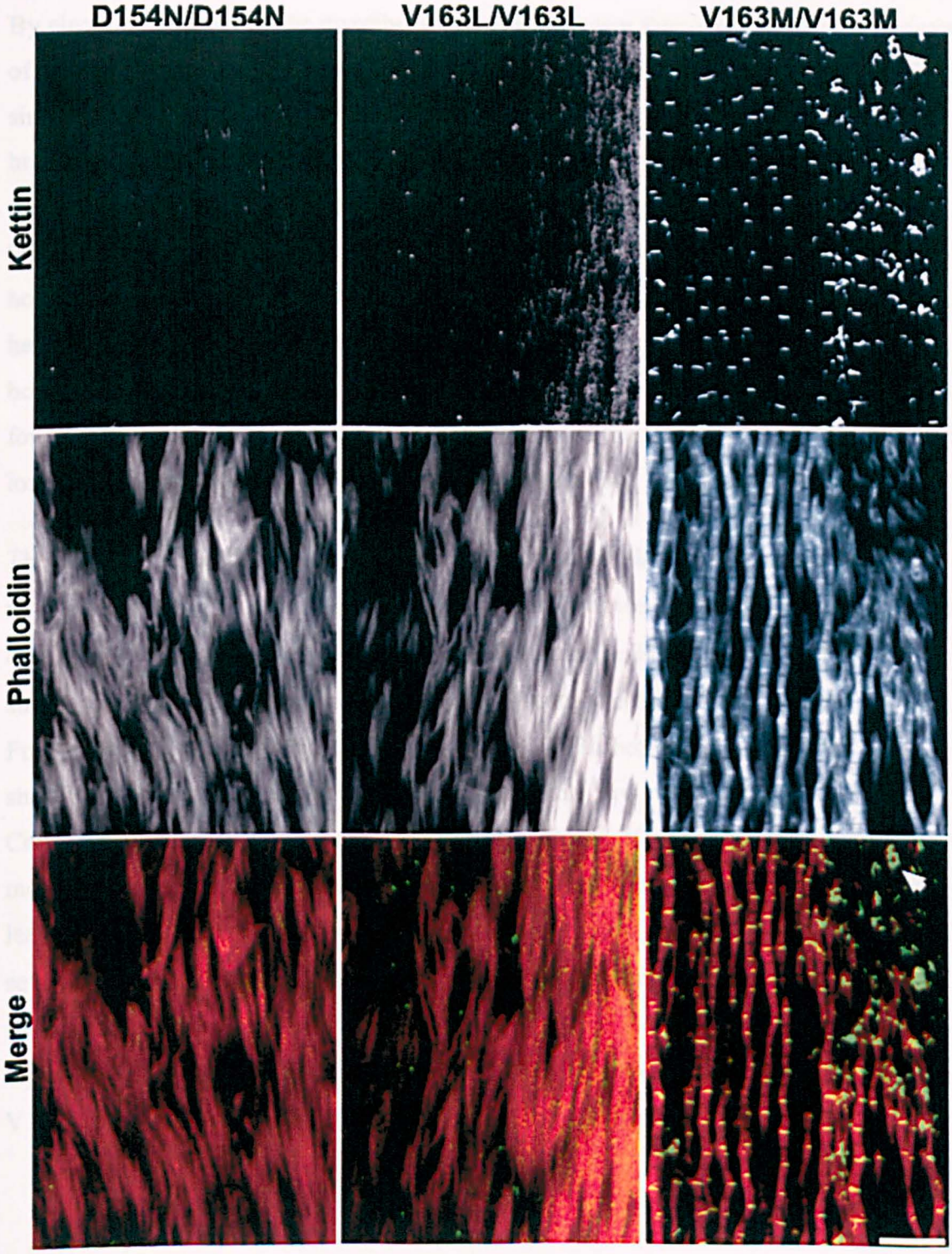

Figure 3.9. Whole muscle light microscopy of intranuclear rod-linked mutants. IFM from *Act88F*^{D154N}, *Act88F*^{V163L} and *Act88F*^{V163M} homozygotes stained with phalloidin and anti-kettin antibody. Arrowheads show Z-rings. Scale bar: 5 µm.

By electron microscopy, the myofibrils are often narrower than in wild type and regions of ordered sarcomeres are found next to regions of disordered sarcomeres (Figure 3.10), similar to the biopsy samples from human patients. Other features include myofibrillar branching, aberrant structure of myofibrils and areas of broken/disorganised thick and thin filaments, although this was not observed in the latter case for D154N, or V163L homozygotes, as they did not form myofibrils (this was not always true for the V163L homozygotes which sometimes formed myofibrils). All three mutants (both heterozygotes and homozygotes) display Z-disc and M-line disruption as well as zebra bodies. The size and frequency of the zebra bodies varies. However the zebra bodies found in these mutants are not detected as often as in the G15R mutant and are not as long (laterally) as the ones caused by the G15R mutation.

The D154, V163L and V163M heterozygote mutants (also V163L/M homozygotes), resulted in a novel ring-like Z-disc structures, which varied in diameter from 0.2 μm to 4 μm (as measured by EM). These structures seen in the EM are likely to be the same structures as the ring-shaped structures seen by confocal microscopy in these mutants. Furthermore, a feature found specifically in the V163L heterozygous mutants was very short sarcomeres with lattice gaps where filaments are missing (Figure 3.10 box). Consistent with the light microscopy, the D154N and V163L mutations showed the most extreme phenotypes as the homozygotes completely abolish myofibrillar structure leaving broken filaments and very long but narrow zebra bodies, which highlights the severity of these mutations (Figure 3.10). It is possible that the muscles in the D154N and of the severely affected V163L mutants were not properly formed during myogenesis. The V163M mutation appears to be less severe compared to D154N and V163L as it permitted the formation of myofibrils in the homozygous state.

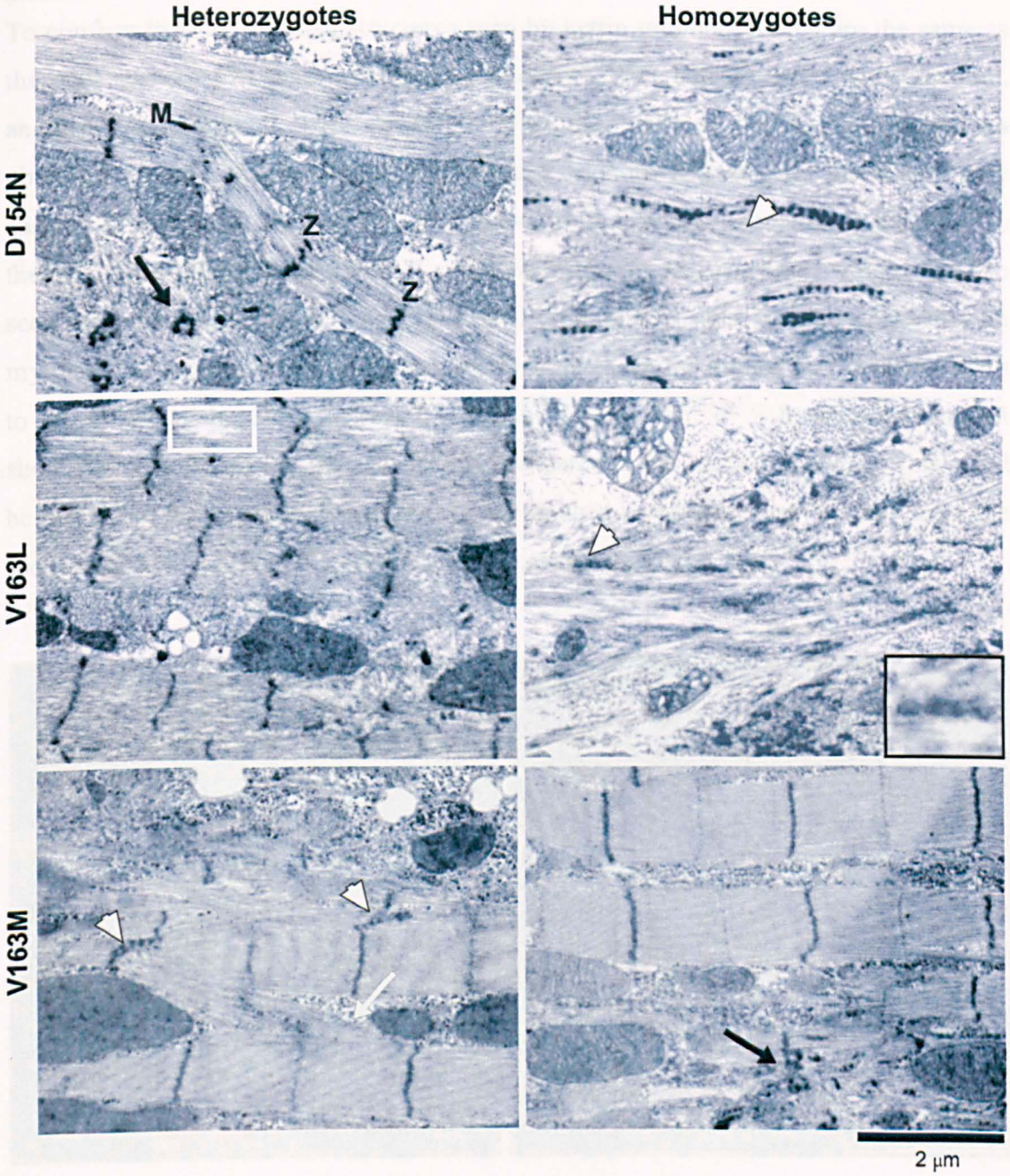

Figure 3.10. TEM images of intranuclear rod-linked mutants. Longitudinal sections of *Act88F*^{D154N}, *Act88F*^{V163L} and *Act88F*^{V163M} heterozygotes and homozygotes. White arrows show thin filaments running between/across adjacent myofibrils. White arrowheads point at zebra bodies. Black arrowheads point at disrupted Z-discs. Z: Z-line, M: M-line. White box shows lattice gap. The black box shows a magnified zebra body.

To confirm that the ring-like structures seen by kettin immunostaining are the same as the ones seen by EM, immunostaining of *Act88F*^{D154N}/+ heterozygotes with α-actinin, another Z-disc protein, was performed. This also showed the ring-like structures observed with the anti-kettin antibody (Figure 3.11 arrow heads). In the same figure spacing of the Z-discs in the mutant is shown to be irregular compared to that seen in the wild type. The Z-discs themselves are bent, broken and irregular, which was also seen with the anti-kettin antibody. The wild type muscle fibre is tightly packed with myofibrils composed of regularly spaced sarcomeres. In the mutant this does not seem to be the case as shown by the very few Z-lines. The *Act88F*^{D154N}/+ heterozygote mutant shown here shows greater muscle disarray compared to the one in Figure 3.8. This could be due to the fact that the section of the fibre imaged in this case was different from the section imaged in Figure 3.8 or due to variations seen between flies.

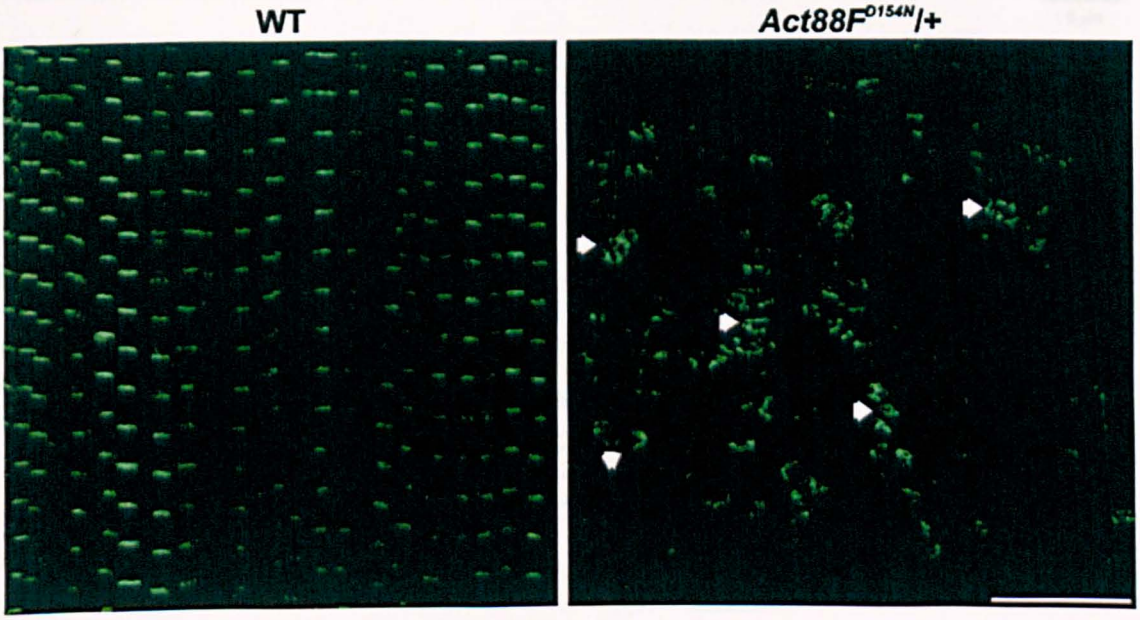

Figure 3.11. Immunostaining with α-actinin antibody of whole fly muscles for wild type and *Act88F*^{D154N}/+ heterozygotes. In the mutant irregular Z-lines which vary in size, and circular structures can be seen. Arrowheads show Z-rings. Scale bar: 10 μm.

In order to understand if the Z-rings are composed solely of Z-disc proteins, immunostaining with myosin was performed. This showed that myosin is also associated with these Z-rings (Figure 3.12 arrows). The expected staining pattern for phalloidin, myosin and kettin in wild type sarcomeres is shown in Figure 3.13. Phalloidin stains actin filaments extending from the Z-discs until close to the H-zone where the thin filaments terminate. Signal from the anti-myosin antibody is only visible at the M-line and at the Z-disc. The thick filaments terminate at the end of the A-band,

which in the IFM is very close to the Z-disc due to very narrow I-bands. As result, a Z-disc staining pattern is observed. The reason for the absence of myosin staining across the thick filament is due to problems with antibody penetration, caused by the very regular thin/thick filament lattice of the IFM. This problem is not seen in other muscles where the lattice is much less regular and more widely spaced so that the anti-myosin antibodies can completely stain the A-band (Ackermann *et al.*, 2009).

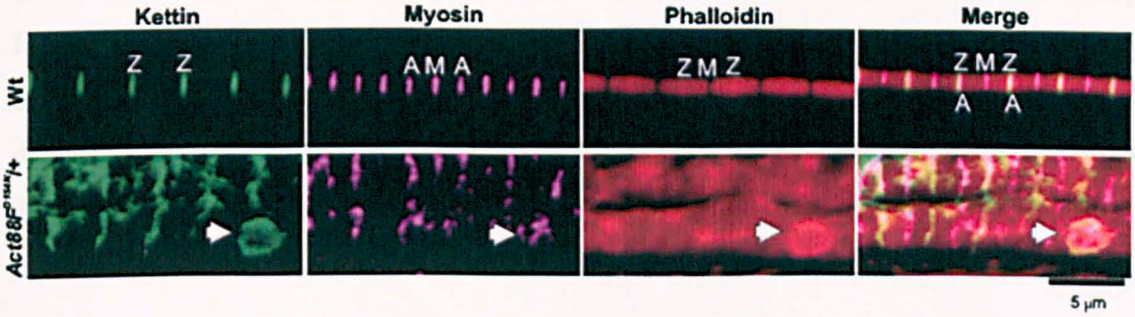

Figure 3.12. Light microscopy of single myofibrils from wild type and *Act88F*^{D154N}/+ heterozygotes. Anti-kettin, anti-myosin antibodies and phalloidin. A: A-band, M: M-line, Z: Z-line.

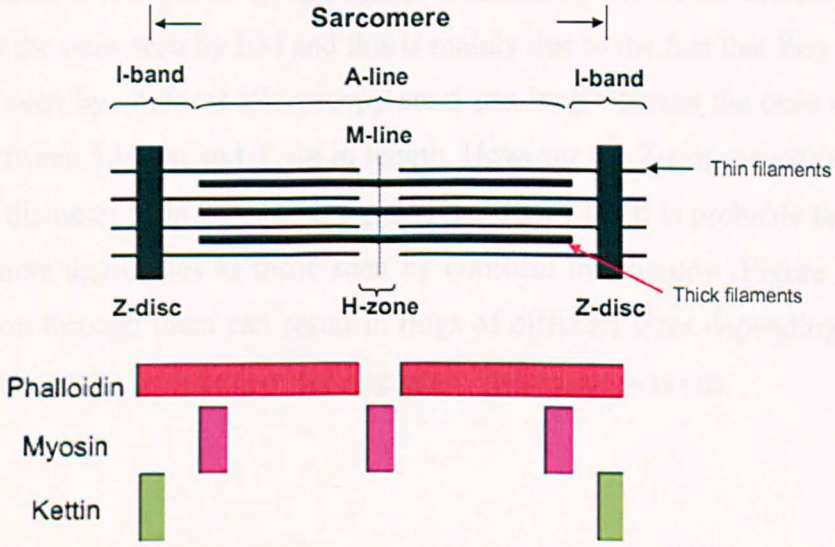

Figure 3.13. Diagram showing the expected position of the fluorescent signal for phalloidin, myosin and kettin in wild type *Drosophila* sarcomeres.

Since single micrographs do not show all the aberrant features observed for each mutation, a selection of micrographs for *Act88F*^{V163M}/+ heterozygotes demonstrates that many different features can be observed for a single mutation (Figure 3.14). EM images show accumulations of actin thin filaments and a multiplicity of Z-disc material. Zebra bodies can be seen as defined by their distinct stripe pattern (Figure 3.14 A) as well as ring-like Z-discs (Figure 3.14 A and B). By EM the zebra bodies and the ring-like Z-discs consist of many round electron dense pieces of Z-disc material (Figure 3.14 A arrow and 3.14 B inset), which from this point forward will be called Z-bodies. Except for Z-rings and zebra bodies, any large aberrant/unstructured accumulations consisting of Z-bodies will be referred to as Z-body aggregates. This term will also be used to describe any other electron dense accumulation in which Z-bodies cannot be distinguished. Large actin and Z-disc material aggregations identified by light microscopy will also be referred to as Z-body aggregates.

Whole muscle confocal imaging shows the co-staining of Z-body aggregates for kettin and actin. The kettin staining seems to be at the periphery of the Z-body aggregate whereas fluorescent phalloidin seems to stain the greater part of this structure. It is not possible to determine if the Z-body aggregates observed by the whole muscle staining are the same as the ones seen by EM and this is mainly due to the fact that they differ in size. The ones seen by confocal microscopy are 5 μm long whereas the ones observed by EM vary between 500 nm and 1 μm in length. However the Z-ring structures shown by EM vary in diameter from 200 nm to 4 μm (Figure 3.14 B). It is probable that the Z-rings are the same aggregates as those seen by confocal microscopy (Figure 3.14 A). Cutting a section through them can result in rings of different sizes depending on how close to the centre or the periphery of the aggregate the section was cut.

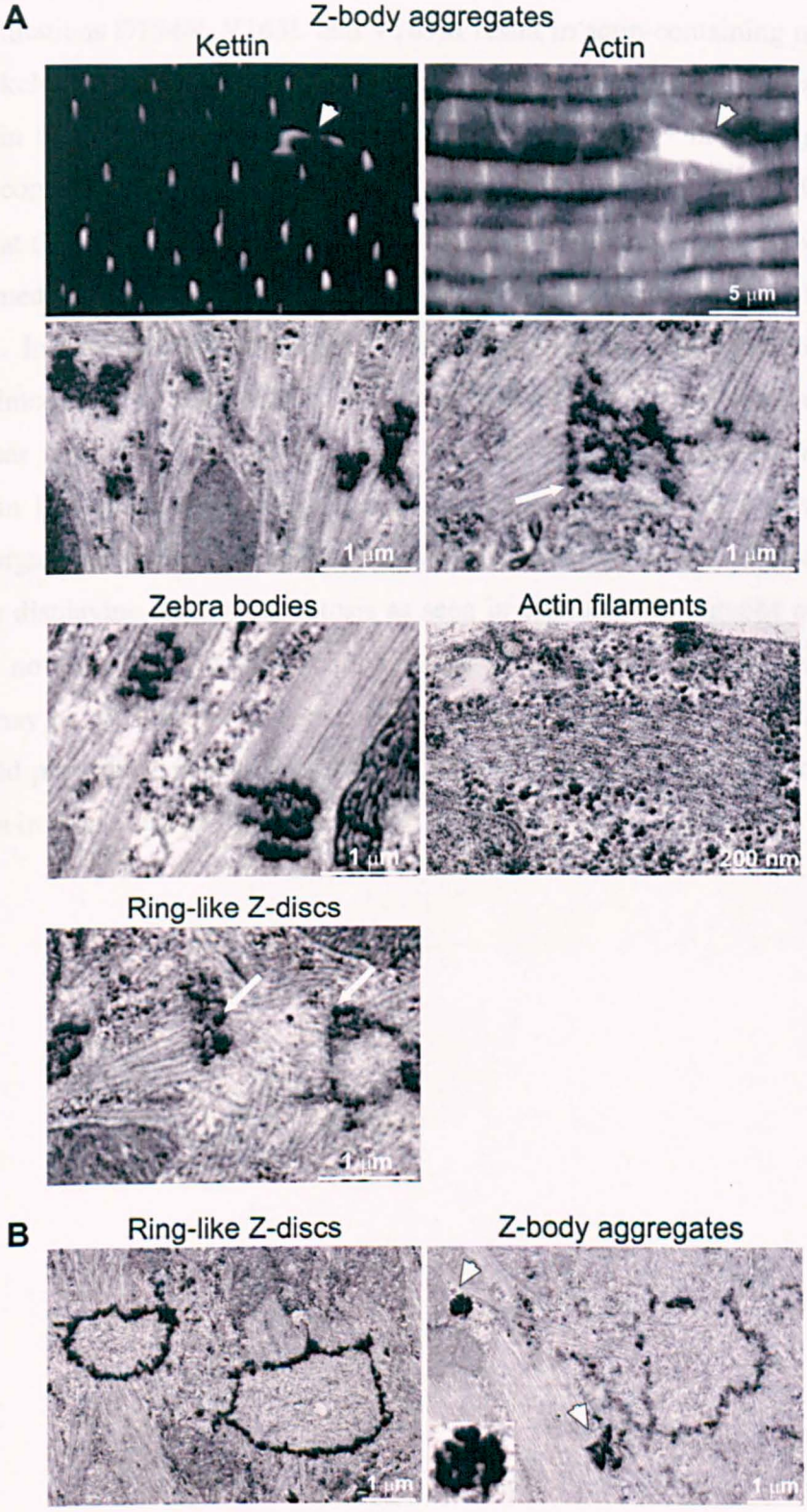

Figure 3.14. Examples of the aberrant structures found in the IR-linked mutants by electron and light microscopy. (A) *Act88F*^{V163M}/+ heterozygote, arrowheads point at Z-body aggregates, white arrows point at Z-bodies. Anti-kettin antibody and phalloidin were used for light microscopy. **(B)** *Act88F*^{D154N}/+ heterozygote, arrowheads point at Z-body aggregates. The inset shows magnification of the Z-body aggregate.

The three mutations D154N, V163L and V163M result in actin-containing nuclear rods in human skeletal muscle and this is also observed in the nuclei of *Drosophila* IFM. The nuclei in these mutants are often enlarged (see $Act88F^{V163L}/+$ heterozygote, Figure 3.15) and contain rod-like structures that consist of filaments. Phalloidin staining confirms that these rods consist of F-actin and span the nucleus (Figure 3.16). This was also confirmed by Z-stacks of whole muscle fibres stained with DAPI and phalloidin (Movie 3.1. Intranuclear rods.avi). In V163L heterozygotes, rods were found in the nuclei of almost every fly examined, and most of the nuclei in the muscle contained rods. Nuclear rods were less common in V163M heterozygotes than in V163L, and infrequent in D154N heterozygotes. The D154N mutation results in the most severe muscle disorganisation but the whole cell may be affected. Most nuclei appear abnormal and may be displaying signs of apoptosis as seen in electron micrographs of 1-day old flies (data not shown). Reduced cell survival could mean that different nuclear processes may be affected including those involved in actin import inside the nucleus, which would prevent the formation of IRs. This could explain the lower frequency of nuclear rods in this mutant.

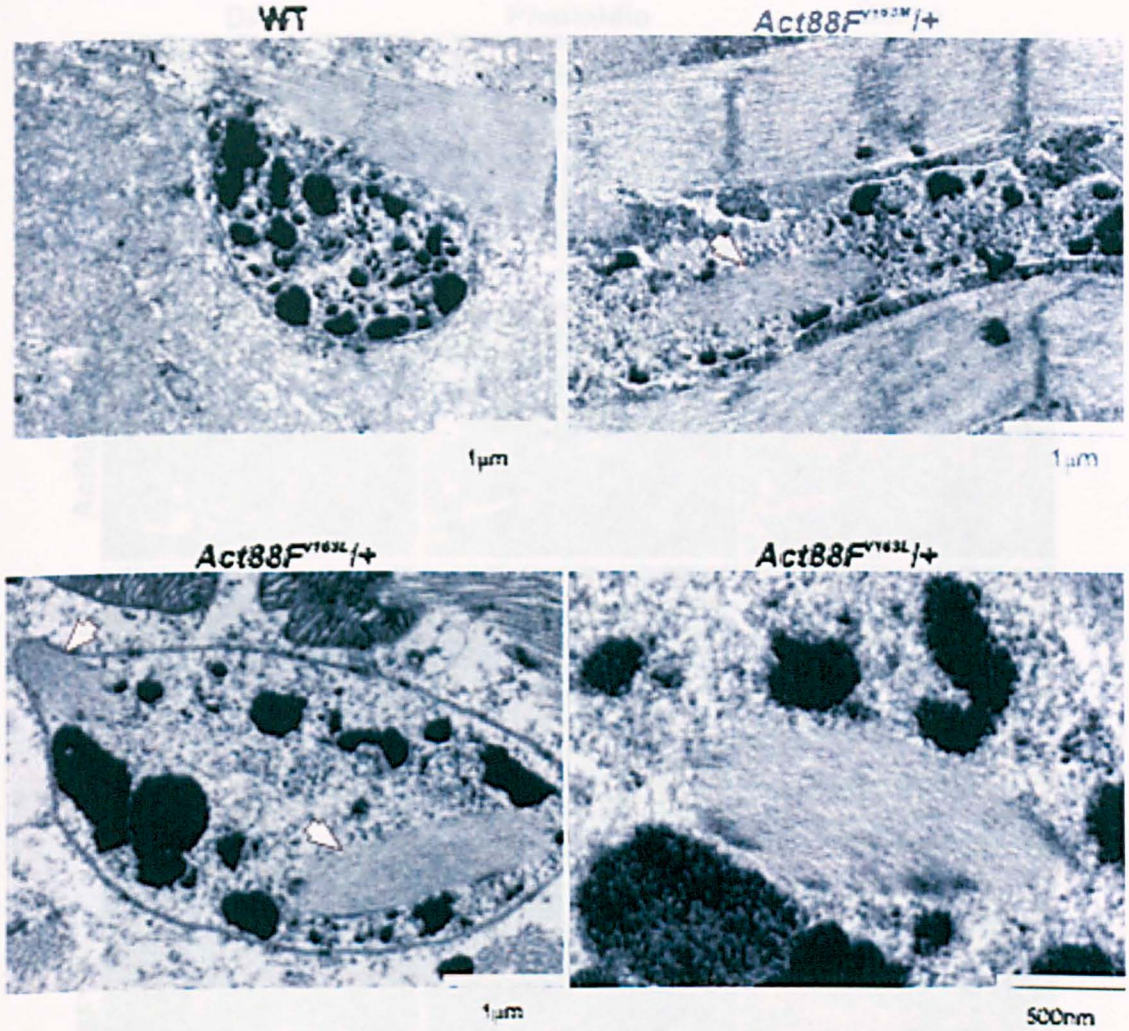

Figure 3.15. Intranuclear rods. TEM images of *Act88F*^{V163L}/+ and *Act88F*^{V163M}/+ heterozygotes showing aggregates inside the nuclei. In the higher magnification of *Act88F*^{V163L}/+ heterozygotes (bottom right panel) the intranuclear aggregates are clearly filamentous.

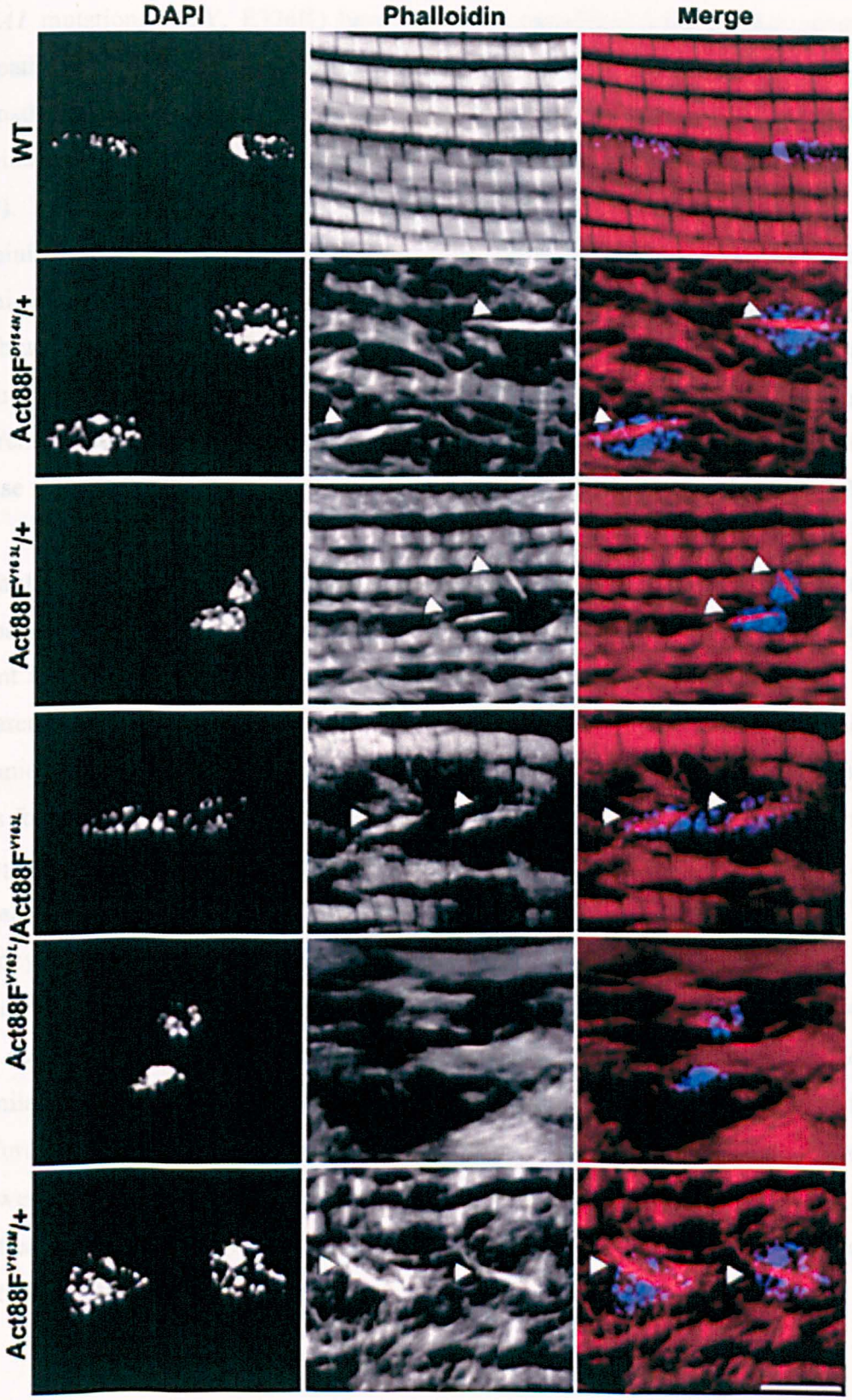

Figure 3.16. Intranuclear actin rods. Whole muscle light microscopy of wild type, *Act88F*^{D154N}, *Act88F*^{V163L} and *Act88F*^{V163M} mutants with DAPI and phalloidin. Arrowheads point at phalloidin-stained nuclear actin rods. Scale bar: 5 µm.

3.5 Is there a correlation between nemaline myopathy and central core disease?

ACTA1 mutations (D3Y, E336K) have also been associated with another congenital myopathy called central core disease (Kaindl *et al.*, 2004). This is a non-progressive myopathy typically caused by mutations in the ryanodine receptor-1 gene (*RYR1*) (Robinson *et al.*, 2006) and in the myosin heavy chain-7 gene (Fananapazir *et al.*, 1993). To identify the disease the patients' muscle biopsies are treated with a stain containing nitroblue tetrazolium (NBT). The principle behind this histochemical technique is that tetrazolium blue acts as an electron acceptor, which becomes reduced to a blue-grey product at the site of the enzyme activity. The intensity of the reaction product is a reflection of the mitochondria within the fibre and varies amongst the different muscle fibre types found in humans. The histopathological feature of the disease is the lack of staining in the centre of the muscle fibre when treated with NBT.

A simultaneous appearance of nemaline rods and central core disease has been observed in a patient with an *ACTA1* mutation (M134V) (Jungbluth *et al.*, 2001). In this particular patient type 1 fibres displayed nemaline bodies whereas type 2 fibres displayed core-like areas. This mixture of rods and cores is more often caused by mutations in *RYR1* (Monnier *et al.*, 2000; Scacheri *et al.*, 2000). Here stained preparations of whole muscle fibres for $Act88F^{V163L}/+$ heterozygotes show that the top section of the fibre appears less damaged or not damaged (observed only by confocal imaging) compared to the more central section (Figure 3.17). This result is presented only for the $Act88F^{V163L}/+$ heterozygous mutant although the other IR-linked mutants also displayed the same characteristic (not shown). The fact that the more central section of the fibre appears more damaged than peripheral regions raises the question as to whether this phenotype is similar to the central core disease phenotype seen in humans. In order to investigate that further transverse muscle sections from wild type and $Act88F^{V163L}/+$ heterozygous flies were stained with NBT, the diagnostic method used to identify central core disease in patient biopsies. However the staining was too pale to see a difference between the wild type and the mutants fibres.

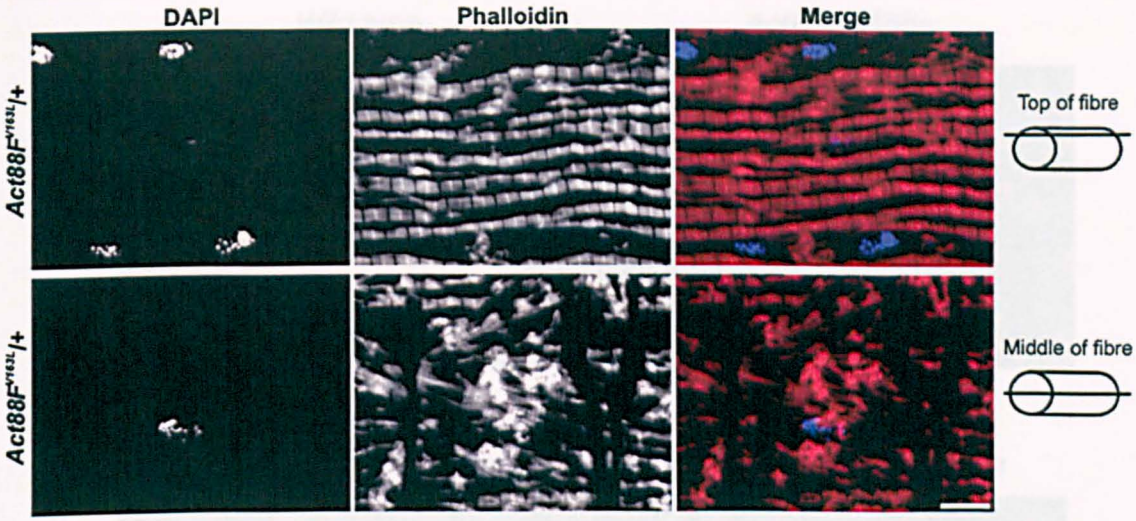

Figure 3.17. Optical sectioning of stained whole muscle from the *Act88F*^{V163L}/+ heterozygote mutant. Upper and lower panels show different optical sections of the same muscle fibre. The top panels are from a section at the top of the fibre, the bottom panels are from the middle section as shown in the cylindrical diagram with the horizontal line, indicating the fibre section that was captured in images. Scale bar: 5μm.

In all the mutants studied here there was variation in the frequency of the different phenotypes amongst flies of the same genotype. The *Act88F*^{V163M} homozygotes are shown as an example. In the wild type thorax the six DLMs are clearly seen and numbered (Figure 3.18). Polarized light images of *Act88F*$^{V163M\ /+}$ heterozygotes shows that the DLM are present however parts of the muscle are not as birefringent because they are damaged (Figure 3.18). In the case of the *Act88F*^{V163M} homozygotes some flies showed the hypercontraction phenotype and their IFM autodestruct (Figure 3.18 bottom left image). However other flies don't hypercontract and their IFM resemble those of the *Act88F*$^{V163M\ /+}$ heterozygotes by polarized light microscopy (Figure 3.18 bottom right image).

Figure 3.18. Polarized light analysis of *Act88F*^{V163M} mutants. In the wild type the six DLMs are numbered I-VI. Arrow points at the sole birefringent IFM of an *Act88F*^{V163M} homozygote and the star at the jump muscle. The flies for all the samples were 1 day old.

Finally, all the different actin mutations give rise to different aspects of the disease in humans and also resulted in novel phenotypes in *Drosophila*. Based on the phenotypic observations the mutants can be split into two groups: those resulting solely in zebra bodies (G15R, I136M, D292V) and those resulting in F-actin/Z-body aggregates, zebra bodies, Z-rings and intranuclear rod aggregates (D154N, V163L/M). Both groups result in general myofibril and sarcomeric disorganization. A summary of all the phenotypic observations made for each heterozygous and homozygous mutant is shown in Table 3.2.

Table 3.2. Summary of observations in heterozygous and homozygous mutants. Note: + indicates the presence of a characteristic and - indicates the absence of a characteristic, nd indicates that it was not possible to determine if a characteristic was present or not.

Act88F Mutation	Intranuclear rods	Zebra bodies	Myofibrils	Aggregates	F-actin	Flight ability	Z-rings
G15R/+	-	+	+	-	+	-	-
I136M/+	-	+	+	-	+	some	-
D154N/+	+	+	-	+	+	-	+
V163L/+	+	+	+	+	+	-	+
V163M/+	+	+	+	+	+	-	+
D292V/+	-	+	+	nd	+	+	-
G15R/G15R	-	+	+	-	+	-	-
I136M/I136M	-	+	+	nd	+	-	-
D154N/D154N	nd	+	-	-	+	-	-
V163L/V163L	+	+	+/-	+	+	-	+
V163M/V163M	nd	+	+	+	+	-	+
D292V/D292V	-	-	+	-	+	-	-

3.6 Detailed single myofibril analysis of the *Act88F* mutations shows aberrant staining patterns.

Detailed single myofibril analysis of the *Act88F* mutations was carried out as part of a collaborative research project with Dr. Peckham (Institute of Molecular and Cellular Biology, Faculty of Biological Sciences, University of Leeds). Single myofibrils from each mutant were stained with a combination of different antibodies against muscle proteins in order to study which proteins are missing or not properly localized in the mutants. For this 1-day-old flies of the correct genotypes were selected, bisected in YMG and stored at -20 °C overnight (Chapter 2, section 2.2.2). The next day the half thoraces kept in YMG on ice were collected by Dr. Michelle Peckham, who proceeded with the single myofibril immunostaining protocol described in Chapter 2 Section 2.2.2. Images from the single myofibril immunostaining are shown in Figure 3.19, 20, 21, which were also prepared by Dr. Peckham.

Mutations in actin might be expected to result in aberrant muscle structure for several reasons. First, the actin itself might not polymerize as well as wild type actin, although the staining of the intact flight muscles from homozygote mutants (Figures 3.5 and 3.10) argues that all of the mutant actins are able to polymerize into F-actin filaments. Second proteins that bind to actin and regulate its length in the sarcomere such as capping protein in the Z-disc, tropomyosin and tropomodulin (the pointed end 'capping' protein) may bind less well to actin filaments, resulting in increased instability and/or variation in thin filament length. Although none of the mutated actin residues lie within

the known myosin binding sites on actin, a change in the binding affinity of actin to tropomyosin, might indirectly affect force generation.

The pattern for tropomyosin immunostaining in wild type muscle shows a strong band at the Z-disc and weaker staining throughout the rest of the sarcomeres, with a fainter strip at the M-line (Figure 3.19). This is due to the fact that the tropomyosin antibody cannot penetrate and bind along the entire length of the actin filament, but does bind at the ends at the thin filaments at the M-line (doublet) and at the Z-line. In the mutant myofibrils G15R, V163M and V163L, this pattern is less regular, and staining near the Z-line is less obvious. This suggests that these mutations may affect tropomyosin binding to the thin filaments. The immunostaining pattern for tropomyosin in I136M, D292V and D154N heterozygotes is similar to that found in wild type muscle. It is surprising that the staining for D154N is not disrupted much, as this mutation has an otherwise severe phenotype in both heterozygous and homozygous flies.

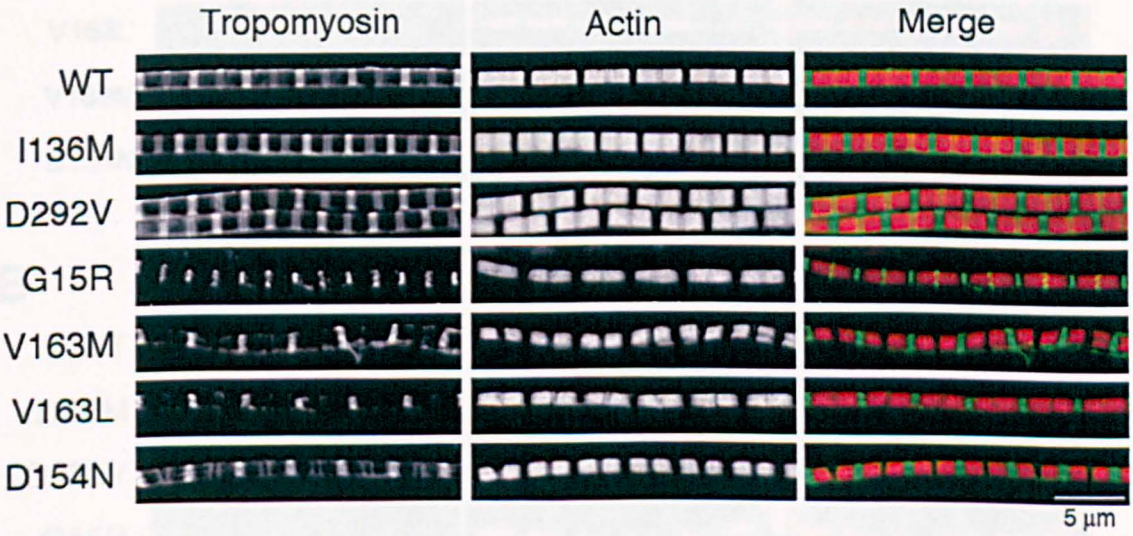

Figure 3.19. Deconvolution images of myofibrils from heterozygous mutants stained for actin and immunostained for tropomyosin.

Thin filaments extend from the opposite Z-discs of a single sarcomere and terminate at the H-zone with their pointed end capped by tropomodulin. For tropomodulin (Figure 3.20 A), a distinctive doublet is observed at the M-line in myofibrils from wild type muscle as expected (Fowler *et al.*, 1993). This doublet pattern is also observed in the myofibrils from the $Act88F^{I136M}$ mutant, which displayed a mild phenotype. M-line staining is also observed for D292V and D154N, though not as a clear doublet, but there

is also evidence of tropomodulin staining throughout the muscle sarcomeres. M-line staining is weak (V163M) or absent for the V163L and G15R mutations, although there is weak staining throughout the sarcomere and even at the Z-line. These results suggest that the interaction of tropomodulin with the thin filaments may be affected in some of the mutants, in particular in G15R, V163L and V163M. Failure to cap thin filaments by tropomodulin could result in aberrant filament growth. Immunostaining for projectin, a myosin binding protein was similar to that found in wild type in all of the mutants with a doublet staining on either size of the Z-line (Figure 3.20 B).

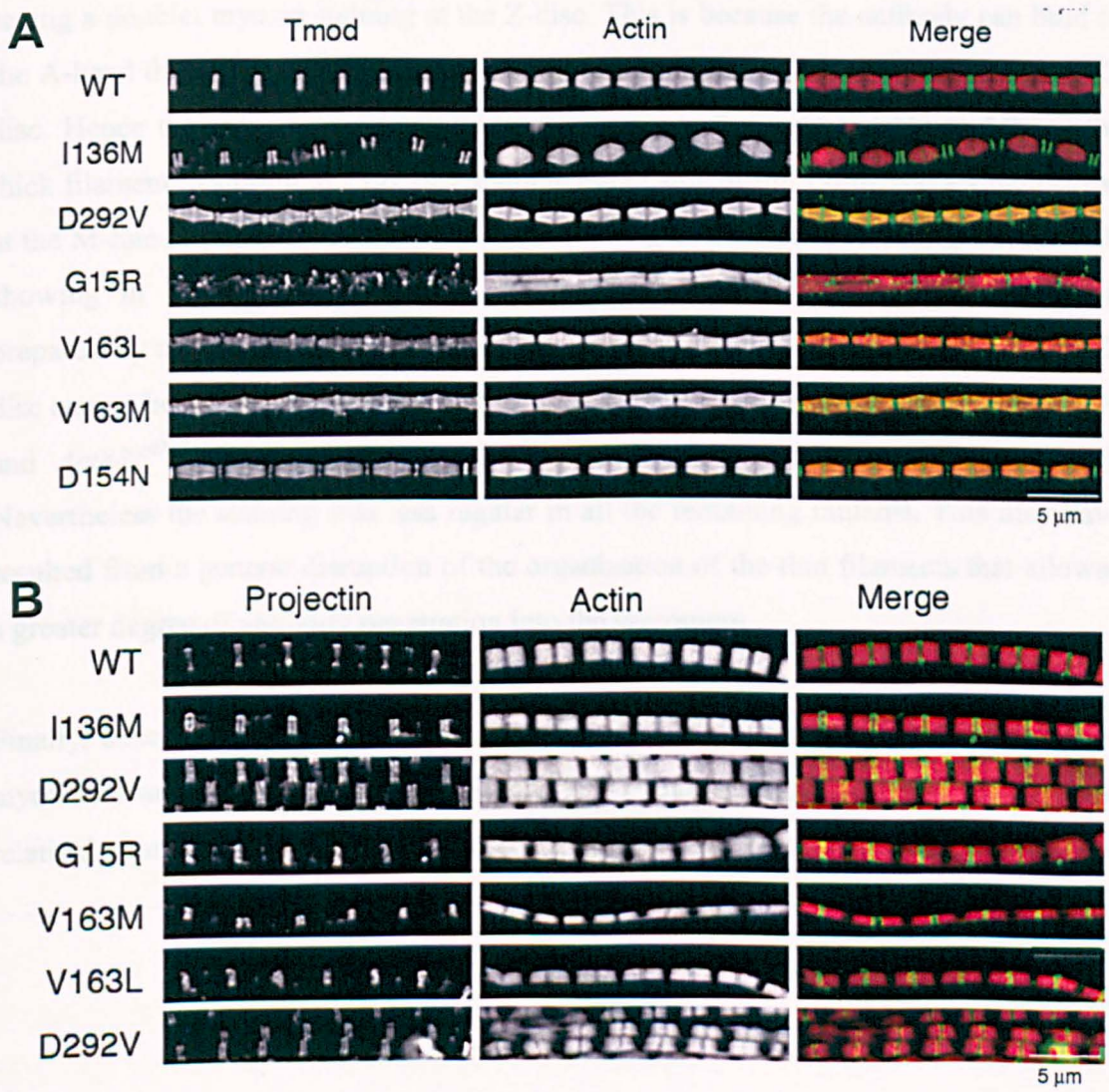

Figure 3.20. Deconvolution images of myofibrils from heterozygous mutants stained for actin and immunostained for (A) Tropomodulin (Tmod) and (B) Projectin.

Like with the tropomyosin antibody that cannot penetrate to stain the thin filament, the myosin antibody does not appear to penetrate in wild type myofibrils and bind to the entire length of the thick filament. As shown before in Figure 3.12 the antibody stains the myosin enriched M-line where the myosin thick filaments originate, as well as the Z-disc. The staining at the Z-line is because the thick filaments terminate at the end of the A-band, which due to the narrow I-bands in the IFM is very close to the Z-disc. In order to visualize the doublet staining at the Z-discs or M-lines for the different antibodies used here, Dr Peckham slightly stretched the single myofibrils during microdissection prior to immunostaining them. Stretching of the myofibrils allowed seeing a doublet myosin staining at the Z-disc. This is because the antibody can bind to the A-band thick filament ends from two adjacent sarcomeres that surround the same Z-disc. Hence the anti-myosin antibody binds mainly to the ends and the middle of the thick filament, resulting in a doublet staining either side of the Z-line and a single stripe at the M-line respectively as well as a weak staining in the sarcomere. Single myofibrils showing in Figure 3.12 from wild type and $Act88F^{D154N}/+$ heterozygous mutant prepared by myself, had not been stretched, which is why the myosin doublet at the Z-disc cannot be visualized. The immunostaining pattern for projectin in the $Act88F^{I136M}/+$ and $Act88F^{D292V}/+$ heterozygous mutants was similar to wild type (Figure 3.20). Nevertheless the staining was less regular in all the remaining mutants. This may have resulted from a general disruption of the organization of the thin filaments that allowed a greater degree of antibody penetration into the sarcomere.

Finally, obscurin co-localized with myosin to a single stripe at the M-line in wild type myofibrils and in all the mutants (Figure 3.21). Interestingly, obscurin staining was relatively normal in the mutants and also displayed a faint localization at the Z-line.

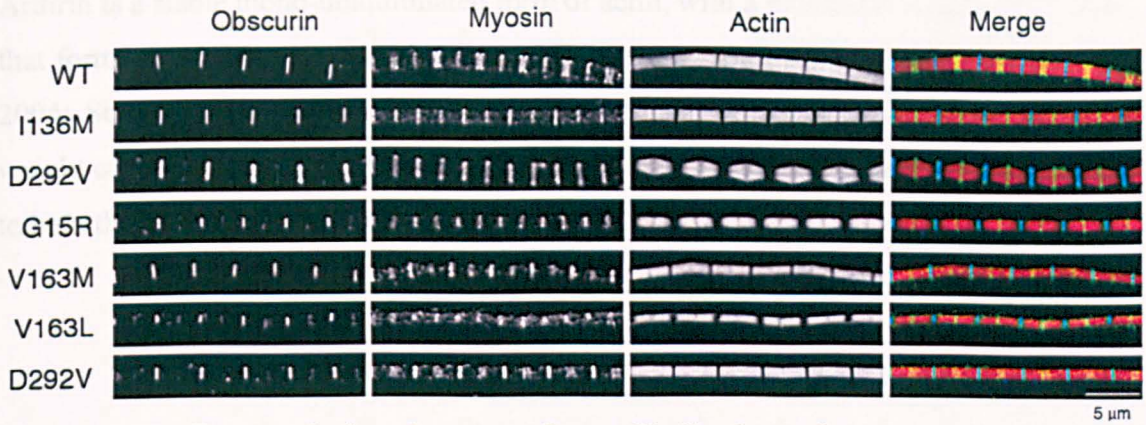

Figure 3.21. Deconvolution images of myofibrils from heterozygous mutants stained for actin and immunostained for myosin and obscurin.

A general observation was that the myofibrils from the mutants were narrower compared to the wild type ones, which is in agreement with the images from the electron micrographs (Figures 3.6 and 3.10).

3.7 Protein analysis of nemaline myopathy mutants

The aberrant muscle structure seen in the different mutants could be due to reduced actin and/or other sarcomeric protein levels. In order to determine if protein levels were altered in the IFM of mutant heterozygotes and homozygotes compared to the wild type flies, 10% 1-D SDS PAGE analysis was performed on dissected intact IFM. Actin null *Act88F*^{KM88} homozygous flies that do not express actin in the IFM were also used as a control. Protein gels (Figure 3.22) show that the actin levels are similar to the wild type in mutant heterozygotes and homozygotes. Actin-myosin ratios measured from three gels showed that the actin levels are decreased in all homozygotes (Figure 3.23). The fact that the actin levels are not significantly reduced in the heterozygous mutants suggests that the muscle phenotypes observed in the IFM are not due to insufficient actin levels but because the mutant actin interferes with the wild type actin function. All the other thin filament proteins and the myosin heavy and light chains (MLC2) are indicated and they are unchanged compared to the wild type. Studies on humans have also shown that nemaline myopathy actin mutants are expressed at relatively normal levels, as are the majority of other sarcomeric proteins examined, with the exception of nebulin, which has more variable levels of expression (Ilkovski *et al.*, 2004).

Arthrin is a stable mono-ubiquitinated form of actin, with a molecular weight of 55 kDa, that forms part of the thin filament in *Drosophila* IFM (Ball *et al.*, 1987; Burgess *et al.*, 2004; Schmitz *et al.*, 2003). The presence of a band corresponding to the molecular weight of arthrin in homozygous $Act88F^{KM88}$ flies has previously been demonstrated not to be arthrin (Clayton *et al.*, 1998).

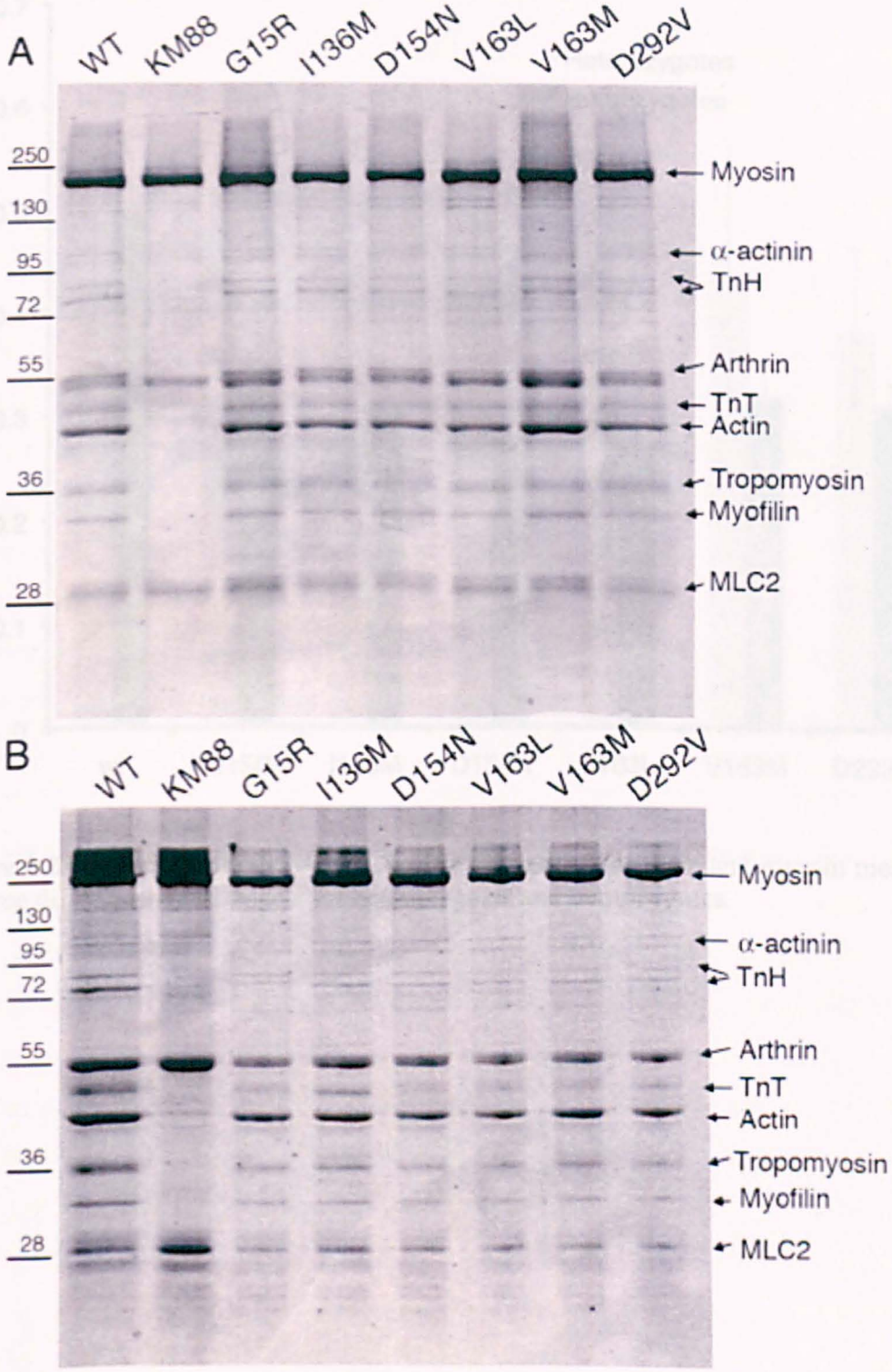

Figure 3.22. Coomassie blue stained 1-D SDS PAGE analysis of sarcomeric proteins from intact IFM. 10% SDS gel of IFM from: **(A)** wild-type, *Act88F* null (KM88) homozygous and *Act88F* heterozygous mutants; **(B)** wild-type, homozygous *Act88F* null (KM88) and *Act88F* mutants. Image created by Dr. Peckham.

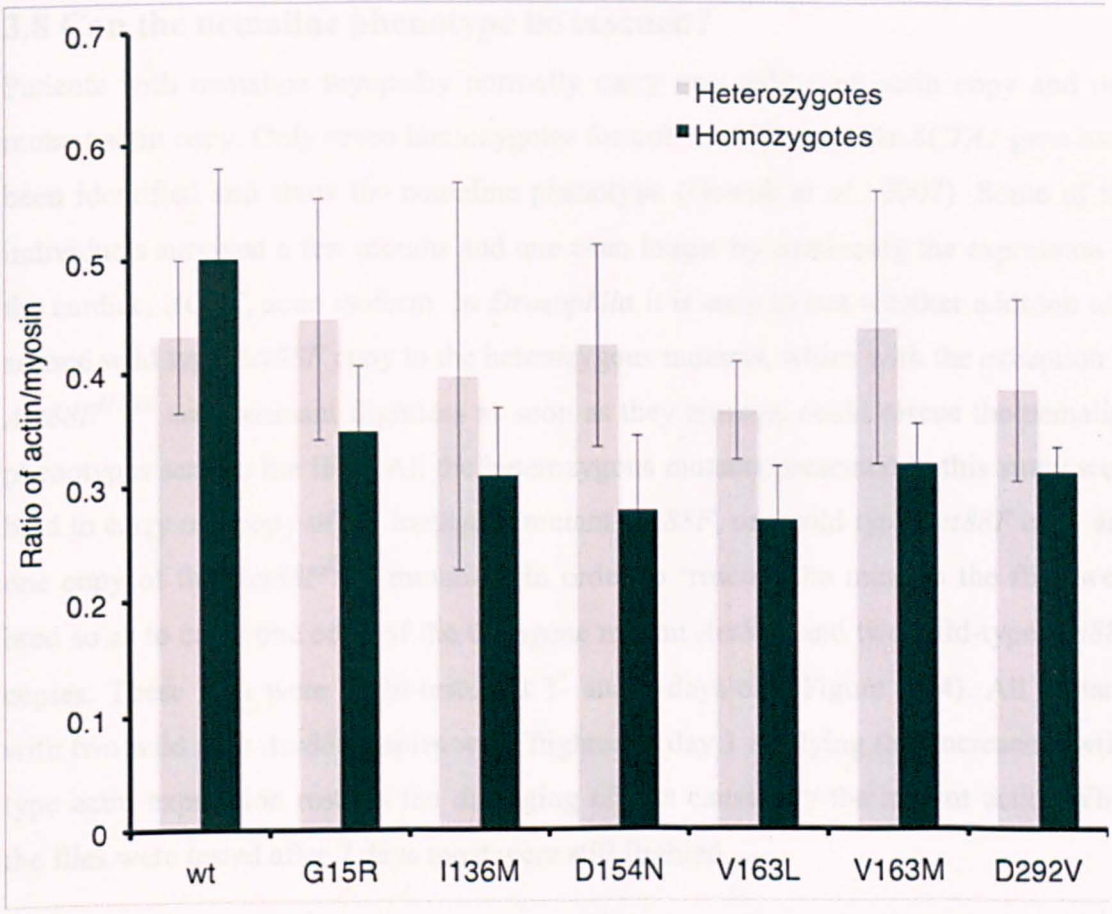

Figure 3.23. Actin-myosin ratios of *Act88F* mutants. The actin and myosin measured by three different 1-D SDS gels for heterozygotes and homozygotes.

3.8 Can the nemaline phenotype be rescued?

Patients with nemaline myopathy normally carry one wild type actin copy and one mutant actin copy. Only seven homozygotes for null mutations in the *ACTA1* gene have been identified and show the nemaline phenotype (Nowak *et al.*, 2007). Some of the individuals survived a few months and one even longer by continuing the expression of the cardiac, *ACTC*, actin isoform. In *Drosophila* it is easy to test whether addition of a second wild type *Act88F* copy to the heterozygous mutants, which with the exception of $Act88F^{I136M}$ are dominant flightless as soon as they emerge, could rescue the nemaline phenotypes seen in the IFM. All the heterozygous mutants presented in this study were bred to carry one copy of the transgene mutant *Act88F*, one wild type *Act88F* copy and one copy of the $Act88F^{KM88}$ mutation. In order to 'rescue' the mutants the flies were bred so as to carry one copy of the transgene mutant *Act88F* and two wild-type *Act88F* copies. These flies were flight-tested at 1- and 7-days-old (Figure 3.24). All mutants with two wild type *Act88F* copies were flighted at day 1 implying that increasing wild-type actin expression rescues the damaging effects caused by the mutant actin. When the flies were tested after 7 days most were still flighted.

However in the case of the $Act88F^{V163L}$ and $Act88F^{D154N}$ 'rescued' mutants the percentage of flighted flies was not as high as for the others and some displayed the wings-up phenotype, which is sometimes associated with muscle hypercontraction. When the IFM are hypercontracted they appear torn from the cuticle and bunched in the middle or either side of the thorax by polarized light microscopy. The correlation between the wings-up and hypercontraction phenotypes is true for IFM mutants for the *Act88F*, *TnI*, *TnT* and *Tm* genes. However, a few *Act88F* mutants display the wings-up phenotype but their IFM are not hypercontracted (An and Mogami, 1996). In order to see if the IFM of the 'rescued' $Act88F^{V163L}$ and $Act88F^{D154N}$ mutants that display the wings-up phenotype are hypercontracted, polarized light microscopy was performed. This showed that the IFM are not birefringent and only the TDT (jumping) muscle can be seen (Figure 3.25). Lack of polarized light signal implies that there is absence of ordered structure in these muscles but does not imply a hypercontracted phenotype. This result is not surprising as these mutants showed the most severe phenotypes in electron microscopy images amongst the transgenics presented in this study.

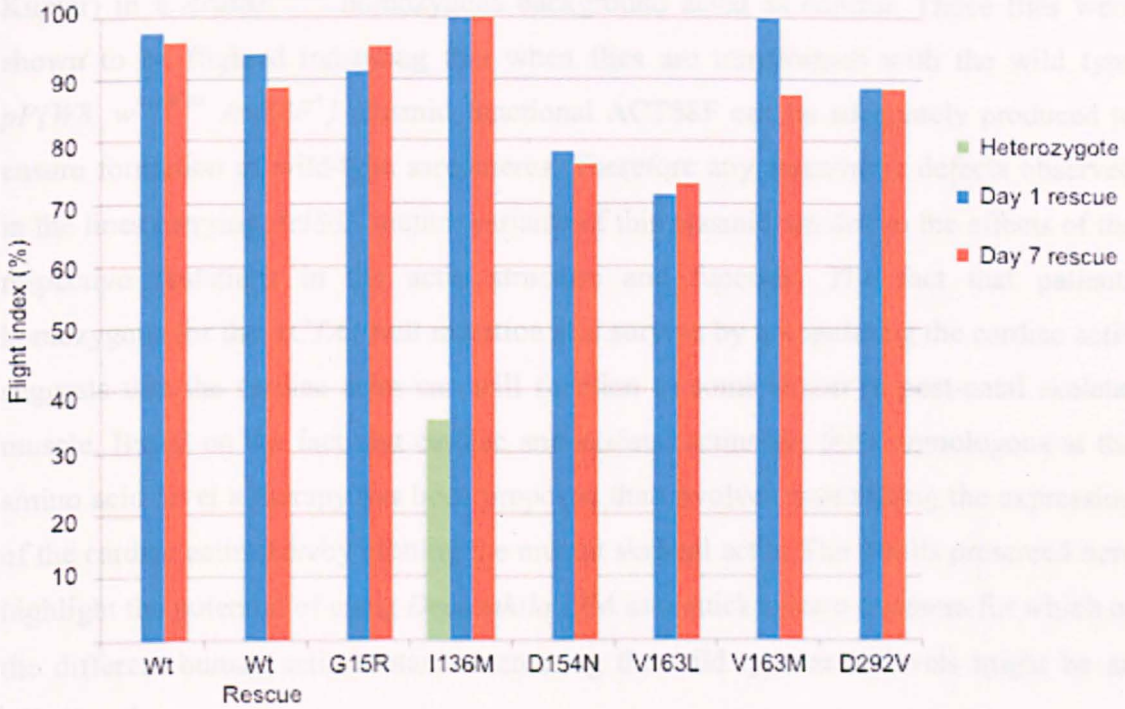

Figure 3.24. Flight-testing of 'rescued' mutants. Flies homozygous for the P-element insert containing wild type *Act88F* in an *Act88F* null background (Wt rescue) were flight-tested at days 1 and 7. Transgenic flies containing two wild type and one transgene mutant *Act88F* copy were flight-tested at days 1 (blue bars) and 7 (red bars). Mutant heterozygotes containing a wild type and a mutant *Act88F* copy were flight-tested at day 1 (green bars).

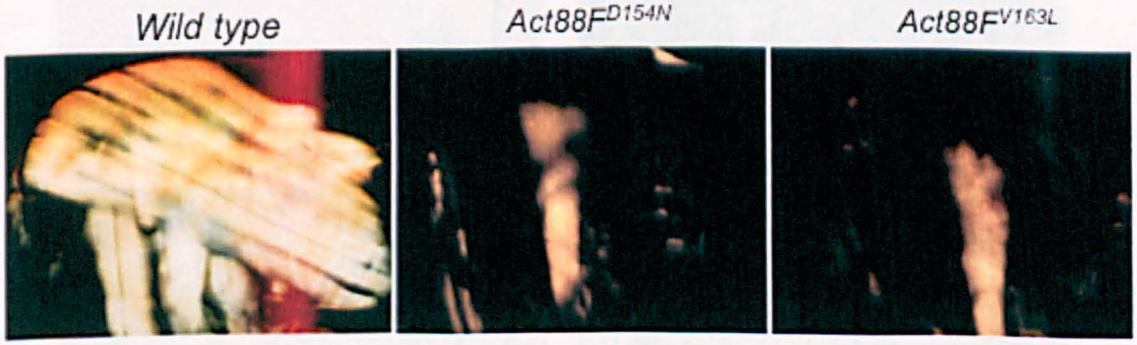

Figure 3.25. Polarized light analysis of *Act88F*^{D154N} and *Act88F*^{V163L} mutants with two wild type *Act88F* copies. The IFM of these mutants are not birefringent despite having two wild type actin copies, only the jump muscle can be seen.

Representative TEM images of the flighted *Act88F*^{V163L} and *Act88F*^{D154N} (Figure 3.26) rescued mutants show normal sarcomeres. In the case of the *Act88F*^{D154N} animals, which despite having two wild type *Act88F* copies were flightless and did not show the wings-up phenotype the sarcomeres also appear normal (Figure 3.26). The 'wild type rescue' line homozygous for the transgenic wild type *Act88F* copy (created by Vikash

Kumar) in a *Act88F*^{KM88} homozygous background acted as control. Those flies were shown to be flighted indicating that when flies are transformed with the wild type *pP{W8, w*$^{+mW.hs}$ *Act88F*$^{+}$*}* plasmid functional ACT88F can be adequately produced to ensure formation of wild-type sarcomeres. Therefore any sarcomeric defects observed in the lines carrying *Act88F* mutant variants of this plasmid are due to the effects of the respective mutations in the actin structure and function. The fact that patients homozygous for the *ACTA1* null mutation still survive by upregulating the cardiac actin suggests that the cardiac actin can still function to some extent in post-natal skeletal muscle. Based on the fact that cardiac and skeletal actins are 99% homologous at the amino acid level a therapy has been proposed that involves maintaining the expression of the cardiac actin thereby diluting the mutant skeletal actin. The results presented here highlight the potential of using *Drosophila* IFM as a quick system to assess for which of the different human actin mutants increasing the wild type actin levels might be an effective therapy.

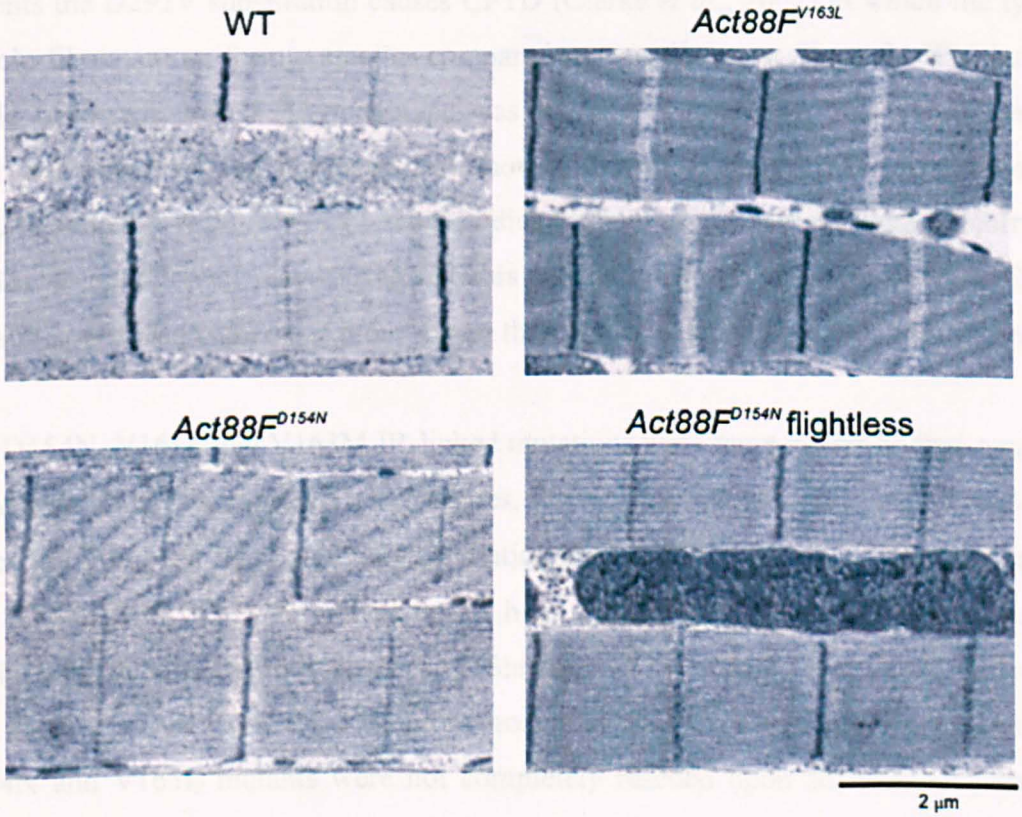

Figure 3.26. TEM images of the D154N and V163L transgenics containing two wild-type and one mutant Act88F copies. The sarcomeres of the rescued mutants appear like that of the wild type, though the D154N mutant was flightless despite having a second wild type actin copy and not displaying the wings-up phenotype.

3.9 Ranking of the nemaline myopathy mutants

The *Act88F* mutants have been ranked according to severity and compared to the published clinical severity of the equivalent mutations in human patients (Table 3.3) (Sparrow *et al.*, 2003; Laing *et al.*, 2009). The criteria used to rank the Drosophila mutants are based on the extent of sarcomeric disruption in each mutant, the flight ability as heterozygotes, and how well the mutations were rescued by adding an extra wild type actin copy.

The mutation I136M was the mildest, it was the only that produced some flighted heterozygotes and showed the less pronounced sarcomeric disruption as heterozygotes and homozygotes (except for D292V). The I136M is also classified as having a mild disease phenotype in patients (Ilkovski *et al.*, 2001). The D292V mutation was more severe than I136M as there were areas showing myofibril disarray and normal myofibrils at whole muscle immunostaining of heterozygous and homozygous flies. In patients the D292V substitution causes CFTD (Clarke *et al.*, 2007) in which the type I muscle fibres are uniformly smaller compared to type II fibres. Since fly IFM have a single fibre type the CFTD phenotype was not seen in the IFM. The G15R mutants (both heterozygotes and homozygotes) showed worse sarcomeric disruption than the D292V mutation with very large zebra bodies throughout the muscle. Patients carrying the G15R mutation displayed AM but this phenotype was not found in flies. These mutations were also ranked as more severe than the I136M mutation in human patients.

The D154N, V163L and V163M IR-linked mutations were more severe as they resulted in the formation of sarcoplasmic aggregates, intranuclear rods, Z-rings and other Z-disc structures. Amongst them the D154N mutation showed the most severe muscle disarray and abolished myofibril formation in the homozygote state. In humans this mutation displays all three nemaline phenotypes (Shröeder *et al.*, 2004). The V163L mutation was less severe than D154N as some homozygous flies did form myofibrils. Both the D154N and V163L mutants were not completely rescued upon addition of a second wild type actin copy. The V163M mutation was less severe; it did not abolish myofibril formation in homozygotes and completely rescued upon addition of a second wild type actin copy, which was not the case with the D154N and V163L mutants. Also based on clinical data in human patients, the V163L mutation is classified as severe congenital

(Goebel *et al.*, 1997a) whereas V163M is described as typical congenital (Sparrow *et al.*, 2003).

Table 3.3. Comparison of the muscle phenotypes caused by the actin mutations in human patients and in the *Drosophila* IFM.

Human biopsy		Drosophila IFM
Mutation	**Classification**	**Phenotypes**
D154N	Severe AM, IR, NM	Zebra bodies, Z-rings, intranuclear rods, Z-body aggregates, muscle structure is more disrupted than V163L, addition of an extra copy of wild type actin does not completely rescue the phenotype
V163L	Severe AM, IR	Zebra bodies, Z-rings, intranuclear rods, muscle structure is more disrupted than V163M, incomplete rescue, addition of an extra copy of wild type actin does not completely rescue the phenotype
V163M	AM, IR	Zebra bodies, Z-rings, intranuclear rods, Z-body aggregates
G15R	AM, NM	Large zebra-bodies throughout muscle
D292V	CFTD	Some zebra bodies and disorganized muscle structure in heterozygotes. Homozygotes have relatively normal muscle structure.
I136M	Mild NM	Minor effects on muscle structure in heterozygotes, zebra bodies only found in homozygotes, small % of flies can fly

3.10 Discussion

3.10.1 Drosophila IFM nemaline myopathy mutants

Three main characteristic features are seen in the muscles of patients with NM; actin filament aggregate myopathy (AM), nemaline myopathy (NM), and intranuclear rods, in which actin filaments form aggregates in the nucleus. Introducing NM-related actin mutations into the *Drosophila* IFM *Act88F* gene has resulted in a range of phenotypes in the muscles that show some important similarities to those seen in human patients. The types of structures observed and degree of severity for each mutation depends to the mutant actin expressed.

The main observation is that the actin mutations affect the ability of the IFM to form normal myofibrils, which in turn results in flightlessness. The only exception are the $Act88F^{I136M}/+$ heterozygotes that retain some flight ability. Homozygous actin mutants still contain actin filaments suggesting that none of the mutations prevent actin polymerization. Reduced myofibril diameter in the D154N and D292V mutants as well as shorter sarcomeres in the V163L mutant suggest that less F-actin is being

incorporated into the myofibrils. The concomitant reduction in myofibrillar volume would result in reduced power output and inability to support flight. However, since all the mutants also have mild to severe disruption of sarcomere organization (similar to patients), the ability of the mutant muscles to power flight would be severely impaired. Other features of the disease identified in *Drosophila* IFM mutants were Z-disc streaming, myofibrillar disruption, branching of the myofibrils to form separate myofibrils that are only connected at the site of branching and 'whirling' of actin filaments. An interesting feature of the IR-linked mutants was the Z-ring phenotype, which has never been previously reported in humans or in other model systems.

The pathological characteristic of nemaline myopathy is the presence of electron-dense rods of different size and shape at the EM level. The rods, which consist of Z-disc material are usually found under the sarcolemma although they can be also seen within the nucleus or within the sarcomere. Here some of the *Drosophila* mutants produced sarcoplasmic Z-body aggregates, which were smaller than the ones seen in humans. The continuous turnover of skeletal muscle proteins in human muscle supports the formation of large protein aggregates. In the IFM of adult flies there is no evidence for repair of damaged muscle or continuous expression of muscle proteins. Hence large protein aggregates may be more difficult to form in the IFM. Furthermore the rods found in patients do not accumulate uniformly within the muscle, some myofibrils contain more rods than others. In *Drosophila* the Z-body aggregates emerge occasionally from the Z-discs or they accumulate in areas lacking any other material. In the patient with the V163M *ACTA1* mutation the cytoplasmic rods were much smaller than the intranuclear rods (Hutchinson *et al.*, 2006). It was observed that the Z-body aggregates of the *Drosophila* V163M mutant were half the length of the IRs (Figures 3.14; 3.16).

Actin filament aggregate myopathy is usually associated with severe NM clinical cases. In patient muscle biopsies actin filament aggregate myopathy is shown as filamentous accumulations within a large region of amorphous material or as large aggregations of actin filaments in the muscle fibre. Here a phenotype resembling actin filament aggregate myopathy was observed in the V163M mutant. EM analysis showed a 1.2 μm long accumulation of filamentous material next to sarcomeres. This accumulation is very small in comparison to the actin filament aggregate myopathy areas that some times occupy a large part of the patient's fibre. The lack of continuous turnover of

muscle proteins in the IFM of adult flies could be why only small protein aggregates can form. The V163M was one of the very severe IFM mutants and represents the only occasion when the actin filament aggregate myopathy -like phenotype was observed. The D154N and V163L mutations also result in actin filament aggregate myopathy in humans but the phenotype was not observed by EM analysis in *Drosophila* IFM. Actin filament aggregate myopathy is a very rare phenotype and is often missed in the human biopsies. This could also be the case here and perhaps if more flies were examined actin filament aggregate myopathy-like phenotypes would be identified in transgenics carrying the D154N and V163L mutations.

The third phenotype associated with the disorder, intranuclear rod myopathy, is also rarely found in human patients. Expressing the three different IR-linked human mutations (D154N, V163L, V163M) in *Drosophila* resulted in the formation of filamentous actin accumulations in the IFM nuclei of all three mutants. The human IRs have been shown to form loosely arranged filamentous actin accumulations like the ones formed in the *Drosophila* IR-linked mutants. However the ones seen in humans can be rod-like which was never the case in any of the three *Drosophila* IR-linked mutants. The IRs in the patient carrying the V163M *ACTA1* mutation varied between 2-8 μm in length (Hutchinson *et al.*, 2006). The Drosophila IRs as measured from confocal images of whole muscle stained with DAPI and phalloidin seem to vary between 5-12 μm. By phalloidin staining the *Drosophila* IRs are similar to the ones observed in cell culture studies (Ilkovski *et al.*, 2004). A similarity between the human, the cell culture and the *Drosophila* IRs is that all three seem to distort the nuclei. Interestingly the filamentous actin accumulations found in *Drosophila* nuclei resemble the actin filament aggregate myopathy-like accumulations found in the sarcoplasm of the V163M mutants. In *Drosophila* IFM intranuclear rods were only observed in the most severe mutants D154N, V163L and V163M. They were mostly seen in the V163L mutants, then in the V163M and rarely seen in the D154N. Among nemaline myopathy patients there is also variability in the percentage of myofibres with intranuclear rods.

For the first time in an intact model genetic organism two of the rare phenotypes of the disease were recapitulated. The *Drosophila* intranuclear rods are very similar to the human ones and are frequently found in the IFM nuclei suggesting that this is a good model system with which to study their appearance. The actin filament aggregate

myopathy-like phenotype was difficult to reproduce, hence *Drosophila* IFM may not be an ideal system to understand the aetiology of this phenotype.

3.10.2 The effects of the *Act88F* mutations vary between muscle fibres of a fly population

A variation in severity of the phenotypes was observed amongst flies carrying the same mutation. This was observed both by EM or whole muscle staining for each mutant. This is not only a feature of *Drosophila* IFM, but also of human patients. Similar phenotypes can be observed in more than one patient such as with the H42Y mutation where 3 out of 4 patients show IR (Sparrow *et al.*, 2003). In contrast the G270C mutation showed high variation in phenotypes across 8 patients from mild to severe nemaline myopathy (Sparrow *et al.*, 2003). The variations in severity between unrelated patients with the same mutation as well as the intra-familial variation suggests that other factors could be affecting the phenotype caused by actin mutations and this may also be the case in *Drosophila.*

Furthermore, a phenotype can be observed more frequently in some patients than in others. For example muscle biopsies of patients suffering from intranuclear rod myopathy show that with some mutants the number of affected nuclei is many (80 % and 75%, Barohn *et al.*, 1994 and Goebel *et al.*, 1997b, respectively) whereas in others the intranuclear rods are infrequent (2 %) (Fukunaga *et al.*, 1980). This could also be the case for the *Drosophila* $Act88F^{D154N}/+$ heterozygous mutants, which do not show IRs as often as the $Act88F^{V163L}/+$ and the $Act88F^{V163M}/+$ heterozygotes.

In addition, the muscle disorganization of the *Act88F* mutants also varied within the same fibre. An example of that was shown in Figure 3.18, for the $Act88F^{V163L}/+$ heterozygous mutant, where sections at the top of the fibre were less disorganized than sections in the centre of the same fibre. Wild type and mutant IFM fibres were treated with NBT, the diagnostic stain used to identify central core disease in patient biopsies, but the fibres turned pale blue, which was not enough to see a difference between the two genotypes. Different fibre types in humans exhibit variations in the intensity with the stain being most effective in type 1 fibres, weakest in type 2A fibres and intermediate in 2B type fibres. Hence it is likely that the *Drosophila* IFM are a type of fibre that can only be poorly stained. The stain used for the *Drosophila* IFM is identical

to the one used for human biopsies. It therefore may be possible to stain the fibres by using a range of different pHs.

3.10.3 The *Drosophila Act88F* mutants vary in severity

In the *Drosophila* IFM mutants there is a correlation between severity and muscle disarray. The I136M mutation was the mildest as it was the only heterozygous mutant that produced some flighted flies and showed the least sarcomeric disruption. This mutant was also classified as mild disease phenotype in patients. The D292V mutation was more severe as it produced areas showing myofibril disarray but also normal myofibrils. In turn the G15R mutation showed worse sarcomeric disruption than the D292V mutation with very large zebra bodies throughout the muscle. The most severe effect both in a heterozygous and homozygous condition have had the D154N, V163L and V163M mutations. The D154N mutation was more severe as it abolished myofibril formation in the homozygous state whereas flies homozygous for the V163L mutation in some cases formed myofibrils thus making this a less severe mutation. The V163M homozygotes are less severe as they always produced myofibrils. Also based on clinical data in human patients, V163L is classified as severe congenital and V163M as typical congenital. Interestingly residues D154 and V163 are in neighbouring β-strands in one of the β-sheets in subdomain 3 of G-actin and produce similar defects (Figure 3.27). Overall the severity ranking of the *Drosophila Act88F* mutations matches the ranking of the human mutations.

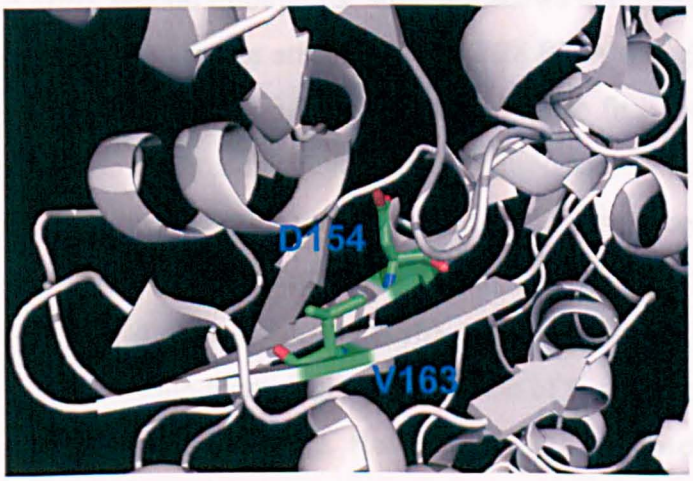

Figure 3.27. G-actin cartoon showing the D154 and V163 residues in the G-actin atomic structure. Image created using Pymol.

The correlation between severity and muscle disarray seen in the *Drosophila* IFM mutants is not surprising. In nemaline myopathy patients the proportion of individual myofibres occupied with nemaline rods, the size of the rod clusters and the degree of myofibrillar disruption appear to correlate with clinical severity. In the muscle fibres of individuals that exhibit the mild nemaline phenotype there is very little sarcomeric disruption by rods and the muscle fibres appear normal at the ultra-structural level. In contrast two individuals affected with the lethal severe congenital form of the disease showed both sarcomeric actin disorganization and regions of the myofibres devoid of sarcomeres (Ilovski *et al.*, 2001).

3.10.4 Molecular effects on actin structure

The D154 and V163 residues reside near a hydrophobic pocket at one end of the hydrophobic cleft in actin subdomain 1. This region of actin is a binding 'hot spot' for a large array of proteins to both G- and F-actin (reviewed in Dominguez, 2004). It mediates important interactions in five G-actin complexes (Bubb *et al.*, 2002; Burtnick *et al.*, 2004; Hertzog *et al.*, 2004; Klenchin *et al.*, 2003; McLaughlin *et al.*, 1993). Hence, mutations that disrupt the molecular surface of this region are highly likely to cause severe phenotypes.

An explanation why the V163L substitution could cause more severe defects than the V163M one came by examining the location of the V163 residue in the G-actin atomic structure. There the V163 residue is depicted as a partially buried amino acid (Figure 3.28 A). A cross section through the structure shows that there are two cavities near the V163 residue pointed by the arrows (Figure 3.28 B). Although methionine has a longer side chain compared to valine it would be possible to fit it into one of the two cavities. However, leucine is a branched hydrophobic amino acid; it would probably not fit as easily and would cause local rearrangement of the surface. Together these observations suggest why the V163L mutation causes a more severe phenotype than V163M in *Drosophila* IFM. Moreover, the V163 residue is located near actin-actin contacts and near the nucleotide-binding cleft. Disruption of that region by the mutation might result in loss of nucleotide binding. However, V163L was previously shown to polymerize similarly to the wild type (Costa *et al.*, 2004).

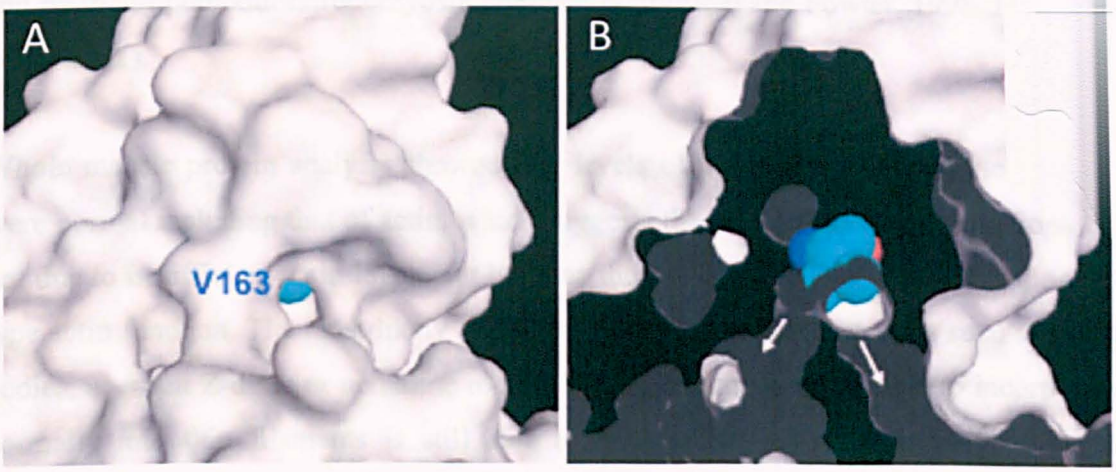

Figure 3.28. G-actin surface sections showing the V163 residue. (A) The V163 residue colored blue is shown to be partially buried. **(B)** Cross section through G-actin showing that V163 occupies a cavity that could accommodate a large amino acid. Images were created using Pymol.

3.10.5 Pointed end capping is affected in NM mutants

The main defect observed is that the actin mutations all affect the ability of the IFM to form normally structured myofibrils, which in turn results in flightlessness. The reduced diameter of the mutant myofibrils suggests that less actin is being incorporated into the myofibrils. The concomitant reduction in myofibrillar volume along with the aberrant sarcomere structure would result in inability to support flight. However, all of the actin mutants formed filaments in the homozygotes, so all the mutant actins maintain their ability to polymerize to form F-actin.

Immunostaining for tropomodulin in the G15R, V163L and V163M mutants showed that its localisation was less regular than in wild type and in other actin mutants. Effects on capping at the pointed end would result in increased rates of polymerisation/depolymerisation and irregular thin filament length. In human skeletal muscle, nebulin, a large protein found in the thin filament bound to actin has been suggested to regulate thin filament length (Labeit *et al.*, 1991). Mutations in nebulin result in congenital myopathies (Pelin *et al.*, 1999) with the patient's actin filament lengths being less well regulated (Ottenheijm *et al.*, 2009). *Drosophila* IFMs do not contain nebulin (Bullard *et al.*, 2006), hence regulation of the thin filament length is likely to depend mainly on capping protein and interactions of the thin filament with other proteins at the Z-disc (Schafer *et al.*, 1993) together with capping of the pointed

end by the tropomodulin/tropomyosin complex (Littlefield and Fowler, 1998; Littlefield *et al.*, 2001).

Whole muscle protein analysis showed that levels of a variety of sarcomeric proteins were normal including that of actin, which suggests that the effects of the mutations are not due to insufficient actin levels but because the mutant actin interferes with the wild type actin function. The most likely explanation for the various structures such as zebra bodies, aberrant Z-discs or nemaline rods is that the mutant actin, unable to incorporate normally into thin filaments is still able to bind to actin binding proteins such as α-actinin and in doing so, forms these aberrant structures.

3.10.6 Summary

The six human congenital actin myopathy mutations that were introduced into *Drosophila* produced similarities to the human phenotypes, including the rare phenotypes associated with the disease and their severity varied according to their human counterparts. Hence *Drosophila* provides a genetically tractable system which can be used to understand the aetiology behind this disease. The next chapter focuses on different genetic approaches that were used to study some of these mutations further.

Chapter 4: Use of genetic approaches to understand the NM phenotypes

4.1 Aims

Having produced a *Drosophila* model for NM, specific aspects of the *Act88F* mutants were investigated to understand the aetiology of certain phenotypes associated with the disease.

4.2 Introduction

To date no intact animal system has been reported where the NM-linked actin mutations have been introduced and that recapitulates all the disease phenotypes. Without an intact animal model system it is difficult to follow the appearance of the different phenotypes associated with congenital actin myopathies and understand their aetiology. The majority of 22 different *ACTA1*-linked actin mutants have been expressed *in vitro*, or examined *in vivo* in cultured fibroblasts, myoblasts or myotubes. These show a variety of defects, including the inability of the protein to fold (two mutants), or the formation of aggregates (Costa *et al.*, 2004; Domazetovska *et al.*, 2007a;b; Ilkovski *et al.*, 2004). However many questions remain unanswered such as why, how and when do the phenotypes associated with congenital actin myopathies appear in the patients? Which actin, wild type, mutant or a combination of both is present in the intranuclear rods?

The *Drosophila Act88F* mutants presented in Chapter 3 show some of the phenotypes associated with the disease such as intranuclear rods, sarcoplasmic rods and actin filament aggregate myopathy, although these are not recapitulated in exactly the same way as in the patients. For example the *Drosophila* intranuclear rods are not as electron dense, rod-like (by EM) and compact as the ones seen in patients. Only one case of actin filament aggregate myopathy was observed by EM (V163M). However, phalloidin-stained actin filaments, which were not assembled into sarcomeres did appear in several mutants. It is not possible to determine if these are similar to the human actin filament aggregate myopathy phenotype as they may had also consisted of myosin thick filaments. The *Drosophila* mutants also displayed sarcoplasmic actin and Z-body aggregates which are the closest representation of the human sarcoplasmic rods, although they are much smaller. The zebra body phenotype, which is uncommon in

humans, is observed frequently for most mutants studied here. Despite the lack of absolute similarity in the appearance of the phenotypes, the *Drosophila* IFM still present an intact animal system with which it can be possible to study these muscle abnormalities.

4.3 Developmental analysis of the intranuclear rod-containing actin mutants

Human patients with intranuclear actin rod myopathy present the rods at birth. This poses a difficulty in investigating how the rods appear in humans and suggests that IR form during development in the womb. *Drosophila* mutants for the IR-linked mutations display the IR phenotype and can therefore be used to understand when during muscle development the IRs first appear. *Drosophila* IFM development occurs during the pupal stage, which lasts approximately four days (96 hours after puparium formation, APF) at 25 °C. In order to see at what point during muscle development the intranuclear actin rods first appear in *Drosophila*, whole muscle imaging was carried in the IFM of pupae. IFM myofibrillogenesis starts at around 48 hours APF (Reedy and Beall, 1993), which coincides with peak *Act88F* expression (Fyrberg *et al.*, 1983). Since expression of the *Act88F* gene starts at early pupal stages (Fyrberg *et al.*, 1983) it is likely that the IR phenotype will be observed only at later pupal stages.

When adult $Act88F^{D154N}/+$, $Act88F^{V163L}/+$ and $Act88F^{V163M}/+$ heterozygous mutants were analyzed by immunofluorescence and EM not all the flies in each genotype showed intranuclear actin rods. Amongst the three mutants the $Act88F^{V163L}/+$ heterozygous flies in all the cases displayed the phenotype. Therefore in order to increase the chances of observing the phenotype at the pupal stages, only the $Act88F^{V163L}/+$ heterozygous pupae were studied. In 60 hour old APF $Act88F^{V163L}/+$ heterozygous pupae intranuclear rods were not found. The intranuclear rods were first observed in the IFM of 70 hour old $Act88F^{V163L}/+$ heterozygous pupae (Figure 4.1 arrows). Muscle disarray is obvious at that stage, the Z-discs vary in size and appear misshaped and Z-rings can be seen (Figure 4.1 arrow heads). This demonstrates that the IRs appear before the muscle development process is finished and muscle contraction has begun.

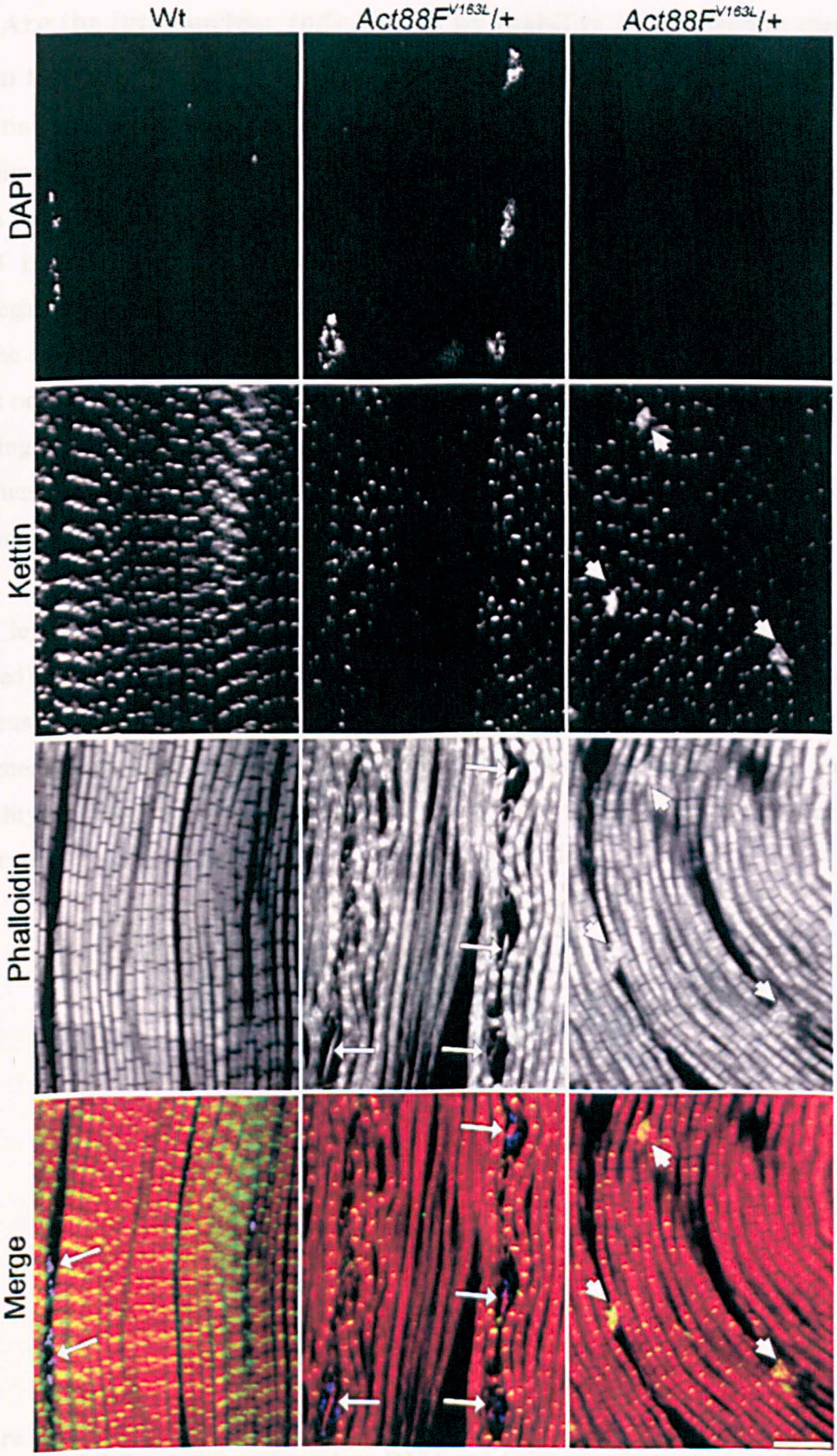

Figure 4.1. Intranuclear actin rods are present at 70 hours APF. Whole muscle light microscopy of wild type and Act88F^{V163L}/+ heterozygous mutant. Arrows indicate IRs and arrowheads Z-rings. Scale bar 5μm.

4.4 Are the intranuclear rods caused by inability to export the mutant actin from the nucleus?

G-actin is exported out of the nucleus via the nuclear export receptor specific for the profilin-actin complex, exportin 6 (Exp6) (Stüven *et al.*, 2003). It contacts primarily actin but the interaction is greatly enhanced in the presence of profilin. Knockdown of *Exp6* in *Drosophila* Schneider cells by RNAi results in the formation of actin aggregates inside the nucleus (Stüven *et al.*, 2003). The existence of the Exp6 pathway for the actin-profilin complex suggests that trafficking of the complex out of the nucleus must occur. The actin D154 and V163 residues are located near the proposed profilin binding sites on actin (Figure 4.2) (Schutt *et al.*, 1993). Hence mutations in these residues may affect the interaction between profilin and actin resulting in detainment of the mutant actin in the nucleus.

Low levels of G-actin as well as short F-actin filaments (that cannot be phalloidin-stained) can be found inside the nucleus. The presence of F-actin filaments inside the nucleus suggests that in the nuclear environment mechanisms exist to support actin polymerization. Therefore abnormally increased actin levels inside the nucleus and the inability to export the mutant actins could result in the formation of intranuclear rods observed in the nuclei of *Drosophila* IFM and human patients.

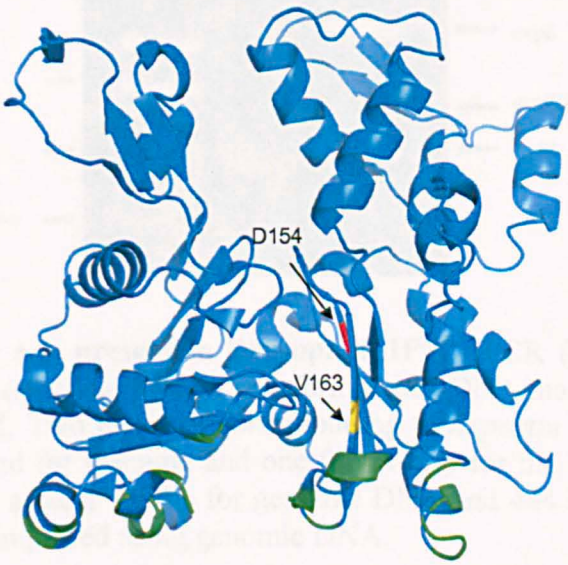

Figure 4.2. The proposed residues involved in profilin binding on actin. G-actin monomer with the position of residues D154 and V163 are shown in red and yellow, respectively. The proposed profilin residues that bind actin are shown in green. Image created in Pymol.

In order to see if *Exp6* is also expressed in the *Drosophila* IFM, PCR was performed to amplify the gene from cDNA made from isolated Drosophila IFM mRNA using the primers listed in Table 1 of Appendix I. Two PCR products were obtained for *Exp6* when cDNA was used. A 615 bp product corresponding to the expected product when IFM cDNA is used confirmed that the gene is expressed there (Figure 4.3). The second 1147 bp band corresponds to the product from genomic DNA probably due to genomic DNA contamination of the mRNA. The *Exp6* PCR product using genomic DNA is 1147 bp, which is the same size as the one of the cDNA (Figure 4.3).

Affymetrix microarray data of isolated IFM from *Drosophila* pupae by Dr Ari Franco show that profilin is also expressed in IFM (personal communication). As Exportin 6, actin and profilin are expressed in the *Drosophila* IFM it was assumed that ACT88F will be exported from the nucleus by the same mechanism described by Stüven *et al.*, 2003.

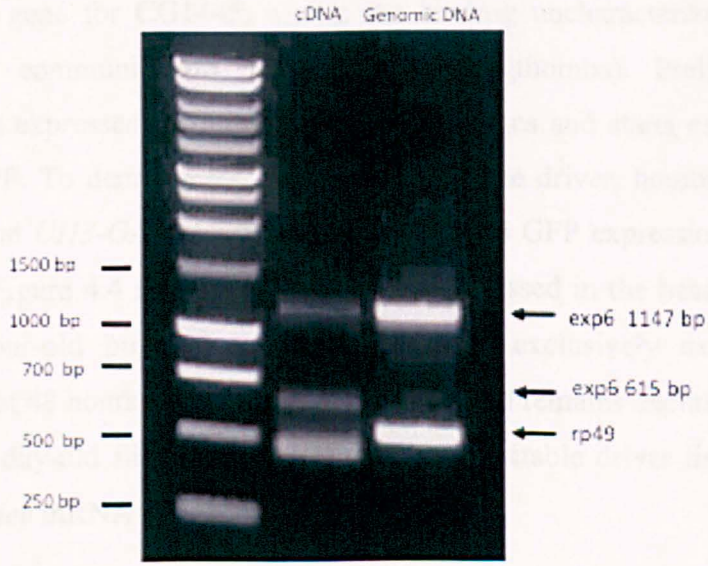

Figure 4.3. *Exportin 6* is present in Drosophila IFM. PCR for *Exportin 6* and the *ribosomal protein 49* (*rp49*) control was performed on cDNA made from RNA isolated from *Drosophila* IFM. Two products corresponding to *Exportin 6* are seen, one is the expected 1146 bp band for genomic and one for 614 bp for the cDNA. The expected band for *rp49* runs at around 609 bp for genomic DNA and 444 bp for the cDNA. The two genes were also amplified using genomic DNA.

The *chickadee* gene of *Drosophila* encodes profilin (Cooley *et al.*, 1992) with the null *chickadee* mutant resulting in late embryonic lethality (Verheyen and Cooley, 1994). The *GAL4*-UAS system offers the advantage of targeting downregulation of gene

expression by RNAi in both a spatial and temporal manner. In order to examine if a reduced ability of actin to bind to profilin results into intranuclear actin rods, an attempt was made to knockdown the profilin mRNA in *Drosophila* IFM. An RNAi line for *chickadee* (stock ID 9553R-3) was purchased from the National Institute of Genetics in Japan, NIG that targets all four reported *chickadee* variants. NIG has used the *Act5C-GAL4* driver at 28 °C which contains the *Actin5C* isoform promoter resulting in ubiquitous silencing of *chickadee*. As reported by the NIG website, the *UAS*-dsRNAi[*chic*] line has an additional 26 off targets. The later include the transcription factor Alhambra (CG1070), the RNA helicase Vasa (CG3506), the histone deacetylase HDAC6 (CG6170) as well as uncharacterized proteins. Though no muscle genes are reported.

The IFM-specific driver *UH3-GAL4* (kind gift of Dr. Upendra Nongthomba) was used to downregulate the expression of *chickadee* exclusively in the IFM at 25 °C. This driver was recovered from an enhancer trap screen. The *UH3-GAL4* insert is localised upstream of the gene for CG1445, a zinc ion binding uncharacterized transcription factor (personal communication, Dr. Upendra Nongthomba). Preliminary results indicate that it is expressed in wing disc in larval stages and starts expressing in the IFM after 30 APF. To demonstrate the specificity of the driver, homozygous flies for the UAS-*GFP* and *UH3-GAL4* inserts were crossed and GFP expression was followed in the progeny. Figure 4.4 shows that the GFP is expressed in the head, abdomen and thorax of 24-hour-old pupae but it then becomes exclusively expressed in the developing IFM at 48 hours APF (Figure 4.4 arrows) and remains exclusively expressed in the IFM of 1-day-old flies. Thus *UH3-GAL4* is a suitable driver line for knocking down the *chickadee* mRNA levels solely in the IFM.

Both the *UH3-GAL4* driver and the *UAS*-dsRNAi[*chic*] lines alone are flighted as heterozygotes (Figure 4.5) suggesting that the inserts do not have an affect on IFM structure or function. The *UAS*-dsRNAi[*chic*] line was driven using the *UH3-GAL4* driver but the flies never emerged and died as pupae. The *dmef2-GAL4* panmuscle driver (Ranganayakulu *et al.*, 1996) was also used to knockdown profilin mRNA. The *GAL4* activity in *Drosophila* is temperature dependent so that at 16 °C it is minimal and at 29 °C maximal (Jarrett, 2000). Since null *chickadee* mutants result in late embryonic lethality (Verheyen and Cooley, 1994), to avoid activation of the *dmef2-GAL4*

panmuscle driver at the embryonic and larval stages, the progeny from the *dmef2-GAL4* cross were first grown at 18 °C (the lowest temperature controlled available room for fly maintenance). Those individuals that had reached the pre-pupal stage were transferred to 25 °C to allow activation of the *dmef2-GAL4* driver. However, the progeny from this cross, died as pupae as did those driven with the *UH3-GAL4* driver. The lethality observed with both *GAL4* drivers could be due to the off-targets reported for this RNAi line.

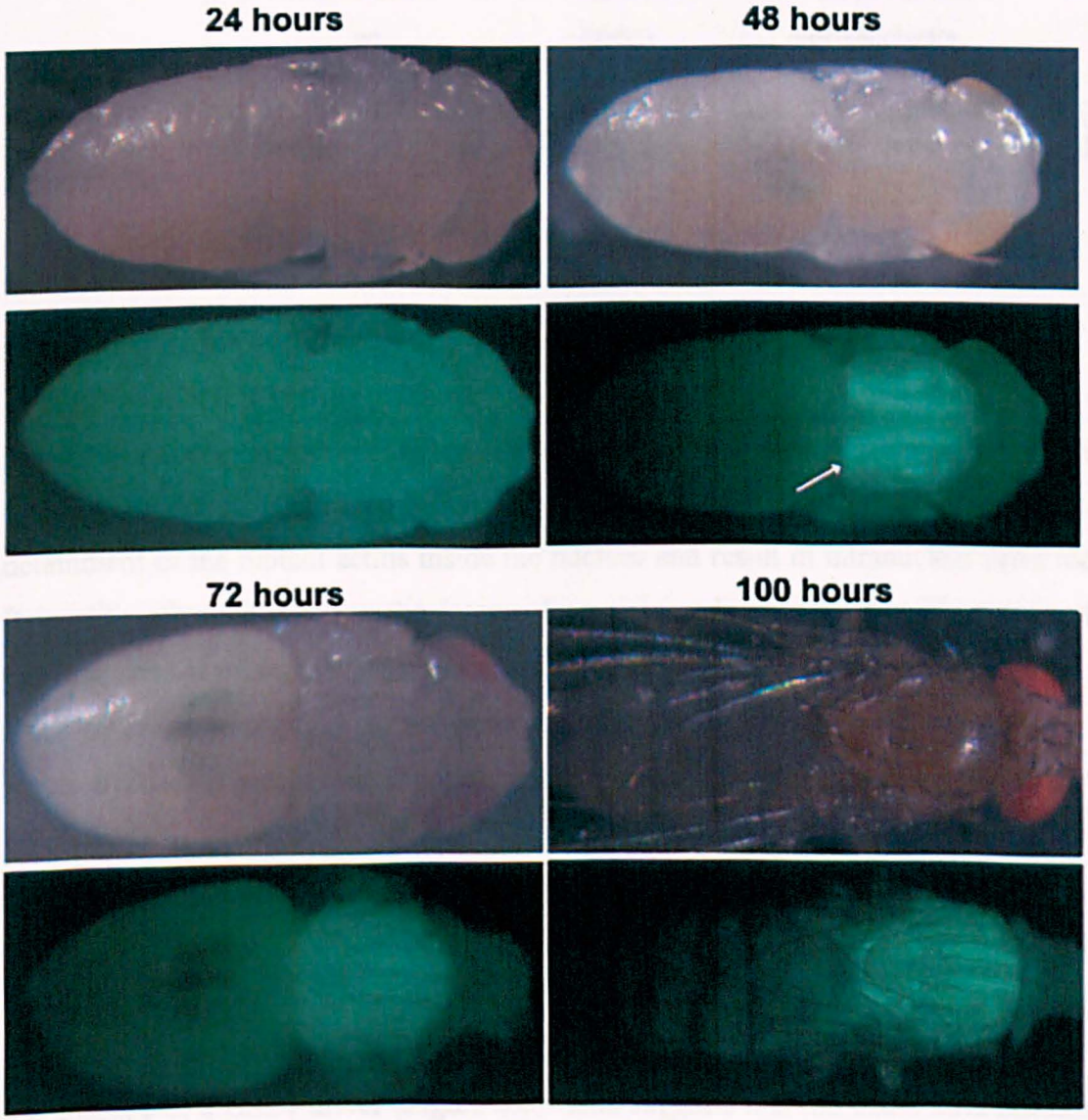

Figure 4.4. Pattern of expression of the *UH3* driver. Peeled pupae and 1-day-old fly are shown under normal light and by GFP imaging of the same specimens.

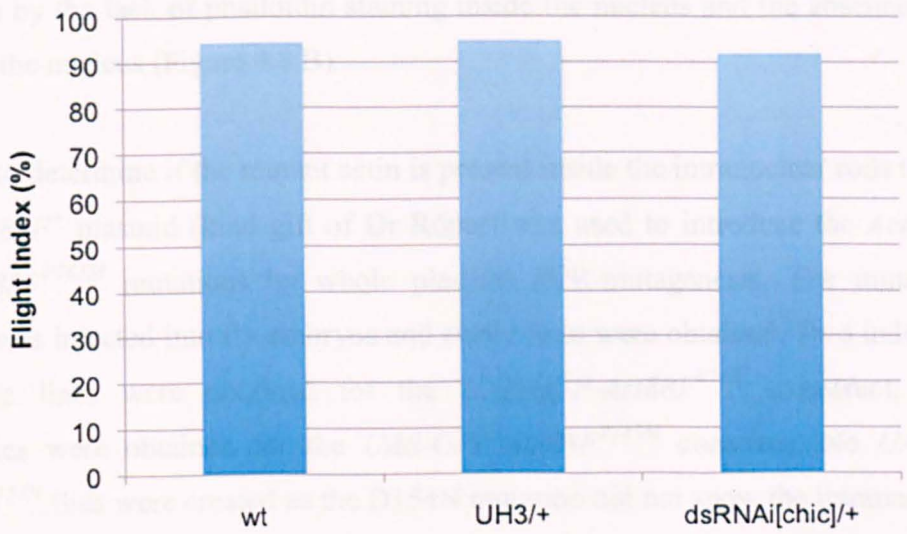

Figure 4.5. Flight ability of *UH3* and dsRNAi[*chic*] flies. The number of flies (n) tested was n = 54 for the wild type, n = 39 for the *UH3-GAL4*/+ and n = 37 for the dsRNAi[*chic*]/+.

4.5 Are the intranuclear rods composed of wild type or mutant actin?

In the *Drosophila* IFM the presence of the Exp6 pathway could mediate the transport of profilin-actin complexes out of the nucleus. This raises the question as to whether inability of the *Act88F* intranuclear rod variants to bind to profilin would lead to detainment of the mutant actins inside the nucleus and result in intranuclear actin rods. It is still unknown whether the intranuclear actin rods seen in nemaline myopathy patients consist of wild type, mutant actin or both species. This was investigated in *Drosophila* by fusing GFP to either the mutant or wild type ACT88F actin, so as to reveal which one localizes in the intranuclear rods. Transgenic flies expressing a *UAS-GFP-Act88F*$^{+}$ insert, where the *GFP* is attached to the 5'- end of the *Act88F* gene through a short linker sequence were previously reported not to cause obvious IFM sarcomeric structural defects, although the flies cannot fly when driven with the panmuscle *dmef2-GAL4* driver (Röper *et al.*, 2005). The *UAS-GFP-Act88F*$^{+}$ transgenic line was obtained from the Bloomington Stock Centre and was found to be flighted in the absence of a *GAL4* driver (Figure 4.6). This suggests that the insert does not affect muscle function and structure when it is not expressed, which was also supported by whole muscle staining (Figure 4.8 A). When the *UAS-GFP-Act88F*$^{+}$/+ flies were driven using the *UH3-GAL4* driver the muscle structure appears normal as expected (Figure 4.8 B) however the flies are flightless (Figure 4.6). Intranuclear rods are not observed

as shown by the lack of phalloidin staining inside the nucleus and the absence of GFP signal in the nucleus (Figure 4.8 B).

In order to determine if the mutant actin is present inside the intranuclear rods the *UAS-GFP-Act88F*$^{+}$ plasmid (kind gift of Dr Röper) was used to introduce the *Act88F*^{V163L} and *Act88F*^{V163M} mutations by whole plasmid PCR-mutagenesis. The mutagenized plasmid was injected into fly embryos and stable lines were obtained. Two independent transgenic lines were obtained for the *UAS-GFP-Act88F*^{V163L} construct, but no transgenics were obtained for the *UAS-GFP-Act88F*^{V163M} construct. No *UAS-GFP-Act88F*^{D154N} flies were created as the D154N mutation did not show the intranuclear rod phenotype as often when compared to the V163 mutation. Both the *UAS-GFP-Act88F*$^{+}$ and *UAS-GFP-Act88F*^{V163L}/+ transgenic lines were flighted in the absence of a *GAL4* driver (Figure 4.6) suggesting that these inserts do not affect muscle function and structure when they are not expressed. This was also supported by whole muscle staining (Figure 4.8 A and Figure 4.9 A). When the *UAS-GFP-Act88F*$^{+}$/+ flies were driven using the *UH3-GAL4* driver the muscle structure appears normal as expected (Figure 4.8 B). However the flies are flightless (Figure 4.6). Intranuclear rods are not observed as shown by the lack of phalloidin staining inside the nuclei and the absence of GFP signal in the nuclei (Figure 4.8 B).

In order to determine if the wild type actin is present in the intranuclear actin rods transgenic flies were created that were heterozygous for the *Act88F*^{V163L} and for the wild type *UAS-GFP-Act88F*$^{+}$ inserts. In order to achieve this, flies homozygous for the *Act88F*^{V163L} insert in the first chromosome and for the *UAS-GFP-Act88F*$^{+}$ insert in the third chromosome were created. These were then crossed to the IFM-specific *UH3-GAL4* driver which was previously put in homozygous *Act88F*^{KM88} actin null background. So in the progeny flies containing one copy of *UH3-GAL4*, one of the *Act88F*^{V163L} insert, one of the *UAS-GFP-Act88F*$^{+}$ insert and two of the *Act88F*^{KM88} insert were generated (Figure 4.7, 4.8 C). Fluorescence microscopy for these flies shows that the GFP signal does not colocalize with the intranuclear actin rods stained with phalloidin (Figure 4.8 C). This suggests that the intranuclear rods are not composed of wild type actin but instead they are composed solely of mutant actin. However, this result could also be due to the fact that the GFP fused to the actin does not allow the protein to enter inside the nucleus. Another interesting result in the same flies was that

the wild type actin fused to GFP did not colocalize with the sarcoplasmic rods (Figure 4.8 C bottom panel). Instead the latter were stained only with phalloidin, which implies that these actin aggregates consist solely of mutant actin. For the bottom panel in Figure 4.8 C DAPI staining is not shown as there were not any nuclei in that section.

The *UH3-GAL4*; *UAS-GFP-Act88F*^{V163L}*/+; Act88F*^{KM88}*/+* flies were also flightless (Figure 4.6). Whole muscle staining with DAPI showed that the *GFP-Act88F*^{V163L} actin localizes inside the nucleus (Figure 4.9 B arrowheads). This shows that the mutant actin is present in the nuclear actin rods and that the GFP does not prevent actin from entering the nucleus. However the GFP-signal appears "grainy" and that was also the case when anti-GFP antibody was used (Figure 4.9 C). These transgenics also displayed sarcoplasmic rods (Figure 4.9 C left phalloidin image arrows) and abnormally large Z-discs (Figure 4.9 C anti-GFP merge arrows and right phalloidin image curly bracket). Given the facts that only mutant actin is present in the intranuclear rods, that the IR-linked residues are near the profilin binding site, and that the exportin 6 pathway is present in *Drosophila* IFM, these observations suggest that inability to export the mutant actin from the nucleus is likely to be one of the underlying causes for the intranuclear rods.

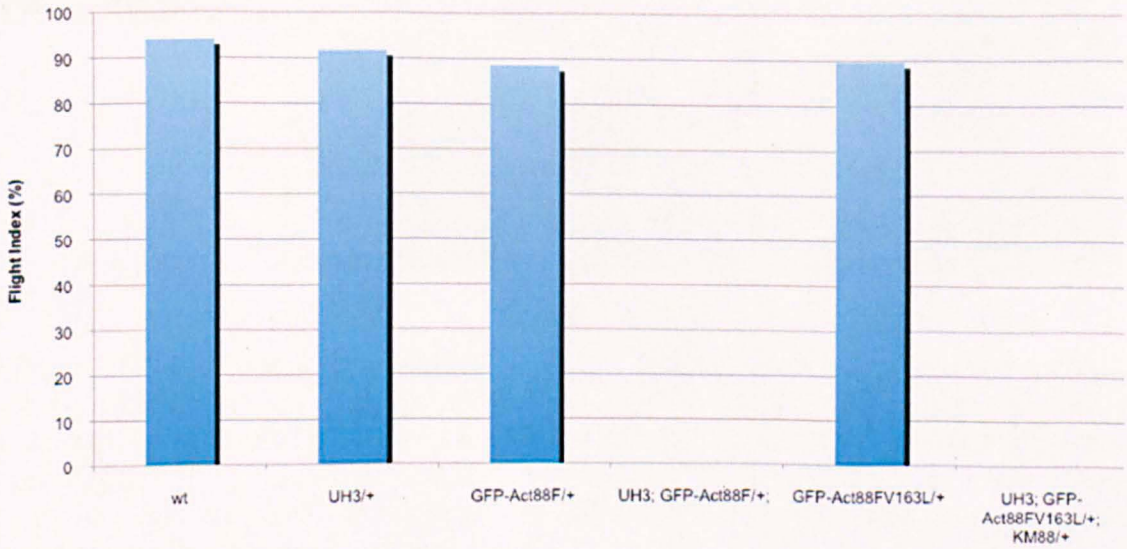

Figure 4.6. Flight-analysis of GFP-Act88F flies. Flight ability of wild type (n = 31), *UH3-GAL4/+* (n = 33), *UAS-GFP-Act88F*$^{+}$*/+* (n = 31), *UH3-GAL4/+*; *UAS-GFP-Act88F*$^{+}$*/+* (n = 40), *UAS-GFP-Act88F*^{V163L}*/+* (n = 26) and *UH3-GAL4/+*; *UAS-GFP-Act88F*^{V163L}*/+*; *Act88FKM88/+* (n = 36) (where n is the number of flies tested).

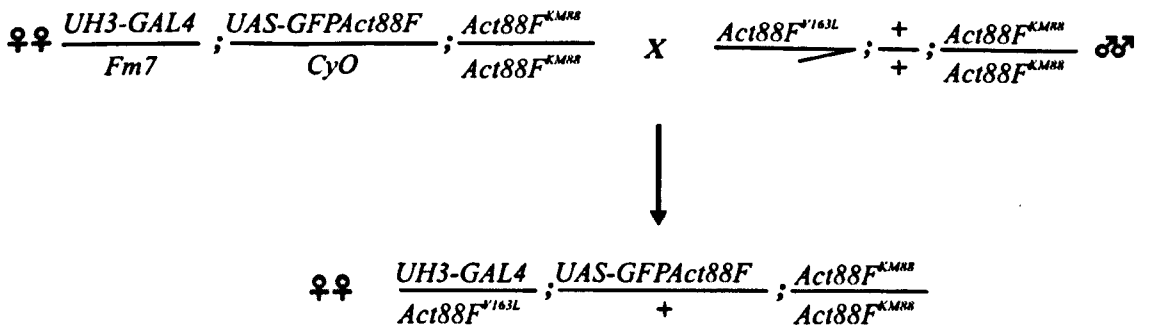

Figure 4.7. Crossing scheme to obtain the *UH3-GAL4/Act88F*^{V163L}; *UAS-GFP-Act88F*$^{+}$/+; *Act88F*^{KM88}/*Act88F*^{KM88} /+ flies.

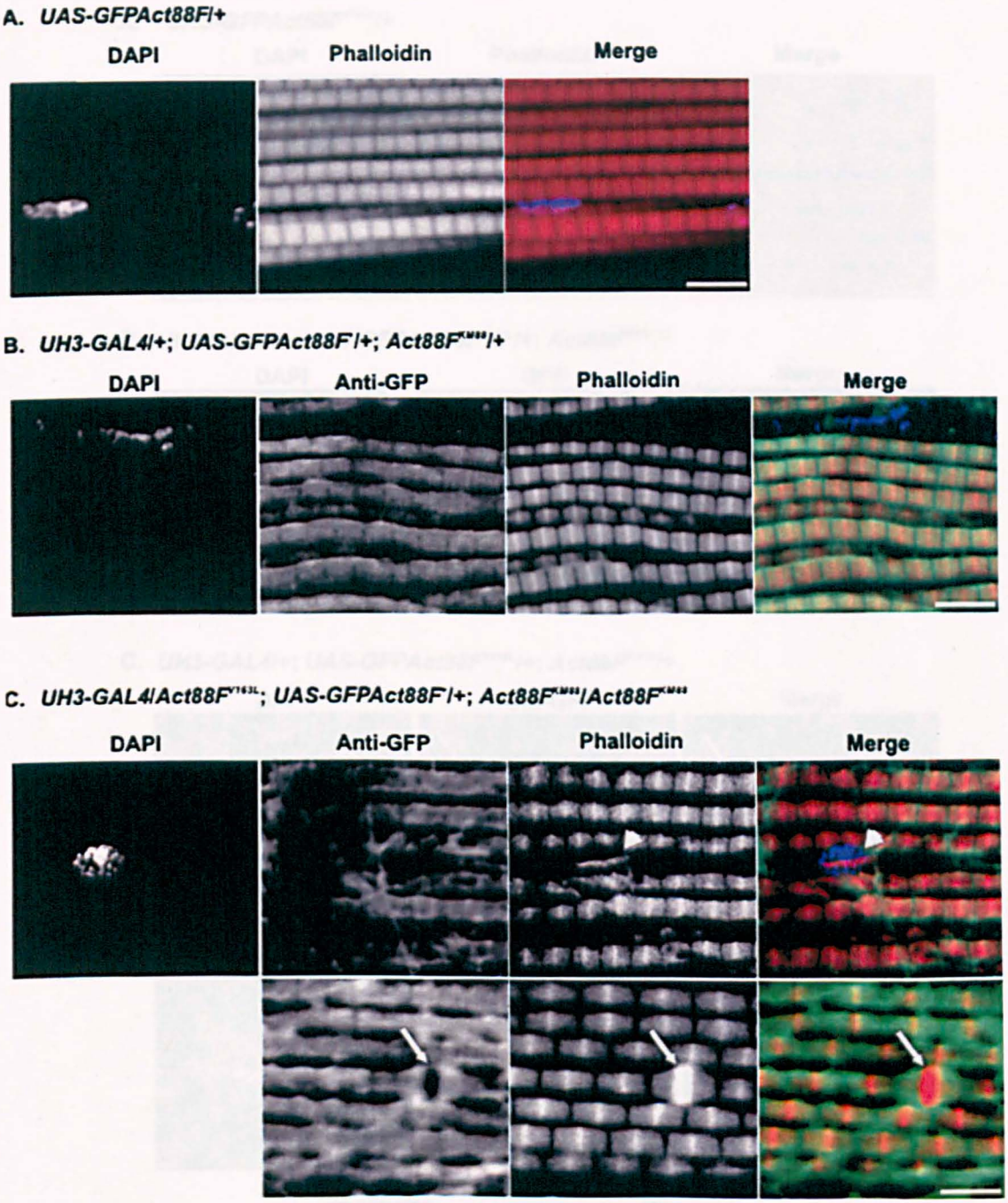

Figure 4.8. Wild type GFP-ACT88F does not localize to intranuclear rods. Whole muscle light microscopy of **(A)** *UAS-GFP-Act88F*$^{+}$*/+; Act88F*^{KM88}*/+* flies with DAPI and phalloidin, **(B)** *UH3-GAL4/+; UAS-GFP-Act88F*$^{+}$*/+; Act88F*^{KM88}*/+* and **(C)** *UH3-GAL4/Act88F*^{V163L}*; UAS-GFP-Act88F*$^{+}$*/+; Act88F*^{KM88}*/Act88F*^{KM88} flies with DAPI, phalloidin and anti-GFP. Arrowheads indicate intranuclear rods and arrows indicate sarcoplasmic aggregates. Scale bars: 5 μm.

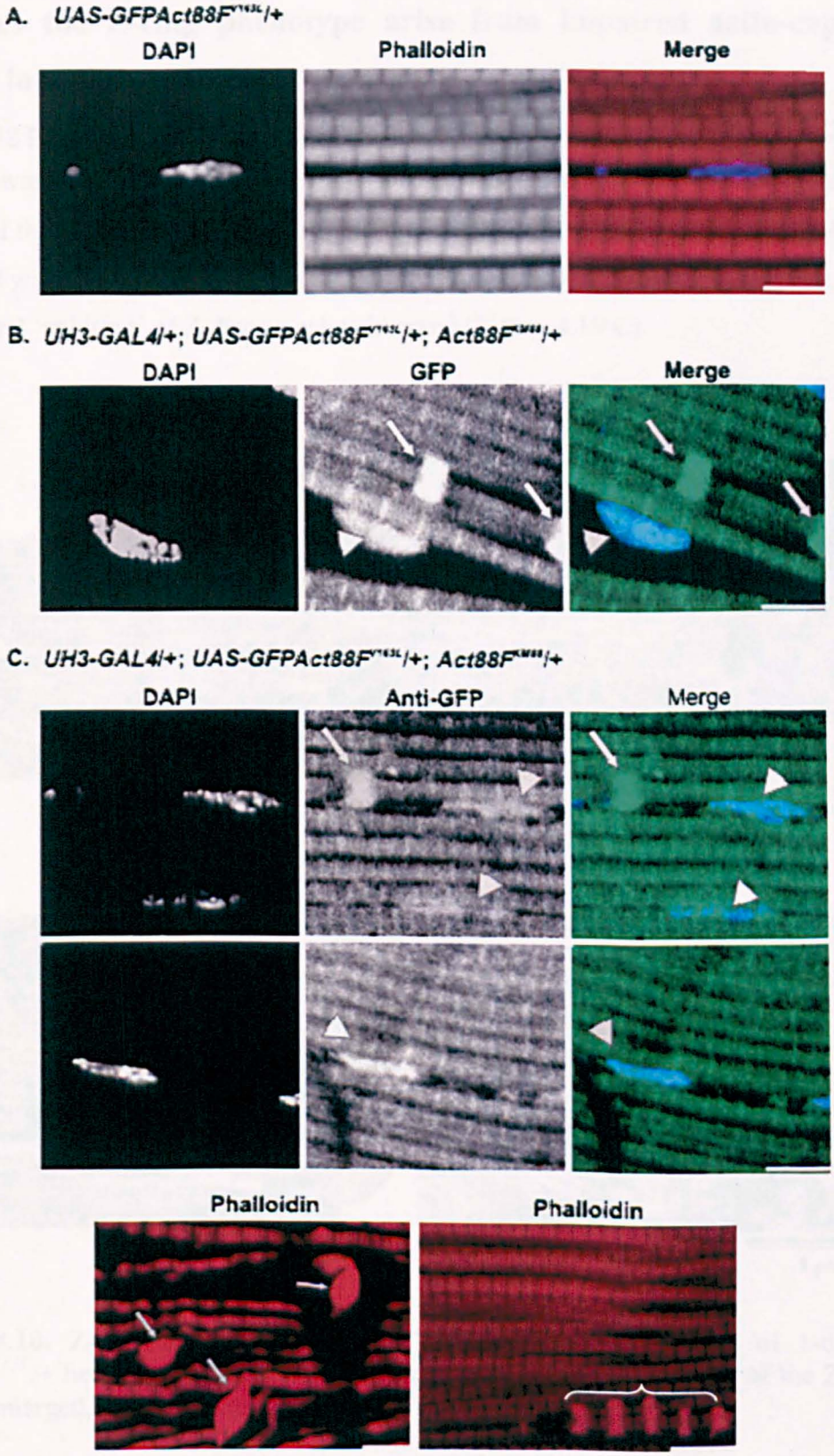

Figure 4.9. The intranuclear rods consist of *GFP-Act88F^{V163L}* actin. Whole muscle light microscopy of **(A)** *UAS-GFP-Act88F^{V163L}*/+ flies with DAPI and phalloidin, *UH3-GAL4*/+; *UAS-GFP-Act88F^{V163L}*/+; *Act88F^{KM88}*/+ flies with: **(B)** and **(C)** DAPI, anti-GFP and phalloidin. Intranuclear rods are indicated by arrowheads, sarcoplasmic aggregates by arrows and large Z-discs are encompassed by the curly bracket. Scale bars: 5 μm.

4.6 Does the Z-ring phenotype arise from impaired actin-capping protein interactions?

The Z-ring phenotype and the appearance of sarcoplasmic aggregates containing Z-disc proteins was a common feature of the *Drosophila* intranuclear rod-linked mutants. Images of the *Act88F*^{V163L}/+ heterozygous adults show parts of the Z-discs are enlarged and filled with material, which is less electron dense than the Z-disc (Figure 4.10 A, B). Also lateral 'splitting' of Z-discs can be observed (Figure 4.10 C).

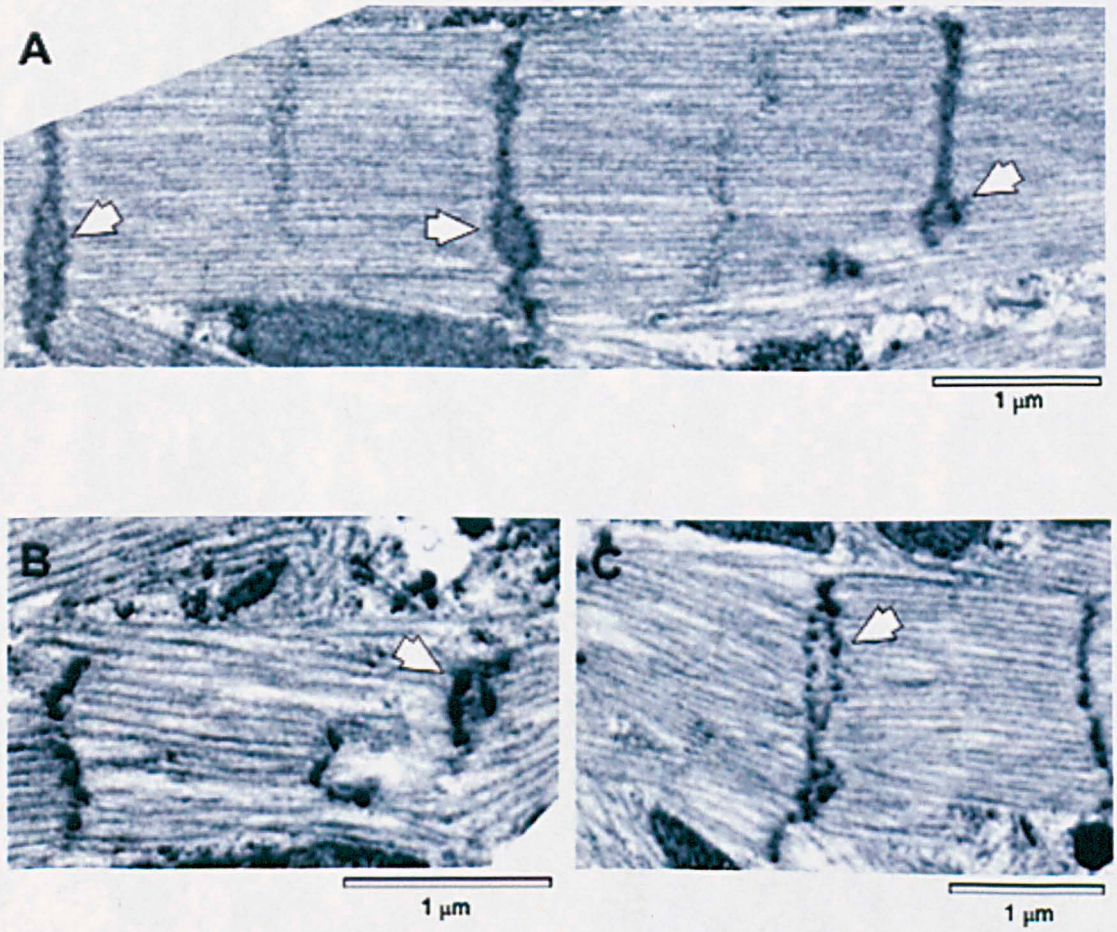

Figure 4.10. Z-disc defects in *Act88F*^{V163L}/+ heterozygotes. TEM of 1-day-old *Act88F*^{V163L}/+ heterozygote adults. **(A, B)** Arrowheads point at the parts of the Z-discs that are enlarged, **(C)** Arrowhead indicates a 'splitting' Z-disc.

Following the analysis of the IFM from 70 hour old pupae, which displayed Z-disc defects, 60 hour old pupae were also examined for both intranuclear rods and Z-disc abnormalities. IFM microdissections of 60 hour old APF pupae are more challenging preparations than those performed at later stages as it is difficult to detect by eye the small and translucent IFM. Also at that stage the developing IFM are not strongly attached to the tendon cells and are often lost during the preparation. In addition, it was thought too soon to notice muscle defects in pupae younger than 60 hours APF as myofibril formation starts at around 40-42 hours APF (Reedy and Beall, 1993b). Based on these facts pupae younger than 60 hours APF were not examined.

For the $Act88F^{V163L}$ mutation 38 heterozygote pupae were examined, 8 $Act88F^{D154N}/+$ and 5 $Act88F^{V163M}/+$ were examined at 60 hour APF. At this age Z-rings can already be seen and are bigger compared to the Z-discs (Figure 4.11 arrowhead). The Z-discs are found not to be properly aligned and are misshaped or smaller compared to the wild type ones. The Z-ring phenotype must not be caused by mechanical damage during use (at least at that age), as the muscles are not in use at 60 hours APF. These observations suggest that the mutant actins are affecting Z-disc assembly during very early muscle development. Moreover no intranuclear actin rods were observed for any of the mutants at this age.

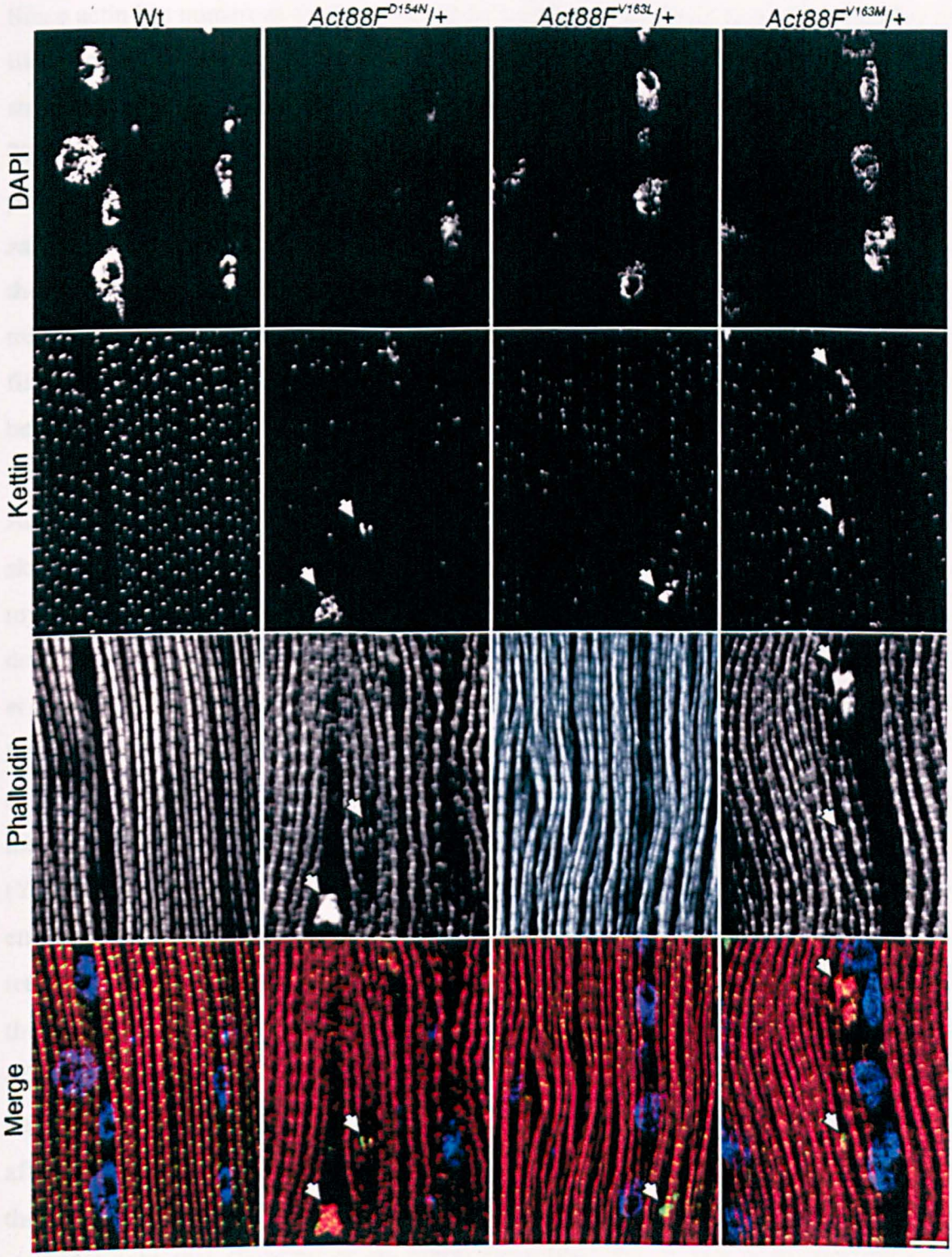

Figure 4.11. Z-rings are present at 60 hours APF. Whole muscle light microscopy of wild type, *Act88F*^{D154N}/+, *Act88F*^{V163L}/+ and *Act88F*^{V163M}/+ heterozygous mutants. Anti-kettin antibody was used to stain the Z-discs. Arrowheads indicate Z-rings. Scale bar 5μm.

Since actin has numerous binding partners it is difficult to pinpoint which interaction is likely to be impaired in the intranuclear rod-linked mutants. In many actin cytoskeletal structures thin filaments elongate principally from their barbed ends (Pollard *et al.*, 2000). In contrast, during IFM myofibrillogenesis the thin filaments elongate from their pointed ends (Mardahl-Dumesnil and Fowler, 2001). This process is regulated by *sanpodo*, the *Drosophila* homologue for the gene encoding for tropomodulin. Because the IR-linked mutants presented several Z-disc abnormalities it was suggested that there might be defective thin filament capping at the barbed end. If the barbed ends of the thin filaments are not capped actin could accumulate and present as electron dense material between the split Z-discs (Figure 4.10 A).

Actin is capped at the barbed end by capping protein (CP), also known as CapZ in skeletal muscle. CP is thought to nucleate thin filament assembly during myofibrillogenesis (Schafer *et al.*, 1995) and to stabilize actin filaments by preventing depolymerization and polymerization from the barbed end (Cooper *et al.*, 1999, Huang *et al.*, 2003). CP is a heterodimeric protein consisting of α and β subunits, which cap the first two actin protomers on the F-actin helix through their flexible C-terminal helical extensions (Wear *et al.*, 2003). In particular, the β tentacle of the CPβ subunit binds to the hydrophobic cleft between subdomain 1 and 3 of the end protomer in the filament (Yamashita *et al.*, 2003). According to the latest model by Narita *et al.*, 2006 for barbed end capping by CP, residue 167 on actin is implicated in the interaction with the β-tentacle of CPβ. Residues D154 and V163 on actin are therefore in close proximity to the proposed area where the β tentacle of the CPβ subunit binds. Furthermore, deletion of 12 amino acids from the C-terminus of the β1 subunit of CPβ in chicken myotubes has been shown to remove the ability of CPβ to bind to actin but otherwise does not affect the formation of the $\alpha\beta$ heterodimer (Hug *et al.*, 1992). The mutation abolishes the formation of the β-tentacle of CPβ, which results in actin aggregates and phalloidin-stained bright foci (Schafer *et al.*, 1985) resembling the Z-ring phenotype seen by immunofluorescence in the IR-linked actin mutants $Act88F^{D154N}$, $Act88F^{V163L}$ and $Act88F^{V163M}$. Altogether these observations raised the hypothesis as to whether actin-CPβ interactions are impaired in the IR-linked mutants.

Homologues of the mammalian CP α and β subunits exist in *Drosophila* which are called capping protein a and b (CPa and CPb) and each has only one reported gene

isoform and transcript in *Drosophila* (Hopmann *et al.* 1996). In order to investigate if the phenotype created by the actin mutants is due to inability to cap actin at the barbed end I looked for existing mutants or CP nulls. However, lines carrying null mutations for the genes are early larval lethal (Hopmann *et al.*, 1996), which highlights the importance of this protein in regulating actin polymerization at the barbed end. Partial loss of function alleles exist that are viable and affect only bristle morphology (Hopmann *et al.*, 1996). For those flies it was reported that flight ability is not affected, which would suggest that the IFM sarcomere structure is normal and devoid of Z-disc defects (Hopmann *et al.*, 1996). Another way to study CPb is to knock down gene expression using RNAi. An RNAi line targeted against the *Drosophila* CPb (transformant ID: 45668) exists and was purchased from the Vienna *Drosophila* RNAi Centre. According to the Vienna *Drosophila* RNAi Center website there is only one reported OFF target coding for the protein, 1-acylglycerol-3-phosphate O-acyltransferase activity (CG3812). As this is not a muscle protein, its targeting by RNAi is unlikely to be causing the Z-disc phenotypes observed here.

When the dsRNAi[*cpb*] flies were driven with either the *UH3-GAL4* and *dmef2-GAL4* drivers the majority were found to be flighted and only 17 % of those driven with *UH3-GAL4* and 22% of those driven with *dmef2-GAL4* were flightless (note that 8 % of the wild type flies fly down or are flightless) (Figure 4.12 A). Furthermore, when using either drivers, the cross resulted in lethality of late pupae. The lethality was quantified by measuring the number of dead and live late pupae and was found to be 23 % and (n = 39) and 55.8 % (n = 34) from crosses using the *UH3*-GAL4 and *dmef2-GAL4* drivers, respectively. These observations show that the RNAi is not effective in every fly thus resulting in pupal lethality when it has been the most effective, flightless adults when it has partially knocked down *cpb* mRNA and flighted adults when the RNAi has not been effective at all. Capping protein is not visible in an SDS-page gel due to its small quantities in muscle and it is not possible to compare the CPb protein levels in the wild type flies and the flies where the *cpb* message was downregulated. Anti-CPb antibody was used to confirm knockdown of *cpb* (kind gift of Dr. Miller) by Western blotting but its signal was very weak in wild type flies and thus it was not possible to use it.

Therefore, semi-quantitative PCR was performed to verify that the *cpb* mRNA had been knocked down. The primers for amplifying *cpb* were designed to span an intron and are listed in Table 1 of Appendix I. PCR was performed under identical conditions with varying cycles (30, 35 and 40) (Figure 4.12 B). The PCR shows that the mRNA for the *cpb* knocked-down flies is reduced only about 37 % at 30 cycles, 40 % at 35 cycles and remained the same at 40 cycles. This is not a surprise as the flight-testing results showed that the majority of the *cpb* knocked-down flies were flighted. When preparing cDNA from *Drosophila* IFM newly eclosed flies were used, which contain high mRNA levels. The mRNA in the IFM is still present in 24 hour *Drosophila* adults but in lower levels when compared to pupae (Fyrberg *et al.*, 1983). It is not possible to choose flightless individuals as newly eclosed flies are not yet mature enough to be flighted. Therefore the mRNA levels were not expected to be found completely knocked down in the PCR performed here.

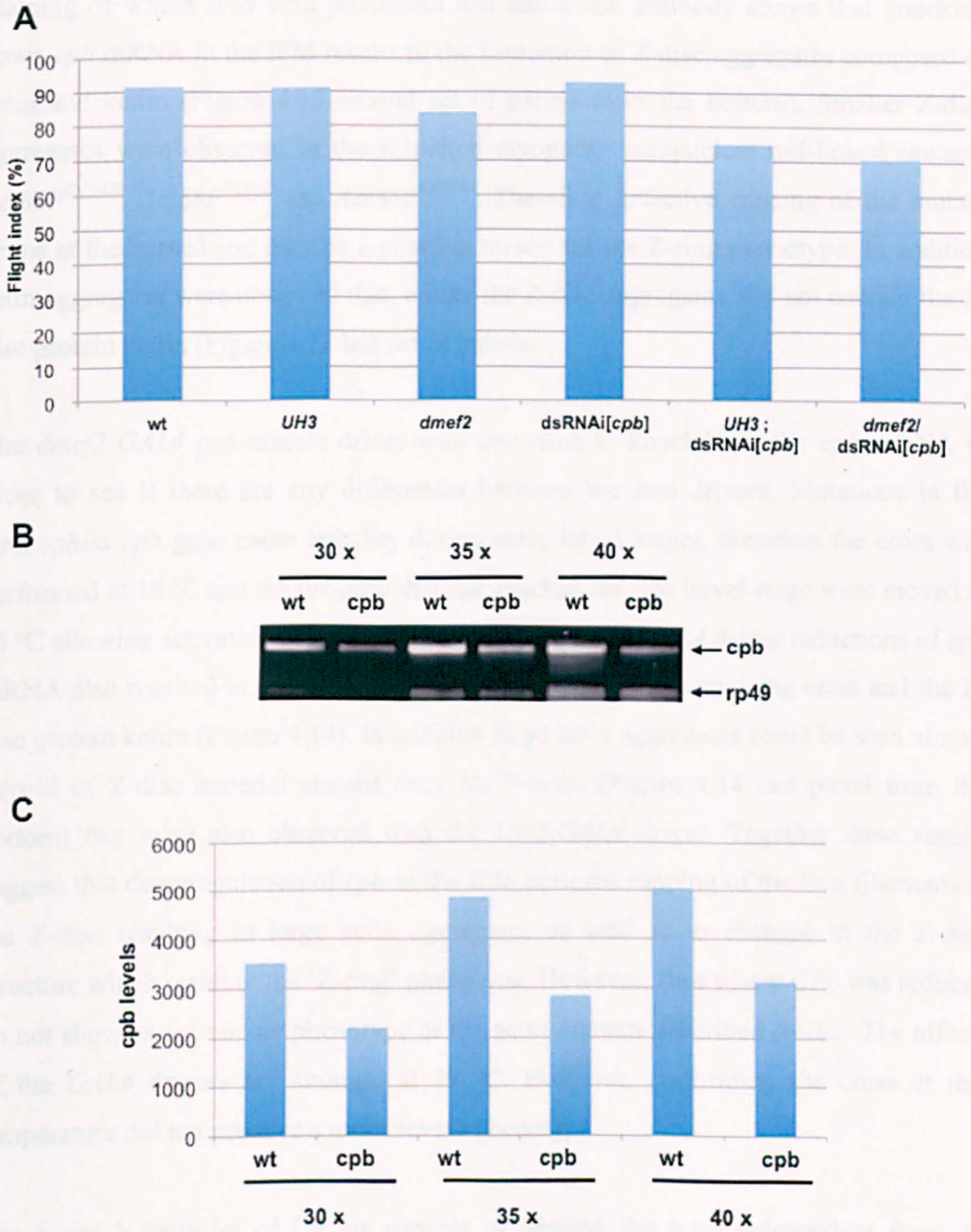

Figure 4.12. Analysis of cpb knockdown mutants. (A) Flight ability of wild type (n = 52), *UH3-GAL4*/+ (n = 52), *dmef2-GAL4*/+ (n = 34), dsRNAi[*cpb*]/+ (n = 45), *UH3-GAL4*/+; dsRNAi[*cpb*] (n = 40) and *dmef2-GAL4*/dsRNAi[*cpb*] (n = 41) flies (where n is the number of flies tested). The UAS and *GAL4* inserts are present as single copies. **(B)** Semi-quantitative PCR of wild type and *dmef2-GAL4*/dsRNAi[*cpb*] flies with 30, 35 and 40 cycles for *cpb* and *rp49* control. **(C)** *cpb* mRNA levels measured from semi-quantitative PCR. Rp49 was used to normalize the *cpb* band intensities between samples/lanes.

Staining of whole IFM with phalloidin and anti-kettin antibody shows that knocking down *cpb* mRNA in the IFM results in the formation of Z-disc aggregates composed of actin and kettin (Figure 4.13 second set of panels from the bottom). Smaller Z-disc aggregates were observed in the nemaline myopathy intranuclear rod-linked mutants $Act88F^{D154N}$, $Act88F^{V163L}$ and $Act88F^{V173M}$. Therefore defective capping of the mutant actins at the barbed end may be a possible reason for the Z-ring phenotype. In addition actin aggregates were observed that, unlike the Z-disc aggregates, did not contain the Z-disc protein kettin (Figure 4.13 last set of panels).

The *dmef2-GAL4* pan-muscle driver was also used to knockdown the *cpb* mRNA in order to see if there are any differences between the two drivers. Mutations in the *Drosophila cpb* gene cause lethality during early larval stages, therefore the cross was performed at 18 °C and the progeny that had reached the late larval stage were moved at 25 °C allowing activation of the *GAL4* driver. The *dmef2-GAL4* driver reductions of *cpb* mRNA also resulted in the appearance of Z-disc aggregates containing actin and the Z-disc protein kettin (Figure 4.14). In addition large actin aggregates could be seen almost devoid of Z-disc material stained only for F-actin (Figure 4.14 last panel from the bottom) that were also observed with the *UH3-GAL4* driver. Together these results suggest that downregulation of *cpb* in the IFM perturbs capping of the thin filaments at the Z-disc resulting in large actin aggregates as well as to changes in the Z-disc structure which result in the 'Z-ring' phenotype. However, flies where CPb was reduced do not show as a dramatic phenotype as the actin mutants described earlier. The effects of the *GAL4* drivers are stronger at 29 °C. However, performing the cross at that temperature did not produce a more severe phenotype.

The a and b tentacles of CP are capable of binding the actin independent from the formation of the heterodimer, hence the effect observed here with knockdown of *cpb* is not due to an inability to cap because the heterodimer cannot form, but because only one subunit caps the barbed end, CPa, which on its own is not sufficient.

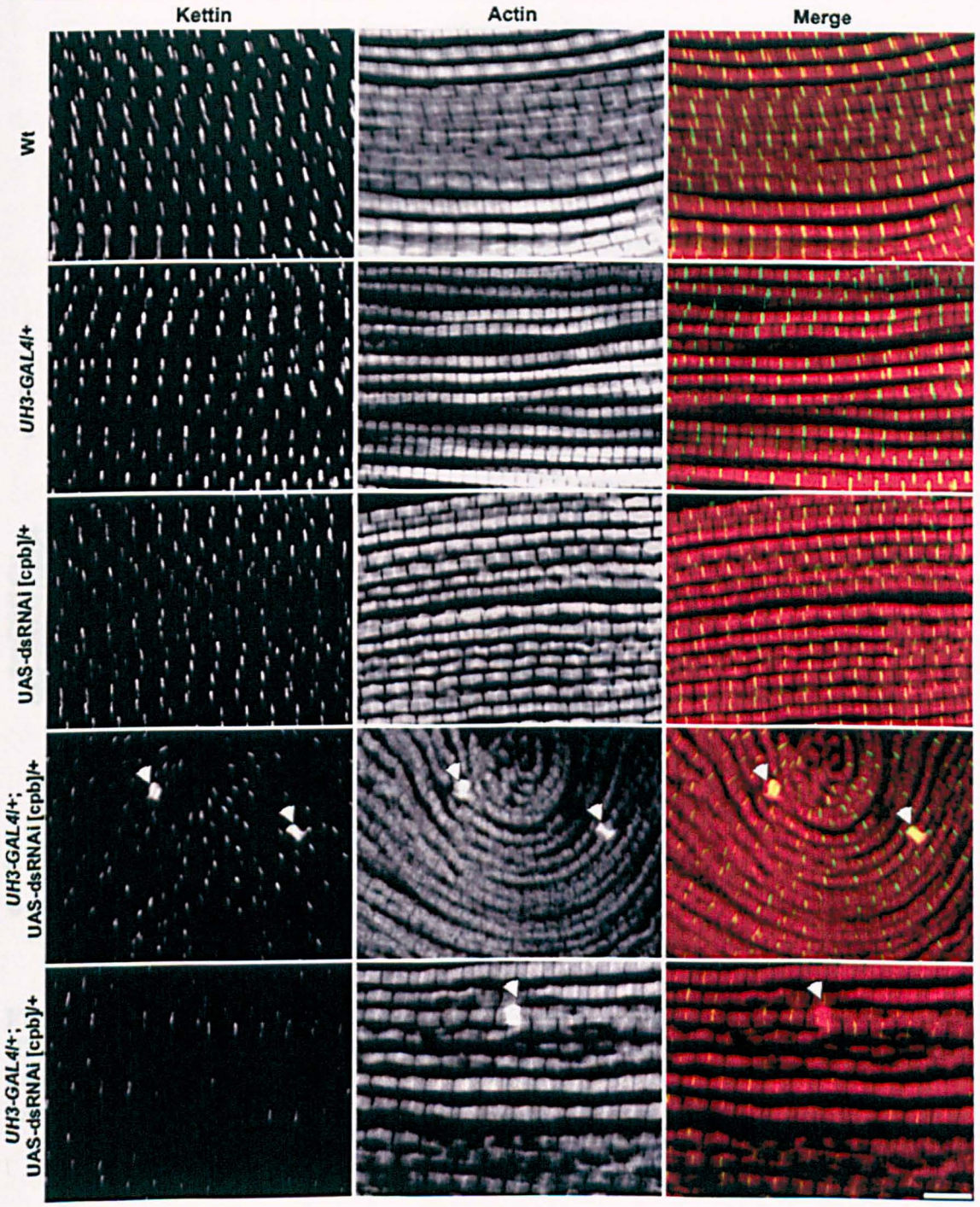

Figure 4.13. Whole muscle light microscopy of *UH3-GAL4*/+;*UAS*-dsRNAi[*cpb*]/+ flies. Anti-kettin and phalloidin staining of of wild type, *UH3-GAL4*/+ heterozygote, *UAS*-dsRNAi[*cpb*]/+ heterozygote and *UH3-GAL4*/+;*UAS*-dsRNAi[*cpb*]/+ flies. Arrowheads indicate Z-disc aggregates. Scale bar: 5 µm.

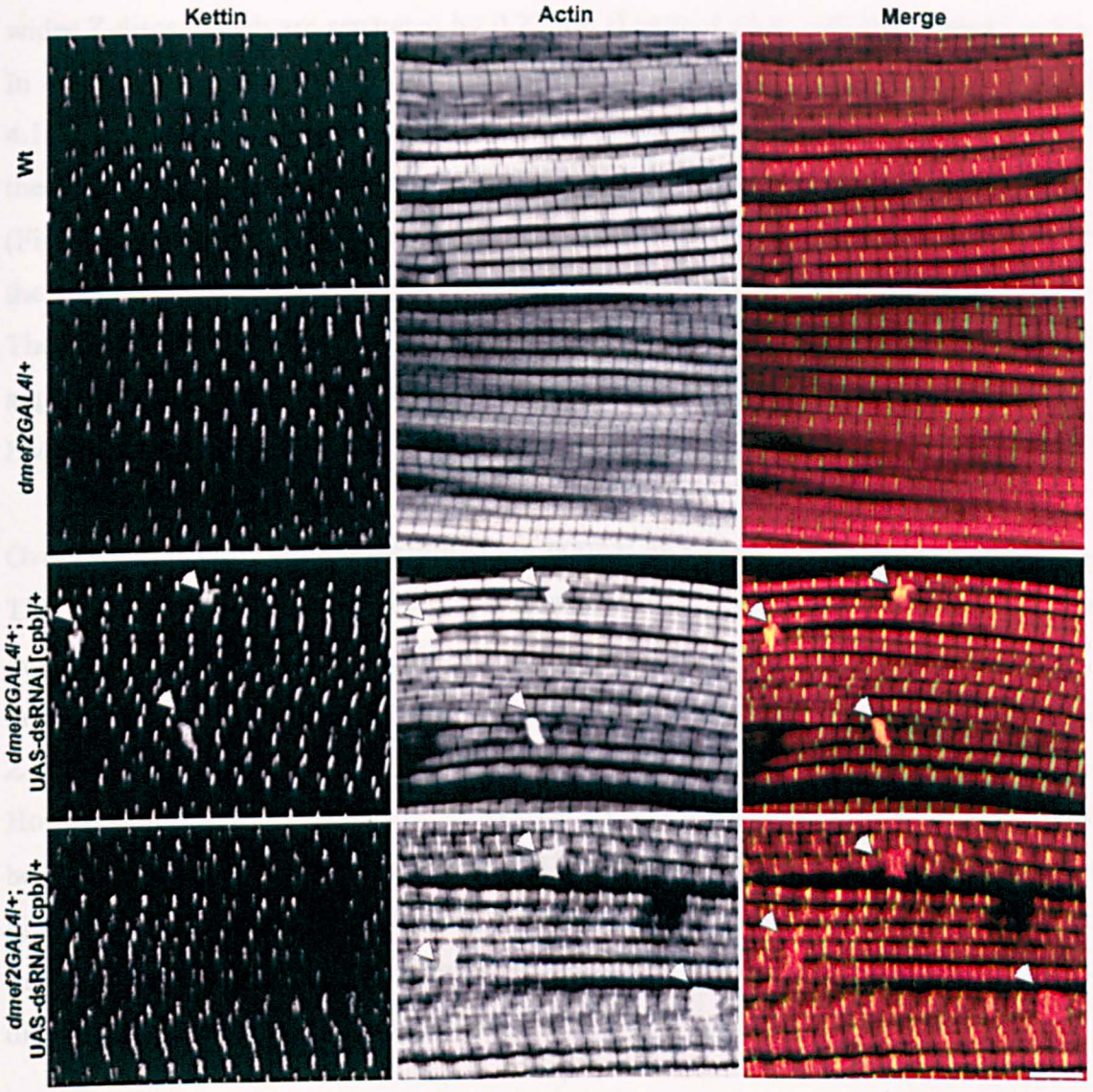

Figure 4.14. Whole muscle light microscopy of *dmef2-GAL4/UAS*-dsRNAi[*cpb*] flies. Anti-kettin and phalloidin staining of wild type, *dmef2-GAL4*/+ heterozygous and *dmef2-GAL4/UAS*-dsRNAi[*cpb*] flies. Arrowheads indicate Z-disc aggregates. Scale bar: 5 µm.

Electron microscopy of flightless *cpb* knockdown flies revealed normal muscle structure; abnormal sarcomeres were rarely seen. Three distinct phenotypes can be identified. The first phenotype is splitting of the Z-discs; in some cases the Z-discs split at one end, but remain attached on the other end (Figure 4.15 A EM image). Immunofluorescence reveals Z-ring like structures like the ones seen in the IR-linked mutants. A second phenotype observed in the *cpb* knockdown flies is characterized by Z-discs that appear to have expanded laterally (Figure 4.15 B). EM and whole muscle immunofluorescence with anti-kettin showed that the Z-discs can be wider than normal or to also surround the sarcomeres. Z-disc-like parallel lines can be seen within these

wider Z-discs, which are separated by 0.22 μm (Figure 4.15 B EM black arrowheads). In other cases Z-discs appear disorganized and wider though only at one end (Figure 4.15 B EM). Interestingly where the Z-discs have laterally expanded and become wider, there is also associated sarcomere damage as shown by the missing thin filaments (Figure 4.15 B EM red asterisk). These enlarged Z-discs bear the closest similarity to the nemaline rods compared to the other sarcoplasmic aggregations seen in this project. The third phenotype observed in the *cpb* knocked down mutants is large sarcoplasmic aggregates that are also reminiscent of the human nemaline rods in size (Figure 4.15 C EM).

Overall the majority of the myofibrils are normal as shown in Figures 4.13 and 4.14. The aberrant Z-discs and sarcoplasmic aggregates are rare and would not be easy to quantify by EM. Hence phalloidin-stained whole muscle images of *UAS*-RNAi[*cpb*] driven with the *dmef2-GAL4* driver were used to quantify them. This showed that large Z-discs and sarcoplasmic aggregates represent only 3 % of the total Z-disc population. However, immunofluorescence is not as sensitive as EM and splitting of Z-discs cannot be identified with this method; hence the percentage of abnormal Z-discs could be higher. A Z-stack from whole muscle immunofluorescence with anti-kettin shows that the sarcoplasmic aggregates and enlarged Z-discs are indeed filled throughout with Z-disc material (Movie 4.1. cpb_dmef2.avi).

Impaired actin-capping at the barbed end could be an explanation for how the nemaline rods seen in humans are formed. Unlike the continual turnover of actin that takes place in vertebrates, in *Drosophila* IFM protein synthesis post-eclosion is not observed, which is probably why large nemaline rods are not seen.

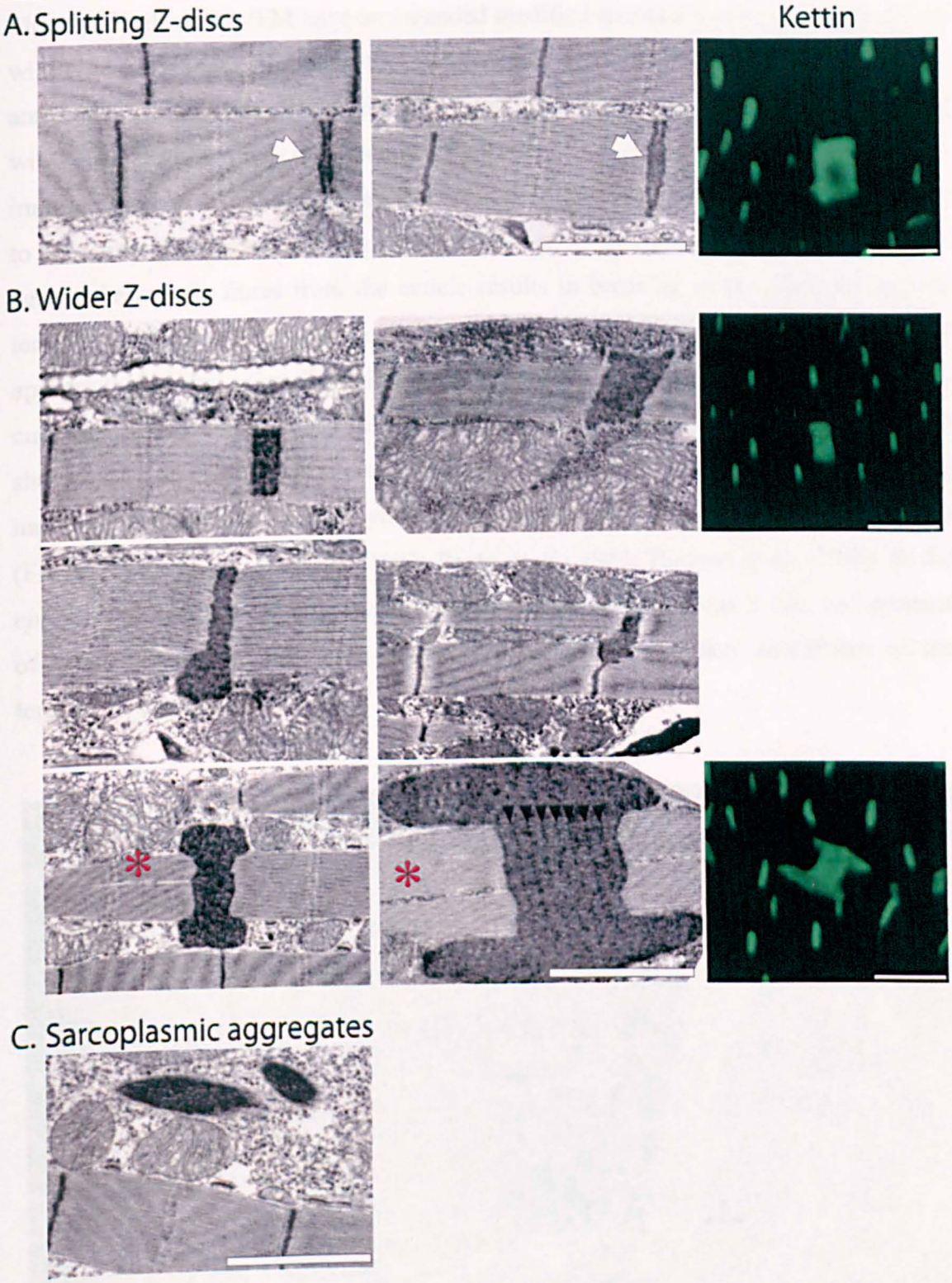

Figure 4.15. Z-disc abnormalities in cpb knockdown flies. TEM images and anti-kettin immunostaining of whole muscle from *UAS*-dsRNAi[*cpb*]/+; *dmef2-GAL4*/+ flies showing **(A)** splitting Z-discs, **(B)** Wider Z-discs, **(C)** sarcoplasmic aggregates. White arrow-heads indicate splitting Z-discs. Black arrowheads indicate parallel Z-lines in the Z-disc aggregate and red asterisks indicate missing sarcomere filaments. Scale bar for immunofluorescence images: 3 μm and for EM images: 2 μm.

The myofibrils of the IFM have an extended modified terminal Z-disc (Figure 4.16). In wild type early pupal muscles, which detach easily from the cuticle these are seen with anti-kettin antibody as bright ends (Zacharias Orfanos, personal communication). In the wild type adult muscle fibres the terminal Z-discs cannot be seen by immunofluorescence following microdissection of the fibre from the thorax. This is due to the terminal Z-discs remaining strongly attached to the cuticle. Hence any attempt to detach the muscle fibres from the cuticle results in breaking of the fibre leaving the terminal Z-discs still attached to it. However in flies with reduced levels of *cpb* it appears that during microdissection the muscle fibre can be easily separated from the cuticle and the terminal Z-discs remain bound to the myofibril (Figure 4.17 arrow). This shows that reduction in *cpb* affects attachment of the terminal Z-discs to the cuticle. The modified terminal Z-discs of myofibrils are connected to the myotendinous junction (Figure 4.16) (Danowski *et al.*, 1992; Pardo *et al.*, 1983; Hudson *et al.*, 2008). In the *cpb* knockdown flies the interaction between the modified terminal Z-disc and proteins of myotendinous junction may be affected resulting in weaker attachment of the terminal Z-discs to the cuticle.

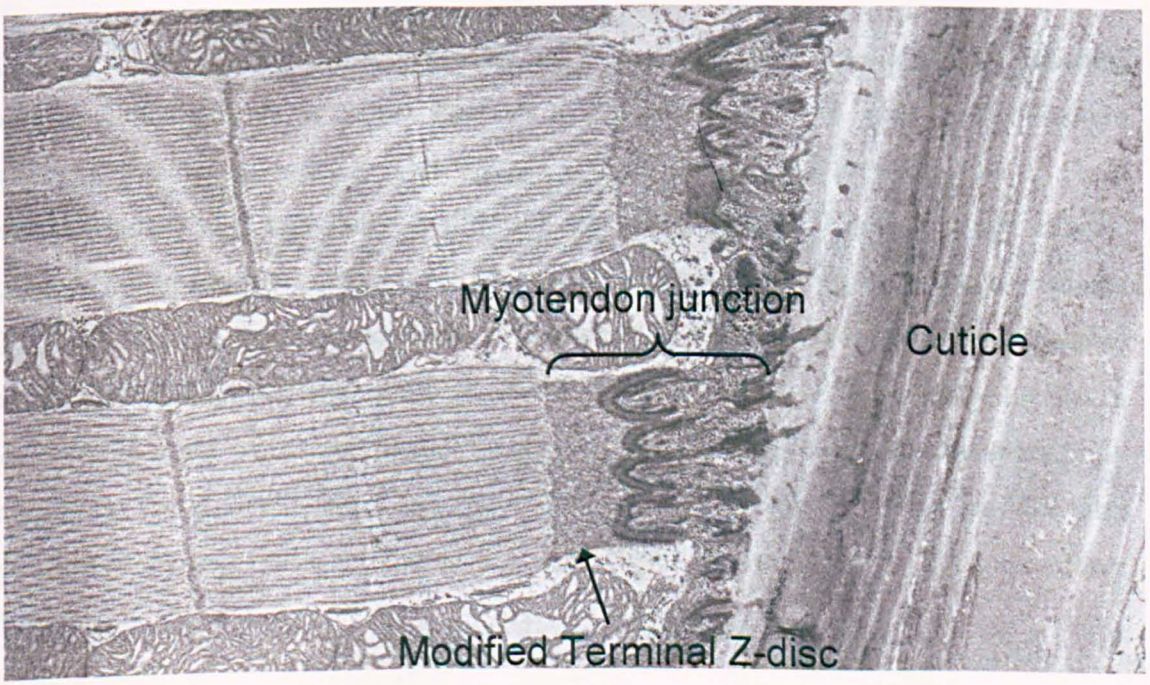

Figure 4.16. Image of the terminal Z-discs of myofibrils attached to the cuticle. Picture reproduced from Prof. Sparrow's original.

Figure 4.17. Image of the terminal Z-discs of single myofibrils from a whole fibre. Anti-kettin immunostaining of whole muscle from *UH3-GAL4*/+; *UAS*-dsRNAi[*cpb*]/+ flies. The terminal Z-discs are the green circles and the green lines are the sarcomere Z-discs. Scale bar: 10 μm.

TEM analysis of the *UAS-GFP-Act88F*^{V163L} flies driven with *UH3-GAL4* showed similar Z-disc defects as those observed in the *cpb* knockdown flies. These include splitting Z-discs and wider Z-discs that show the zebra body pattern (Figure 4.18 A, B white asterisk) with some surrounding the myofibrils (Figure 4.18 B top left image). Large zebra body structures often as long as a sarcomere were found in the sarcoplasm (Figure 4.18 C, right). Electron dense structures resembling the sarcoplasmic aggregates of the *cpb* knockdown flies were also seen (Figure 4.18 C, left). A stripy pattern is observed in areas of the aggregates, suggesting that these may possibly be zebra body structures. The Z-disc defects observed in the *UAS-GFP-Act88F*^{V163L} flies coincide with splitting of the myofibrils (Figure 4.18 A, B red asterisk) as seen in the *cpb* knockdown flies.

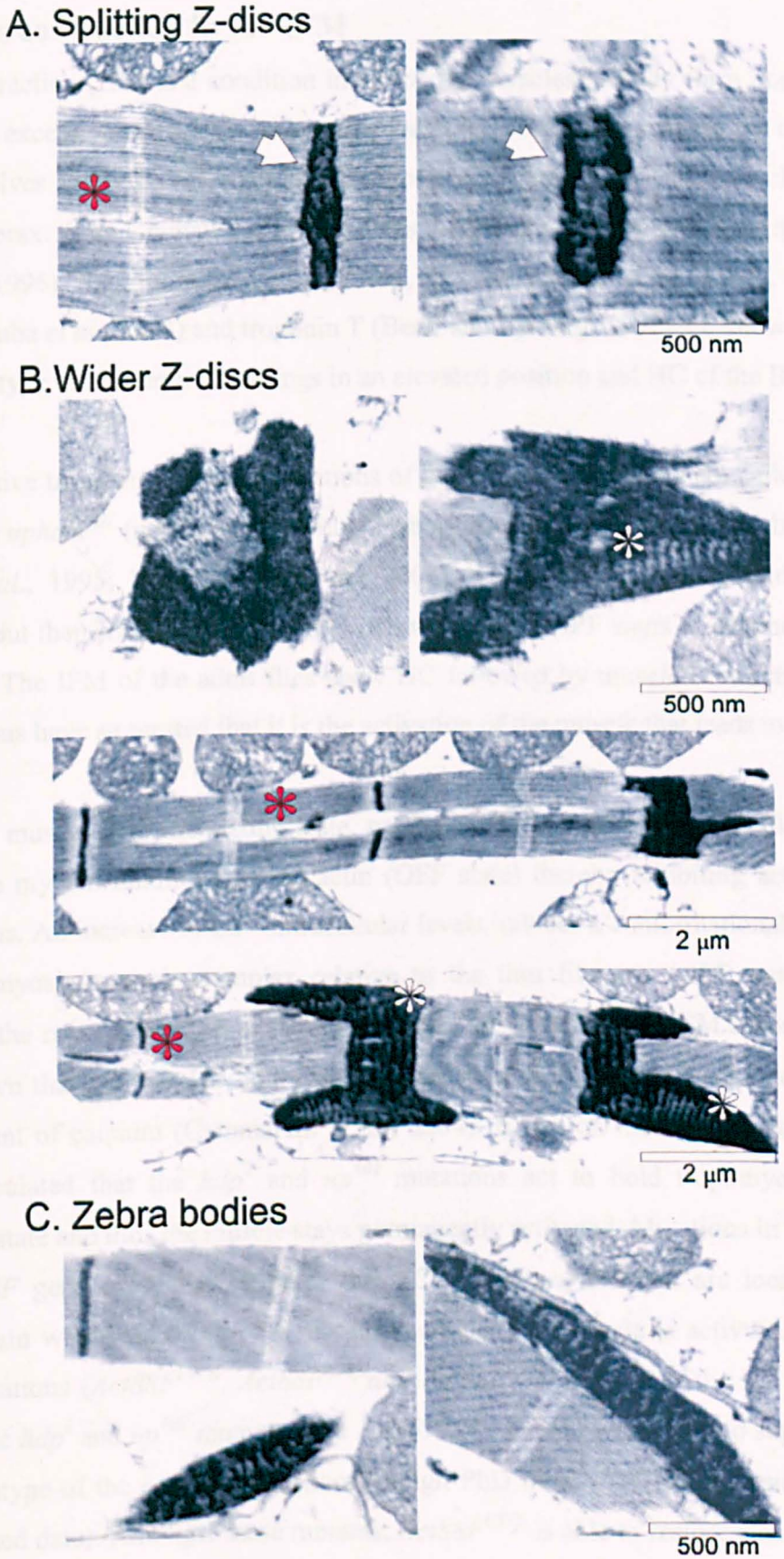

Figure 4.18. Z-disc abnormalities in *UAS-GFP-Act88F*^{V163L} flies. TEM images showing **(A)** splitting Z-discs, **(B)** wider Z-discs, **(C)** zebra bodies. White arrow-heads indicate splitting Z-discs. White asterisk indicates parallel Z-lines in the Z-disc aggregates and red asterisks indicate splitting of myofibrils. Scale bars are indicated.

4.7 Hypercontraction in the IFM

Hypercontraction (HC) is a condition in which the muscles initially form normally but then show excessive contraction (Nongthomba *et al.*, 2003). This causes the muscles to rip themselves apart and for material to gather at the centre or at either attachment site on the thorax. Some mutations in the *Drosophila* muscle genes for actin (An and Mogami, 1996), flightin (Reedy *et al.*, 2000), myosin (Kronert *et al.*, 1995), troponin I (Nongthomba *et al.*, 2003) and troponin T (Beall and Fyrberg, 1991) are known to result in a phenotype characterized by wings in an elevated position and HC of the IFM.

The recessive troponin missense mutations of the *TnI* and *TnT* genes are called $heldup^2$ (hdp^2) and $upheld^{101}$ (up^{101}), respectively (Fyrberg *et al.*, 1990; Beall and Fyrberg, 1991; Prado *et al.*, 1995; Nongthomba *et al.*, 2003). The IFM of these mutants develop normally but then when they begin to twitch at 78 hours APF signs of degeneration are observed. The IFM of the adult flies show HC followed by muscle destruction. These observations have suggested that it is the activation of the muscle that leads to HC.

When the muscle is in the resting state, tropomyosin lies across the thin filament and blocks the myosin binding sites on actin (OFF state) thereby inhibiting actin-myosin interactions. An increase in Ca^{2+} intracellular levels induces a conformational change in the tropomyosin/troponin complex relative to the thin filament (OFF state) thereby exposing the myosin binding sites and initiating force generation. EM reconstructions have shown that hdp^2 acts to hold tropomyosin away from the blocked state, which is independent of calcium (Cammarato *et al.*, 2004). Based on these observations it has been speculated that the hdp^2 and up^{101} mutations act to hold tropomyosin in the activated state and thus the muscle stays permanently activated. Mutations in residues of the *Act88F* gene exist that suppress the HC phenotype and that are located where tropomyosin would lie on the F-actin surface when the muscle is activated. Three of these mutations ($Act88F^{E57K}$, $Act88F^{E93K}$ *and* $Act88F^{R254H}$) suppress the HC phenotype of both the hdp^2 and up^{101} mutants. The $Act88F^{E334Q}$ mutant was found to suppress only the phenotype of the hdp^2 mutant (Sarah Haigh PhD thesis, 2003, University of York, unpublished data). Amongst these mutants, $Act88F^{E57K}$ is able to restore also flight. The CFTD-causing actin residue D292 is also located in the tropomyosin binding area of actin. Hence the $Act88F^{D292V}$ could potentially act as a suppressor of the hdp^2 and up^{101} mutants.

4.7.1 *Act88F*^{D292V} is a suppressor of the *hdp*^{2} *and up*^{101} phenotype

In vitro motility studies using 50% wild type and 50% D292V mutant actin extracted from patient biopsies provide strong evidence that the D292V mutation causes a functional abnormality of the actin-myosin contractile unit by altering tropomyosin dynamics (Clarke *et al.*, 2007). The authors found that addition of tropomyosin abolished motility in the presence of the troponin complex and high Ca^{2+} concentrations. Residue D292 is located on the surface of the F-actin structure (Figure 4.19 A arrow). In the presence of high Ca^{2+} concentrations ('ON state') the predicted location of tropomyosin is to the left of residue D292 (Figure 4.19 B, C). In low Ca^{2+} concentrations ('OFF' state) tropomyosin is predicted to be in contact with residue D292 (Figure 4.19 C). The authors proposed that the D292V mutation obstructs actomyosin interactions by stabilizing tropomyosin in the 'OFF' state, which would result in a hypocontractile phenotype.

In the *Act88F*^{D292V}/+ heterozygote flies different combinations of wild type and mutant actin on the thin filament would cause tropomyosin shifting to be more difficult or not take place where mutant actin predominates, thereby blocking muscle contraction. This could result in some areas of the thin filament being able to contract and others not resulting in muscle damage.

To test whether the D292V mutation results in a hypocontractile phenotype, *Act88F*^{D292V} homozygous flies were crossed to the troponin I *hdp*^{2} as well as troponin T *up*^{101} flies to see if the *Act88F*^{D292V} mutant actin suppresses the hypercontractile phenotype of those mutants. In the progeny male flies that were hemizygous for either one of the troponin mutations and heterozygous for the actin mutation were flight-tested and were found to be flighted (Figure 4.20). Therefore the *Act88F*^{D292V} actin mutant, which is predicted to inactivate muscle contraction, can act as a suppressor of the troponin mutations that lead to constant muscle activation. The fact that the D292V mutation leads to inactivation of muscle contraction also explains why the IFM of *Act88F*^{D292V} homozygotes do not show any structural defects. In these flies the IFM are composed solely of ACT88F^{D292V} actin, which means that contraction cannot take place at any part of the myofibril. This is in contrast to the heterozygote mutants, which consist of a mixture of wild type and mutant actin leading to muscle contraction in some parts of the myofibril and not in others.

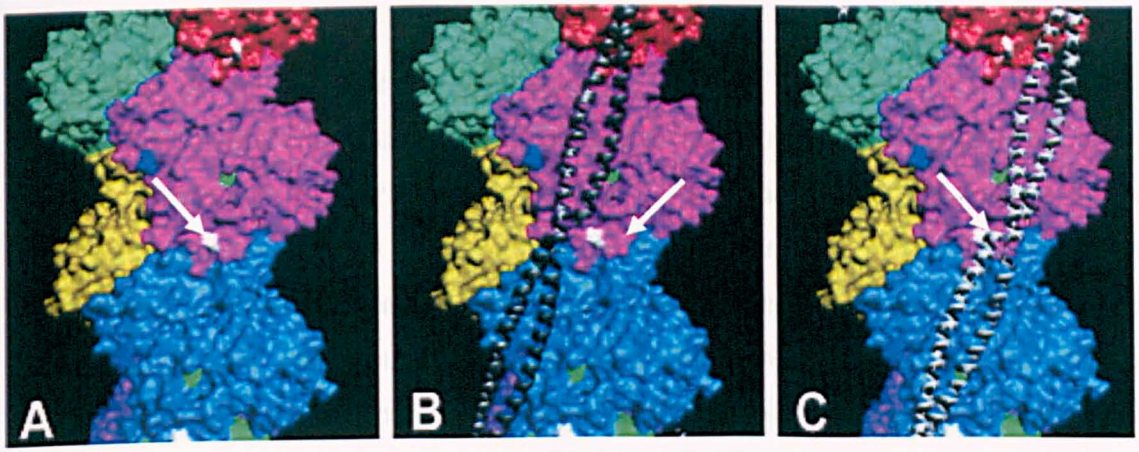

Figure 4.19. Location of D292V mutation in the F-actin structure and its relation to tropomyosin. (A) D292V is shown in white, each actin monomer is colored differently. The position of tropomyosin (white double helix) is shown in the high Ca^{2+} state **(B)** and in the low Ca^{2+} state **(C)**. Picture adapted from Clarke *et al.*, 2007.

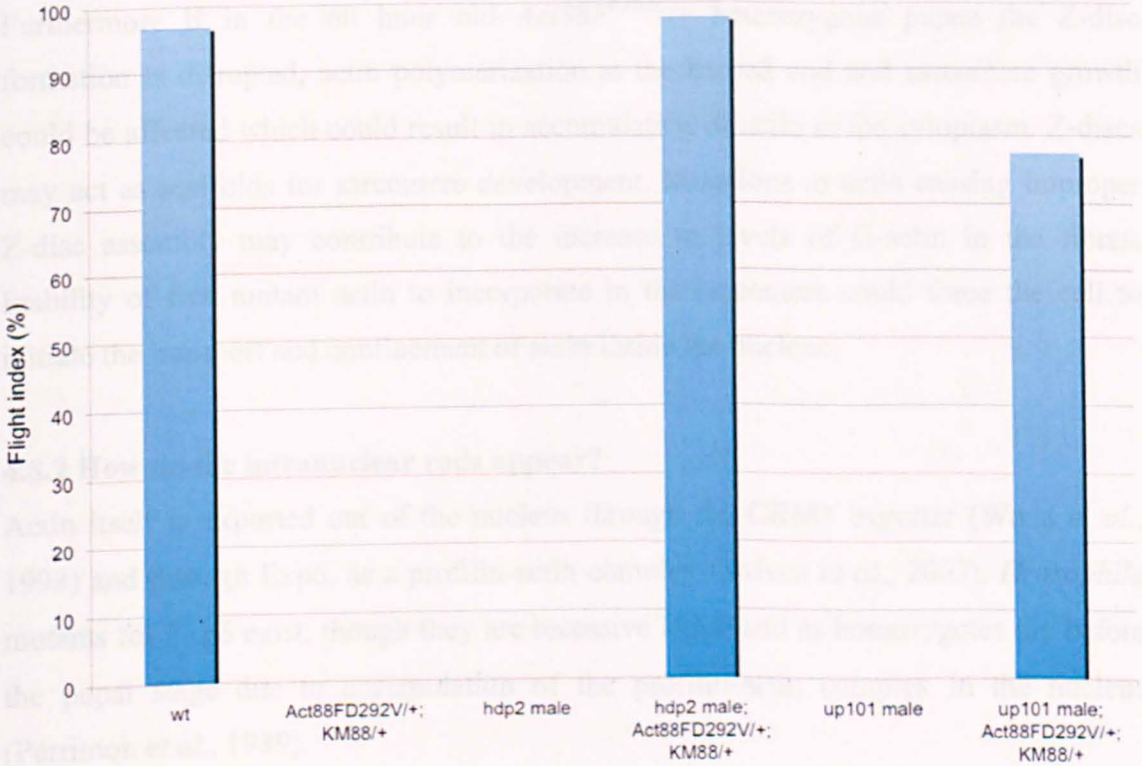

Figure 4.20. Suppressing of the *hdp*^{2} and *up*^{101} mutations. Flight-testing for wild-type (n = 32), *Act88F*^{D292V}/+; *KM88*/+ (n = 20), male *hdp*^{2} (n = 22), male *hdp*^{2}/+; *Act88F*^{D292V}/+; *KM88*/+ (n = 47), male up^{101} (n = 20) and male *up*^{101}; *Act88F*^{D292V}/+; *KM88*/+ (n = 31) flies. Where 'n' is the number of flies tested.

4.8 Discussion

4.8.1 When do the intranuclear rods appear?

Developmental analysis of intranuclear rod-linked heterozygous actin mutants showed that the intranuclear rods form by 70 hours APF. There can be many explanations as to why the intranuclear rods do not appear earlier, by 60 hours APF. One reason is that the actin levels inside the nucleus are not high enough at earlier stages to induce actin polymerization and rod formation. Fyrberg *et al,* 1983 have reported that expression of ACT88F begins at early pupal stages but becomes more strongly expressed at mid and late pupal stages (Fyrberg *et al.*, 1983). IFM myofibrillogenesis starts at around 40-42 hours APF (Reedy and Beall, 1993b), which is also when the ACT88F expression levels peak (Fyrberg *et al.*, 1983). Hence 60 hours APF is perhaps too early to observe the intranuclear rods as the myofibrillogenesis has proceeded for only 12 hours.

Furthermore if in the 60 hour old $Act88F^{V163L}/+$ heterozygous pupae the Z-disc formation is disrupted, actin polymerization at the barbed end and sarcomere growth could be affected which could result in accumulation of actin in the cytoplasm. Z-discs may act as scaffolds for sarcomere development. Mutations in actin causing improper Z-disc assembly may contribute to the increase in levels of G-actin in the fibres. Inability of free mutant actin to incorporate in the sarcomere could force the cell to initiate the transport and confinement of actin inside the nucleus.

4.8.2 How do the intranuclear rods appear?

Actin itself is exported out of the nucleus through the CRM1 exporter (Wada *et al.*, 1998) and through Exp6, as a profilin-actin complex (Stüven *et al.*, 2003). *Drosophila* mutants for Exp6 exist, though they are recessive lethal and as homozygotes die before the pupal stage due to accumulation of the profilin-actin complex in the nucleus (Perrimon *et al.*, 1989).

Indeed actin cycling in the nucleus may even help to regulate actin levels (Miralles *et al.*, 2003). The presence of actin rods in the nucleus suggests that the D154N, V163L/M mutations interfere with its export from the nucleus, and this effect should be strongest for V163L where the intranuclear rods were most common. The position of these substitutions is in the region of the monomer towards the barbed end, where profilin is known to bind. Therefore it is possible that formation of the profilin-actin complex in

the nucleus is affected, and hence exportin is unable to transport actin out of the nucleus. In yeast cells deficient for profilin or carrying a single point profilin mutation, thick actin bars are detected which may have formed as a result of improper regulation of actin assembly (Haarer *et al.*, 1990; 1996).

In the actin structure the nucleotide (ATP or ADP) is bound between subdomains 3 and 4 (Kabsch *et al.*, 1990). In the 'tight-state' of the actin-profilin crystals (Schutt *et al.*, 1993), the nucleotide β-phosphate forms H-bonds to the amide nitrogens of S14, G15 and M16 in one of the actin loops and to D157 in the other actin loop. The γ-phosphate of the nucleotide is bound to S14, D157, G158 and V159. As the G-actin interdomain contact is established via the nucleotide-binding site (Frieden *et al.*, 1980; Frieden *et al.*, 1985; Crosbie *et al.*, 1994; Muhlrad *et al.*, 1994; Strzelecka-Golaszewska *et al.*, 1995) mutations in the nucleotide-binding cleft could influence binding to profilin. Based on these observations it could be speculated that mutations in the actin residue D154 may affect binding to profilin and inability to export actin from the nucleus. In yeast the double actin mutation D154A/D157A is lethal (Wertman *et al.*, 1992).

Actin contains two nuclear export signals (NESs) that are recognized by the export factor CRM1/exportin1 (Kudo *et al.*, 1998). The IR-linked actin residues are near one of the two NESs on actin, hence the mutations may be affecting processes involving the NESs resulting in actin detainment inside the nucleus. In addition the inability to export actin from the nucleus might also be coupled with abnormally increased levels of F-actin entering the nucleus. If the mutant actins are less stable in filaments, free G-actin may have a higher probability of entering the nucleus. Hence, if levels of G-actin become high in the nucleus, then it could polymerize and form the observed actin rods. In support of this hypothesis developmental analysis of the IR-linked mutants showed that the mutant actin is affecting Z-disc and sarcomere assembly before the IRs start to appear. Lastly and importantly the fact that the intranuclear rods appear before the muscle is fully formed suggests that they may also appear in human patients before the end of gestation.

4.8.3 Are both wild-type and mutant actins present inside the intranuclear rods?

It is not yet known whether the human intranuclear rods contain solely mutant actin or a combination of wild type and mutant actin. Previous studies in a mouse myoblast culture system have demonstrated that the V163L/M ACTA1 mutants are capable of forming actin aggregates inside the nucleus (Domazetovska *et al.*, 2007a;b). *Drosophila* IFM mutants heterozygous for the $Act88F^{V163L}$ mutation show the intranuclear rod phenotype thus offering the advantage of having an intact animal system, which expresses both wild type and mutant actins. Here it was possible to examine which one of the two actin species is located inside the intranuclear actin rods by fusing GFP to each one of them. Analysis of flies expressing one wild type *GFP-Act88F* and one $Act88F^{V63L}$ copy did not show co-localisation of the GFP with the intranuclear rods suggesting that these structures do not contain any wild type actin. However the *GFP-*$Act88F^{V63L}$/+ heterozygous mutant showed co-localisation of the GFP within the intranuclear rods suggesting that the intranuclear actin rods consist of mutant actin. Furthermore an unexpected result was that the sarcoplasmic rods also contained solely mutant actin as the wild type GFP-fused actin was excluded from these aggregates. This further highlights the advantage of studying the disease in an intact animal system as it has allowed the identification of the actin species found in IRs.

4.8.4 Barbed end actin capping is affected in the intranuclear rod-linked mutants

Capping protein prevents polymerization or depolymerisation of the thin filaments from the barbed end. The protein is a heterodimer of subunits α and β each of which is composed of a base and a flexible tentacle, which binds directly the actin monomer (Narita *et al.*, 2006). The CPa and CPb subunits bind to distinct regions of the terminal actin protomers at the barbed end (Narita *et al.*, 2006). The actin D154 and V163 residues reside near the proposed binding site for the β-tentacle of CP. Thus mutations in these residues could affect binding of the β-tentacle of CP at the fast growing end of the thin filaments resulting in aberrant Z-disc structures and actin aggregates.

To test this hypothesis *cpb* was knocked down using the dsRNAi[*cpb*] line and two different *GAL4* drivers, an IFM-specific (*UH3-GAL4*) and a pan muscle (*dmef2-GAL4*) driver. Using both drivers the result was actin aggregates, enlarged Z-discs and Z-ring structures stained with anti-kettin and phalloidin like the ones seen in whole muscle immunostaining of the intranuclear rod-linked mutants. This suggests that a failure or

reduced ability to cap the actin barbed ends resulting in continuous addition of actin monomers at the Z-disc, alters the Z-disc structure and results in actin aggregates. Failure to cap the thin filament barbed ends could be a major underlying cause of nemaline bodies observed in human patients.

4.8.5 *Act88F*^{D292V} can act as a suppressor for the HC phenotype

Suppressor mutations can also help to understand the aetiology of some nemaline phenotypes. In the 'OFF' state tropomyosin lies across the actin filament on the proposed myosin binding site and inhibits actomyosin interactions. The residue D292 forms part of the tropomyosin binding site and it has been suggested that the D292V mutation might obstruct actomyosin interactions by stabilizing tropomyosin in the 'OFF' state (Clarke *et al.*, 2007). Here the hypercontractile phenotypes of the TnI and TnT mutants were suppressed by introducing the *Act88F*^{D292V} mutant actin, supporting the idea that the D292V mutation obstructs actomyosin interactions and prevents muscle contraction. This highlights the advantage of adopting an intact animal system where genetic approaches can be applied to understand how a mutation can disrupt muscle function.

Finally, eight ACTA1 mutations (E4K, G46D, E205D, L221P, E241K, D292V, P307S and P332S) are known to result in CFTD in humans (Laing *et al.*, 2009). The eight residues mutated in CFTD patients are all located close to tropomyosin-binding sites on actin in both the high (ON) and low-Ca^{2+} states (OFF) (Figure 4.21). Therefore it can be speculated that the CFTD mutations share a common disease mechanism whereby the tropomyosin sliding is disrupted, resulting in inability to regulate actomyosin interactions. Although the eight CFTD mutations may obstruct actomyosin interactions there are other ACTA1 mutations that are also predicted to perturb actin/tropomyosin interactions and do not cause CFTD (Sparrow *et al.*, 2003). Therefore disruption of actin/tropomyosin interactions cannot be the sole aetiology for CFTD and other factors must be involved.

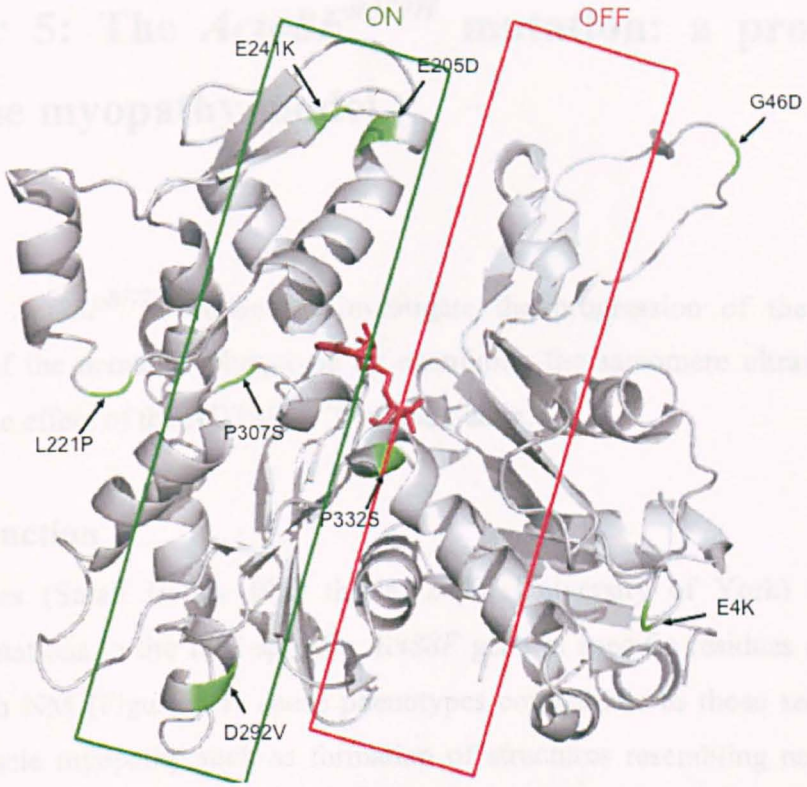

Figure 4.21. Position of the eight CFTD-linked ACTA1 mutations. Cartoon of G-actin complexed with ATP (red), the residues which are mutated in CFTD are shown in green. The green box indicates where tropomyosin lies on actin when in the 'ON' state and the red box the position of tropomyosin on actin when in the 'OFF' state. Image created using Pymol.

4.8.6 Summary

Different genetic approaches were used to further understand the aetiology of the severe *Drosophila* mutations D154N and V163L/M. It was found that the intranuclear and sarcoplasmic rods appear during muscle development. Fusing GFP to both wild type and mutant actin, showed that the mutant actin is present in both intranuclear and sarcoplasmic rods, whereas wild type actin was excluded from these structures. Knock down of the *cpb* mRNA produced the same Z-disc abnormalities as seen in the intranuclear rod-linked mutants, suggesting insufficient capping of actin by cpb may be the cause of sarcoplasmic rods. The D292V mutation was believed to cause hypercontraction. This was confirmed by suppressing two known hypercontractile mutants of the *TnI* and *TnT* genes. In the next chapter the nemaline myopathy mutation, R372H, was used to study the development of the nemaline phenotype.

Chapter 5: The *Act88F*^{R372H} mutation: a progressive nemaline myopathy model.

5.1 Aims

Use of the *Act88F*^{R372H} mutant to investigate the progression of the *Drosophila* equivalent of the nemaline phenotype by examining the sarcomere ultrastructure and determine the effect of the ACT88F^{R372H} mutant actin.

5.2 Introduction

Initial studies (Sarah Haigh, PhD thesis, 2003, University of York) showed that genomic mutations in the IFM-specific *Act88F* gene at specific residues associated in humans with NM (Figure 5.1) cause phenotypes comparable to those seen in human skeletal muscle myopathy such as formation of structures resembling nemaline rods, variable sarcomere lengths as well as aberrant thin filament assembly. In particular four *ACT88F Drosophila* (A138V, R256C, G268D, R372H) mutations corresponding to six *ACTA1* nemaline mutations (A138P, R256H/L, G268R/C, R372H) (Figure 5.1) result in similar phenotypes to those seen in human biopsies. As homozygotes, three of these *Act88F* mutants (A138V, R256C, G268D) do not form sarcomeres during early myogenesis and show the zebra body phenotype (Figure 5.2 B, C). The flies also exhibit muscle disarray (Figure 5.3 C, D, E, F) and as heterozygotes they were flightless. The *Act88F*^{R372H} mutant displayed normal myogenesis and the pupae show normal myofibrils (Figure 5.2 D). However, as heterozygotes the flies that emerged could fly at first but became flightless as time progressed and developed the nemaline phenotype (Figure 5.3 G, H).

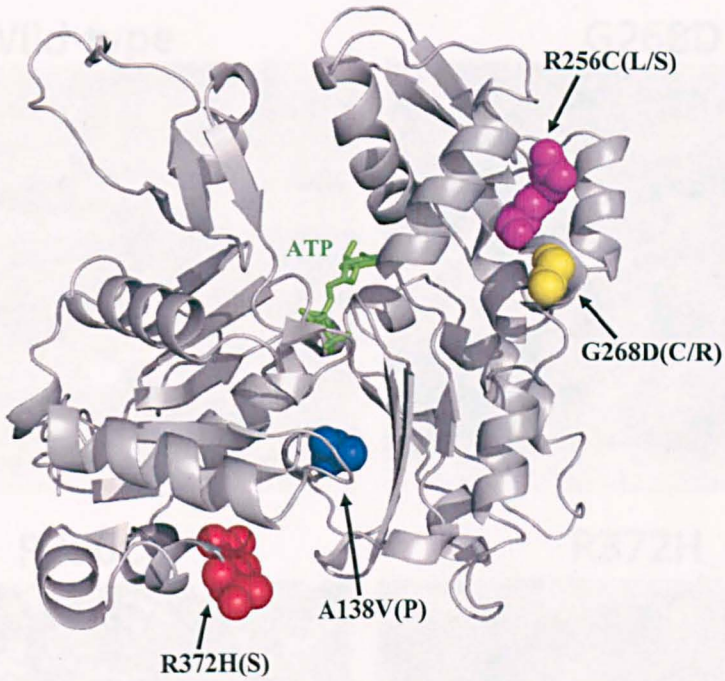

Figure 5.1. The position of the four *Drosophila* Act88F mutations in actin. Cartoon of the ATP-bound G-actin showing in space-fill the position of the four *Drosophila* Act88F mutations which correspond to the six human nemaline mutations (in parenthesis). The positions of A138V, R256C, G268D and R372H are shown in blue, purple, yellow and red, respectively. The ATP is shown as sticks. Image produced using Pymol.

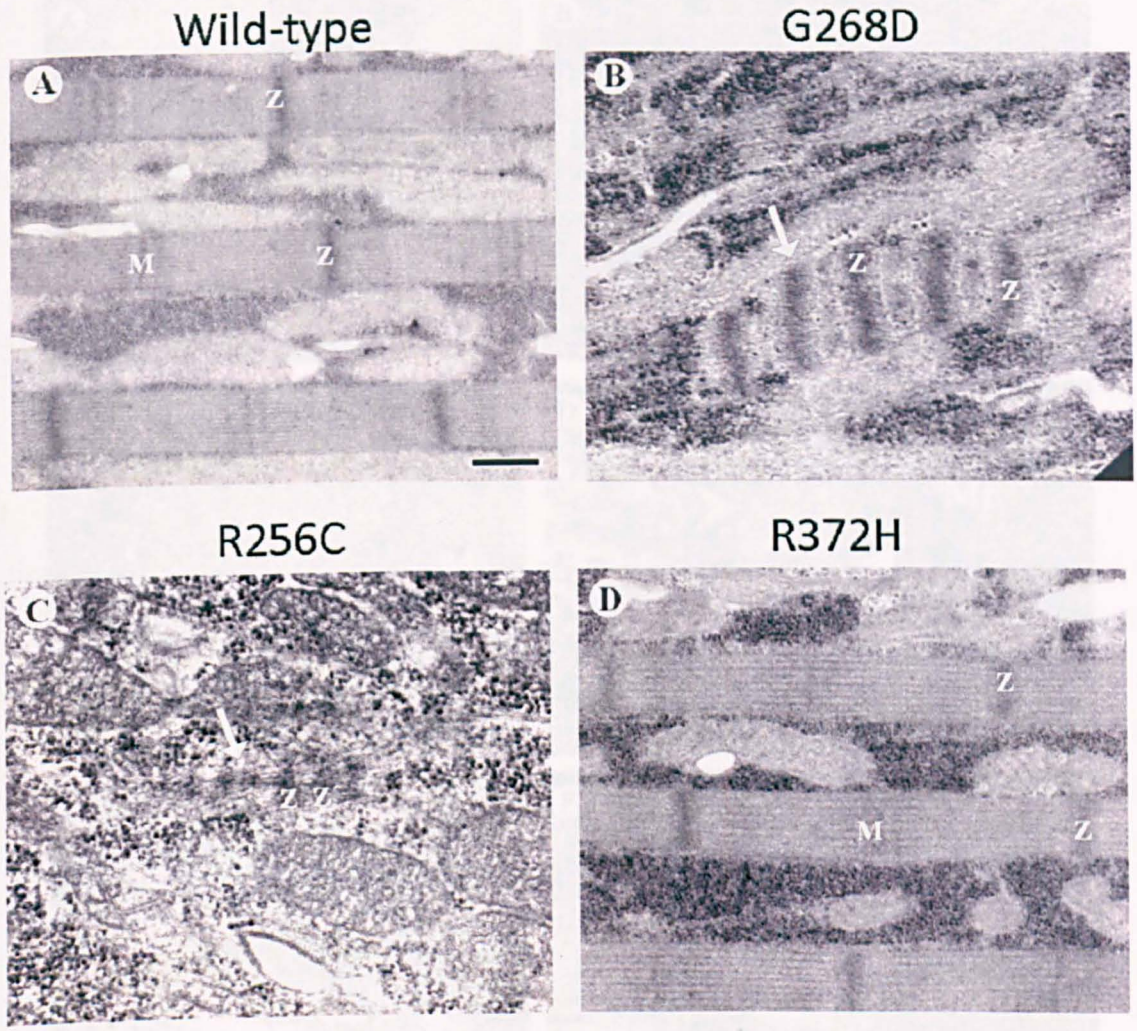

Figure 5.2. TEM images of (A) wild-type, (B) *Act88F*^{G268D}, (C) *Act88F*^{R256C} and (D) *Act88F*^{R372H} 44 hours old pupae. White arrows point at zebra bodies. M: M-line, Z: Z-line. Scale bar: 250 nm. Taken from Sarah Haigh, PhD thesis, 2003.

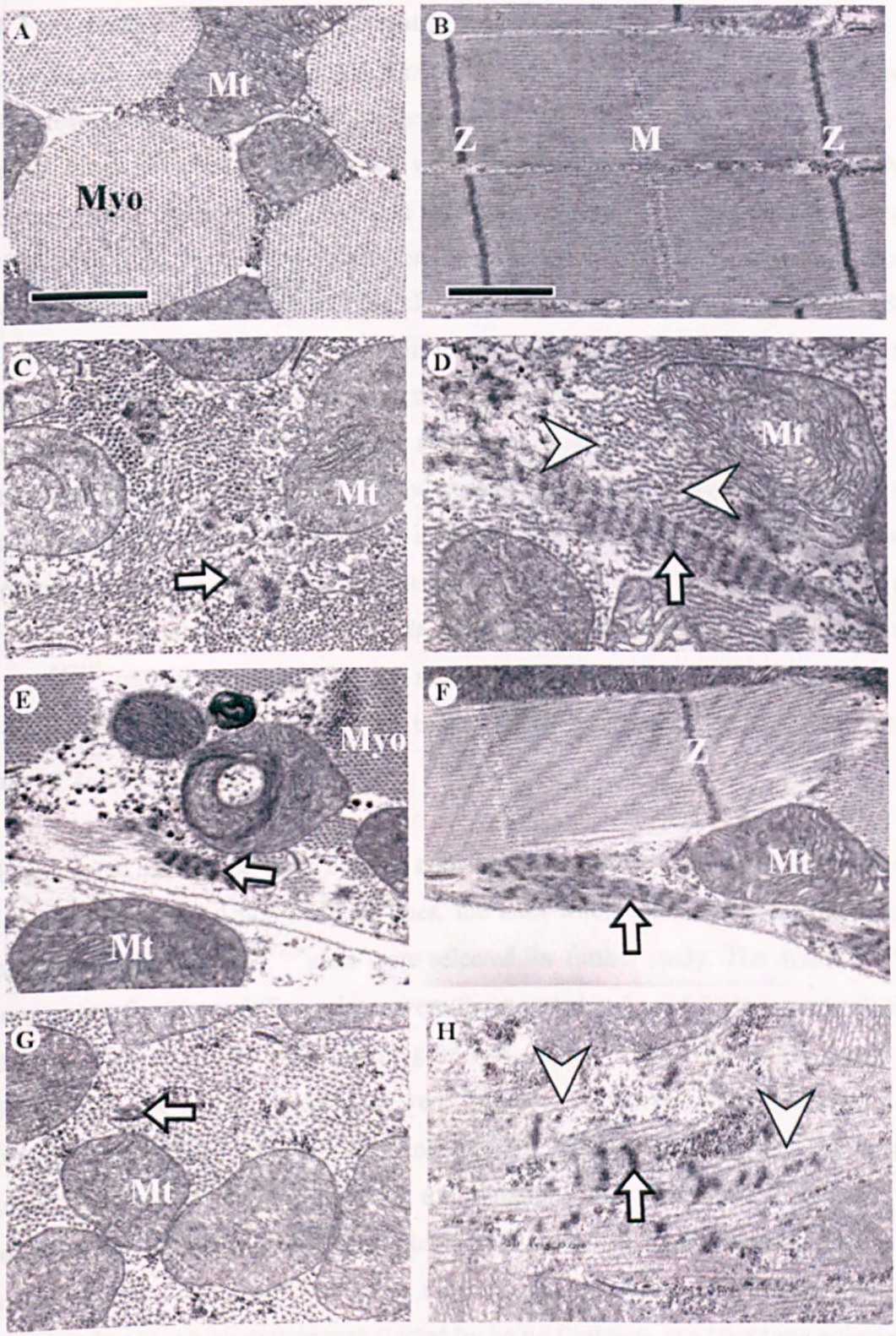

Figure 5.3. TEM images of (A), (B) wild-type; (C), (D) $Act88F^{G268D}$; (E), (F) $Act88F^{R256C}$ and (G), (H) $Act88F^{R372H}$ adult flies. The panels on the left are transverse sections and on the right longitudinal sections. White arrows point at zebra bodies, white arrow heads point at disorganised filaments. M: M-line, Z: Z-line, Myo: myofibril, Mt: mitochondrion. Scale bar: 1 μm. Taken from Sarah Haigh PhD thesis, 2003.

5.3 The *Act88F*^{R372H}/+ heterozygotes lose their flight ability

The transgenic line with the genomic *Act88F*^{R372H} mutation used for EM analysis shown in Figures 5.2 and 5.3 was lost. However we were in possession of a line carrying a P-element insert for *Act88F*^{R372H}, which was located in the third chromosome. When studying *Act88F* mutants it is important that the P-element insert carrying the mutant *Act88F* gene is not in the third chromosome but instead is located on the first or second chromosome. The reason for this is that the wild type actin gene as well as the ACT88F null mutation (*Act88F*^{KM88}) also reside in the third chromosome. In order to study the *Act88F* mutants in a homozygous state or be able to extract mutant actin for biochemical experiments the wild type actin gene must not be present. Since the P-element insert containing *Act88F*^{R372H} is located in the third chromosome it was not possible (except by recombination) to eliminate the wild type *Act88F* copy. It was therefore easier to create a transgenic line that would allow to control the number of the *Act88F*^{R372H} mutant and wild type *Act88F* gene copies. The objective was to 'hop' the *Act88F*^{R372H} transgene to the first or second chromosome. This was achieved by crossing the *Act88F*^{R372H} mutant line to an active transposase coding line (Δ2-3) (Chapter 2, section 2.1.4).

This generated 33 lines carrying a single copy of the *Act88F*^{R372H} mutation in the first or second chromosome. Amongst those lines, the ones where the inserts generated good expression of the *Act88F*^{R372H} gene were selected for further study. The *Act88F*^{R372H}/+ heterozygous flies from different lines were flight-tested at 1- and 7- days post eclosion and were compared to the wild type (Figure 5.4). At day 1 the flight ability varied for different lines and at day 7 most lines were flightless. However, there were some lines that were still flighted at day 7 (data not shown), which suggested that the muscle structure was not severely affected by the mutation. Therefore these lines were not studied further. As the aim of this chapter was to use the R372H mutant to follow the disease progress, a line with an initial normal muscle structure (identified by being flighted at day 1), which deteriorates (tested by being flightless at a later time point) was needed. Line 16 gave the best flight ability at day 1 and the flies were flightless after 7 days and therefore it was selected for further analysis.

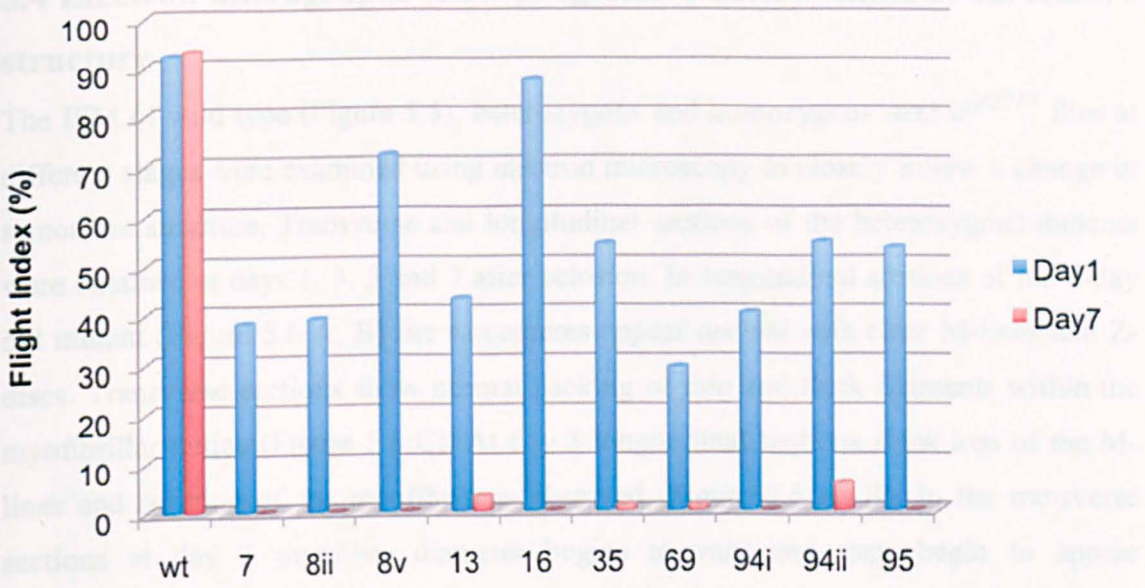

Figure 5.4. Flight index for wild type and lines of *Act88F*^{R372H}/+ heterozygous flies. 1- and 7-days old wild type and *Act88F*^{R372H}/+ heterozygous flies were flight-tested.

5.4 Electron micrographs show progressive deterioration of sarcomere structure

The IFM of wild type (Figure 5.5), heterozygous and homozygous *Act88F*^{R372H} flies at different stages were examined using electron microscopy to closely follow a change in sarcomere structure. Transverse and longitudinal sections of the heterozygous mutants were obtained at days 1, 3, 5 and 7 after eclosion. In longitudinal sections of the 1-day old mutant (Figure 5.6 A, B) the sarcomeres appear normal with clear M-lines and Z-discs. Transverse sections show normal packing of thin and thick filaments within the myofibrillar lattice (Figure 5.6 C). At day 3 longitudinal sections show loss of the M-lines and splitting of the myofibrils is observed (Figure 5.6 A, B). In the transverse sections at day 3 myofibre diameter begins to vary and gaps begin to appear (Figure 5.6 C arrow). At day 5 the Z-lines are damaged greatly and the M-lines are no longer visible. The sarcomere is disorganised and some zebra bodies have developed (Figure 5.7 B arrow-head). Myofibril branching is also observed (result not shown). Transverse sections at day 5 (Figure 5.7 C) show that the myofibrils are not as tightly packed as those of 1-day-old flies, and display gaps. The sarcomeres of 7-day-old flies appear more disorganized with large zebra bodies forming between them that are found more frequently in the muscles than in 5-day old flies (Figure 5.7 A arrow-head). In addition to the lack of visible M-lines already observed at 5-day old flies, the Z-discs are also difficult to discern. These observations show that there is progressive sarcomeric damage explaining why on day 1 the mutants can fly but become flightless by day 7.

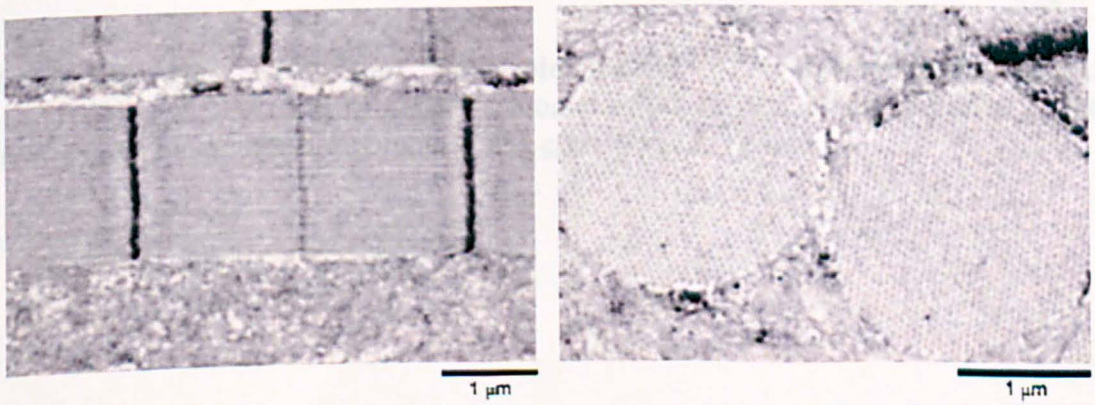

Figure 5.5. TEM images of longitudinal and transverse sections from wild type flies.

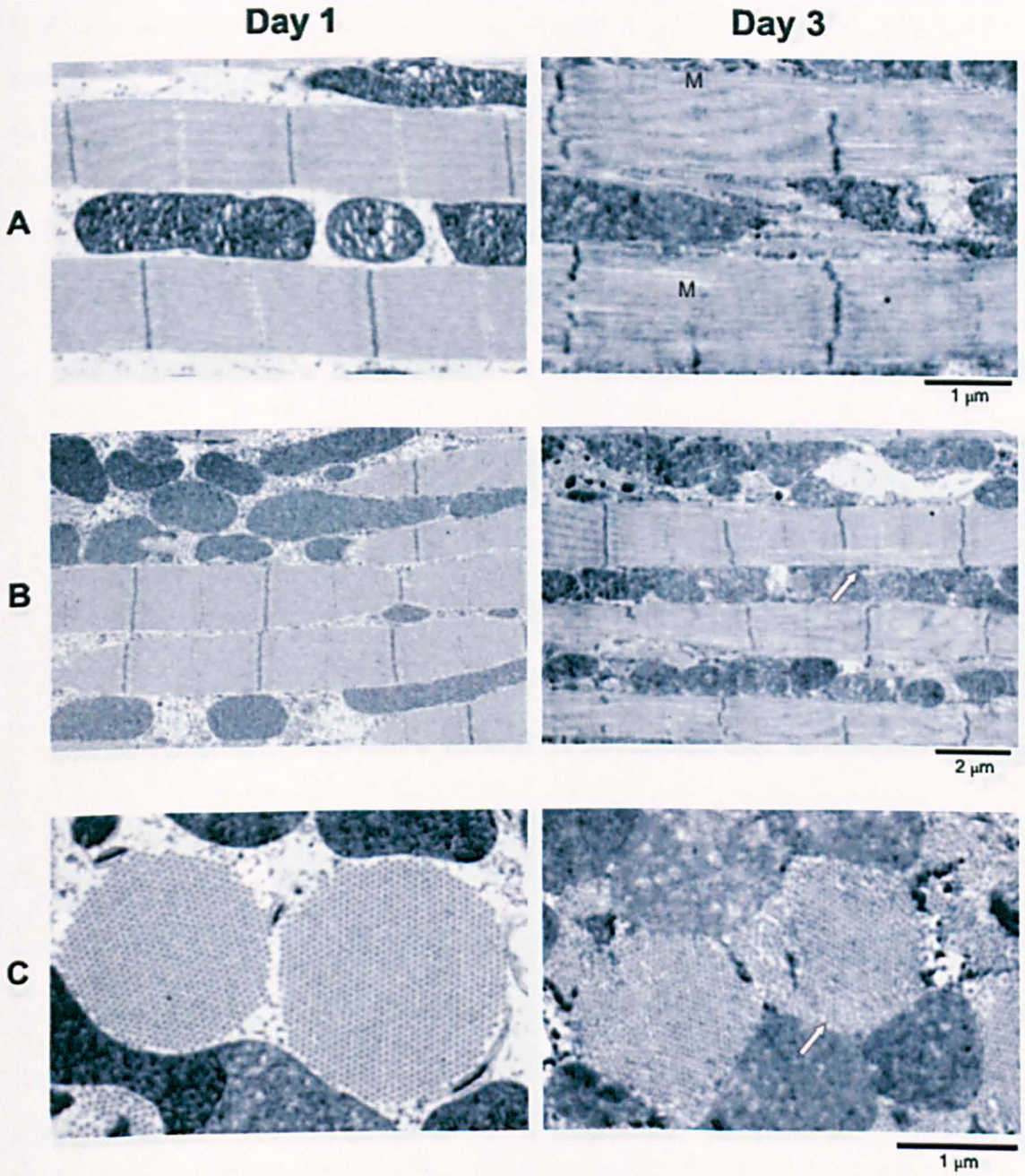

Figure 5.6. TEM of 1- and 3-day old *Act88F*^{R372H}/+ heterozygotes. (A) LS magnification at 8.200, **(B)** LS magnification at 4.200, **(C)** TS magnification at 11.500. Arrows indicate myofibril fraying in B and gaps in C. M: M-line.

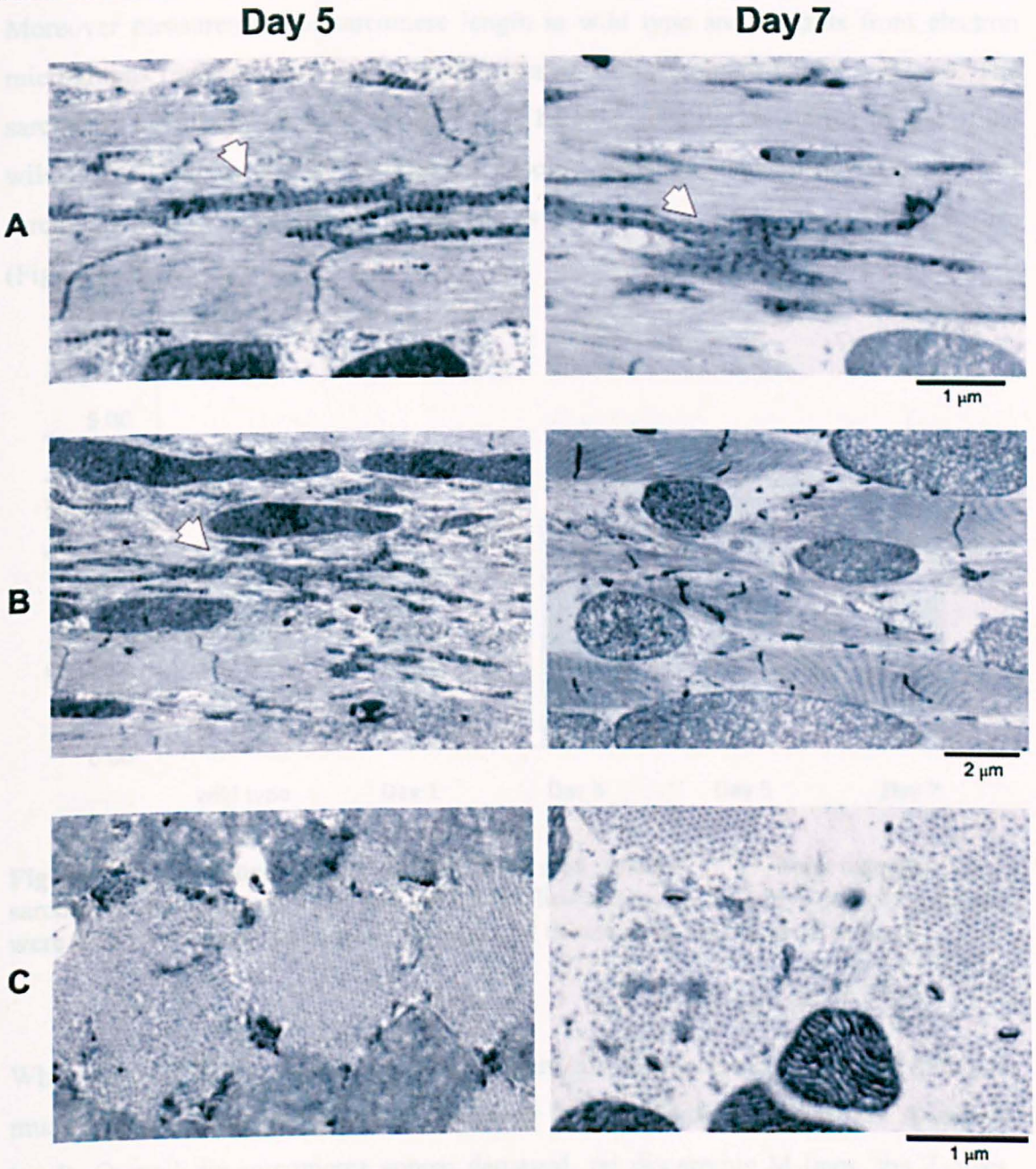

Figure 5.7. TEM of 5- and 7-day old *Act88F*^{R372H}/+ heterozygotes. (A) LS magnification at 8.200, **(B)** Ls magnification at 4.200, **(C)** TS magnification at 11.500. Arrowheads point at zebra bodies.

Moreover measurement of sarcomere length in wild type and mutants from electron micrographs revealed very large variations in mutant sarcomere length with age. The sarcomere length of 1-day-old $Act88F^{R372H}$/+ heterozygous flies is similar to that of the wild type flies. However as the mutants become older the standard deviation of their sarcomere length increases with time and is greater than that of the wild type flies (Figure 5.8).

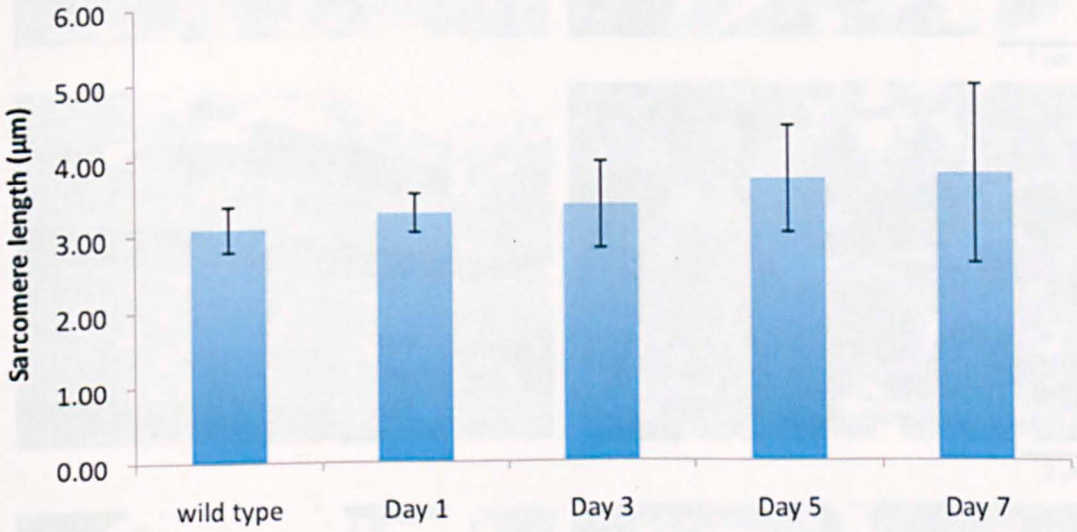

Figure 5.8. Sarcomere length of wild type and $Act88F^{R372H}$/+ heterozygotes. The sarcomere lengths from 3 day old wild type flies and 1-, 3-, 5- and 7-day-old mutants were measured from EM images, the standard deviation is shown as error bars.

When $Act88F^{R372H}$ homozygous mutants were examined already on day 1 there is muscle disarray with zebra bodies extending from the Z-discs (Figure 5.9 A arrow-head). Overall the sarcomeres appear damaged, no discernible M-lines, the Z-discs appear damaged and broken (Figure 5.9 B arrows) and there are filaments gaps (Figure 5.9 B). In transverse sections large empty patches are seen inside the myofibrils (Figure 5.9 C arrow). By day 3 large electron dense bodies start to appear (Figure 5.9 A arrow-head). No sarcomeric structure is present and the fibre is filled with broken filaments. Many more large empty gaps are seen inside the myofibrils in transverse sections (Figure 5.9 C arrows). Hence in the absence of a wild type actin copy the $Act88F^{R372H}$ homozygotes already show muscle disarray from day 1 with progressive muscle damage to the point of no obvious sarcomeric structure being present by day 3.

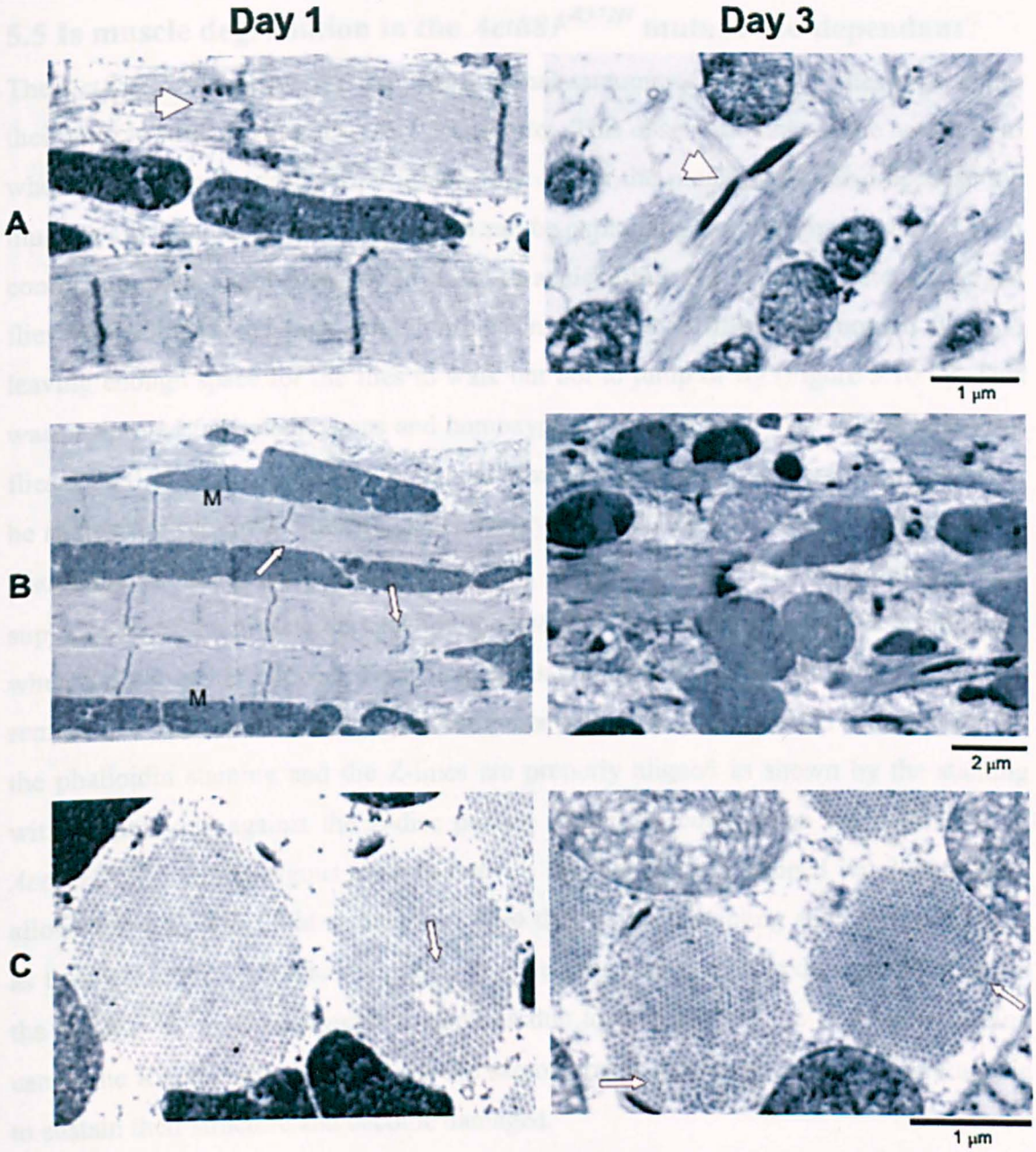

Figure 5.9. TEM of 1- and 3-day old *Act88F*^{R372H} homozygotes. (A) LS magnification at 8.200, **(B)** Ls magnification at 4.200, **(C)** TS magnification at 11.500. Arrowheads point at zebra bodies and electron dense bodies. Arrows indicate damaged Z-discs in B and gaps in C. Arrowheads indicate zebra and electron dense bodies. M: M-line

5.5 Is muscle degradation in the *Act88F*^{R372H} mutant use-dependant?

The *Act88F*^{R372H} mutants initially form normal sarcomeres but as the flies grow older their muscle structure progressively deteriorates. This observation raised the notion as to whether the sarcomeric disarray is not only due to the mutation but also because the muscles are being used. This hypothesis can be explored if the flies are prevented from contracting their flight muscles. In order to achieve this the wings of newly emerged flies were clipped and flies were confined in a Petri dish filled with normal fly food leaving enough space for the flies to walk but not to jump or fly (Figure 5.10 C). This was performed for heterozygous and homozygous mutants as well as wild type control flies. The flies were aged under these conditions and collected at different time points to be analysed by confocal microscopy. Heterozygous mutants without clipped wings were also aged in a standard culture vial as a control. Figure 5.10 demonstrates that suppression of the muscle degradation in *Act88F*^{R372H}/+ heterozygous flies occurs only when the wings are clipped. Their myofibrils are similar to the wild type control and remain like this even after 10 days. Actin is arranged in thin filaments as suggested by the phalloidin staining and the Z-lines are properly aligned as shown by the staining with an antibody against the Z-disc protein zetalin. In comparison the myofibrils of *Act88F*^{R372H}/+ heterozygous mutants kept in the vial without clipped wings that were allowed to use their flight muscles show no thin filament staining and aberrant Z-lines as they get older. This result suggests that the progressive muscle damage observed in the *Act88F*^{R372H}/+ heterozygous mutants is due to the fact that the muscles are being used. The R372H mutation weakens the sarcomeres which upon contraction are unable to sustain their structure and become damaged.

When *Act88F*^{R372H} homozygotes confined in the Petri dish were collected at later stages their muscles broke during dissections and no myofibril separation was possible. There is no phalloidin staining suggesting the integrity of the thin filaments has been compromised (Figure 5.10). Therefore in the case of the homozygotes where muscle damage has already begun at 1-day old flies as shown by EM (Figure 3.8), clipping their wings cannot prevent further muscle degradation.

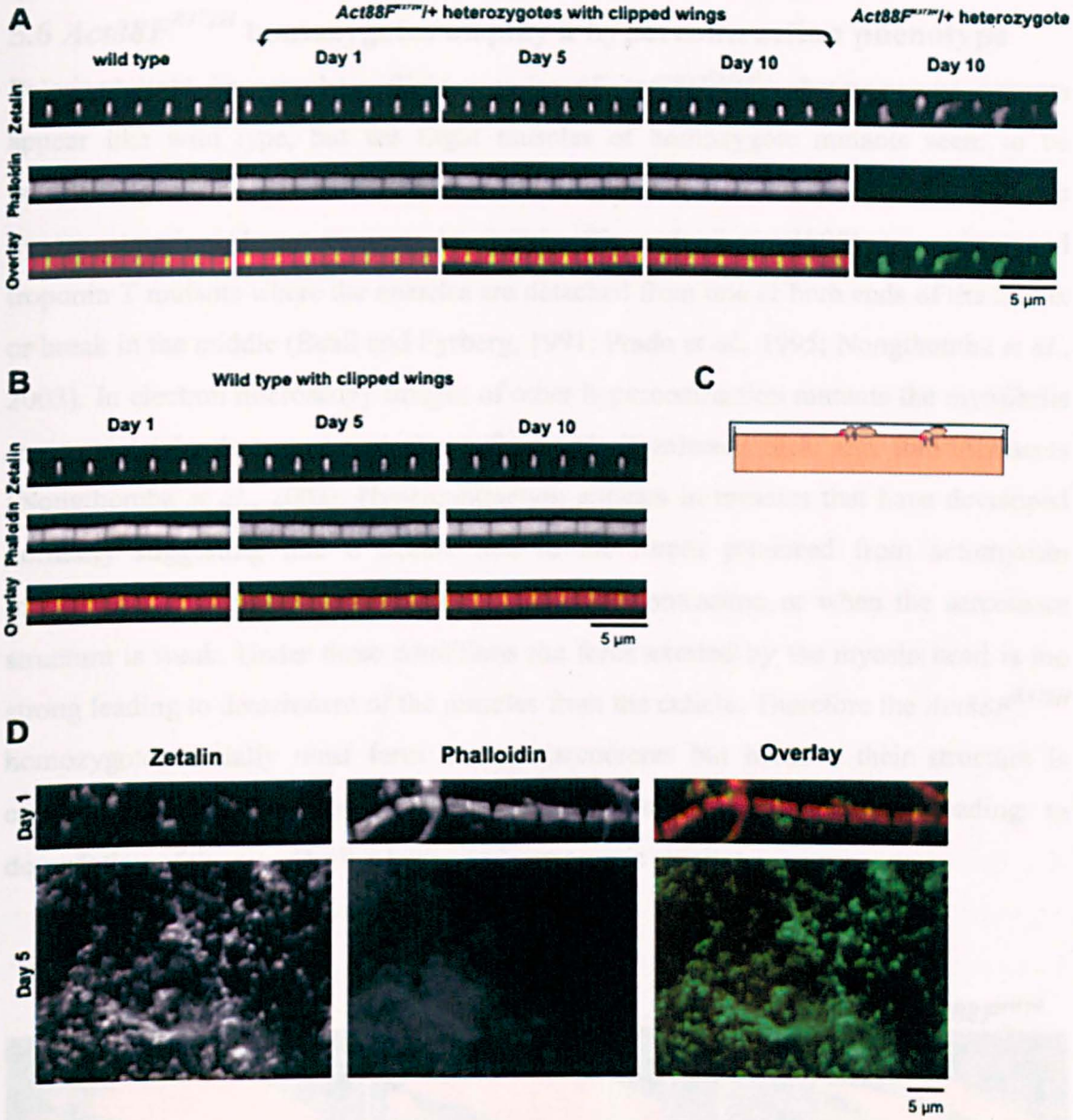

Figure 5.10. Light microscopy of myofibrils stained for actin and immunostained for zetalin. Myofibrils isolated from **(A)** wild type fly kept in standard vial, $Act88F^{R372H}$/+ heterozygote fly with clipped wings confined in petri plate (at different time points), and at the right end $Act88F^{R372H}$/+ heterozygote fly without clipped wings grown in a standard vial. **(B)** Single myofibrils from wild type flies with clipped wings at different time points. **(C)** Cartoon showing flies confined in a fly food-filled Petri-plate. **(D)** $Act88F^{R372H}$ homozygotes: at the top is a myofibril from newly emerged flies and at the bottom whole muscle from 5-day-old flies with clipped wings confined in a petri plate. Anti-zetalin antibody and TRITC-phalloidin were used. Scale bars are indicated.

5.6 *Act88F*^{R372H} homozygotes display a hypercontraction phenotype

Polarized light images show flight muscles of *Act88F*^{R372H}/+ heterozygous mutants appear like wild type, but the flight muscles of homozygote mutants seem to be detached from one end of the semi-thorax (Figure 5.11). This is reminiscent of the hypercontraction phenotype seen in myosin (Kronert *et al.*, 1995), troponin I and troponin T mutants where the muscles are detached from one or both ends of the thorax or break in the middle (Beall and Fyrberg, 1991; Prado *et al.*, 1995; Nongthomba *et al.*, 2003). In electron microscopy images of other hypercontraction mutants the myofibrils are completely destroyed and show fields of disordered thick and thin filaments (Nongthomba *et al.*, 2003). Hypercontraction appears in muscles that have developed normally suggesting that it occurs due to the forces produced from actomyosin interactions in response to aberrant regulation of contraction or when the sarcomere structure is weak. Under these conditions the force exerted by the myosin head is too strong leading to detachment of the muscles from the cuticle. Therefore the *Act88F*^{R372H} homozygotes initially must form normal sarcomeres but because their structure is compromised they cannot withstand muscle contraction, eventually leading to degradation of the myofibrillar lattice and sarcomeric structure.

Figure 5.11. Polarized light microscopy of *Drosophila* semi-thoraces. The IFM of the *Act88F*^{R372H}/+ heterozygotes appear normal, however in the *Act88F*^{R372H} homozygote the muscles have detached from one end of the cuticle (arrow).

5.7 Mechanical properties of the *Act88F*^{R372H}/+ sarcomere.

The *Act88F*^{R372H}/+ heterozygote mutants can fly initially but become flightless over time and display progressive myofibril disarray as shown by TEM images. When the wings of newly emerged *Act88F*^{R372H}/+ mutants were clipped and the flies were confined in petri plates so as to prevent them from using their flight muscles, the myofibrils did not display any structural damage over time. This would suggest that the muscles become damaged only when they are being used. An explanation why this could happen is that the muscles are mechanically compromised and gradually become damaged upon contraction and lose their structure. In order to pursue this hypothesis single myofibril mechanics were performed in order to measure the passive force produced from wild type and *Act88F*^{R372H}/+ heterozygote myofibrils. Single myofibrils are the smallest structures of muscle cells that maintain the complete contractile machinery. These features make them the optimal specimen for muscle mechanics.

The number of thick filaments from wild type and newly emerged *Act88F*^{R372H}/+ heterozygote myofibrils was measured from transverse TEM images before performing the myofibril mechanics. This was done to ensure that the force signal produced from each genotype was generated from a similar group of thick and thin filaments per myofibril. From 6-8 myofibrils, it was found that the number of thick filaments varied between 900 and 1200 among flies for each genotype (Table 5.1). Although the mean and variance within the myofibrils of the same fly do not vary significantly, there is a large variation between flies. This is an unexplained developmental phenomenon always observed in *Drosophila* IFM (Prof. Sparrow, personal communication).

As there was no significant difference between the number of thick filaments in the wild type and mutant myofibrils, single myofibril force measurements were performed at the University of Cologne, in Germany, in collaboration with Prof. Pfitzer's laboratory. The apparatus used for the experiments involves attaching single myofibrils to a length-driving tungsten stiff needle at one end and to the coated tip of an atomic force cantilever (AFC) at the other end (Figure 5.12); upon stretching of the myofibril with the length-driving needle the force can be recorded. Throughout these experiments Dr. Bogdan Iorga operated the apparatus and analyzed the force transients obtained and produced Figures 5.13, 5.14 and 5.15, which are presented in this chapter.

Table 5.1. Number of thick filaments present in the myofibrils of newly emerged wild type and $Act88F^{R372H}$/+ heterozygous flies. The number of thick filaments from 6-8 myofibrils was measured for each fly.

Genotype	Fly	Number of thick filaments
Wild type	1	1103 ± 14
	2	900 ± 33
	3	1239 ± 25
	4	945 ± 19
	5	977 ± 17
$Act88F^{R372H}$/+	1	1060 ± 44
	2	1021 ± 11
	3	925 ± 22
	4	904 ± 13
	5	920 ± 38

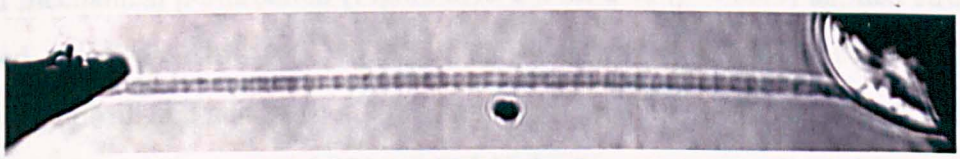

Figure 5.12. Brightfield image of a single mounted myofibril. Single IFM myofibril attached to length-driving tungsten stiff needle on the left and to the tip of an AFC on the right.

The passive force was recorded in successive stretch protocols applied to fully relaxed single myofibrils (Chapter 2 section 2.5.2). Briefly, single myofibrils were extended step-wise to 2% - 4%, 3% - 6% and 4% - 8% of their slack sarcomere length (SL) (Figure 5.13 A), and at each stage the force was measured. Stretching protocols higher than 8% were not carried out, as they would cause the myofibrils to break.

For a single applied sequential stretching protocol (2% - 4%), the passive force responsiveness of mutant myofibrils was significantly reduced ($p < 0.01$) when compared with that of wild-type myofibrils at a given applied stretch (mean ± SEM, $n = 3$): at 2 % applied stretch, $F_p = 17.7 \pm 0.4$ kPa for $Act88F^{R372H}$ and $F_p = 31.6 \pm 2.9$ kPa for wild-type myofibrils; at 4% applied stretch, $F_p = 31.7 \pm 2.7$ kPa for $Act88F^{R372H}$ and $F_p = 51.3 \pm 2.5$ kPa for wild-type myofibrils (Figure 5.13 B, C). Moreover during the applied stretch ramp to the 6 % level, the mutant myofibril has broken (Figure 5.13 B, grey trace of the force transient). The same event happened with the wild-type myofibril but upon a greater applied stretch, i.e., during the ramp to the 8 % level (Figure 5.13 C, light grey trace of the force transient) and the passive force responsiveness upon the corresponding stretch was reduced (Figures 5.13 B and C). Corresponding video files are shown in Table 5.2. The fact that less force is required to stretch the mutant myofibrils compared to the wild type ones and that the mutant myofibril brakes during the 8% stretch ramp, suggested that their structure is much weaker.

Video analysis of the myofibrils discussed in Figure 5.13 B and C showed that the observed sarcomeric stretch upon identical applied stretch is larger for mutant myofibrils than for wild-type ones and, for both myofibril types, is smaller than the applied mechanical perturbation (Figure 5.15 B). At 2 % ($p < 0.05$) applied stretch the observed stretch is 1.158 ± 0.093 % for the wild type and 1.767 ± 0.107 % for the mutant myofibril, and at 4 % ($p < 0.001$) applied stretch the observed stretch is 1.970 ± 0.036 % for the wild type and 3.175 ± 0.065 % for the mutant myofibril (Figure 5.15 B). This disagreement between applied and observed stretch of *Drosophila* IFM myofibrils has been observed by others (Hao *et al.*, 2004). This is due to the glue used to attach the myofibril to the length-driving needle and the tip of the AFC is more compliant than the myofibril itself, resulting in the glue also being stretched along with the myofibril. The consequence of this is that the myofibril becomes less stretched than expected.

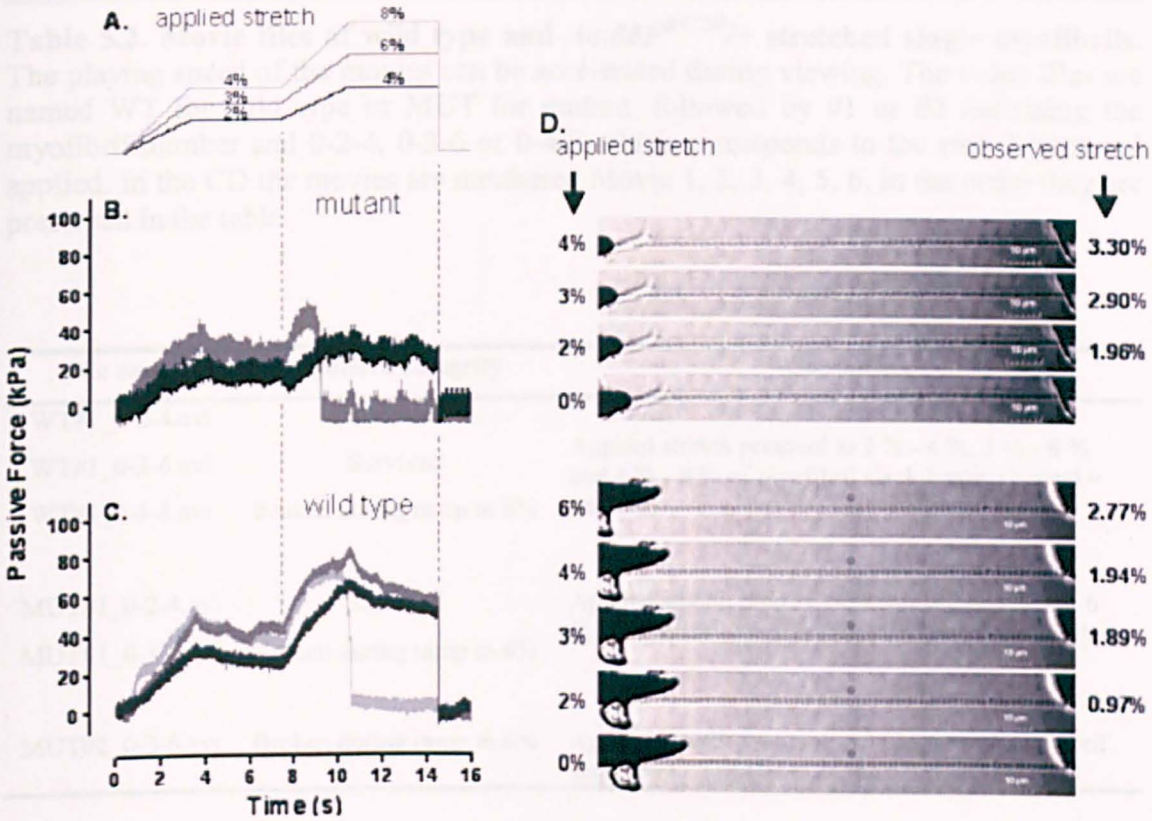

Figure 5.13. Myofibril force measurements. The force transient for a mutant **(B)** and wild-type **(C)** myofibril upon applied stretch **(A)** expressed as percentage of the slack length of the entire mounted myofibril. Force is normalized to CSA (kPa). The black transient corresponds to the protocol of the successive 2% and 4% applied stretch; the dark grey transient corresponds to the protocol of the successive 3% and 6% applied stretch; the light grey transient (only for the wild-type myofibril, C) corresponds to the protocol of the successive 4% and 8% applied stretch. The duration of each steady applied stretch is 4 seconds followed by a ramp of 3 seconds. The mutant myofibril has the diameter = 1.4 μm (CSA = 1.54 μm^2) and the initial slack length = 121.0 μm (N = 33 sarcomeres). The wild-type myofibril has the diameter = 1.85μm (CSA = 2.69 μm^2) and the initial slack length = 133.2 μm (N = 37 sarcomeres). **(D)** Microphotographs of mutant (top) and wild-type (bottom) myofibrils at different moments during the steady slack, just before the next ramp or rapid release. The imposed (left) and measured (right) stretched lengths are indicated.

Table 5.2. Movie files of wild type and *Act88F*^{R372H}/+ stretched single myofibrils. The playing speed of the movies can be accelerated during viewing. The video files are named WT for wild type or MUT for mutant, followed by #1 or #2 indicating the myofibril number and 0-2-4, 0-3-6 or 0-4-8 which corresponds to the stretch protocol applied. In the CD the movies are numbered Movie 1, 2, 3, 4, 5, 6. in the order they are presented in the table

File name	Myofibril Integrity	Comments
WT#1_0-2-4.avi	Survived	Applied stretch protocol to 2 % - 4 %, 3 % - 6 % and 4 % - 8 % of myofibril slack length (1 pixel = 160 nm)
WT#1_0-3-6.avi	Survived	
WT#1_0-4-8.avi	Broken during ramp to 8%	
MUT#1_0-2-4.avi	Survived	Applied stretch protocol to 2 % - 4 % and 3 % - 6 % of myofibril slack length (1 pixel = 106.9 nm)
MUT#1_0-3-6.avi	Broken during ramp to 6%	
MUT#2_0-3-6.avi	Broken during ramp to 6%	Applied stretch protocol to 3 % - 6 % of myofibril slack length (1 pixel =160 nm)

In addition, before the same mutant myofibril was subjected to the second stretching protocol (3% - 6%), its slack SL was measured as larger than its initial slack (SL_0) by 1.49 % (indicated by arrow in Figure 5.14), suggesting a remnant structural plastic deformation. This was not the case for the wild-type myofibril, which did not show a significant plastic deformation before commencing the third stretching protocol (4% - 8%), i.e. only by 0.1 5% and 0.23 % after the first and second applied stretching protocol, respectively. Therefore the fact that the mutant myofibril exhibits substantial plastic deformation upon stretching supports the idea that it is prone to become damaged upon use. Furthermore its estimated stiffness seems to be at least 2.5 - 3 times smaller than that of wild-type control for all the applied stretches (Figure 5.14).

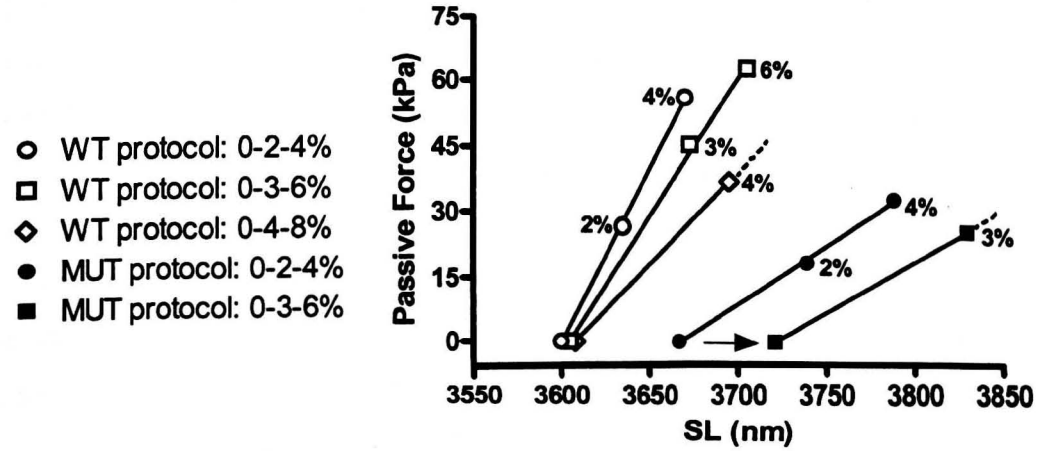

Protocol	Stiffness for wild type	Stiffness for mutant
0-2-4 (kPa)	0.8014 ± 0.02227	0.2700 ± 0.009593
0-3-6 (kPa)	0.6342 ± 0.02984	0.2370
0-4-8 (kPa)	0.4230	Broken during ramp

Figure 5.14. The passive force responsiveness upon stretch of mutant and wild-type myofibrils. Force is normalized to CSA (kPa). SL (nm) is the observed sarcomere length of wild-type (open symbols) and mutant (closed symbols) myofibrils stretched to the applied values indicated in percents (%). Circles correspond to the first applied protocol (2% - 4%), squares to the second one (3% - 6%) and diamonds to the last protocol (4% - 8%) applied to the myofibrils. The arrow indicates the plastic deformation observed for the mutant myofibril by 1.49% of its initial slack sarcomere length (SL_0). Dashed lines indicate that upon the protocol "4% - 8%" for wild type and "3% - 6%" for mutant, myofibrils brake-down during the application of the final ramp. Slopes of the best-fit linear regression estimate the stiffness (kPa/nm).

Less passive force is required to achieve a higher observed stretch for the mutant myofibril compared to the wild type (Figure 5.15 A, B). The estimated stiffness acquired for the mutant is similar (Figure 5.15 C), which denotes the linearity of the passive force-sarcomere length relationship shown in Figure 5.14. The linearity implies that the elastic component predominates in the mutant myofibrils. However, a small viscous component cannot be completely neglected, at least for the wild-type myofibril, since a peak in the force responsiveness was observed at the end of each ramp of stretching before reaching a the steady state. Mutant myofibrils did not display a clear peak of passive force even when the ramp of the stretching was faster (transients not shown). Overall these results suggest that myofibrils isolated from the IFM of $Act88F^{R372H}/+$ heterozygotes are mechanically less stiff and more fragile than wild-type controls supporting the hypothesis that this mutation has structural consequences on myofibrillar filaments.

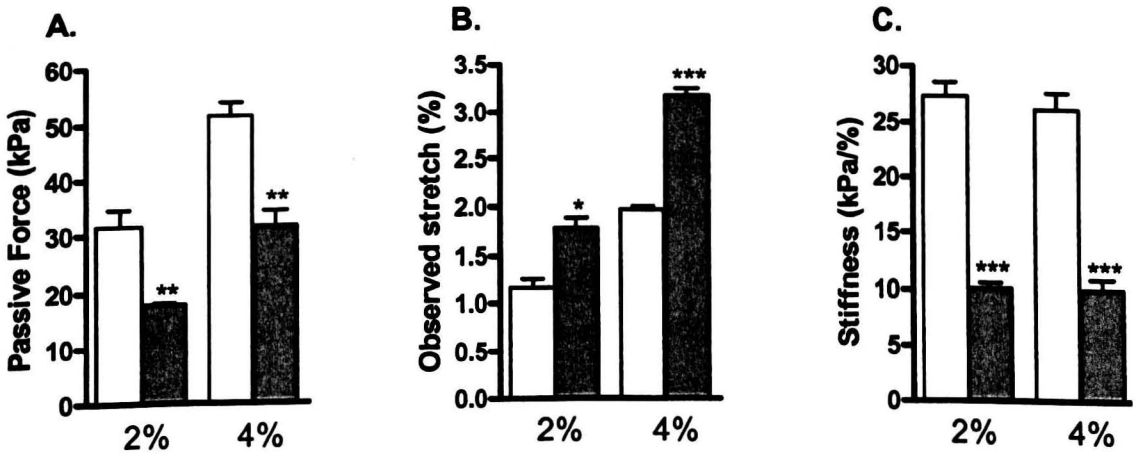

Figure 5.15. Passive force, observed stretch responsiveness and stiffness of wild-type and mutant myofibrils. (A) Passive force and **(B)** observed stretch responsiveness upon identical applied stretch (2% and 4% of the slack myofibrillar length) for wild-type (white bars) and mutant (grey bars) myofibrils are shown. For each myofibril, force was normalized to CSA (kPa). The observed stretch was normalized to its slack length, expressed in % and then averaged. **(C)** Mean ± SEM values for stiffness expressed as the passive force induced by 1% observed stretch of slack myofibrils are shown. Significance level between values of $n = 3$ mutant and wild-type myofibrils: * ($p < 0.05$), ** ($p < 0.01$), *** ($p < 0.001$).

5.8 Is the reduced myofibrillar stiffness in the *Act88F*^{R372H}/+ heterozygote mutants a result of weakened F-actin/ α-actinin interactions?

The R372 residue is not known to be in direct contact with other major sarcomeric proteins such as tropomyosin, myosin or the troponin complex and it is therefore less likely that the R372H mutation will directly affect the actin binding to any of those proteins. The reduced stiffness seen in the myofibrils of *Act88F*^{R372H}/+ heterozygous mutants compared to the wild type ones could be due to a weakened interaction of actin with a binding partner situated in the Z-disc. α-Actinin is a Z-disc protein involved in cross-linking the actin thin filaments within the Z-disc (Saide *et al.*, 1989; Lakey *et al.*, 1990). The binding constant of actin for α-actinin has been measured to be 2.1μM (van Straaten *et al.*, 1999). α-Actinin exists as an anti-parallel homodimer with the actin binding domains at opposite ends of the homodimer (Djinovic-Carugo *et al.*, 1999, Tang *et al.*, 2001). Actin thin filaments of adjacent sarcomeres overlap and terminate within the Z-disc where they are linked by transversely oriented α-actinin molecules that form ladder-like structures within the thin filaments (Figure 5.16 B) (Meyer and Aebi., 1990; Vigoreaux, 1994). Cryo-EM reconstructions of α-actinin decorated F-actin (McGough *et al.*, 1994) and biochemical data (Mimura and Asano, 1987; Lebart *et al.*, 1993) place the α-actinin binding site on residues 83-117 and 350-372 of the actin monomer. The R372 residue is on the outer surface of the thin filament (Figure 5.16 A) and is located in one of the two proposed α-actinin binding sites on actin (Lebart *et al.*, 1993).

The *Act88F* mutation, E93K, is in the other α-actinin binding site (Sparrow *et al.*, 1995) on actin and results in a hypercontraction phenotype similar to that seen in the polarized light images of the *Act88F*^{R372H} homozygous mutant (Figure 5.11). A weakened interaction between α-actinin and the actin thin filaments caused by a mutation could lead to detachment of the thin filaments from the Z-discs upon muscle contraction. Detachment of the thin filaments from the Z-discs of *Act88F*^{R372H} homozygotes were also observed in EM images (Figure 5.17). This would explain why the R372H actin mutation affects the attachment of the thin filaments at the Z-disc and why a reduced stiffness of the mutant myofibrils was observed.

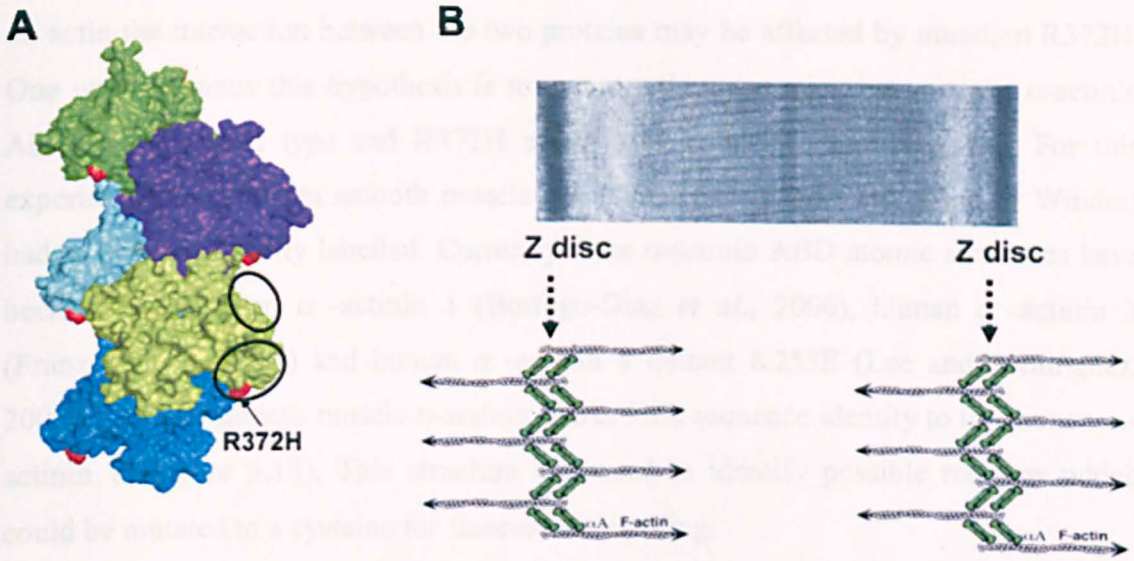

Figure 5.16. The R372 residue is in the proposed α-actinin binding site on actin. (A) In the F-actin helix the R372 residue in each actin monomer is shown in red and the two black circles surround the proposed α-actinin binding sites on actin. **(B)** In the Z-discs α-actinin (αA) homodimers form cross-bridges with actin filaments (other proteins that are not shown here are also involved in the attachment of thin filaments on the Z-disc). Picture adapted from Djinovic-Carugo *et al.*, 2001.

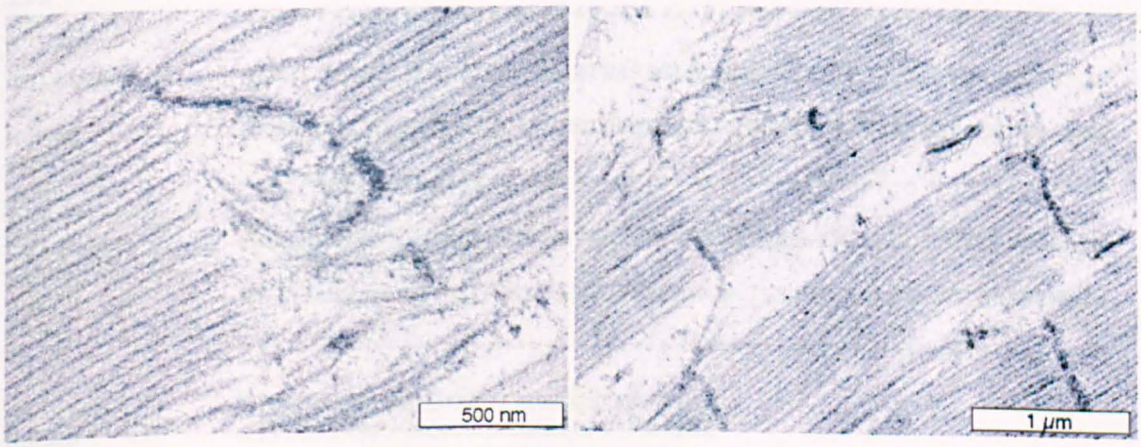

Figure 5.17. TEM of 7-day-old *Act88F*^{R372H} homozygotes showing thin filaments detaching from the Z-disc. Scale bars are indicated.

5.9 Purification of the *Gallus gallus* α-actinin ABD^{S103C} mutant

Given the fact that the R372 residue is within one of the two proposed α-actinin ABD on actin the interaction between the two proteins may be affected by mutation R372H. One way to pursue this hypothesis is to measure the interaction between the α-actinin ABD and the wild type and R372H actins using fluorescence anisotropy. For this experiment, the chicken smooth muscle α-actinin ABD (a kind gift from Dr Winder) had to be fluorescently labelled. Currently three α-actinin ABD atomic structures have been solved: human α -actinin 1 (Borrego-Diaz *et al.*, 2006), human α -actinin 3 (Franzot *et al.*, 2005) and human α -actinin 4 mutant K255E (Lee and Dominguez, 2008). Chicken smooth muscle α-actinin shares 98% sequence identity to the human α -actinin 1 (Figure 5.18). This structure was used to identify possible residues which could be mutated to a cysteine for fluorescent labelling.

```
Chicken     MDHHYDPQQTNDYMQPEEDWDRDLLLDPAWEKQQRKTFTAWCNSHLRKAGTQIENIEEDF
60
Human       MD-HYDSQQTNDYMQPEEDWDRDLLLDPAWEKQQRKTFTAWCNSHLRKAGTQIENIEEDF
59          ** *** ***************************************************

Chicken     RDGLKLMLLLEVISGERLAKPERGKMRVHKISNVNKALDFIASKGVKLVSIGAEEIVDGN
120
Human       RDGLKLMLLLEVISGERLAKPERGKMRVHKISNVNKALDFIASKGVKLVSIGAEEIVDGN
119         ************************************************************

Chicken     VKMTLGMIWTIILRFAIQDISVEETSAKEGLLLWYQRKTAPYKNVNIQNFHISWKDGLGF
180
Human       VKMTLGMIWTIILRFAIQDISVEETSAKEGLLLWCQRKTAPYKNVNIQNFHISWKDGLGF
179         ********************************* ************************

Chicken     CALIHRHRPELIDYGKLRKDDPLTNLNTAFDVAEKYLDIPKMLDAEDIVGTARPDEKAIM
240
Human       CALIHRHRPELIDYGKLRKDDPLTNLNTAFDVAEKYLDIPKMLDAEDIVGTARPDEKAIM
239         ************************************************************

Chicken     TYVSSFYHAFSGAQKAETAANRICKVLAV 269
Human       TYVSSFYHAFSGAQKAETAANRICKVLAV 268
            ****************************
```

Figure 5.18. Protein sequence alignment of the chicken and human α-actinin ABDs. Identical residues are indicated by a star. The accession number for the chicken α-actinin 1 ABD is NM_204127 and for the human α-actinin 1 (ACTN1) ABD from transcript variant 3 is NM_001130005. Sequence alignment was performed using Clustal W2.

The α-actinin ABD consists of 269 residues. The structure solved by Borrego-Diaz *et al.*, 2006 only resolves residues 30-253. α-Actinin ABD naturally contains three cysteines, two of which are buried beneath the surface (C42 and C181). The last cysteine (C264) was not solved in the structure. Serine 103 was mutated to a cysteine for two reasons; (1) it is not close to the proposed actin-binding site (Figures 5.19 A, B) and (2) it is solvent exposed (Figure 5.19 C, D). The NH_2-terminal His-tagged α-actinin ABD S103C variant was overproduced and purified as described in Chapter 2 Section 2.4.3., the purification steps and purity at each stage are shown in Figures 5.20 A, B, C, D, E.

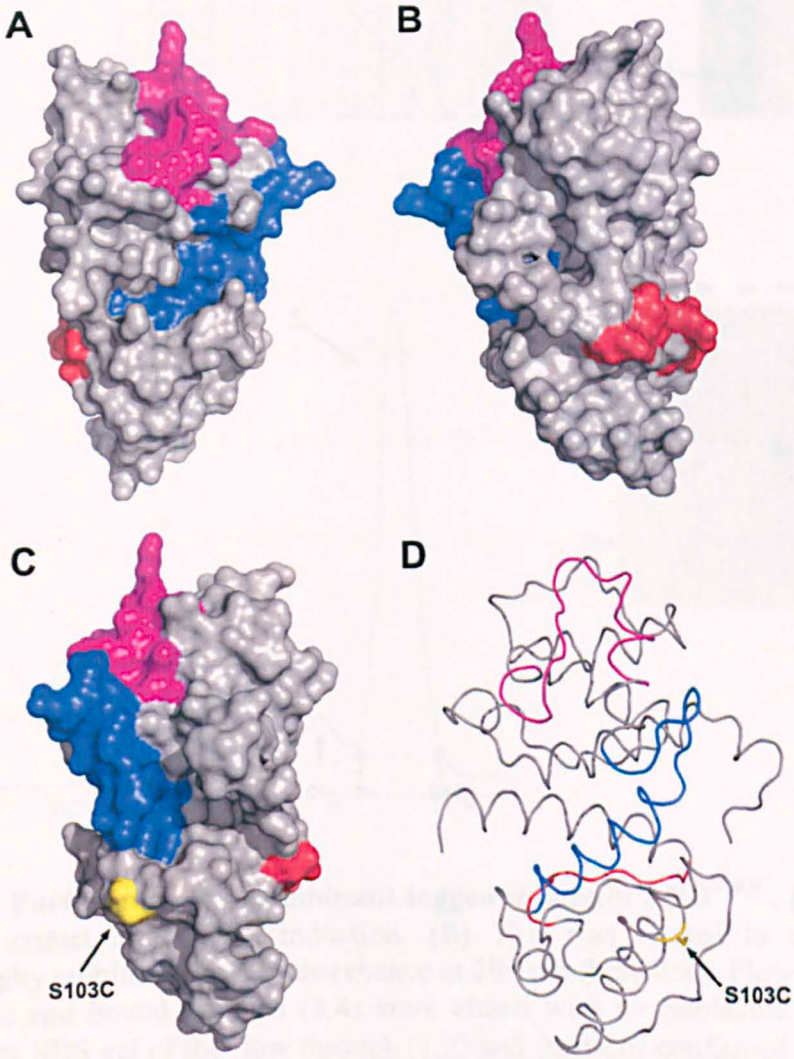

Figure 5.19. Crystal structure of human smooth muscle α-actinin ABD isoform 1 (residues 30-253) with the three proposed actin-binding sites (ABS). (A and B) ABS1 is shown in red, ABS2 in blue and ABS3 in purple. **(C)** The surface S103 residue that was mutated into a cysteine is shown in yellow. **(D)** The free S103 is shown as stick. Pdb file (2EYI) taken from Borrego-Diaz *et al.*, 2006, pictures were made using Pymol.

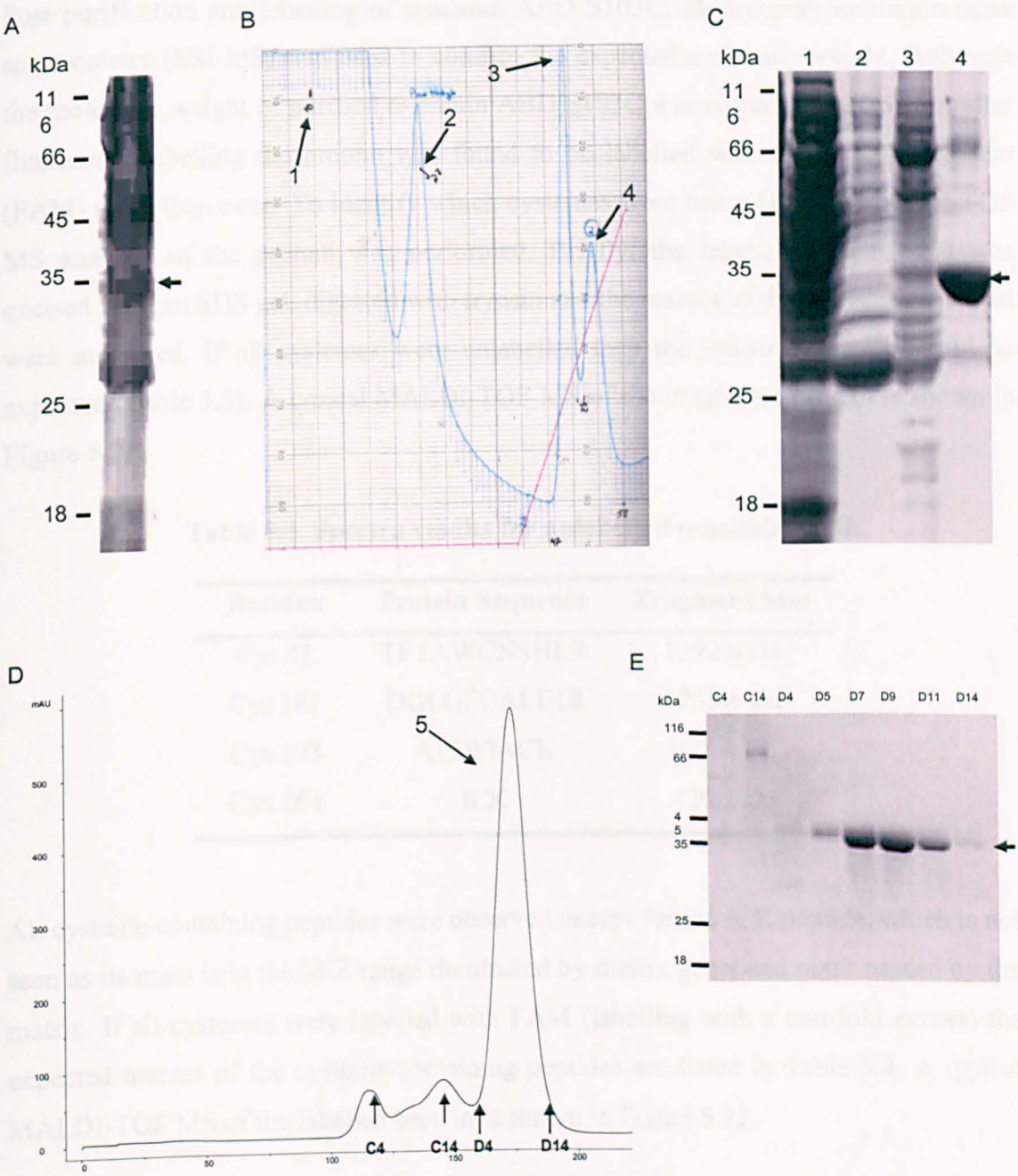

Figure 5.20. Purification of recombinant tagged α-actinin ABD^{S103C}. (A) 10% SDS gel of cell extract after IPTG induction. **(B)** This was treated to nickel-affinity chromatography monitored by UV absorbance at 280 nm (blue line). Flow through (1,2) was collected and bound proteins (3,4) were eluted with an imidazole gradient (red line). **(C)** 10% SDS gel of the flow through (1,2) and fractions confirmed that α-actinin ABD^{S103C} is in peak 4. **(D)** Gel filtration profile monitored by absorbance at 280 nm on a Superdex S75 26/60 column of flow through. **(E)** 10% SDS gel of fractions from the three elution peaks shows that α-actinin ABD^{S103C} is present in the fractions D4 to D14. α-Actinin ABD^{S103C} bands in 10% SDS PAGE gels are indicated by an arrow.

Post purification and labelling of α-actinin ABD S103C, electrospray ionisation mass spectrometry (ESI-MS) was used to confirm the expected molecular weight. Although the molecular weight of purified α-actinin ABD S103C was correct (33616.4 Da), after fluorescent labelling the protein was found to be labelled with 5-carboxyfluorescein (FAM) more than once. To identify which cysteines were being labelled MALDI-TOF MS analysis of the protein was performed. Briefly, the labelled protein band was excised from an SDS gel, digested with trypsin and the masses of the peptides generated were measured. If all cysteines were unlabelled then the following peaks would be expected (Table 5.3). A typical MALDI-TOF MS of the unlabelled protein is shown in Figure 5.21.

Table 5.3. Spectra results for unlabelled α-actinin ABD.

Residue	Protein Sequence	Fragment Size
Cys 42	TFTAWCNSHLR	1392.6 Da
Cys 181	DGLGFCALIHR	1258.6 Da
Cys 103	ALDFIACK	937.4 Da
Cys 264	ICK	420.2 Da

All cysteine-containing peptides were observed except for the ICK peptide, which is not seen as its mass is in the M/Z range dominated by matrix generated noise caused by the matrix. If all cysteines were labelled with FAM (labelling with a two-fold excess) the expected masses of the cysteine-containing peptides are listed in Table 5.4. A typical MALDI-TOF MS of the labelled protein is shown in Figure 5.22

Table 5.4. Spectra results for labelled α-actinin ABD.

Residue	Protein Sequence	Fragment Size
Cys 42	TFTAWC*NSHLR	1780.7 Da
Cys 181	DGLGFC*ALIHR	1646.7 Da
Cys 103	ALDFIAC*K	1325.5 Da
Cys 264	IC*K	808.1 Da

The MALDI-TOF MS of the labelled α-actinin ABD S103C clearly shows that all four cysteines became labelled. The buried cysteines (C42 and C181) must become exposed during the labelling procedure. Whether this is due to protein 'breathing', a less compact structure or due to the S103C mutation is not known. C264, which was not seen in the crystal structure, is also labelled. The termini of proteins are usually not observed in X-ray crystallography due to the high flexibility. The labelling of C264 demonstrates that this region of the protein is solvent exposed. The genetically engineered cysteine (S103C) is also labelled. However, as it stands it is not possible to use this variant of α-actinin ABD due to labelling of all cysteines. Even if conditions were sought to suppress labelling of the buried cysteines (C42 and C181) the solvent exposed cysteine (C264) would still be labelled. Therefore wild type α-actinin ABD was used instead to label the intrinsic cysteine, C264.

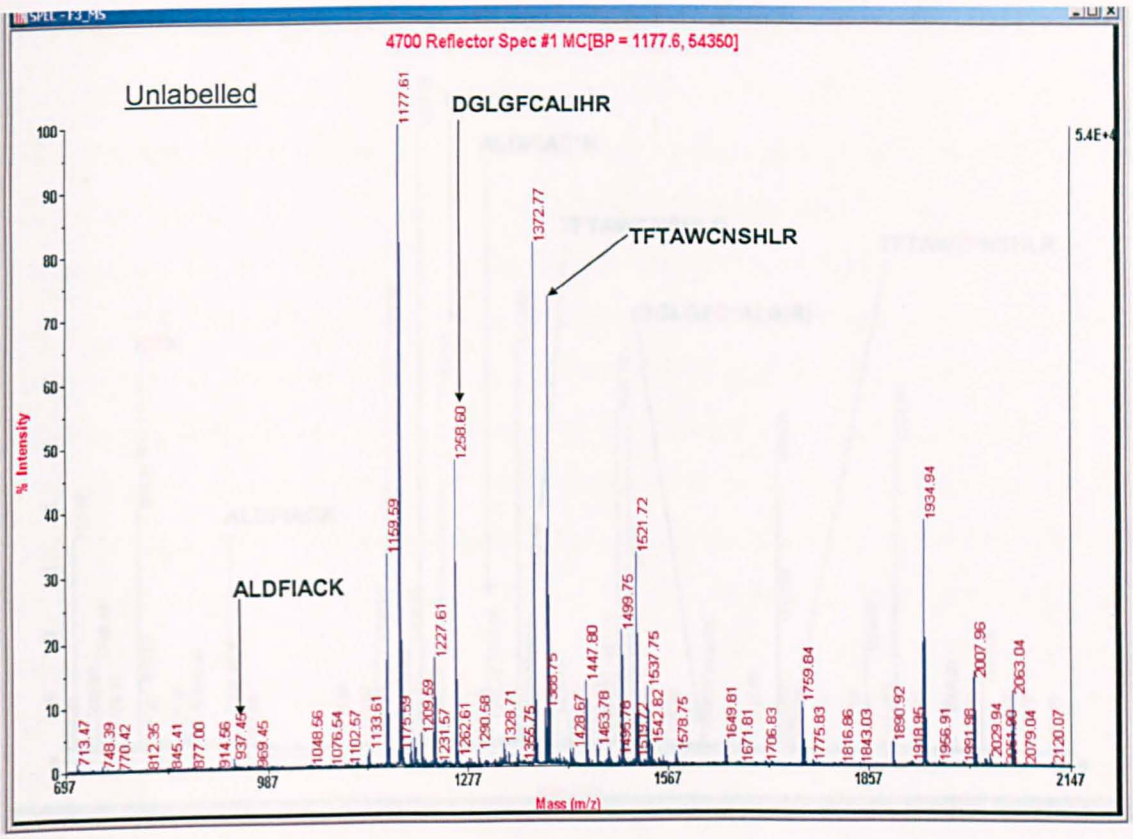

Figure 5.21. Spectra of unlabelled α-actinin ABD^{S103C}. Arrows are pointing at the cysteine containing fragments. The smallest cysteine-containing fragment is not visible. Analysis and representation of spectra carried out by Adam Dowle at the Technology Facility of the Biology Department.

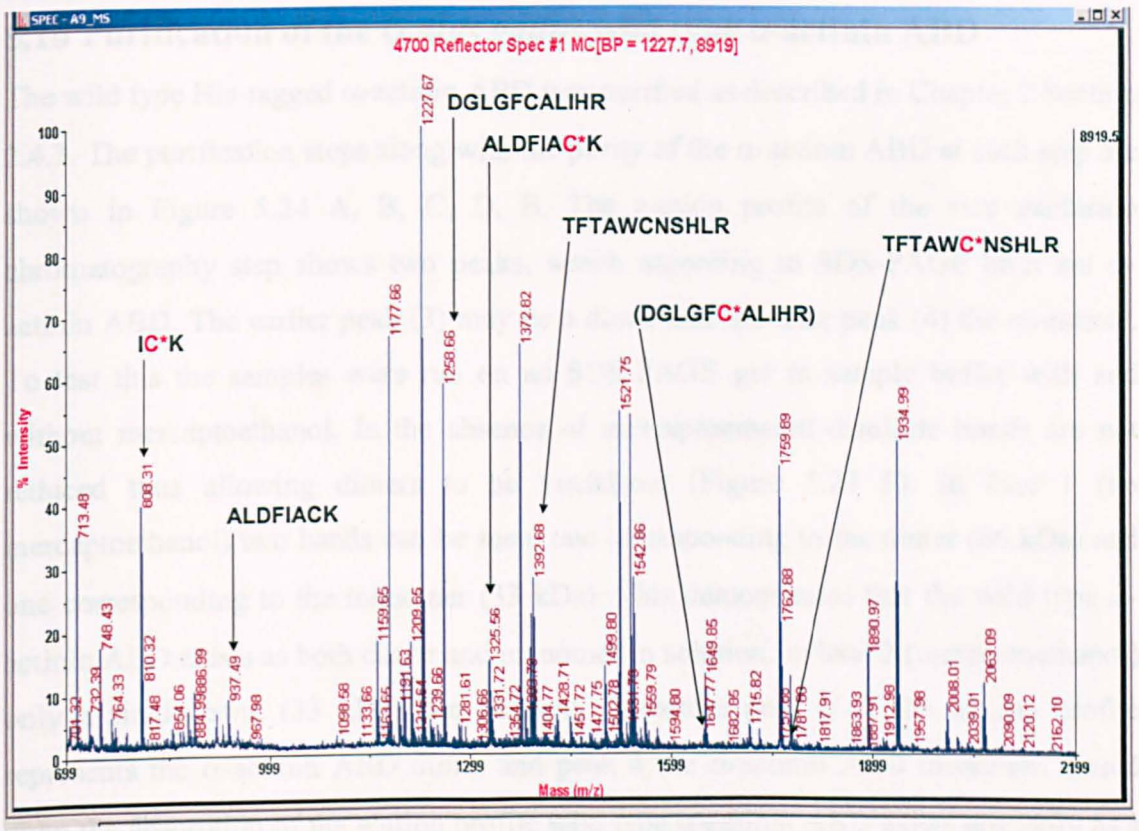

Figure 5.22. Spectra of labelled α-actinin ABD^{S103C} labelled with two fold molar excess of fluorophore. The spectra show that all four cysteines are labelled in the sample, as well as some peaks of unlabelled fragments. Analysis and representation of spectra carried out by Adam Dowle at the Technology Facility of the Biology Department.

5.10 Purification of the *Gallus gallus* wild type α-actinin ABD

The wild type His-tagged α-actinin ABD was purified as described in Chapter 2 Section 2.4.3. The purification steps along with the purity of the α-actinin ABD at each step are shown in Figure 5.24 A, B, C, D, E. The elution profile of the size exclusion chromatography step shows two peaks, which according to SDS-PAGE both are α-actinin ABD. The earlier peak (3) may be a dimer and the later peak (4) the monomer. To test this the samples were run on an SDS-PAGE gel in sample buffer with and without mercaptoethanol. In the absence of mercaptoethanol disulfide bonds are not reduced thus allowing dimers to be visualized (Figure 5.23 F). In lane 1 (no mercaptoethanol) two bands can be seen, one corresponding to the dimer (66 kDa) and one corresponding to the monomer (33 kDa). This demonstrates that the wild type α-actinin ABD exists as both dimer and monomer in solution. In lane 2 (mercaptoethanol) only a single band (33 kDa) can be seen. Therefore peak 3 of the elution profile represents the α-actinin ABD dimer and peak 4 the α-actinin ABD monomer. Based upon the absorption of the elution profile wild type α-actinin ABD exists primarily as a dimer in solution. As the overexpressed α-actinin ABD lacks the dimerization domain, mercaptoethanol has demonstrated that dimerization occurs probably due to an exposed cysteine. The tendency of α-actinin ABD to dimerize caused problems with labelling. Figure 5.24 shows that labelling of α-actinin ABD results in the labelling of the dimer, despite DTT being present in the labelling reaction. In addition to this multiple labelling was still occurring, suggesting the internal cysteines (C42 and C181) are still exposed. To overcome this problem, the role of kosmotropes was explored. Kosmotropes added to protein solutions lead to dehydration of the protein surface and increase the strength of the hydrophobic interaction causing stabilization of the structure. Sucrose, a known kosmotrope, was used in the labelling buffer (2 M). ESI-MS of the labelled protein resulted in no dimerization of α-actinin ABD although it still shows labelling of the buried cysteines (Figure 5.25 A). Although ESI-MS is not quantitative, the relative intensities of the peaks with and without sucrose suggest that less multiple labelling is occurring in the presence of sucrose (Figure 5.25 A, B).

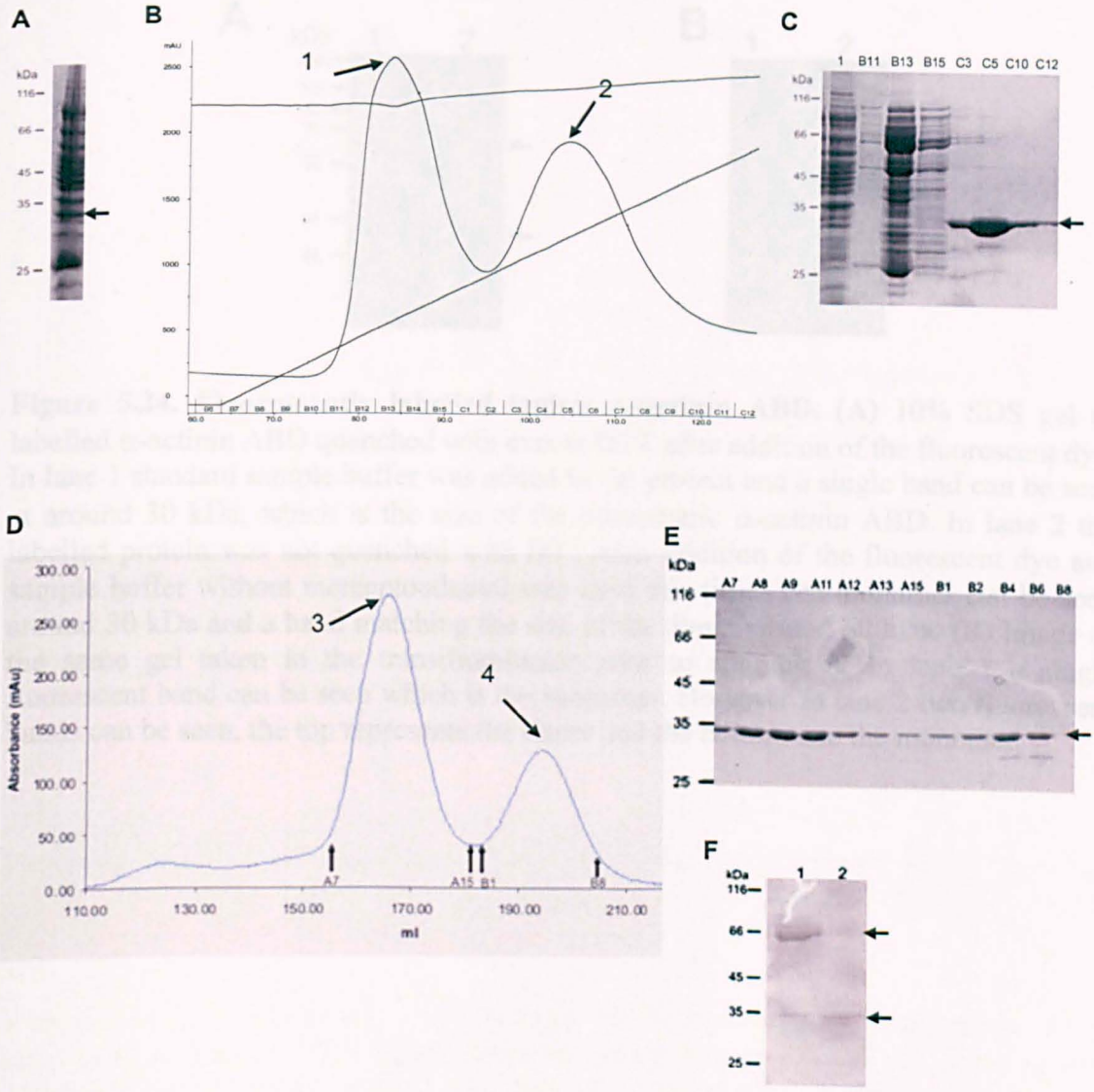

Figure 5.23. Purification of recombinant tagged α-actinin ABD. (A) 10% SDS PAGE gel of cell extract after IPTG induction. α-Actinin ABD is indicated with an arrow. **(B)** This was treated to weak-anion exchange chromatography (DE52) monitored by UV absorbance at 280 nm (blue line). Flow through (1) was collected and bound proteins (2) were eluted with an imidazole gradient (bottom line). **(C)** 10% SDS PAGE gel of the flow through (lane 1) and fractions confirmed that α-actinin ABD is in fractions C3 to C12. **(D)** Gel filtration profile monitored by absorbance at 280 nm on a Superdex S75 26/60 column of flow through. **(E)** 10% SDS PAGE gel of fractions from the two elution peaks shows α-actinin ABD is present in both. **(F)** 10% SDS PAGE gel of fraction A9 prepared in sample buffer without mercaptoethanol (lane 1) shows it contains an α-actinin ABD dimer at 66 kDa and a monomer at around 33 kDa. Fraction A9 prepared in standard sample buffer (lane 2) shows monomeric α-actinin ABD. All α-actinin ABD are indicated by arrow.

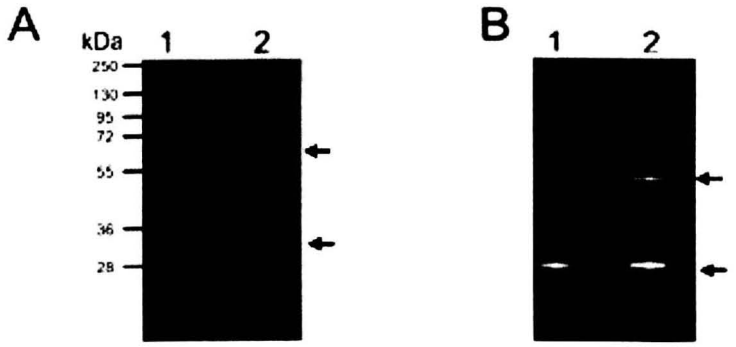

Figure 5.24. Fluorescently labelled tagless α-actinin ABD. (A) 10% SDS gel of labelled α-actinin ABD quenched with excess DTT after addition of the fluorescent dye. In lane 1 standard sample buffer was added to the protein and a single band can be seen at around 30 kDa, which is the size of the monomeric α-actinin ABD. In lane 2 the labelled protein was not quenched with DTT after addition of the fluorescent dye and sample buffer without mercaptoethanol was used this time. The monomer can be seen around 30 kDa and a band matching the size of the dimer around 60 kDa. **(B)** Image of the same gel taken in the transilluminator prior to staining it. In lane 1 a single fluorescent band can be seen which is the monomer. However in lane 2 two fluorescent bands can be seen, the top represents the dimer and the bottom one the monomer.

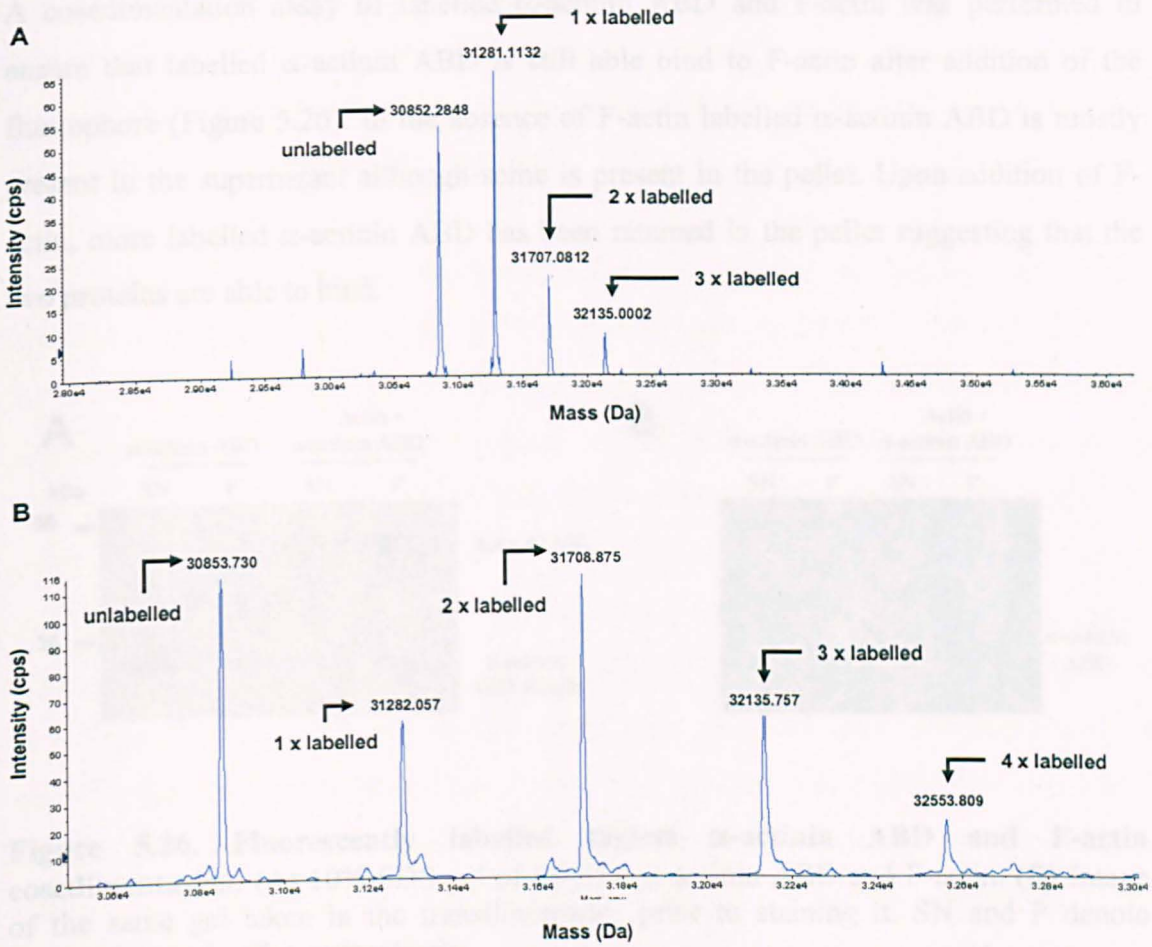

Figure 5.25. The effect of a kosmotrope on FAM-labelling of α-actinin ABD monitored by ESI-MS. The reconstructed masses of the raw ESI-MS data for α-actinin ABD showing unlabelled, single-, double-, triple- and quadruple labelling of exposed cysteines in the presence **(A)** and absence **(B)** of sucrose.

A cosedimentation assay of labelled α-actinin ABD and F-actin was performed to ensure that labelled α-actinin ABD is still able bind to F-actin after addition of the fluorophore (Figure 5.26). In the absence of F-actin labelled α-actinin ABD is mostly present in the supernatant although some is present in the pellet. Upon addition of F-actin, more labelled α-actinin ABD has been retained in the pellet suggesting that the two proteins are able to bind.

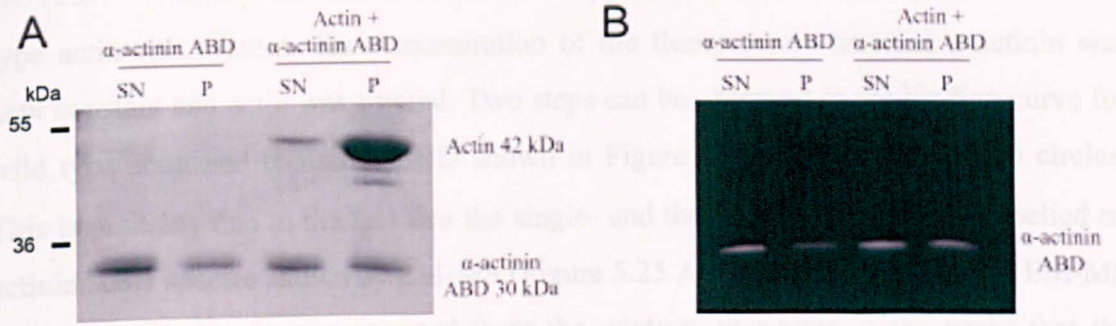

Figure 5.26. Fluorescently labelled tagless α-actinin ABD and F-actin cosedimentation. (A) 10% SDS gel of labelled α-actinin ABD and F-actin. **(B)** Image of the same gel taken in the transilluminator prior to staining it. SN and P denote supernatant and pellet, respectively.

5.11 Fluorescence anisotropy measurements of α-actinin ABD and F-actin

Fluorescence anisotropy is concerned with changes of the plane of polarised light upon protein complexation. For instance, when a protein is excited with vertical polarised light, the light is emitted in the same polarised plane, if the protein is not tumbling during the excited state (~ ns timescale). However, if the protein tumbles out of this plane, the light is remitted in a different plane. During the course of the experiment, the intensity of both the vertical and horizontal planes is measured. The changes from the vertical to the horizontal plane (depolarisation) are therefore dependent on changes in the speed of protein tumbling. The largest fluorescence change measured is when a small protein (fast tumbler) binds to a large protein (slow tumbler). Hence, protein interactions can be detected when the smaller of two interacting partners is fused to a fluorophore and binds to a larger partner (this maximizes the difference in signal

between bound and unbound states). The amount of polarization observed is proportional to the amount of protein complex formed, which is proportional to the concentration of the binding partners in solution. Hence by titrating one of the two proteins a binding curve can be generated.

Here fluorescence anisotropy was performed to compare the binding of fluorescently labelled wild type α-actinin ABD to wild type and ACT88F^{R372H} mutant F-actin. ACT88F^{R372H} actin was extracted from homozygous *Act88F*^{R372H} flies to ensure no wild type actin was present. The concentration of the fluorescently labelled α-actinin was kept constant and actin was titrated. Two steps can be observed in the binding curve for wild type actin and α-actinin ABD shown in Figure 5.27 as closed and open circles. This is probably due to the fact that the single- and the double-fluorescently labelled α-actinin ABD species shown by ESI-MS (Figure 5.25 A) bind to actin. Although ESI-MS is not quantitative, it was assumed from the relative intensities of the peaks that the amount of double-labelled α-actinin ABD will be less than that of the single-labelled α-actinin ABD. Hence, given the fact that the change in anisotropy is concentration dependent, it was assumed here that the smaller step in the binding corresponds to the double-labelled α-actinin ABD which must be present in smaller amounts (Figure 5.27 closed circles). The second step in the binding must correspond to the single-labelled α-actinin ABD (Figure 5.27 open circles). A binding curve was generated from the single-labelled α-actinin ABD readings using SigmaPlot and the dissociation constant (K_d) of the wild type actin for the α-actinin ABD was shown to be 0.39 μM ($R^2 = 0.9006$).

In the mutant the two step binding is not as obvious. Closed and open triangles were used to plot the readings assuming there are two different steps in the binding due to the single and double-labelled α-actinin ABD binding to R372H actin. A binding curve was generated using the open triangle readings and the K_d of the R372H actin was shown to be 5.21 μM ($R^2 = 0.9278$), approximately 13.35-fold weaker than that of the wild type actin. Hence reduced affinity of the mutant actin for α-actinin could explain the detachment of the thin filaments from the Z-discs seen in the images of *Act88F*^{R372H} homozygous flies.

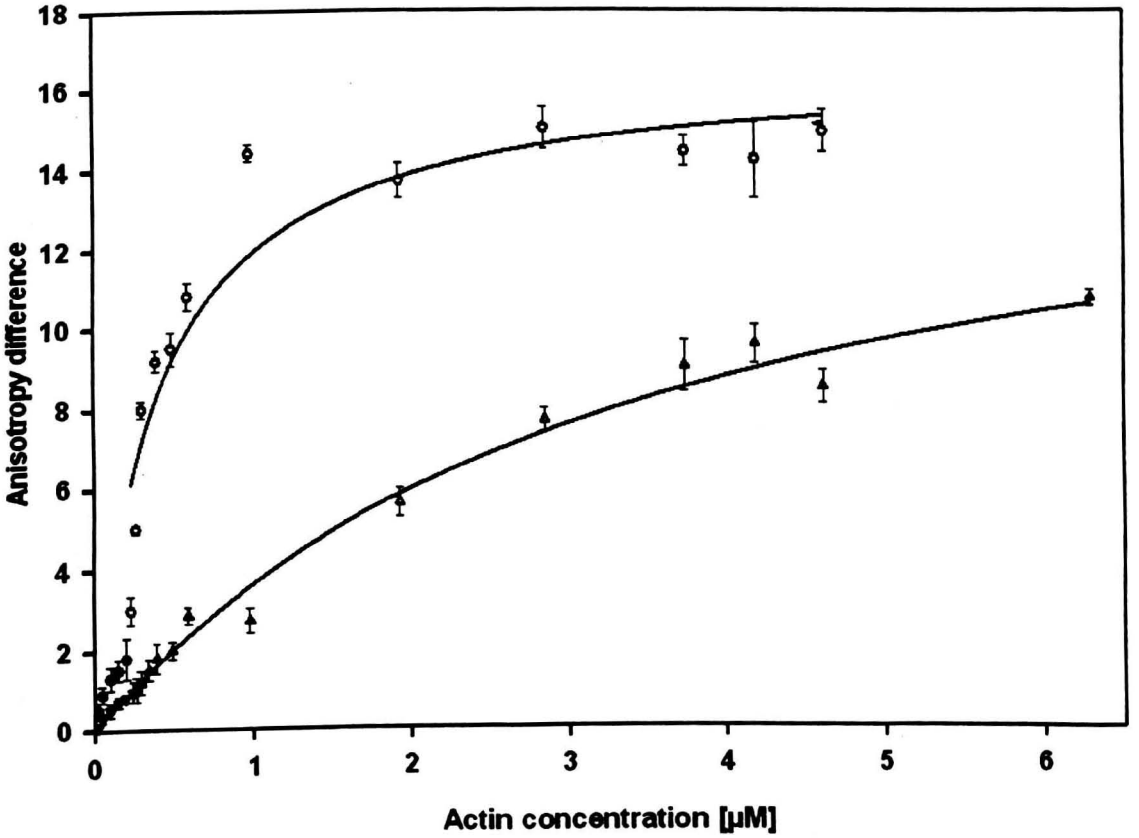

Figure 5.27. Binding curves for α-actinin ABD interacting with wild type and R372H-mutant F-actin. The curves are produced by plotting the average anisotropy difference versus F-actin concentration corrected for dilution effects. Open and closed circles correspond to the wild type actin. Closed and open triangles correspond to the R372H actin. Vertical error bars show errors in anisotropy values. Although the first and second open circle readings in the wild type were considered when drawing the binding curve, SigmaPlot did not permit the line to intercept them.

5.12 Discussion

5.12.1 Two pathways leading to NM

Four *Act88F* mutations in *Drosophila* IFM (A138V, R256C, G268D, R372H), which correspond to six *ACTA1* nemaline mutations (A138P, R256H/L, G268R/C, R372H) seen in humans show the *Drosophila* equivalent of the human nemaline phenotype. Three of the mutants (A138P, R256H/L, G268R/C) do not form any sarcomeres during sarcomerogenesis and the flies never fly. However one mutant, *Act88F*^{R372H}, forms normal sarcomeres during muscle development as seen by 1 day old flies which can fly, lose their flight ability within 7 days. TEM images from 1- to 7-day-old *Act88F*^{R372H}/+

heterozygous flies show that there is progressive sarcomeric damage explaining why they become flightless. When newly eclosed flies were prevented from using their flight muscles, no sarcomere deterioration was observed and the muscles appeared normal even when the flies were 10 days old. This suggested that the mutant myofibrils become damaged upon use. Interestingly, wild type confined flies whose wings had not been clipped were flight-tested after 1 and 3 days and did not make any attempts to fly, jump or beat their wings when released. It was found after four hours that 85% of them could fly (n = 22). This implies that wild type flies were not using their flight muscles when confined. Therefore the Petri-dish confinement method is a useful technique for preventing IFM usage. This observation suggests that there are at least two pathways leading to a nemaline myopathy phenotype. The first pathway is characterized by an inability to form normal sarcomeres. The second pathway, which is seen in the $Act88F^{R372H}$ mutant, results from the inability to maintain thin filament organization that causes loss of sarcomere structure.

5.12.2 The R372H mutation weakens myofibril mechanical stiffness

The IFM of the $Act88F^{R372H}/+$ heterozygous mutants are normal when the flies emerge but progressively deteriorate due to usage. In addition the thin filaments of $Act88F^{R372H}$ homozygous flies appeared torn from the Z-discs. These observations led to the proposal that the mutation may weaken the thin filament attachment to the Z-disc. Hence when the sarcomere contracts the thin filaments become more likely detached from the Z-disc. This was investigated by single myofibril mechanical experiments. However this technique using myofibrils from *Drosophila* IFM has a number of problems associated with it.

First due to their very small size, myofibrils pose some difficulties such as insecure attachment to the force transducers (Hao *et al.*, 2004). Though measurements of the passive force produced from *Drosophila* IFM single myofibrils have been obtained by wrapping them around the force transducers and reinforcing the attachment with glue (Dickinson *et al.*, 1997; Kulke *et al.*, 2001; Hao *et al.*, 2004). However it was not possible to use these experimental setups during this study. Instead the myofibrils were touched to glue-coated length-driving tungsten stiff needle at one end and an AFC at the other end. As the myofibrils behaved as rigid rods, due to their well known high

stiffness compared to vertebrate myofibrils, the first challenge was securely attaching them to the needle and the AFC. However, merely touching them with either the needle or the tip of the AFC would cause the myofibrils to 'bounce' off. If on the other hand the pressure applied was too great the myofibrils would break at the point of contact. These facts made their manipulation and the mounting procedure very difficult and laborious. Furthermore, following an overall inspection of the myofibrillar suspension with the microscope (40x-90x magnification, phase-contrast) it was evident that the mutant myofibrils manifest a tendency to aggregate more than wild-type ones, suggesting a different surface electrical charge. They also had a reduced ability to sediment within the same time compared to the wild-type ones (90 minutes). These difficulties acted as a 'filter' in selecting the mutant myofibrils to be subjected to mechanical analysis.

Wild type IFM myofibrils are known to be very stiff and do not contract more than ~ 3 % (Peckham *et al.*, 1990). As previously shown it is very difficult to obtain sufficient stretch to produce a sarcomere length change (Hao *et al.*, 2004). This was also the case here as too great a stretch would break the myofibril. In the laboratory where these experiments were performed, single myofibril mechanical experiments with cardiac smooth muscle are routinely performed. Cardiac muscle is far less stiff than the *Drosophila* IFM and mounting or stretching cardiac myofibrils is a lot easier and a large set of samples can quickly be processed. The high passive stiffness of *Drosophila* IFM posed a great challenge and as a result not many IFM myofibrils could be processed. For a larger and representative myofibrillar population of IFM from the mutant, the differences in mechanical parameters (stiffness, plastic deformation) could be even larger.

The high passive stiffness of the IFM myofibrils posed a third obstacle. The wild type myofibrils were stiffer than the glue, which resulted in deformation of the glue upon stretching. Different combinations of glue and nitrocellulose were tried out but this problem could not be overcome. Therefore there is an associated error with the measurement of the wild type sarcomere length change. The *Act88F*^{R372H}/+ heterozygotes myofibrils were more fragile than wild type as was observed during handling and isometrically mounting them between the needle and the tip of the AFC.

They were found to be mechanically less stiff, displayed plastic deformation and would break during the third stretching protocol. The observed mechanical weakness of the mutant myofibrils demonstrates that glue deformation due to stretching is insignificant, because the mutant myofibrils are more compliant than the glue. Although there is an error in the stiffness in the wild type, the mutant sarcomere must be mechanically compromised and explains why myofibrillar damage is use-dependent.

5.12.3 Weakening of the F-actin R372H/α-actinin interaction causes NM

R372 is on the exposed surface of the F-actin helix, within one of the two proposed α-actinin ABD sites. These observations suggest that the R372H mutation has reduced the F-actin/α-actinin binding, weakening the attachment of the thin filaments on the Z-disc as seen in the EM images of *Act88F*^{R372H} homozygotes. The reduced myofibrillar mechanical stiffness observed for the mutant supports this hypothesis. The ACT88F^{E93K} mutation resides on a residue located in the other α-actinin ABD site and displays the hypercontraction phenotype as does the ACT88F^{R372H} mutation. This suggests that weak binding to α-actinin ABD may be the molecular basis of pathogenesis for both mutations. Indeed ACT88F^{R372H} actin extracted from *Drosophila* IFM displayed a 13.35 -fold weaker interaction with the α-actinin ABD. A 10-fold weakening in the F-actin/α-actinin binding has also been reported for the human ACTA1 K336E mutation, which is associated with nemaline myopathy and cardiomyopathy (D'Amico *et al.*, 2006). The fact that the binding constant between R372H F-actin and α-actinin is only 13.35-fold weaker from that of the wild type F-actin to α-actinin is not surprising. As heterozygotes, the R372H mutants are able to fly at day 1 thus the effect of the mutation must be subtle. However, the damaging effect of the mutation in *Drosophila* IFM is progressive which is in contrast to the situation in humans, as nemaline myopathy is normally a non-progressive disorder. The reason behind this difference could be due to repair and regenerative mechanisms present in human muscle, which are apparently absent from *Drosophila* IFM.

The interaction of chicken smooth α-actinin ABD with *Drosophila Act88F* F-actin has not been previously measured. However, in other systems the affinity between chicken smooth muscle α-actinin and α-actinin ABD with rabbit F-actin has been reported. The temperatures, buffer conditions and biochemical approaches used vary from the

conditions used here. The K_d for α-actinin ABD with rabbit F-actin has been shown by stop-flow measurements to be 0.82 μM at 15 °C and 2.38 μM at 25 °C (Kuhlman *et al.*, 1992), whereas cosedimentation measurements have shown the K_d to be 0.23 μM and to be unaffected by temperature (Bennette *et al.* 1984). However, they find that the interaction is weakened 5-fold in the presence of Ca^{2+}. The wide discrepancy between reported values of the K_d for the F-actin/α-actinin binding could be due to Ca^{2+} ions present in the distilled water, as certain groups used EGTA in their buffers.

In *Drosophila* there is a single α-actinin gene whose differential splicing results in two α-actinin muscle isoforms (104 kDa and 107 kDa). Their protein sequences are identical except for the amino acids that join the actin-binding domain to the first spectrin repeat (Roulier *et al.*, 1992). This part of the sequence contains a 22 amino acid insertion resulting in the larger isoform. The 104 kDa isoform is expressed in the IFM and leg muscles whereas the 107 kDa isoform is predominantly expressed in the larval supercontractile muscles and visceral tissues of the adults (Roulier *et al.*, 1992; Vigoreaux *et al.*, 1991). Substitution of the 104 kDa isoform for the 107 kDa isoform results in flightless flies with reduced α-actinin levels (Roulier *et al.* 1992). The myofibrils of newly emerged flies look normal but the Z-bands degenerate as the flies become older. These results suggested that normal α-actinin levels are not required for sarcomere assembly in the IFM but are for maintaining sarcomere structure. It is therefore not surprising that the R372H mutant, in which F-actin/α-actinin binding is weakened, can develop normal sarcomeres. That the *Act88F*^{R372H} myofibrils degenerate as the flies become older in similar ways to where the α-actinin 104 kDa isoform levels is substituted for the 107 kDa isoform supports the idea that weakened actin/α-actinin interactions are the mode of pathogenesis in the R372H mutant.

Finally it should be pointed out that in yeast, the residue 372 of actin is a histidine (H372). Mutation of this residue to an arginine (the reverse of what has been done here) causes a mitochondrial-vacuole phenotype and the actin cytoskeleton appears depolarised (McKane *et al.*, 2005). The authors also find that *in vitro* the H372R actin shows slightly faster polymerisation that the wild type actin.

5.12.4 Summary

Congenital actin myopathy mutations that were studied in Chapter 3 and 4 resulted in sarcomeric defects being present during muscle development. Unlike previous Drosophila actin mutants for congenital actin myopathies, the IFM of the R372H mutant form normally but then the nemaline myopathy phenotype is generated over time. A variety of biophysical approaches was used to understand this progressive muscle disarray. It was observed that the myofibrils were less stiff by single force measurements. This was because the attachment of the thin filaments by α-actinin to the Z-discs was weakened.

Chapter 6: *Drosophila* IFM as a model system for studying arthrogryposes

6.1 Aims

To express the IFM-specific TnI and TnT isoforms using the *GAL4/UAS* expression system in the IFM to rescue the hdp^3 and up^1 nulls, respectively. To express and study IFM mutations of the genes encoding for TnI and TnT responsible for arthrogryposis. To express a truncated TnT to investigate the role of its COOH-terminus.

6.2 Arthrogryposis

Distal arthrogryposes are a group of disorders characterized by permanent contractures of two or more body areas that affects limb function (Bamshad *et al.*, 1996a; b). The disorder has multiple unknown origins but in some cases is caused by mutations in fast skeletal muscle *TnI* and *TnT* genes. There are four mutations in the gene encoding for fast TnI (Sung *et al.*, 2003; Kimber *et al.*, 2006; Jiang *et al.*, 2006; Robinson *et al.*, 2007) and one mutation in the gene encoding fast TnT (Sung *et al.*, 2003) that cause arthrogryposis in humans (Table 6.1). In *Drosophila* IFM-specific TnI and TnT isoforms exist that could be used to introduce the human arthrogryposis mutations. Nulls also exist for these genes so that mutations can be studied in the absence of the wild type protein.

Table 6.1. Human mutations in *TnI* and *TnT* genes responsible for arthrogryposis and their *Drosophila* counterparts.

Disease	Humans	*D. melanogaster*	References
Arthrogryposis	Fast TnT R63H	TnT K43H	Sung *et al.*,2003
Arthrogryposis	Fast TnI R156@	TnI K245@	Robinson *et al.*, 2007
Arthrogryposis	Fast TnI R174G	TnI V256G	Sung *et al.*, 2003
Arthrogryposis	Fast TnI ΔK175	TnI ΔK257	Jiang *et al.*, 2006
Arthrogryposis and myopathy (changes in type II fibres)	Fast TnI ΔK176	TnI ΔE258	Kimber *et al.*, 2006
-	-	TnT E314@	-

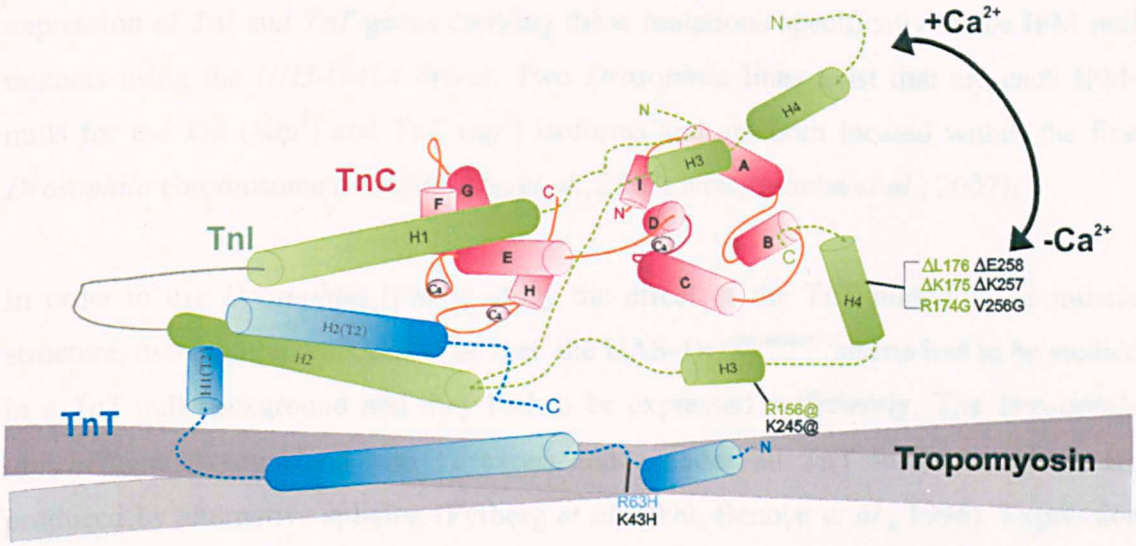

Figure 6.1. Diagram of the tertiary structure of the troponin complex in the thin filament and localization of troponin mutations. TnI, TnT and TnC are coloured in green, blue and red respectively with alpha helices represented as cylinders and coils represented as lines. Movement of the TnI NH_2-terminus is upon Ca^{2+} activation is indicated. Diagram and labeling of protein domains are based on the X-ray crystal structure of the partial troponin complex solved by Takeda *et al.*, 2003. The localization of mutations causing arthrogryposis (green and black for humans and *Drosophila*, respectively) are approximately represented in each troponin subunit. The tropomyosin dimer is shown in grey. 'Original in colour'

Expression of mutations in the TnI and TnT encoding genes had to be high and restricted to the IFM. The *Act88F* mutations in the previous chapters were expressed using the native *Act88F* promoter, which drives high levels of expression specifically in the IFM. Overexpression of the IFM-specific TnT isoform gene under the control of the very strong *Act88F* gene promoter was shown to cause reduction of the endogenous TnT, TnI, actin and tropomyosin levels and muscle abnormalities (Marco-Ferreres *et al.*, 2005). Hence the *Act88F* gene promoter could not be used for the expression of the mutations in the *TnI* and *TnT* genes. The spatial and temporal transcriptional regulation of both the *TnT* and *TnI* genes is very complicated and requires two regulatory elements upstream and downstream of the transcription initiation site (Mas *et al.*, 2004; Marín *et al.*, 2004). Trying to reconstruct this arrangement to successfully express the *TnI* gene would not be trivial. We were in possession of the adult wild type IFM-specific TnT clone as part of a collaborative project with Dr Nongthomba, in which mutations could be readily introduced. Dr. Ferrús of the Cajal Institute, Spain, provided other *UAS-TnI* transgenic construct lines to be expressed as part of a collaborative project within the MYORES network. Therefore the aim was to use the *GAL4/UAS* system to drive the

expression of *TnI* and *TnT* genes carrying these mutations specifically in the IFM null mutants using the *UH3-GAL4* driver. Two *Drosophila* lines exist that are each IFM-nulls for the TnI (hdp^3) and TnT (up^1) isoforms and are both located within the first *Drosophila* chromosome (Nongthomba *et al.*, 2003; Nongthomba *et al.*, 2007).

In order to use *Drosophila* IFM to study the effect of the TnT mutations in muscle structure, two requirements had to be met: the UAS-$TnT^{[mutation]}$ inserts had to be studied in a *TnT* null background and they had to be expressed sufficiently. The *Drosophila upheld* gene is organized into 11 exons and encodes all TnT isoforms, which are produced by alternative splicing (Fyrberg *et al.* 1990, Benoist *et al.*, 1998). Expression of the different isoforms is regulated by a single promoter (Benoist *et al.*, 1998). A *TnT* mutant exists, $upheld^1$ (up^1), in which defective splicing of exon 10a results in lack of TnT message and protein in the IFM (Nongthomba *et al.*, 2007). Hemizygous male up^1 mutants and up^1/+ heterozygote female are flightless (Deak *et al.*, 1982). The IFM of the up^1 hemizygous mutants lack normal sarcomeres though short sarcomere-like structures have been reported and zebra bodies (Nongthomba *et al.*, 2007). The up^1/+ heterozygote females show myofibrillar branching, Z-disc and M-line streaming but display more myofibrillar organization than up^1 hemizygotes (Nongthomba *et al.*, 2007). Therefore, the up^1 hemizygous mutant was used for studying the UAS-$TnT^{[mutation]}$ transgenics in *TnT* null background. The mating scheme for obtaining lines expressing *UAS-TnT* in *TnT* null background is shown in Chapter 2, section 2.6.7, Figure 2.7 A.

Like with the *UAS-*$TnT^{[mutation]}$ inserts, in order to use *Drosophila* IFM to study the effect of the TnI mutations in muscle structure the *UAS-*$TnI^{[mutation]}$ inserts had to be studied in a TnI null background and they had to be adequately expressed. A TnI mutant exists, $heldup^3$ (hdp^3), in which alternative splicing of the IFM/TDT-specific exon 6b1 is affected (Barbas *et al.*, 1993). As a result the IFM/TDT *TnI* RNA isoforms are not expressed resulting in an IFM/TDT TnI null. The hdp^3 hemizygotes and hdp^3/+ heterozygote adults are dominant flightless and display aberrant muscle structure (Barbas *et al.*, 1991; Deak *et al.*, 1982; Prado *et al.*, 1999). The muscles initially form normally but autodestruct when hypercontraction starts at 70-75 hours APF (Nongthomba *et al.*, 2003). Hence, the hdp^3 mutant was used to study the *UAS-*$TnI^{[mutation]}$ transgenics in wild type *TnI* null backgrounds. The mating scheme for

obtaining lines expressing *UAS-TnI* in wild type *TnI* null background is shown in Chapter 2, section 2.6.7, Figure 2.7 A.

When this project started it was originally thought that the *UH3-GAL4* insert was in the second *Drosophila* chromosome and could therefore be used to create lines that contained this insert and either the *TnI* or *TnT* nulls, which are located in the first chromosome. Therefore hdp^3 and up^1 lines were created that also carried the *UH3-GAL4* driver in the second chromosome. However, it was discovered late on in the research that there are two *GAL4* (pGawB enhancer trap) drivers in the stock - one on the first chromosome expressing in the IFM and another on the second chromosome expressing in the midgut. This meant that in the hdp^3; *UH3-GAL4* and up^1; *UH3-GAL4* lines that were created, because the *UH3-GAL4* insert was selected to be in the second chromosome, expression of the *UAS-TnI* and *UAS-TnT* constructs could not be achieved in the IFM. A way to circumvent this problem is to recombine the *UH3-GAL4* driver into the same chromosome as the up^1 and hdp^3 genes. However, as creating/studying the arthrogryposis mutants was the last piece of research that was carried out there was not sufficient time left to perform the recombinations. Therefore the *dmef2-GAL4* panmuscle driver, which is in the third chromosome (Ranganayakulu *et al.*, 1996), was used instead to express the arthrogryposis constructs. The mating scheme for obtaining lines expressing *dmef2-GAL4* in wild type *TnI* or *TnT* null background is shown in Chapter 2, section 2.6.7, Figure 2.7 B.

Transgenics carrying the wild type $UAS\text{-}TnI^+$ and $UAS\text{-}TnT^+$ constructs were created in order to rescue the IFM *TnI* (hdp^3) and *TnT* (up^1) gene nulls. Also transgenics for the $UAS\text{-}TnI^{[mutation]}$ and $UAS\text{-}TnT^{[mutation]}$ inserts carrying the arthrogryposis mutations were created and studied. All crosses described in this chapter, involving *dmef2-GAL4* flies, the vials were kept at 18 °C where the *GAL4* driver shows weak expression. Those individuals that had reached the pre-pupal stage were then transferred to 25 °C or 29 °C to allow increased expression of the *dmef2-GAL4* driver.

6.3 Troponin T mutants

A single mutation in the human fast skeletal isoform TnT, R63H, has been discovered that causes arthrogryposis. It is found within the region of TnT that binds the NH_2-terminus of TnC (Sung *et al.*, 2003). Protein sequence alignment of the *Drosophila* IFM-specific TnT and the human fast skeletal muscle TnT isoform (Figure 6.2) shows that the human protein is poorly conserved compared to that of *Drosophila* one (25% sequence homology). Based on the sequence alignment residue K43 of *Drosophila* TnT was mutated into H43 to recapitulate the human residue R63 of TnT responsible for arthrogryposis.

```
Human_TNNT1     MSDTEEQEYEEEQPEEEAADEEEEAPEEPEPVAEPEEERPKPSRPVVPPLIPPKIPEGER 60
Human_TNNT3     MSDEEVEQVEEQYEEEEEAQEEEEVQEDT-AEEDAEEEKPRPK------LTAPKIPEGEK 53
Drosophila      MSDDEEYTGEGDPEFIKRQDQKRSDLDDQLKEYITEWRK--------------------- 39
                *** *    *                          *

Human_TNNT1     VDFDDIHRKRMEKDLLELQTLIDVHFEQRKKEEEELVALKERIERRRSERAEQQRFRTEK 120
Human_TNNT3     VDFDDIQKKRQNKDLMELQALIDSHFEARKKEEEELVALKERIEKRRAERAEQQRIRAEK 113
Drosophila      -------RSKEEDELKKLKEKQAKRKVTRAEEEQKMAQRKKEEEERRVREAEEKKQREIE 92
                              *  *          *  **      *   * **   **    *

Human_TNNT1     ERERQAKLAEEKMRKEEEEAKKRAEDDAKKKKVLSNMGAHFGGYLVKAEQKRGKRQTGRE 180
Human_TNNT3     ERERQNRLAEEKARREEEDAKRRAEDDLKKKKALSSMGANYSSYLAKADQKRGKKQTARE 173
Drosophila      EK--RMRLEEAEKKRQAMLQAMKDKDKKGPNFTIAKKDAGVLGLSSAAMERNKTKEQLEE 150
                *     * *             *             *       *          *

Human_TNNT1     MKVRILSERKKPLDIDYMGEEQLRARSAWLPPSQPSCPAREKAQELSDWIHQLESEKFDL 240
Human_TNNT3     MKKKILAERRKPLNIDHLGEDKLR----------------DKAKELWETLHQLEIDKFEF 217
Drosophila      EKKISLSFRIKPLAIEGFGEAKLR----------------EKAQELWELIVKLETEKYDL 194
                 *  *  * *** *   **  **                  ** **     **  *

Human_TNNT1     MAKLKQQKYEINVLYNRISHAQKFRKGAG---KGRVGGRWK------------------- 278
Human_TNNT3     GEKLKRQKYDITTLRSRIDQAQKHSKKAGTPAKGKVGGRWK------------------- 258
Drosophila      EERQKRQDYDLKELKERQKQQLRHKALKKGLDPEALTGKYPPKIQVASKYERRVDTRSYD 254
                    * * *    *  *                    *

Human_TNNT1     ------------------------------------------------------------
Human_TNNT3     ------------------------------------------------------------
Drosophila      DKKKLFEGGYNTVYAETLEKTWQERQERFTQRTKSKLPKWFGERPGKKAGEPETPEGEED 314

Human_TNNT1     ------------------------------------------------------------
Human_TNNT3     ------------------------------------------------------------
Drosophila      AKADEDIVEDDEEVEEEVVEEEDEEAEEDEEEEEEEEEEEEEEEEEEEEEEEEEEEEEEE 373
```

Figure 6.2. Sequence alignment of *Homo sapiens* troponin T type 1 (skeletal, slow) (TNNT1), troponin T type 3 (skeletal, fast) (TNNT3) and *Drosophila melanogaster* IFM-specific troponin T isoform. The human TnT residue R63 is highlighted in yellow and *Drosophila* homologue K43 in cyan. *Drosophila* residue E314 is also highlighted in cyan. Sequence alignment was performed using Clustal W2 software. The accession number for human TNNT1 is P13805, human TNNT3 is NP_006748 and for *Drosophila* TnT is AAR24586.1. The asterisk denotes conserved residues.

In contrast to vertebrates, the *Drosophila* TnT IFM isoform has a negatively charged Glu-rich, COOH-terminal extension. The human and *Drosophila* TnT proteins are poorly conserved, it is hitherto unknown what the functional importance of the *Drosophila* TnT poly-E tail. Therefore, a stop codon at residue E314 was introduced (Figure 6.2) leading to a loss of 70 amino acids in the COOH-terminus. It was also of interest to investigate if *Drosophila* $TnT^{E314@}$ will integrate into the myofibrils since previous studies have shown that a human truncated TnT mutant (E180@) does not integrate into muscle fibres (Jin *et al.*, 2003).

First, the wild type *UAS-TnT*$^{+}$ construct was expressed in an *up*^{1} background. If expression of wild type TnT in the IFM restored the flight ability or suppressed the muscle abnormalities of the *up*^{1} male mutant it would suggest that the *UAS-TnT*$^{[mutation]}$ inserts can also be adequately expressed thus allowing this system to be used to study the *UAS-TnT*$^{[mutation]}$ constructs. The mating scheme to obtain lines expressing the *UAS-TnT* and *dmef2-GAL4* inserts in wild type *TnT* null backgrounds is shown in Chapter 2, section 2.6.7, Figure 2.6.3.

Transgenic flies carrying the *UAS-TnT*$^{+}$ insert in the *up*^{1} background were created and driven with the *dmef2-GAL4* driver. Control flies carrying a single copy of the *dmef2-GAL4* or the *UAS-TnT*$^{+}$ inserts are flighted (Figure 6.4, Table 6.2) suggesting that the presence of the inserts does not cause any muscle defects. Control *up*^{1}; *UAS- TnT*$^{+}$/+ ; + and *up*^{1}; + ; *dmef2-GAL4* flies were flightless showing that the *UAS-TnT*$^{+}$ and *dmef2-GAL4* inserts alone cannot rescue the *up*^{1} phenotype. Males expressing wild type TnT in the *up*^{1} background (*up*^{1}; *UAS-TnT*$^{+}$/+; *dmef2-GAL4*/+) from crosses kept at 25 °C were flightless (Figure 6.4. Table 6.2) and showed the wings-up phenotype characteristic of muscle hypercontraction (Figure 6.5). This suggested that the IFM TnT null cannot be rescued by expression of the *UAS-TnT*$^{+}$. Male progeny expressing wild type TnT in the presence of the native TnT gene (+; *UAS-TnT*$^{+}$/+; *dmef2-GAL4*/+) were also flightless (Figure 6.4).

In the case of the mutants, flies bearing single copies of the *UAS-TnT*^{K43H} or *UAS-TnT*$^{E314@}$ inserts were flighted, suggesting that the inserts do not cause any muscle defects (Figure 6.4, Table 6.2). Control *up*^{1}; + ; *UAS-TnT*^{K43H}/+ and *up*^{1}; +; *UAS-TnT*$^{E314@}$/ + flies were flightless showing that the *UAS-TnT*$^{[mutation]}$ inserts alone cannot

rescue the up^1 phenotype. Expression of the *UAS-TnT*^{K43H} and *UAS-TnT*$^{E314@}$ mutants in up^1 background with *dmef2*-GAL4 (up^1; + ; *UAS-TnT*^{K43H}*/dmef2-GAL4* and up^1; + ; *UAS-TnT*$^{E314@}$*/dmef2-GAL4*) resulted in flightless flies at 25 °C (Figure 6.4, Table 6.2), which showed the wings-up phenotype (Figure 6.5). Expression of the *UAS-TnT*^{K43H} and *UAS-TnT*$^{E314@}$ mutants in the presence of a wild type TnT copy also resulted in flightless flies (+; + ; *UAS-TnT*^{K43H}*/dmef2-GAL4* and +; + ; *UAS-TnT*$^{E314@}$*/dmef2-GAL4*) (Figure 6.4) with the wings up phenotype.

Table 6.2 Number of male flies tested for the TnT mutation and deletion of the polyE tail.

Genotype	Number of flies
wt	27
+/Y; + ; *dmef2-GAL4*/+	45
up^1/Y; + ; +	35
up^1/Y; + ;*dmef2-GAL4*/+	28
+/Y; *UAS-TnT*$^+$/+; /+	21
up^1/Y; *UAS-TnT*$^+$/+ ;+	18
up^1/Y; *UAS-TnT*$^+$/+ ; *dmef2-GAL4*/+	31
+/Y; *UAS-TnT*$^+$/+ ; *dmef2-GAL4*/+	22
+/Y; + ; *UAS-TnT*^{K43H}/+	30
+/Y; + ; *UAS-TnT*$^{E314@}$/+	37
up^1/Y; + ; *UAS-TnT*^{K43H}/+	30
up^1/Y; + ; *UAS-TnT*$^{E314@}$/+	29
up^1/Y; + ; *UAS-TnT*^{K43H}*/dmef2-GAL4*	32
up^1/Y; + ; *UAS-TnT*$^{E314@}$*/dmef2-GAL4*	26
+/Y; + ; *UAS-TnT*^{K43H}*/dmef2-GAL4*	34
+/Y; + ; *UAS-TnT*$^{E314@}$*/dmef2-GAL4*	32

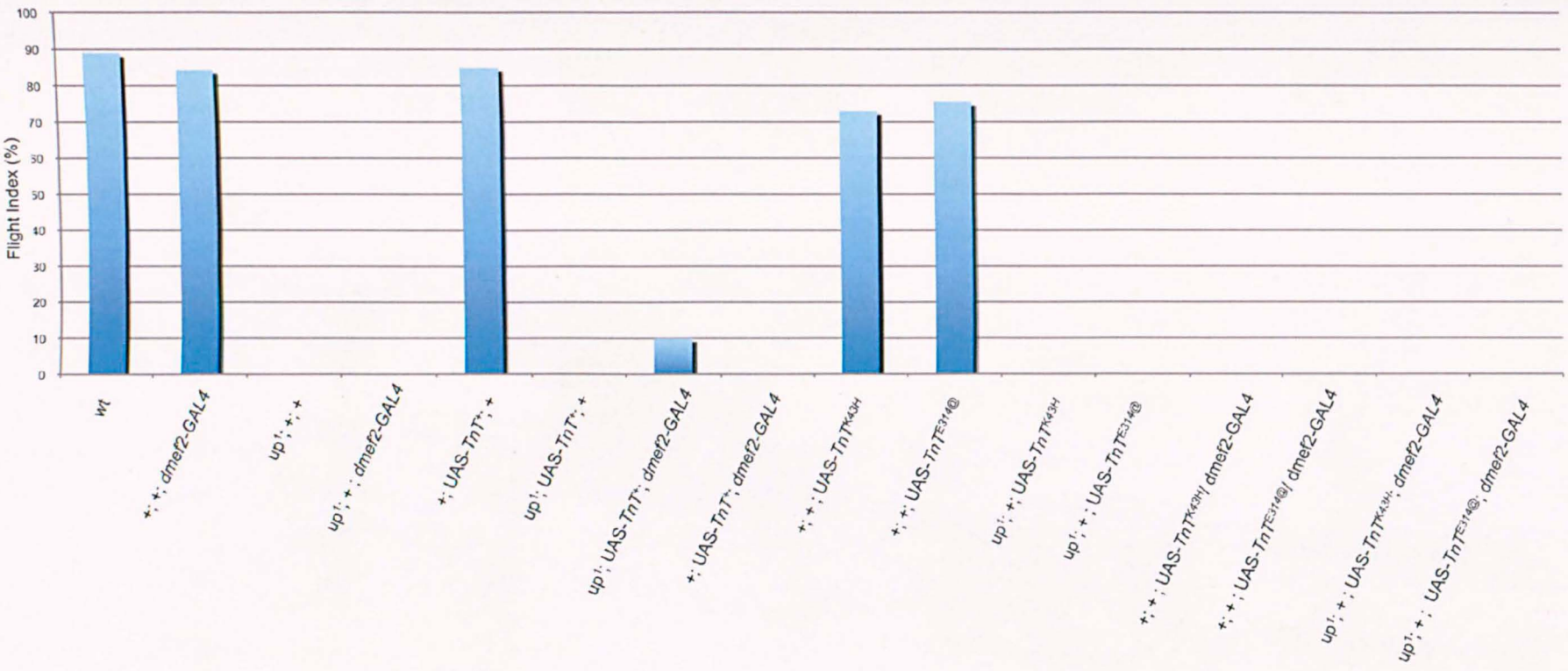

Figure 6.4. Flight testing of male wild type UAS-*TnT*$^{+}$ flies and mutant variants grown at 25 °C. The inserts: UAS-*TnT*$^{+}$, UAS-*TnT*^{K43H}, UAS-*TnT*$^{E314@}$ and *dmef2-GAL4* are present as single copies.

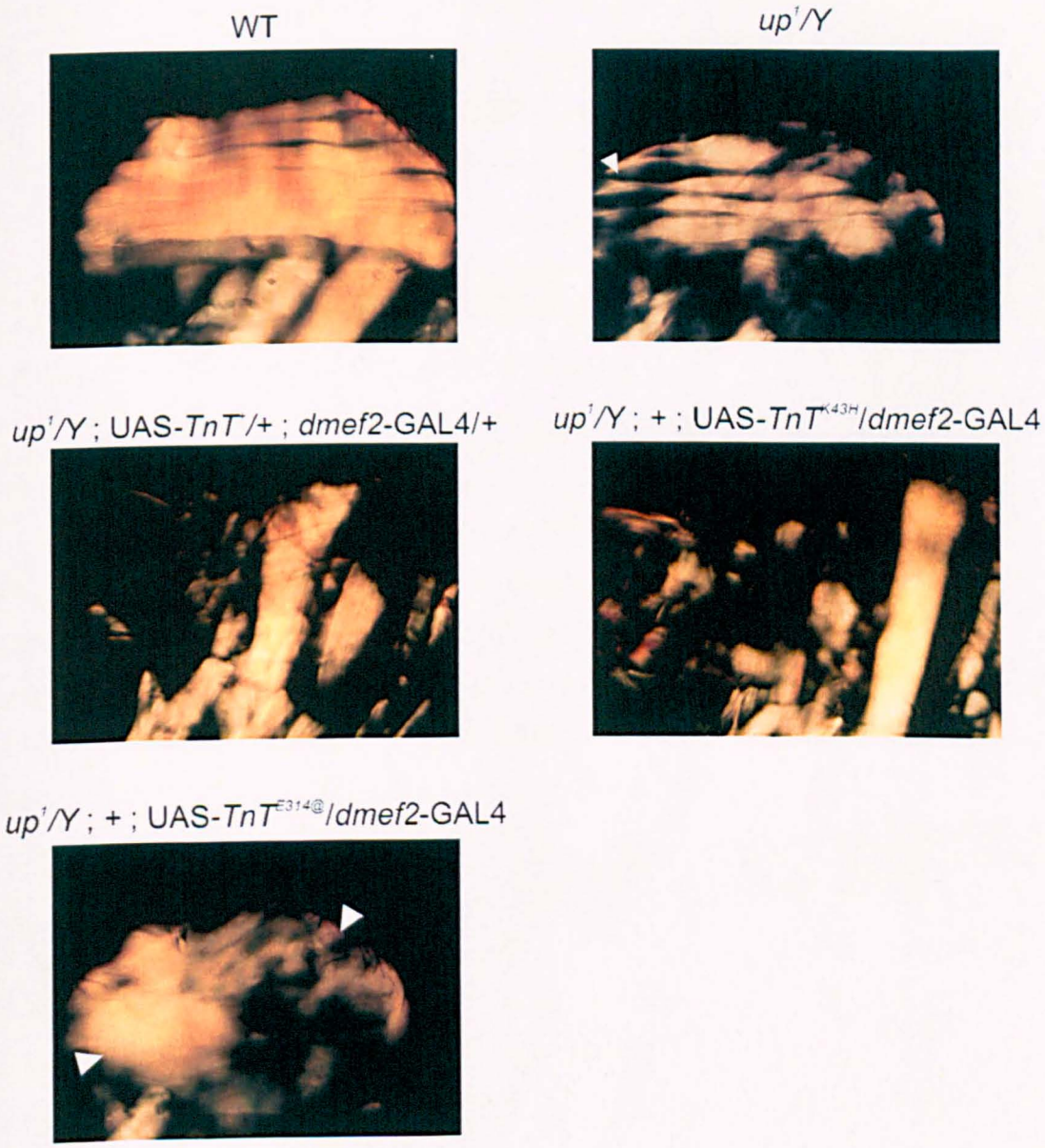

Figure 6.5. Polarized light microscopy of male wild type *UAS-TnT*$^{+}$ flies and mutant variants. Arrowheads show hypercontracted muscles.

The *UAS-TnT*$^{+}$, *dmef2-GAL4* and *UAS-TnT*$^{[mutation]}$ inserts were also expressed in *up*^{1}/+ heterozygote females which on their own are completely flightless (Figure 6.6). Control *up*^{1}/+ ; UAS-*TnT*$^{+}$/+ ; + flies were flightless showing that the UAS-*TnT*$^{+}$ insert alone cannot restore flight ability. When the UAS-*TnT*$^{+}$ insert was expressed, 30% of the *up*^{1}/+; UAS-*TnT*$^{+}$/+; *dmef2-GAL4*/+ progeny were flighted (Figure 6.5, Table 6.3). This shows that some rescue can be achieved in the *up*^{1}/+ heterozygote females. Perhaps the presence of the *hdp*$^{+}$ allele in these flies allows for some rescuing. However, it should be noted that the *GAL4* activation is not the same in every fly. Less active *GAL4* in some of the progeny may account for incomplete rescue. Such was the situation for the *cpb* knockdown flies in Chapter 4.

For the mutants, control female flies bearing single copies of the UAS-*TnT*^{K43H} or UAS-*TnT*$^{E314@}$ inserts were flighted (+; + ; UAS-*TnT*^{K43H}/+ and +; + ; UAS-*TnT*$^{E314@}$/ +), suggesting that the inserts do not cause any muscle defects (Figure 6.6). Control *up*^{1}/+; + ; UAS-*TnT*^{K43H}/+ and *up*^{1}/+; + ; UAS-*TnT*$^{E314@}$/ + flies were flightless showing that the UAS-*TnT*$^{[mutation]}$ inserts alone cannot restore flightness in *up*^{1}/+ heterozygote females. Expression of the UAS-*TnT*^{K43H} insert in wild type heterozygote background (*up*^{1}/+; + ; UAS-*TnT*^{K43H}/*dmef2-GAL4*) resulted in flightless flies (Figure 6.6, Table 6.3). However, expression of the UAS-*TnT*$^{E314@}$ insert in wild type heterozygote background (*up*^{1}/+; + ; UAS-*TnT*$^{E314@}$/*dmef2-GAL4*) resulted in 70% flight ability (Figure 6.6, Table 6.3). The presence of the wild type *up*$^{+}$ gene may be responsible for the flight rescuing in this case. Polarized light microscopy should be performed for both the K43H and E314@ flightless progeny, so as to see if the muscle defects are less pronounced compared to the *up*^{1}/+ flies.

Table 6.3 Number of female flies tested for the *TnT* mutation and deletion of the polyE tail.

Genotype	Number of flies
wt	20
+ ; + ; *dmef2-GAL4*/+	25
up^1/+ ; + ; +	12
up^1/+ ; + ; *dmef2-GAL4*/+	24
up^1/+ ; *UAS-TnT*$^+$/+; *dmef2-GAL4*/+	28
+ ; + ; *UAS-TnT*^{K43H}/+	37
+ ; + ; *UAS-TnT*$^{E314@}$/+	45
up^1/+ ; +; *UAS-TnT*^{K43H}/+	35
up^1/+ ; +; *UAS-TnT*$^{E314@}$/+	31
+ ; + ; *UAS-TnT*^{K43H}/*dmef2-GAL4*	47
+ ; + ; *UAS-TnT*$^{E314@}$/*dmef2-GAL4*	28
up^1/+ ; + ; *UAS-TnT*^{K43H}/*dmef2-GAL4*	21
up^1/+ ; + ; *UAS-TnT*$^{E314@}$/*dmef2-GAL4*	18

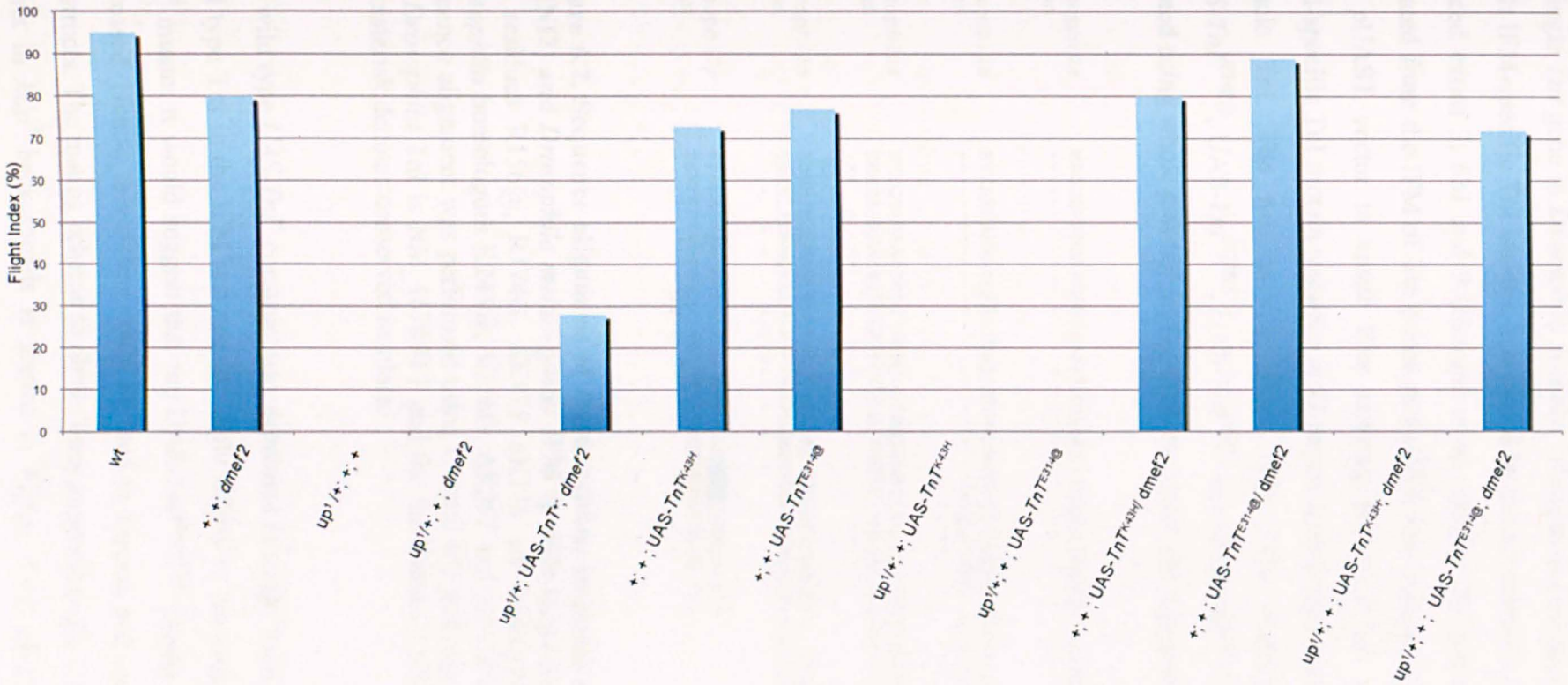

Figure 6.6. Flight testing of female wild type UAS- *TnT*$^{+}$ flies and mutant variants grown at 25 °C. The inserts: *UAS-TnT*$^{+}$, *UAS-TnT*^{K43H}, *UAS-TnT*$^{E314@}$ and *dmef2-GAL4* are present as single copies.

6.4 Troponin I arthrogryposis mutants

A single *TnI* gene in *Drosophila* encodes 13 exons and produces all TnI isoforms. The adult IFM-specific TnI isoform is encoded by the constitutive exons and the alternative spliced exons 3, 6b1 and 9 (Herranz *et al.*, 2005). The mRNA of this isoform was isolated from the IFM of late pupae and cDNA was created. The gene was inserted in the pUAST vector to create flies carrying the *UAS-TnI*$^{+}$ insert. The *Drosophila* IFM-specific TnI protein sequence is 87 amino acids longer than the human fast skeletal muscle TnI. The two proteins show only 25% homology (Figure 6.7). The *UAS-TnI*$^{K245@}$, UAS-*TnI*^{N256G}, UAS-*TnI*$^{\Delta K257}$ and UAS-*TnI*$^{\Delta E258}$ mutant constructs were created using whole plasmid mutagenesis to model arthrogryposis in Drosophila.

```
Drosophila   MADDEKKAAAPAAAPAAAAKPAAPAAAPAANGKAAPAANGKAAPAAAAAPAGPPKDPNDP 60
Human        ------------------------------------------------------------

Drosophila   KVKAEEAKKAKQAEIERKRAEVRKRMEEASKAKKAKKGFMTPERKKKLRLLLRKKAAEEL 120
Human        ----------------------------MSQCKKRNR--AITARRQHLKSVMLQIAATEL 30
                                          *  **        *   *       ** **

Drosophila   KKEQERKAAERRRIIEERCGSPRNLSDASEGELQEICEEYYERMYICEGQKWDLEYEVRK 180
Human        EKEESRREAEKQNYLAEHCPPLHIPGSMS--EVQELCKQLHAKIDAAEEEKYDMEVRVQK 88
              **  *  **      * *       *  * ** *          *  * * *  * *

Drosophila   KDWEINDLNAQVNDLRGKFVKPALKKVSKYENKFAKLQK---KAAEFNFRNQLKVVKKKE 237
Human        TSKELEDMNQKLFDLRGKFKRPPLRRVRMSADAMLKALLGSKHKVCMDLRANLKQVKKED 148
               *  * *    ******  * *  *        *              *  ** ***

Drosophila   FTLEEEEKEKKPDWSK---GKPGDAKVKEEVEAEA 269
Human        TEKERDLRDVG-DWRKNIEEKSGMEGRKKMFESES 182
               *       ** *    * *    *   * *
```

Figure 6.7. Sequence alignment of *Homo sapiens* troponin I type 1 (skeletal, fast) (TNNI2) and *Drosophila melanogaster* IFM specific troponin I isoform. The human TnI residues R156@, R174G, ΔK175 ΔK176 are highlighted in yellow and the *Drosophila* homologues K245@, V256G, ΔK257 and ΔE258 are highlighted in cyan. Sequence alignment was performed using Clustal W2 software. Accession number for the *Drosophila* TnI is NM_167608.1 and for the human TNNI2 is NP_001139313.1. The asterisk denotes conserved residues.

The wild type *UAS-TnI*$^{+}$ construct was expressed in a *hdp*^{3} background. If expression of wild type TnI in the IFM restored the flight ability or the muscle abnormalities of the *hdp*^{3} mutant it would suggest that the UAS-*TnI*$^{[mutation]}$ inserts can also be adequately expressed. Hence, this system could be used to express and study the UAS-*TnI*$^{[mutation]}$ constructs. The mating scheme to obtain lines expressing the *UAS-TnI* and *dmef2-GAL4* inserts in *hdp*^{3} backgrounds is shown in Figure 2.6.3 of Chapter 2. Due to time

constraints, the pupae from these crosses were grown at 29 °C where the *GAL4* activity is higher instead of 25 °C, which was the case for the *UAS-TnT* constructs.

Control flies carrying a single copy of the *dmef2-GAL4* or the *UAS-TnI*$^{+}$ inserts are flighted (Figure 6.4) showing that the inserts does not cause any muscle defects. Control *hdp*^{3}; *UAS-TnI*$^{+}$/+ ; + and *hdp*^{3}; + ; *dmef2-GAL4* male flies were flightless showing that the *UAS-TnI*$^{+}$ or the *dmef2-GAL4* inserts alone cannot rescue the *hdp*^{3} phenotype. Male progeny expressing wild type TnI in *hdp*^{3} background (*hdp*^{3}; *UAS-TnI*$^{+}$/+; *dmef2-GAL4*/+) from crosses kept at 29 °C (Figure 6.8, Table 6.4) were 100 % flighted indicating that the *dmef2-GAL4* driver can achieve expression of the *UAS-TnI* inserts at high enough levels to rescue the flight ability of *hdp*^{3} (Figure 6.8, Table 6.4). However, overexpression of TnI in males already bearing the wild type TnI copy (+; *UAS-TnI*$^{+}$/+; *dmef2-GAL4*/+) resulted in flight reduction.

Control TnI male flies bearing only the *UAS-TnI*$^{[mutation]}$ inserts were flighted suggesting that the integration of the inserts is not affecting muscle function. Control male *hdp*^{3}; + ; *UAS-TnI*$^{K245@}$, *hdp*^{3}; + ; *UAS-TnI*^{V256G}, *hdp*^{3}; + ; *UAS-TnI*$^{\Delta K257}$ and *hdp*^{3}; + ; *UAS-TnI*$^{\Delta A258}$ flies were flightless showing that the *UAS-TnT*$^{[mutation]}$ inserts alone cannot rescue the *hdp*^{3} phenotype. In the presence of the *dmef2-GAL4* driver the *TnI*$^{K245@}$ mutation resulted 14 % flighted progeny (*hdp*^{3}; +; *UAS-TnI*$^{K245@}$; *dmef2-GAL4*), *TnI*^{V256G} mutation resulted 3.57 % flighted progeny (*hdp*^{3}; + ; *UAS-TnI*^{V256G} ; *dmef2-GAL4*), the *TnI*$^{\Delta K257}$ mutation resulted in 44 % flighted progeny (*hdp*^{3}; + ; *UAS-TnI*$^{\Delta K257}$; *dmef2-GAL4*), whereas the *UAS-TnI*$^{\Delta E258}$ mutation resulted in 40 % flighted progeny (*hdp*^{3}; + ; *UAS-TnI*$^{\Delta E258}$; *dmef2-GAL4*) (Figure 6.8, Table 6.4). These results suggest that the mutations affect muscle function. However, in contrast to the male TnI null (*hdp*^{3}), the K245@ and ΔK257 arthrogryposis mutants and to a lesser extent the V256G and ΔE258 ones, form birefringent dorso ventral and dorsal longitudinal muscles (Figure 6.9). Hence, they suppress to different degrees the muscle degeneration phenotype of the TnI null. As this work was the last part of the project there was not enough time to study these mutants further and to express the *UAS-TnI*$^{+}$ constructs in *hdp*^{3}/+ heterozygote females.

In the presence of a single wild type TnI copy expressing the four mutant inserts using the *dmef2-GAL4* driver resulted in reduced flight ability compared to the wild type

which was mostly pronounced in the $TnI^{K245@}$ (75 % flight ability) TnI^{V256G} (64 % flight ability), and $TnI^{\Delta K257}$ (62 % flight ability) and $TnI^{\Delta E258}$ (75 % flight ability) mutants (Figure 6.8, Table 6.4). The presence of excess TnI protein when the $UAS\text{-}TnI^{+}$ was expressed in wild type (hdp^{+}) background also resulted in reduced flight ability.

Table 6.4 Number of male flies tested for the *TnI* arthrogryposis mutations.

Genotype	Number of flies
wt	26
+ ; + ; *dmef2-GAL4*/+	41
hdp^3/Y ; + ; *dmef2-GAL4*/+	30
hdp^3/Y ; + ; +	31
+/Y ; $UAS\text{-}TnI^{+}$; +	28
hdp^3/Y ; $UAS\text{-}TnI^{+}$; +	19
+/Y ; + ; $UAS\text{-}TnI^{+}$/*dmef2-GAL4*	35
hdp^3/Y ; $UAS\text{-}TnI^{+}$;*dmef2-GAL4*	52
+/Y ; + ; $UAS\text{-}TnI^{K245@}$/+	50
+/Y ; + ; $UAS\text{-}TnI^{V256G}$/+	82
+/Y ; + ; $UAS\text{-}TnI^{\Delta K257}$/+	63
+/Y ; + ; $UAS\text{-}TnI^{\Delta E258}$/+	24
hdp^3/Y; + ; $UAS\text{-}TnI^{K245@}$/+	25
hdp^3/Y; + ; $UAS\text{-}TnI^{V256G}$/+	31
hdp^3/Y; + ; $UAS\text{-}TnI^{\Delta K257}$/+	28
hdp^3/Y; + ; $UAS\text{-}TnI^{\Delta E258}$/+	24
hdp^3/Y; + ; $UAS\text{-}TnI^{K245@}$/*dmef2-GAL4*	35
hdp^3/Y; + ; $UAS\text{-}TnI^{V256G}$/*dmef2-GAL4*	32
hdp^3/Y; + ; $UAS\text{-}TnI^{\Delta K257}$/*dmef2-GAL4*	36
hdp^3/Y; + ; $UAS\text{-}TnI^{\Delta E258}$/*dmef2-GAL4*	30
+/Y ; + ; $UAS\text{-}TnI^{K245@}$/*dmef2-GAL4*	45
+/Y ; + ; $UAS\text{-}TnI^{V256G}$/*dmef2-GAL4*	50
+/Y ; + ; $UAS\text{-}TnI^{\Delta K257}$/*dmef2-GAL4*	32
+/Y ; + ; $UAS\text{-}TnI^{\Delta E258}$/*dmef2-GAL4*	29

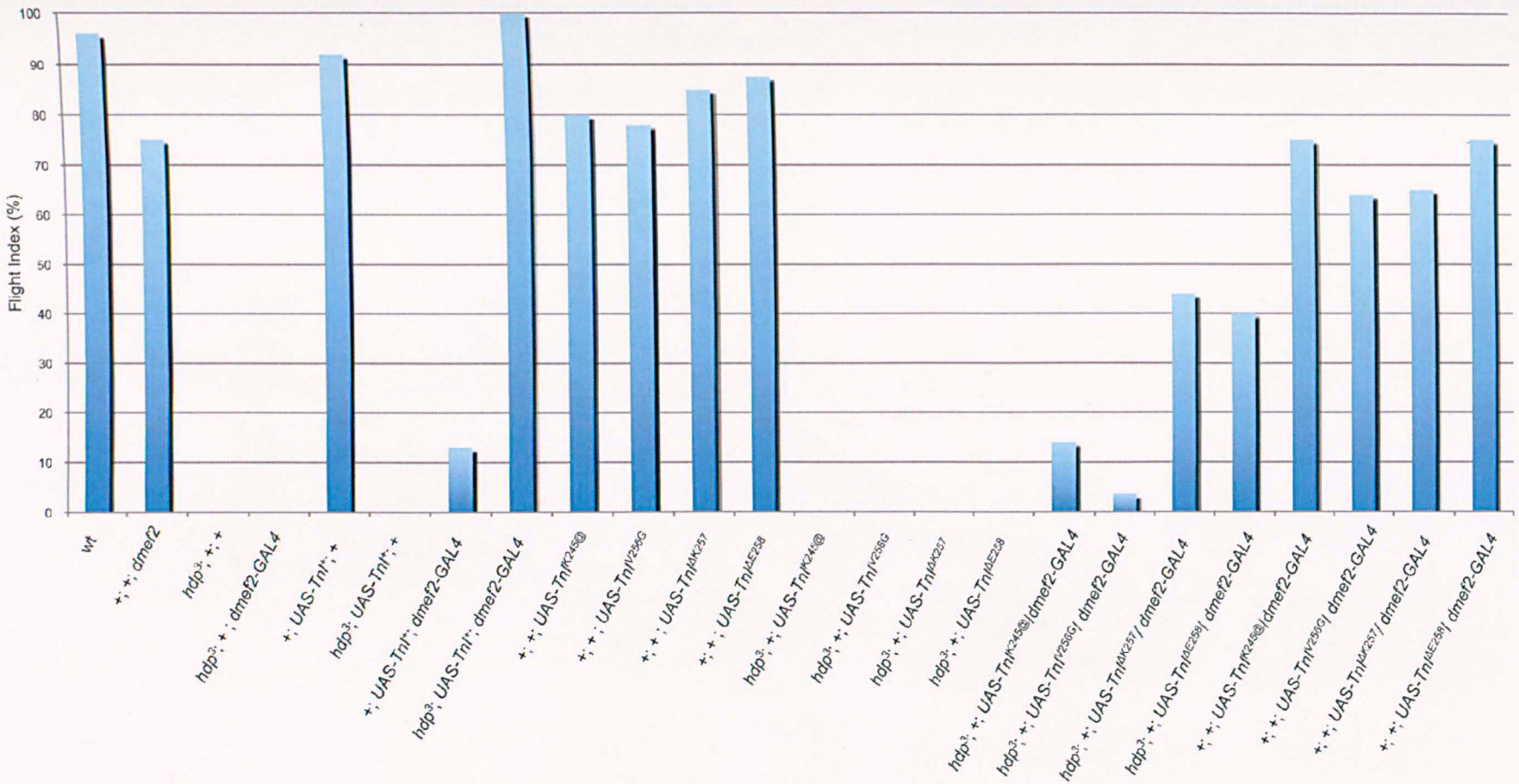

Figure 6.8. Flight testing of male wild type UAS-*TnI*$^{+}$ flies and mutant variants at 29 °C. The inserts: *UAS-TnI*$^{+}$, *UAS-TnI*$^{K245@}$, *UAS-TnI*^{V256G}, *UAS-TnI*$^{\Delta K257}$, *UAS-TnI*$^{\Delta E258}$ and *dmef2-GAL4* are present as single copies.

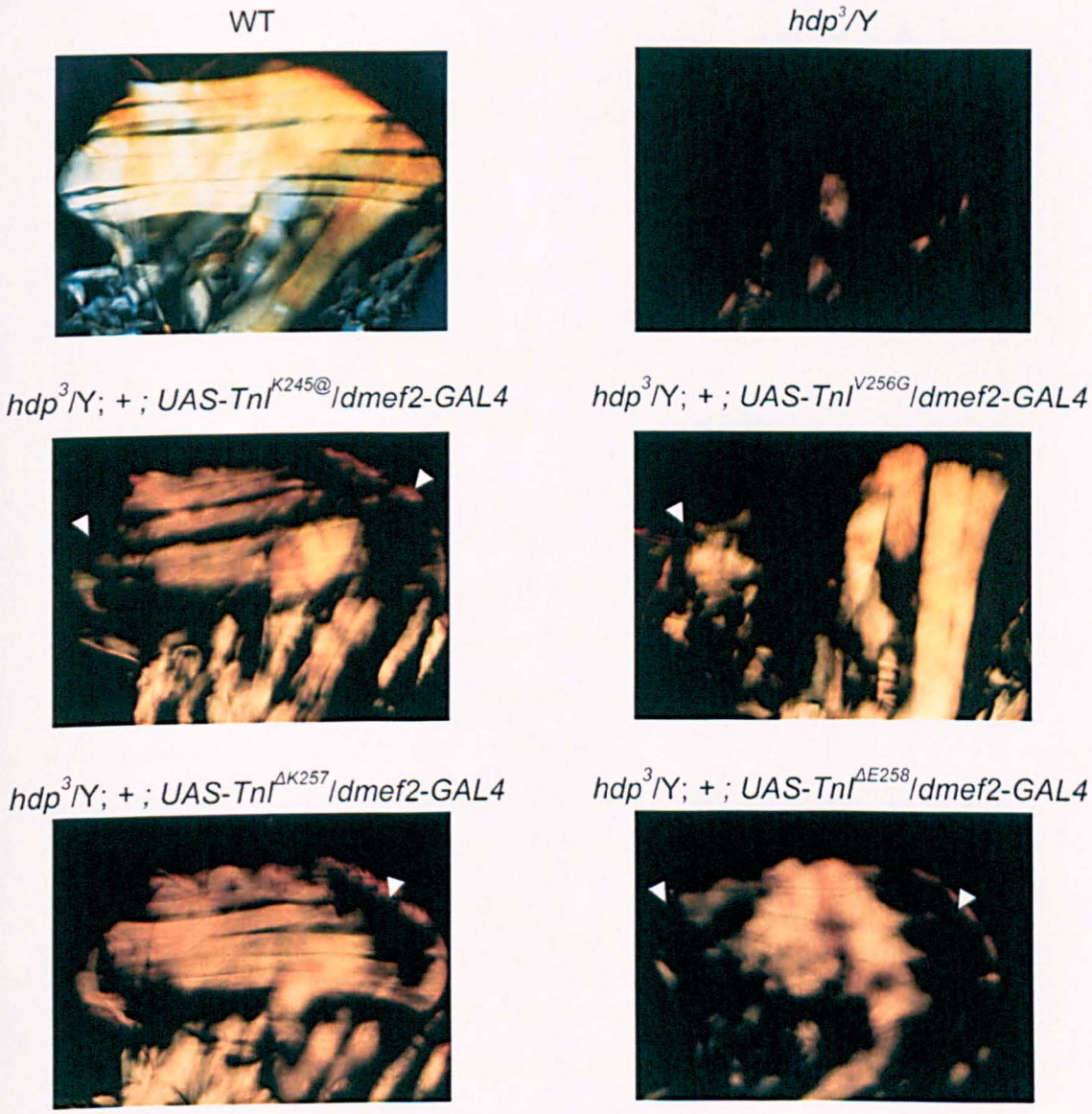

Figure 6.9. Polarized light microscopy of male *UAS-TnI* mutant variants. Arrowheads show hypercontracted muscles detached from the cuticle.

6.5 Discussion

TnI and *TnT* arthrogryposis mutations were expressed using the *GAL4/UAS* system. The mutations were expressed in IFM *TnI* (hdp^3) and *TnT* (up^1) null backgrounds. The null mutations result in lack of TnI and TnT mRNA in the IFM (Nongthomba *et al.*, 2003; Nongthomba *et al.*, 2007). Male flies are flightless; their muscles are hypercontracted and display the wings up phenotype. To establish if the mutant genes can be expressed sufficiently using this strategy the nulls had to be rescued by expressing the wild type genes. Rescuing the flight ability or the muscle phenotype would show that this system can be used to express the mutant constructs.

However, the IFM up^1 null could not be rescued using the *dmef2-GAL4* driver and the flies were flightless and still displayed the wings up phenotype. The *UH3-GAL4* driver has been used more recently to express the *UAS-TnT*$^+$ construct at 25 °C by Prof. Sparrow (personal communication) and this did not rescue the phenotype of the up^1 mutation either. The IFM-specific isoform is encoded by an mRNA made by constitutive exons and by the mutually exclusive 10a and 10b exons (Fyrberg *et al.*, 1990; Benoist *et al.*, 1998; Herranz *et al.*, 2005; Nongthomba *et al.*, 2007). The exon 10b isoform is present during all stages of muscle development and later becomes replaced by the exon 10a isoform, which is present in late pupae and adult flies (Nongthomba *et al.*, 2007). The up^1 mutation causes defective splicing of the alternative TnT exon 10a but does not affect expression of the exon 10b isoform. The UAS-*TnT*$^+$ encoding the exon 10a isoform was expressed in an up^1 background from the early pupal stage. This is concomitant with the expression of the native exon 10b isoform. Expression of exon 10a isoform during early development may interfere with the function of exon 10b isoform. This could result in defective muscle development instead of rescuing the up^1 mutation. In fact, others have shown that the overexpression of TnT in the IFM using the very strong *Act88F* gene promoter causes flightless flies characterized by a decrease in the levels of thin filament proteins (Marco-Ferreres *et al.*, 2005). The authors report the increase in TnT during early stages of adult muscle formation followed by a decrease in the TnT, tropomyosin, TnI and actin levels. The decrease in thin filament protein levels was not only due to degradation but also their mRNA levels were also diminished. Hence, early expression of the exon 10a isoform up^1 pupae may lead to muscle abnormalities. Functional differences between the 10a and 10b TnT isoforms have been hypothesized to occur due to differences in

phosphorylation sites (Nongthomba *et al.*, 2007). Since the IFM up^1 null could not be rescued here, *Drosophila* cannot be used yet as a model system to study *UAS-TnT* mutants.

If the concomitant expression of the IFM adult TnT 10a isoform with the 10b is indeed causing defects in early pupal stages, one could use a driver that permits the expression of the *UAS-TnT* constructs at late stages of pupal development. Also, using the existing drivers one could perform shifts in temperature so that the flies are grown at 18 °C where the *GAL4* activity is weak and then transferred to 25 °C or 29 °C degrees where the *GAL4* activity is stronger. The $GAL80^{ts}$ driver, which is the native repressor of *GAL4* in yeast (Lohr *et al.*, 1995) could also be used. The *GAL4* transcription activation domain is blocked at temperatures below 30 °C degrees when the $GAL80^{ts}$ driver becomes active. Introduction of the $GAL80^{ts}$ driver into the system could be a possible way to circumvent parallel expression of the 10b and 10a isoforms during early pupal stages.

Rescuing of the *TnI* hemizygote null was successful. Expression of the TnI arthrogryposis mutations resulted in either flighted or flightless flies with some mutations affecting flight ability more than others. From actin-myosin ATPase studies using the human proteins, the mutations have been hypothesized to result in hypercontractile phenotypes (Robinson *et al.*, 2006). In *Drosophila*, homologous transgenic mutations resulted in hypercontracted muscles. One way to study which TnI function is affected is to search for suppressor mutations in other proteins or in TnI. The mutations in *TnI* are located at one of the interaction sites with tropomyosin (Ferrus, 2005). Hence, suppressor mutations in the tropomyosin gene could be tested. There was not enough time during this project to test the *TnI* gene mutations in hdp^3/+ heterozygote females, which is an important experiment to perform.

There was not enough time to further analyze the *TnI* and *TnT* transgenic lines presented in this chapter. An important experiment would be to compare the level of expression of the *TnT* and *TnI* genes between the wild type and transgenic flies for the different constructs using RT-PCR.

6.6 Summary

The inability to rescue the flight ability or muscle abnormalities of the up^1 mutant shows that *Drosophila* cannot be used yet for the study of *UAS-TnT* mutants. Expression of wild type *TnI* in the IFM rescued flight ability. Some *TnI* mutants were flighted whereas others displayed the hypercontracted muscle phenotype. The biochemical study of these mutants was not completed.

Chapter 7: General Discussion

7.1. *Drosophila* IFM as a possible model for studying human nemaline myopathy

Of the currently known 3714 human disease genes, 657 are estimated to have sufficiently well conserved homologues to be analyzed in *Drosophila*. Amongst the various muscle components there is a variation in gene redundancy, sequence identity, inserts and isoform splicing. The conserved homologues of the sarcomeric components some show high protein sequence similarity e.g. Act88F and α-actinin, but others show poor sequence similarity e.g. the TnI and TnT. The work presented here dealt with both highly and poorly conserved homologues, the Act88F actin and the troponin complex, with respect to modelling two human muscle diseases.

The high sequence similarity between *ACTA1* and *Act88F* has allowed the study of 7 different NM-causing point mutations in the IFM. These actin mutations were chosen because they result in different disease symptoms in humans; actin filament aggregate myopathy, nemaline myopathy, intranuclear rods and congenital fibre type disproportion. All the mutants resulted in Z-disc and M-line disruption, zebra bodies, myofibre splitting/branching, 'whirling' of actin filaments and areas of broken/disorganised thick and thin filaments; which are seen in human patients. Concerning the major disease phenotypes, large nemaline bodies were not observed, however the IRs were recapitulated by the mutants that expressed only the human IR-linked mutations. Actin filament aggregate myopathy was not observed, though an actin filament aggregate myopathy-like phenotype was found in one case but it was not as pronounced as in humans.

Each of the *Act88F* mutants displayed an array of different characteristics, though they all produced a general muscle weakness (flightlessness) caused by the inability of the IFM to form normal myofibrils. However, at day 1 the I136M mutation resulted in some flight ability and the R372H mutation in completely flighted flies. The myofibrils of $Act88F^{I136M}/+$ and $Act88F^{R372H}/+$ heterozygotes appeared relatively and completely normal at day 1, respectively. The I136M mutation resulted in characteristic features of NM such as occasional and small zebra bodies. It was observed with the R372H mutation that the muscle progressively deteriorates and is accompanied by the formation of zebra bodies due to use over time. This suggested that there can be at least

two pathways leading to nemaline myopathy. The first pathway is characterized by an inability to form normal sarcomeres and the second pathway seen in the case of the *Act88F*^{R372H} mutant by an inability to maintain thin filament and subsequently sarcomere structure, followed by the appearance of aberrant Z-disc structures.

Another mutation, G15R, resulted in greater muscle disorganisation than the I136M and R372H mutations, with very large zebra bodies seen throughout the muscle and within the myofibrils themselves. The V163M mutation resulted in IRs, a novel ring like Z-disc structure and an actin filament aggregate myopathy-like phenotype. Actin filament aggregate myopathy is usually associated with severe clinical phenotypes in humans. In Drosophila based on the characteristics of each mutation V163M is a severe mutation. A different amino acid substitution of the same residue, V163L, resulted in all the above features with the exception of the actin filament aggregate myopathy-like phenotype and occasionally abolished myofibril formation in the homozygous state. These features were also caused by the D154N mutation, which always abolished myofibril formation in the homozygous state. The actin filament aggregate myopathy-like phenotype was not observed here either. Actin filament aggregate myopathy and intranuclear rod myopathy are often missed in the human biopsies due to their rarity. This could also be the case here and if more flies were examined it might be possible to identify actin filament aggregate myopathy in flies with the D154N and V163L mutations. However, the AM phenotype in flies is only identifiable by EM, which is an expensive and time-consuming method. In addition the AM-like aggregation seen in the V163M mutant is very small and difficult to find by eye. Hence, further processing of flies to identify AM with this method was not pursued.

The D292V mutation was studied because it causes congenital fibre type disproportion (CFTD), a disease that many patients with nemaline myopathy exhibit (Iannaccone *et al.*, 1987; Miike *et al.*, 1986; Ryan *et al.*, 2003). In those patients, the type I muscle fibres are uniformly smaller compared to type II fibres. Although loss of sarcomeres is an important cause of weakness in *ACTA1* nemaline myopathies, it is not the case for *ACTA1* CFTD as a disease because sarcomeric structure is intact (Laing *et al.*, 2004; Clarke *et al.*, 2007). Hence, there might be a distinct characteristic underlying CFTD. The distribution of mutant ACTA1 is unlikely to be a cause as it is produced in all skeletal muscle fibres. An explanation could be that the presence of different protein

isoforms between type I and II fibres result in the mutant actin disrupting a type I-specific interaction with tropomyosin or with another actin-binding protein. In Drosophila, IFM abnormal fibre type I or II differentiation cannot be studied as the IFM consist of only one fibre type. Nevertheless, *Drosophila Act88F*^{D292V} mutants displayed relatively normal and disrupted myofibrils, with some being half the size of the normal ones. This mutation resulted in sarcomeric defects in *Drosophila* IFM and in cytoplasmic aggregates in culture cell studies (Clarke *et al.*, 2007). In humans this mutation does not disrupt sarcomere structure nor does it cause sarcoplasmic rods (Laing *et al.*, 2004). The reason behind this difference is probably the fact that *Drosophila* IFM lack the continuous protein turnover and muscle repair mechanisms present in the patients' musculature.

In nemaline myopathy patients the proportion of individual myofibres occupied with nemaline rods, the size of the rod clusters and the degree of myofibrillar disruption appear to correlate with clinical severity. In the muscle fibres of individuals that exhibit the mild nemaline phenotype there is very little sarcomeric disruption by rods and the muscle fibres appear normal at the ultra-structural level. In contrast, two individuals affected with the lethal severe congenital form of the disease showed both sarcomeric actin disorganization and regions of the myofibres devoid of sarcomeres (Ilovski *et al.*, 2001). An important question is if the degree of sarcomeric disruption in *ACTA1* nemaline myopathies is an important factor that influences whether nemaline bodies form *in vivo* (Clarke *et al.*, 2007). Studying nemaline myopathy mutations in *Drosophila* IFM showed that the degree of myofibrillar abnormalities correlates with the formation of sarcoplasmic and nuclear aggregates. The D154N, V163L and V163M mutations showed the most pronounced sarcomeric disruption and resulted in sarcoplasmic and intranuclear rods. Whereas the G15R, I136M and D292V that showed less sarcomeric disruption did not result in any type of rods.

For the same mutation it was noted that the severity amongst flies of the same line varied. This is not only a feature of *Drosophila* IFM, but also of human patients (Sparrow *et al.*, 2003). In some cases similar phenotypes are observed in more than one patient such as the H42T mutation where 3 out of 4 patients show IR (Nowak *et al.*, 1999; Sparrow *et al.*, 2003); Q43R leading to typical nemaline myopathy in 2 patients (Wallgren-Pettersson and Laing, 2001; Sparrow *et al.*, 2003); H75L/R leading to severe

nemaline myopathy in 2 patients (Laing *et al.*, 2009); N117T leading to mild nemaline myopathy in 2 patients (Sparrow *et al.*, 2003) and M134V resulting in mild nemaline myopathy in 2 patients (Nowak *et al.*, 1999; Jungbluth *et al.*, 2001; Sparrow *et al.*, 2003). In contrast, the G270C mutation showed high variation in phenotypes across 8 patients from mild to severe nemaline myopathy (Ilovski *et al.*, 2001; Sparrow *et al.*, 2003). Furthermore, apart from the variations in severity between unrelated patients with the same mutation there is also intra-familial variation. This was also true here for the *Drosophila* V163L mutation, which in the homozygous state would some times abolish myofibril formation and other times not. Also all three IR-linked mutations sometimes displayed the wings-up phenotype when a single copy of the mutant actin and two of the wild type were present. These observations suggest that other factors could be affecting the IRs caused by actin mutations in both flies and humans.

7.2 Actin rods

The pathological hallmark of nemaline myopathy is the presence of dark staining bodies called nemaline rods. In the EM these rods appear as electron-dense bodies of different size and shape and usually found in the sarcoplasm or within the sarcomere. Occasionally they emerge from the Z-discs or they accumulate in an area lacking sarcomeric material. The rods do not accumulate uniformly within the muscle, as some myofibrils seem to contain more rods than others. The rods consist of actin and other Z-disc proteins, however it is unknown whether it is the mutant or the wild type actin or both (Laing *et al.*, 2009).

In *Drosophila* large nemaline bodies were rarely observed (by whole muscle staining). However, small Z-body aggregates were frequently observed in the muscles of the very severe intranuclear rod-linked *Act88F* mutants. Differences in the size of the rods and sarcomeric disruption between patients and *Drosophila* are probably due to the very much reduced levels of muscle protein expression and repair mechanisms in adult flies (Smith *et al.*, 1970). In humans muscle repair mechanisms may prevent muscle disorganisation and continuous protein turnover will support the formation of protein aggregates. For example the intranuclear rod-linked 60 hour APF pupae already show severe muscle disarray and Z-body aggregates formation. As there are reduced levels of protein turnover in the adult fly, the Z-body aggregates cannot accumulate more protein to match the size of the human ones.

Interestingly in flies carrying both the mutant *Act88F*^{V163L} and wild type *GFPAct88F*$^{+}$ alleles, the GFP signal was excluded from the phalloidin-stained sarcoplasmic actin rods. This suggested that only the mutant ACT88F^{V163L} actin is present in the sarcoplasmic rods. Indeed, expressing *GFPAct88F*^{V163L} in the IFM resulted in very large sarcoplasmic GFP-aggregates. Never before has it been shown that in muscles the mutant actin alone accumulates in the sarcoplasmic rods, which may also be the case in humans. An explanation for the large GFPACT88F^{V163L} aggregates is that they may be due to higher levels of expression driven by *GAL4*, as opposed to the native *Act88F* promoter used to express *Act88F*^{V163L}. This supports the hypothesis that the absence of large nemaline bodies in the IFM is due to the lack of protein turnover in the adult flies.

The *ACTA1* mutations causing sarcoplasmic and intranuclear rods in patients also form identical structures in cell cultures studies fibroblasts, myotubes (Costa *et al.*, 2004; Ilovski *et al.*, 2004; Domazetovska *et al.*, 2007a, b). However, the tissue culture studies are not always ideal as the R183G and the D292V CFTD-causing mutation caused intranuclear rods cytoplasmic rods, respectively to form in culture despite the fact that these phenotypes were not found in the patients (Ilovski *et al.*, 2004; Clarke *et al.*, 2007). There could be two reasons for that disagreement: 1) the artificial situations in tissue cultures may result in different effects compared to those seen in patients (Feng and Marston, 2009) or 2) because some nemaline myopathy characteristics are overlooked in the biopsies (Ryan *et al.*, 2003). In *Drosophila* IFM the intranuclear rod phenotypes were only observed in transgenics expressing human intranuclear rod-linked ACTA1 mutations further highlighting the suitability of this model for studying congenital actin myopathies.

7.2.1 Sarcoplasmic rods are caused by inability to cap actin

Studying congenital actin myopathies in *Drosophila* IFM not only allowed the identification of the actin species present in the sarcoplasmic rods but also helped to understand how the rods may be forming. A mutant CP in chicken myoblasts lacking the C-terminal β-tentacle region results in abnormal phalloidin-stained actin aggregates resembling those seen by whole muscle immunostaining in the *Drosophila* IFM D154N and V163L/M *Act88F* mutants (Schafer *et al.*, 1985). The actin D154 and V163 residues reside near the proposed binding site for the β-tentacle of CP. Thus mutations

in these residues could affect CPb binding at the fast growing end of the thin filaments resulting in aberrant Z-disc structures and actin aggregates. When *Drosophila cpb* was knocked down by RNAi using the IFM-specific (*UH3*) and pan muscle (*dmef2*) *GAL4* drivers, Z-ring structures were observed with both drivers resembling those seen in the intranuclear rod-linked mutants. These results suggested that a failure or reduced ability to cap the actin barbed ends resulting in continuous addition of actin monomers at the Z-disc alters the Z-disc structure and results in actin aggregates and aberrant Z-disc structures. Failure to cap the thin filament barbed ends could be one of the underlying cause of nemaline bodies observed in human patients.

In support of these observations when a CPβ1 mutant that poorly binds actin was expressed in mice, it resulted in myofibril disruption with sarcomeric and Z-disc defects (Hart and Cooper, 1999). Moreover, mutations in *Drosophila* genes encoding the capping protein α and β subunits result in abnormal accumulation of actin in eye-imaginal discs and retinal degeneration (Delalle *et al.*, 2005) or dramatically increase F-actin levels in *Drosophila* bristles (Hopmann and Miller, 2003). Together these observations support the hypothesis that reduced capping of the barbed end of the thin filaments could result in the formation of sarcoplasmic actin rods.

Interestingly, chicken cultured myotubes transfected with α-actinin mutants that lack any part of the region from the beginning of the fourth spectrin repeat to the start of the EF hands present α-actinin doublets, Z-line hypertrophy (up to 20-fold of the typical width) and nemaline-like body formation (Zhang *et al.*, 2009). All these phenotypes were also seen in the *cpb* knockdown flies studied here. The reported α-actinin doublets are reminiscent of the splitting Z-discs shown in the *cpb* knockdown flies.

7.3 Actin in the nucleus

Actin has no nuclear localisation signal (NLS) but cofilin, a G-actin and F-actin binding protein, has an NLS and can translocate actin in the nucleus (Ohta 1989; Pendleton *et al.*, 2003). The concentration of nuclear actin is 100-1000 times greater than the concentration required for actin to spontaneously polymerize *in vitro* (Pollard *et al.*, 2000). The pool of polymerized actin in the nucleus was found to be 20% of the total nuclear actin (McDonald *et al.*, 2006).

Several actin binding proteins have been detected in the nucleus such as, profilin (binds to G-actin and promotes nucleotide exchange) (Skare *et al.*, 2003), the point end binding proteins CapG (Onoda *et al.*, 1993), tropomodulin (Kong and Kedes, 2004), the barbed end binding protein CapZ (Ankenbauer *et al.*, 1989), cofilin (Nishida *et al.*, 1987) and zyxin (promotes actin-polymerization) (Nix *et al.*, 1997; Fradelizi *et al.*, 2001). This indicates that although actin may not necessarily be in a polymerized state, it must still be in a functional form. In fact nuclear actin has been associated with diverse nuclear activities (reviewed in Jockusch *et al.*, 2006) such as chromatin remodelling, nuclear structure and stability, mRNA export and RNA polymerase I, II, III activity.

Normally cytoplasmic F-actin is identifiable by its binding to the toxin phalloidin. However, cell culture studies have shown that the filamentous nuclear actin structures are not stained by phalloidin. This suggested that the form of nuclear F-actin differs from the conventional form of F-actin in the cytoplasm (Pederson and Aebi, 2002, 2005; Jockusch *et al.*, 2006). A monoclonal actin antibody generated against the skeletal muscle actin-profilin complex recognizes a specific conformation of the actin molecule that is not prevalent in the cytoplasm but is present in the nuclei of certain cell types (Gonsior *et al.*, 1999). The antibody recognises three regions of actin that are buried upon polymerisation.

In *Drosophila* IFM the intranuclear actin rods are stained with phalloidin. This is most likely due to the fact that they polymerize in such large structures. The same was observed for cell myoblast studies (Domazetovska *et al.*, 2007 a; b).

7.4 Actin rods in the nucleus

A nuclear exporter was recently discovered that is specific for the profilin-actin complex named exportin 6 (Exp6). Exp6 is a conserved protein found in a wide variety of organisms from amoeba to vertebrates (Stüven *et al.*, 2003). Knockdown of *Exportin 6* in *Drosophila* Schneider cells by RNAi results in the formation of actin aggregates inside the nucleus (Stüven *et al.*, 2003). Nuclear actin aggregates have also been visualized in cells that were subjected to stress such as heat shock (Welch and Suhan, 1985; Ono *et al.*, 1996) or ATP depletion (Sanger *et al.*, 1983). Treatment with toxins such as dimethylsulfoxide was also shown to result in paracrystaline actin arrays

in the nucleus of the slime mould *Dictyostelium amoebae* (Fukui, 1978; Fukui and Katsumaru, 1979; Ono *et al.*, 1993). However, nuclear actin aggregates can also appear naturally during spore formation by *Dictyostelium discoideum* (Fukui and Katsumaru, 1979; Sameshima *et al.*, 1994). Overexpression of leiomodin, an actin nucleator, has also been reported to result in the formation of intranuclear actin rods (Chereau *et al.*, 2008). Hence a variety of causes, from cell stress to disruption of actin binding proteins and proteins involved in the export of actin from the nucleus, can result in the formation of intranuclear rods. Several actin-binding proteins exist in the nucleus to support formation of actin aggregates.

Actin is exported out of the nucleus through the CRM1 exporter (Wada *et al.*, 1998) and through exportin 6, as a profilin-actin complex (Stuven *et al.*, 2003). Indeed actin cycling in the nucleus may even help to regulate actin levels (Miralles *et al.*, 2003). The presence of actin rods in the nucleus suggests that the D154N, V163L/M mutations interfere with its export from the nucleus. This effect is strongest for V163L where the intranuclear rods were most common. Several reasons could account for the intranuclear actin rod phenotype seen in the *Drosophila* IFM and in human patients. The IR-linked residues are near the profilin binding site on actin. Therefore one explanation could be that mutations in these residues disrupt the profilin-actin interaction and the formation of the complex in the nucleus. Hence, exportin is unable to transport actin resulting in the mutant actin being retained in the nucleus and aggregating once certain levels of actin have accumulated.

Actin has two putative nuclear export signals (170-181 and 211-222) that are highly conserved and have been shown to be functional by mutational analysis and cell transfection (Wada *et al.*, 1998). The *ACTA1* mutations that lead to intranuclear rods in patients are not located within these sequences but some e.g. V163L/M are found close by (Figure 3.7) (Hutchinson *et al.*, 2006) and they may affect nuclear export of actin.

This lack of export via CRM1 (G-actin) and Exp6 (profilin-actin complex) and coupled with increased levels of actin entering the nucleus would result in IRs. If the mutant actins are less stable in filaments, free mutant G-actin may have a higher probability of entering the nucleus. Interestingly, if levels of free tropomodulin increase in cell cultures, tropomodulin begins to be observed in the nucleus (Kong and Kedes, 2004).

Mouse myoblasts and fibroblasts transfected with GFP-tagged *ACTA1* intranuclear rod-mutants showed that the mutant actins can accumulate in the nucleus and form rod structures (Domazetovska *et al.*, 2007 a; b). Live-cell imaging has demonstrated that the nuclear aggregates form within the nucleus rather than forming in the cytoplasm and then translocated to the nucleus (Domazetovska *et al.*, 2007a). Hence, the nuclear environment supports the formation of intranuclear rods. However, it is not yet known if the wild type or mutant actin species is present in the human IRs. Here, it was possible to coexpress the wild type *GFPAct88F* and the $Act88F^{V163L}$ actin genes. This showed that the GFP signal is excluded from the IRs, suggesting that wild type actin is not present in the IRs. When the wild type *Act88F* and the $GFPAct88F^{V163L}$ actin genes were coexpressed, the mutant GFP-tagged actin was incorporated into the IRs, suggesting that the mutant actin is only present in the IRs. However, coexpression of wild type GFP-tagged actin and V163M untagged actin in mouse myoblasts showed that the wild type GFP-tagged actin also localised in the intranuclear rods (Domazetovska *et al.*, 2007b). These observations were in mononucleated cells and not in the mature multinucleated muscle fibres of a whole organism, which is the case in this thesis. Artificial cell culture environments may not produce different effects compared to a study in the context of a whole organism.

The intranuclear rods seen in *Drosophila* IFM, like those reported in the tissue culture studies distort the shape of the nuclei. In fact those in cell culture studies were shown to be motile (Domazetovska *et al.*, 2007b). In cells the Z-disc proteins α-actinin, γ-filamin and myotilin have been reported to be components of intranuclear actin rods (Domazetovska *et al.*, 2007a). Here, the Z-disc protein kettin was not found to colocalize with the intranuclear rods by immunostaining.

Interestingly, amongst the different thin filament proteins causing congenital myopathies, only mutations in actin result in intranuclear rods.

7.5 Understanding the effect of a single mutation in muscle structure

To date there are more than 196 known *ACTA1* mutations responsible for the nemaline phenotype (Laing *et al.*, 2009). The mutations are spread throughout the actin gene hence actin interactions with many different proteins can be affected. Actin is a protein involved in many cell functions with numerous binding partners. Some mutations in

actin are likely to disrupt more than one protein-protein interactions leading to loss of functions and making it difficult to pinpoint which interaction is affected. *Drosophila* IFM is a tractable system for studying the effects of mutations in muscle structure. An unanswered question is whether the muscle weakness in NM patients is solely due to the skeletal muscle atrophy. It is unknown whether certain mutations could induce specific alterations in the contractile function, which would contribute to the muscle weakness. This question was answered by studies in the $Act88F^{D292V}$ and $Act88F^{R372H}$ mutants.

7.5.1 Characterisation of the R372H mutation using genetic, mechanical and biochemical approaches

The R372H mutant allowed a study of how the progression of the *Drosophila* equivalent of NM using different approaches. First, confining the flies to prevent the muscles from contracting showed that the muscle damage is use-dependant in this mutant. Single myofibril mechanical experiments showed that the mutant myofibrils were less stiff compared to wild type ones, and displayed plastic deformation. This suggested that the myofibrils were mechanically compromised consistent with the observation that the thin filaments appeared torn from the Z-discs of this mutant. The R372 residue is located in one of the α-actinin binding sites on actin identified by other (Lebart *et al.*, 1993). This raised the hypothesis that the R372H mutation could affect the F-actin/α-actinin interactions within the Z-discs, weakening the attachment of the thin filaments to the Z-disc. Fluorescence anisotropy measurements showed that the binding constant of the R372H mutant actin for α-actinin was indeed 13-fold weaker than with wild type actin. A 10-fold weakening in the F-actin/α-actinin binding has also been reported in an *ACTA1* K336E mutation associated with nemaline myopathy and cardiomyopathy (D'Amico *et al.*, 2006). The $Act88F^{R372H}$ mutant has allowed to use several methods in order to understand how a single mutation affects muscle structure.

Mutations of the α-actinin gene are known, which result in nemaline bodies. For example deletion of the COOH-terminal residues 730-897 of chicken α-actinin results in hypertrophy of the Z-disc in 7-8 day myotubes, which resembles nemaline bodies (Schultheiss *et al.*, 1992; Lin *et al.*, 1998). Another α-actinin mutant lacking the region from the beginning of the fourth spectrin repeat to the start of the EF hands also results in Z-disc hypertrophy, formation of nemaline-like bodies and splitting of the Z-discs as

seen by α-actinin doublets in immunofluorescence staining of cultured chicken myotubes (Zhang *et al.*, 2009).

Similar to the *Act88F*^{R372H} mutant, other *Drosophila* models of a human skeletal muscle disease are reported that have been studied both genetically and biochemically (Shcherbata *et al.*, 2007). Fluorescence anisotropy was used to measure the human and *Drosophila* versions of dystroglycan (Dg) interacting with both human and *Drosophila* dystrophins (Dys). It was found that *Drosophila* Dg binds both human and *Drosophila* Dys with similar K_d (~ 20 μM). Human Dg also binds Dys from both species with similar K_d (~ 5 μM). These data showed that the Dys-Dg interaction is conserved between humans and *Drosophila* (Shcherbata *et al.*, 2007), which further supports *Drosophila* is a suitable system for studying human muscle diseases.

7.5.2 Genetic interactions revealed that D292V causes a hypocontractile phenotype

The residue D292 forms part of the Tm binding site on actin and *in vitro* motility studies predicted that the CFTD D292V mutation obstructs actomyosin interactions by stabilizing tropomyosin in the 'OFF' state (Clarke *et al.*, 2007). Indeed the ACT88F^{D292V} mutation suppresses the hypercontractile phenotypes of the *hdp*^{2} and *up*^{101} mutants. This suggested that the presence of sarcomere defects caused by the ACT88F^{D292V} is a consequence of functional abnormalities. This highlights the advantage of using a genetic organism whereby suppressor mutations counteract the effect of another mutation. The D292V adds to another four *Act88F* mutations that form part of the tropomyosin binding site on actin, and were previously shown to suppress the *hdp*^{2} and *up*^{101} mutations (Sarah Haigh PhD thesis, 2003, University of York).

The hypercontractile phenotype displayed by the troponin mutants can be suppressed by mutations in other proteins of the contractile machinery. For example the *hdp*^{2} phenotype can be suppressed by mutations in genes encoding tropomyosin (also suppressor of *up*^{101}) (Naimi *et al.*, 2001), TnI (Prado *et al.*, 1995) and the myosin heavy chain (Kronert *et al.*, 1995; Nongthomba *et al.*, 2003). The mutation in the tropomyosin gene suppresses both the *hdp*^{2} and *up*^{101} phenotypes and is thought to do so by disrupting the interactions of Tm with TnT and/or actin (Naimi *et al.*, 2001). One of the TnI mutations is thought to affect its interaction with TnT and affects a region close to

the interaction site with TnC (Prado *et al.*, 1995). Hence, it was proposed that hypercontraction results from misregulation of muscle contraction. The myosin heavy chain mutations map to two functionally important regions of the myosin head: the ATP binding and entry sites, which could perturb the myosin ATPase cycle and the actin-binding domain that could sterically hinder the actomyosin interaction (Rayment *et al.*, 1993). In fact disrupting the effectiveness of the myosin head and thus the transduction of force to the thin filament can prevent hypercontraction in hdp^2 flies crossed with myosin null mutants (Beall and Fyrberg, 1991; Nongthomba *et al.*, 2003). Based on these observations, it has been speculated that the force exerted by the myosin head can also drive hypercontraction.

7.6 The effects of muscle protein mutations on Z-disc assembly

Analysis of *Act88F* mutants has shown that the Z-disc structure can be affected in different ways and produce three phenotypes: Z-rings, zebra bodies and Z-body aggregates. The most likely explanation for these structures is that the mutant actin, unable to polymerise and incorporate normally into thin filaments, is still able to bind to actin binding proteins e.g. α-actinin and in doing so, forms these aberrant structures.

In *Drosophila* actin and Troponin H (a tropomyosin isoform) have been demonstrated to localise to the zebra bodies by immuno-gold labelling (Dr Bullard, personal communication). In particular, the anti-actin antibody co-localises with the electron dense bodies and filaments between them. The anti-TnH antibody recognises the thin filaments that project from them. These findings suggest that the zebra bodies might be aberrant Z-discs. The spacing of the Z-discs in *Drosophila* zebra bodies is always ~200 nm. An explanation for this regular spacing could be due to kettin, the high molecular weight modular protein present in *Drosophila* that spans from the Z-disc through the I-band and the edge of the A-band by binding to F-actin (Figure 7.1) (Bullard *et al.*, 2005). Its NH_2-terminal domain is at the centre of the Z-disc (van Straaten *et al.*, 1999) and spans 93 nm of the thin filaments protruding from the Z-disc with a further 30 nm located within the Z-disc (Figure 7.1) (van Straaten, *et al.*, 1999). Two kettin molecules extending from the opposing Z-discs of a single sarcomere would result in regular ~ 200 nm spacings like the ones seen in the zebra bodies. Kettin consists of 35 Ig domains separated by short linker sequences and binds to actin with a stoichiometry of one Ig linker molecule to one actin subunit (van Straaten, *et al.*, 1999),

suggesting that the function of kettin is to stabilize the thin filament (Burkart *et al.*, 2007). Hence this could be an explanation as to why thin filaments are seen protruding from the Z-discs of the zebra bodies.

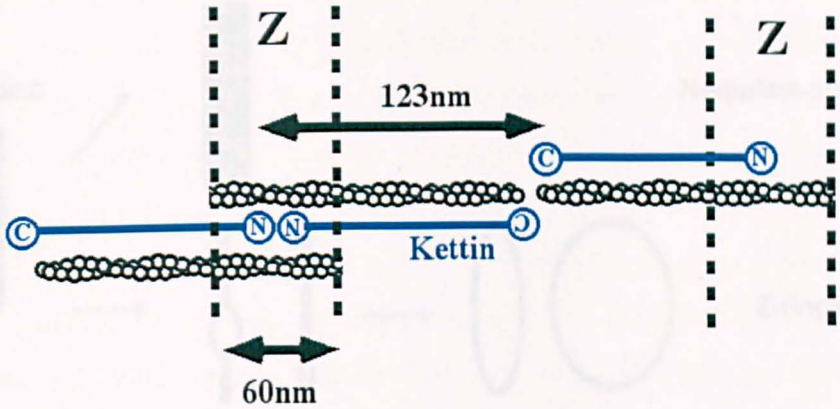

Figure 7.1. Regular spacing of zebra bodies may be caused by kettin. The Z-discs (Z) are shown as vertical dashed lines, 60 nm in width, the actin thin filament helices extend from the Z-disc, kettin is shown in blue with its N- and C-termini indicated as N and C respectively and the length of a kettin polypeptide is indicated to be 123 nm. Image produced by Dr. Bullard.

The zebra bodies may be formed due to abnormal sarcomere development or after splitting of the Z-disc due to mechanical damage (Figure 7.2). A break in the Z-disc followed by regeneration can lead to the zebra body phenotype. The nemaline-like bodies caused by *cpb* knockdown are very closely compacted zebra bodies. These are probably caused due to unregulated growth at the barbed end of the filament resulting in continuous addition of actin subunits. Insufficient capping of the thin filaments at the barbed end could be resulting in Z-ring structures (e.g. intranuclear rod-linked mutants and *cpb* knock down). Mechanical damage of the Z-rings could further result in zebra body formation. The Z-body aggregates do not show a zebra body pattern. Instead they appear as degraded Z-discs that maintain their parallel arrangement. Each degrading Z-disc appears to consist of small Z-bodies. Sometimes the parallel arrangement is not fully maintained and an aggregation of Z-bodies forms. Other electron dense structures without a distinguishable pattern may also be Z-body aggregations.

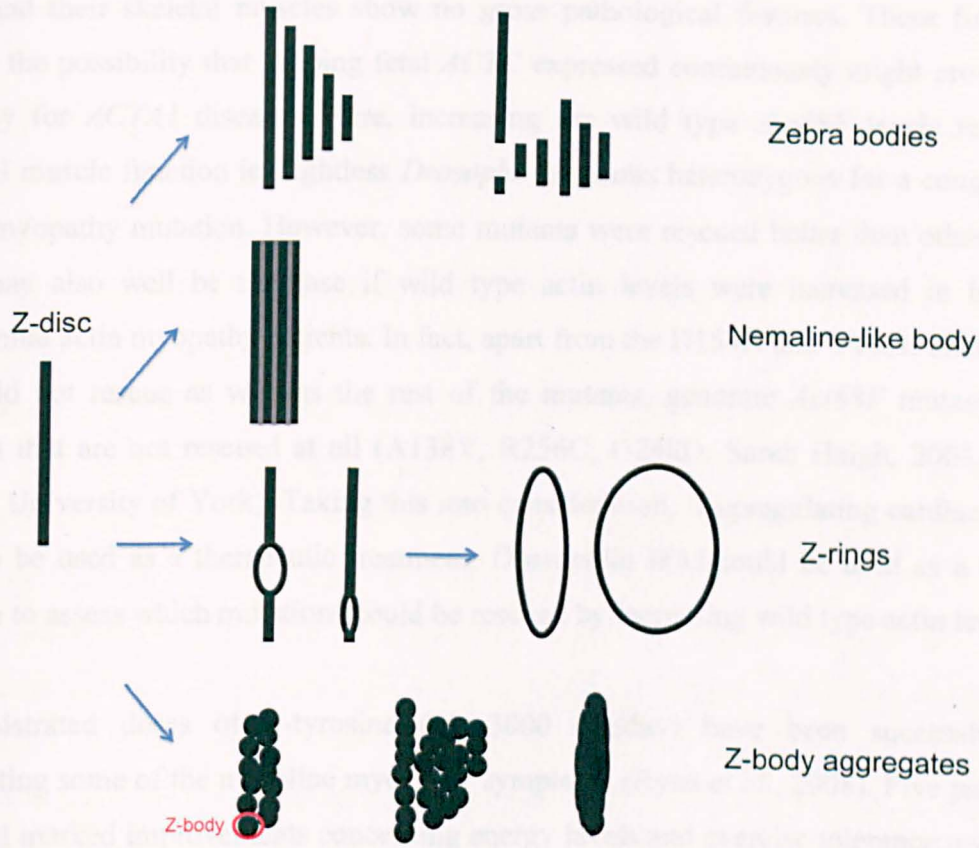

Figure 7.2. Different Z-disc phenotypes observed in the *Act88F* mutants. Abnormalities in Z-disc structure result in nemaline-like bodies, Z-rings, zebra bodies and Z-aggregates consisting of Z-bodies (indicated by red circle).

7.7 Rescuing of the nemaline phenotype

The *ACTA1* mutations affect many actin functions hence therapies focused at individual functions are unlikely to be effective and the therapy of choice would be one that is independent of actin function. In humans upregulating the skeletal muscle *ACTA1* gene would not rescue the congenital actin myopathy phenotypes, as it would lead to overexpression of both wild type and mutant variants. Another candidate that could be used is cardiac α-actin (ACTC). The skeletal and cardiac muscle ACTA1 and ACTC actins share 99 % sequence homology (Kumar *et al.*, 1997). ACTC1 is the major striated actin in fetal heart and skeletal muscle and is replaced by ACTA1 during the later stages pre-parturition (Ordahl, 1986). Recently fetal *ACTC* was used to successfully rescue the skeletal muscle α-actin-null mice (Nowak *et al.*, 2009), which otherwise die 9 days after birth (Crawford *et al.*, 2002). The rescued mice survive to old

age, and their skeletal muscles show no gross pathological features. These findings raised the possibility that keeping fetal *ACTC* expressed continuously might provide a therapy for *ACTA1* diseases. Here, increasing the wild type *Act88F* levels restores normal muscle function in flightless *Drosophila* mutants heterozygous for a congenital actin myopathy mutation. However, some mutants were rescued better than others and this may also well be the case if wild type actin levels were increased in human congenital actin myopathy patients. In fact, apart from the D154N and V163L mutations that did not rescue as well as the rest of the mutants, genomic *Act88F* mutants are known that are not rescued at all (A138V, R256C, G268D, Sarah Haigh, 2003, PhD thesis, University of York). Taking this into consideration, if upregulating cardiac actin was to be used as a therapeutic treatment, *Drosophila* IFM could be used as a quick system to assess which mutations could be rescued by increasing wild type actin levels.

Administrated doses of L-tyrosine (250-3000 mg/day) have been successful in alleviating some of the nemaline myopathy symptoms (Ryan *et al.*, 2008). Five patients showed marked improvements concerning energy levels and exercise tolerance upon L-tyrosine treatment without side effects. The mechanism of this result is not known but may be effective through effects of catecholamines on muscle (Dr. K. North personal communication). The ease of growing flies cheaply and fast in large numbers allows their use to screen for therapeutic drugs. However, both in nematodes and flies there are limitations in drug discovery. Given the fact that metabolic pathways in humans and invertebrates differ, administrating drugs to alleviate/cure disease symptoms in nematodes and flies may have an adverse effect in humans due to toxic metabolites, side-effects or they may no be effective at all. Nevertheless, *C.elegans* has been successfully used to discover the molecules serotonin and prednisone for the treatment of Duchenne Muscular Dystrophy symptoms (Bessou *et al.*, 1998; Gaud *et al.*, 2004; Carre-Pierrat *et al.*, 2006). This example shows that it is possible to discover therapeutic drugs invertebrate models to treat human myopathies.

Other proposed therapeutic approaches include allele-specific knock down by RNAi (Nowak *et al.*, 2008). However this approach must be made effective *in vivo* (Xia *et al.*, 2006). Although 75% of the mutations are found in individual families, the Wobble hypothesis leads to a variation of the third base in each codon. Targeting these variations by RNAi would require sequencing of each family member and given the fact

that new mutations appear almost as frequently as known mutations, RNAi therapy would need to be tailored to each individual. Third, not all mutations are amenable to RNAi. With 40 % of the body mass consisting of muscle (Netter, 2006), targeting of effective treatments for the mutated protein is a daunting task.

7.8 Is Drosophila IFM a good model for studying human thin filament myopathies?

Drosophila is not a perfect model and limitations in using flies to study human muscle disease have been stated throughout this chapter. Briefly, the human phenotypes cannot always be reproduced (in this thesis actin filament aggregate myopathy) and if so it is not always identical (in this thesis IRs were loosely packed instead of rod-like). Key human sarcomeric proteins, e.g. nebulin and titin, are missing in flies and other sarcomeric proteins are present only in *Drosophila* e.g. sallimus isoforms, flightin. A pathogenic protein interacts with other cellular proteins; hence since some of the proteins in *Drosophila* are different from the putatively interacting proteins in man one could potentially obtain false positive or negative results of interaction if the human disease protein cannot interact with a genuine target protein in *Drosophila*. Sufficient amounts of protein, for example myosin and actin, can be extracted from the IFM for studying protein-protein interactions (Anson *et al.*, 1995; Silva *et al.*, 2003). However, some muscle proteins are not as abundant as myosin and actin, hence the choice of biophysical techniques can be limited for such proteins. Screening for potential drugs to alleviate NM may or may not be possible in *Drosophila* given the differences in metabolic pathways to humans.

Studying a muscle disorder in a system where there is no innate immune response or muscle regeneration can be a disadvantage, as the model does not fully mimic the disease. However, the absence of muscle regeneration (satellite cells have not been found) in adult *Drosophila* can act as an advantage over other animal systems where muscle repair mechanisms are in place. The *mdx* mice, with only a mild dystrophy, have been used for studying Duchenne Muscular Dystrophy (Sicinski *et al.*, 1989). With the exception of the diaphragm, which is the most affected muscle, the other muscles show signs of the disease during the first six weeks of life, but subsequently show little signs of weakness and the mice have a near-normal lifespan (Collins *et al.*, 2003). The dystrophy remains subtle and non-lethal in these mice as expansion of satellite cells

allows them to adapt to degeneration and show muscle recovery (reviewed in Durbeej and Campell, 2002). Unlike mouse models of muscle disease that often show modest phenotypes, introducing mutations in *Drosophila* equivalent genes can impair muscle structure and often recapitulate the clinical phenotypes of human patients (as discussed in Chapter 1, section 1.4).

While *Drosophila* has only been used as a model for studying human muscle disease for the last decade, it is well equipped with all the necessary tools for studying skeletal myopathies. With a complete genome sequence and a plethora of genetic tools, genes can be identified, mapped, cloned rapidly and their expression can be spatially and temporally controlled. The organism is easily amenable and muscle defects can be readily identified and studied. Furthermore, if a mutation is too severe it may result to death thus preventing studying of the muscle defects in mice. The IFM, which are an isolated group of muscles, is dispensable for the viability of the fly and permits one to study even the most severe mutations.

Drosophila IFM meet most of the requirements to act as a genetic model system for NM. Using the *Act88F* mutants it was possible to reproduce to some extent the different congenital actin myopathy phenotypes in the IFM such as intranuclear rods, sarcomeric and myofibrillar abnormalities. The actin-aggregate filament myopathy phenotype was not reproduced. Large nemaline bodies were only observed when *GFPAct88F*^{V163L} was expressed using a *GAL4* driver. This might be due to overexpression of the ACT88F^{V163L} or less likely the GFP moiety. Hence *Drosophila* IFM is a suitable model with which to study how the IR, sarcoplasmic rods and myofibrillar disarray are caused. Furthermore, genetic approaches have helped to understand how the large nemaline bodies form. It was shown that only mutant actin is present in the intranuclear and sarcoplasmic rods. For such a small organism, flies still permit a variety of biochemical and mechanical approaches to understand the mechanism of disease as demonstrated with the studies of the R372H ACT88F mutation in this thesis. Moreover each *Act88F* mutation resulted in different phenotypes and matched in severity those of the human patients. This further shows that *Drosophila* IFM is a suitable model for studying NM.

However, the work on troponins and their role in arthrogryposis has raised issues concerning the use of *Drosophila* in studying this disease. First the *Drosophila* TnI and

TnT genes share little homology to the human counterparts due to large insertions/deletions. As a result, the *Drosophila* equivalent of the human mutant residues causing arthrogryposis could not be identified with certainty. In order to study the arthrogryposis TnI and TnT mutations the *UAS-TnI* and *UAS-TnT* constructs had to be sufficiently expressed. The way to establish if that was feasible involved rescuing the wild type IFM nulls. The TnI null was rescued but the TnT null could not be. The *UAS-TnT*$^{+}$ was expressed in an *up*^{1} background. The *up*^{1} mutation causes defective splicing of the alternative TnT exon 10a. This exon is used to generate an IFM-specific isoform, which in IFM development replaces the earlier expressed exon 10b isoform (Nongthomba *et al.*, 2007). Here expression of the exon 10a isoform was initiated from the early pupal stage when the exon 10b isoform is still expressed. The presence of exon 10a isoform during early development may interfere with the function of exon 10b isoform. This would not allow rescuing of the *up*^{1} mutation. Therefore *Drosophila* IFM are not yet a suitable system for modelling TnT arthrogryposis mutations.

7.9 Future work

Future directions should include isolating the IR-linked *Act88F* actins from the IFM to biochemically study their interactions to cpb and profilin. Weakened interaction of the actin mutants to profilin would strengthen the hypothesis that the mutant actin/profilin complex is retained in the nucleus thus resulting in actin IRs. If the binding of those actins to cpb is weakened, it would suggest that aberrant Z-disc assembly is due to the inability to cap the barbed ends of the filaments in the mutants.

The levels of expression of the GFP tagged-wild type ACT88F^{+} and ACT88F^{V163L} actins, using the *UH3*-GAL4 driver are unknown. Western blot analysis with anti-GFP and anti-actin antibodies for the *UH3*-GAL4/+; *UAS-GFPAct88F*^{V163L}/+ and *UH3-GAL4*/+; *UAS-GFPAct88F*$^{+}$/+ flies would reveal the expression levels of GFP-tagged wild type and GFP-tagged mutant actins. This would allow comparison to the native ACT88F protein levels.

Other future work should include developmental analysis of the G15R and D292V mutants by light microscopy of whole IFM. It is thought that the D292V mutant actin disrupts tropomyosin interactions. Biochemical analysis could be carried out to understand if the interaction of ACT88F^{D292V} and tropomyosin is weakened.

Furthermore, it is unknown what proteins other than actin accumulate in the Drosophila IRs. Whole muscle immunostaining showed that kettin did not localise in the IRs. Whole muscle immunostaining for different proteins such as the actin nucleator formin (Evangelista *et al.*, 2003) and α-actinin (present in human rods) can be carried out.

Tropomodulin overexpression in cell cultures results in intranuclear rods (Kong and Kedes, 2004). Although *sanpodo*, the *Drosophila* homologue of tropomodulin, has previously been overexpressed, an intranuclear rod phenotype was not reported in those flies (Kong and Kedes, 2004). The phenotype may have been overlooked or if the muscles were not properly treated the intranuclear rods could have been lost. In this thesis fixing the IFM prior to permeabilisation was crucial in order not to lose the intranuclear rods. An interesting experiment would be to perform whole muscle staining with anti-sanpodo antibody in flies overexpressing *sanpodo* and see if they also show the intranuclear rod phenotype.

For the rescue of the TnT up^1 null, to prevent parallel expression of the TnT 10a isoform with that of the TnT 10b isoform, a different driver could be used where expression occurs at a later stage during pupal development. Introduction of the $GAL80^{ts}$ driver into the system may also be a way to circumvent this problem. Shifts in temperature so that the flies are grown at 18 °C where the *GAL4* activity is weak and then transferred to 25 °C or 29 °C degrees at late pupal stages is another possible experiment. For the TnI mutants expression of the *UAS-TnI* constructs in $hdp^3/+$ heterozygote females should be followed. Studying the *UAS-TnI* mutant constructs also requires further investigation.

Appendix I

Table 1. List of primers. Mutagenized residues are underscored and shown in bold. The '-' indicates that the primer was used for gene amplification.

Gene	Mutation /-	Forward primer 5'- 3'	Reverse primer 3'- 5'
α-actinin Actin Binding Domain	S103C	GGATTTCATTGCCT**G**CAAAGGAGTCA	TGACTCCTTTG**C**AGGCAATGAAATCC
	-	GCGCGCCATATGATCGAAGGTCGTATGGATCATCACTACGACCCGC	GCGCGCCTCGAGTTAGACTGCAGAACCTTGCAAATACG
Actin88F	I136M	CGTGGCCAT**G**CAGGCCGTGCTCTCCCTG	CAGGGAGAGCACGGCCTG**C**ATGGCCACG
	D154N	ACCGGTATTGTGCTG**A**ACTCCGGCG	CGCCGGAGT**T**CAGCACAATACCGGT
	V163L	TGTCTCCCACACC**C**TGCCCATCTATGAGGG	CCCTCATAGATGGGCA**G**GGTGTGGGAGACA
	V163M	TGTCTCCCACACC**A**TGCCCATCTATGAGGG	CCCTCATAGATGGGCA**T**GGTGTGGGAGACA
	D292V	CATCCGCAAGG**T**TCTGTATGCCAACTCCGT	ACGGAGTTGGCATACAGA**A**CCTTGCGGATG
Troponin I	K245@	CGCTGGAGGAGGAGGAG**T**AGGAGAAAAAGATAAAAGA	TCTTTTATCTTTTTCTCCT**A**CTCCTCCTCCTCCAGCG
	V256G	AAAGATGCCGCTGTGCTA**GG**TAAGGCCAAAAAGTAA	TTACTTTTTGGCCTTA**CC**TAGCACAGCGGCATCTT
	ΔK257	GATGCCGCTGTGCTAAATGCCAAAAAGTAAGGTACC	GGTACCTTACTTTTTGGCATTTAGCACAGCGGCATC
	ΔE258	GCCGCTGTGCTAAATAAGAAAAAGTAAGGTACCGCA	TGCGGTACCTTACTTTTTCTTATTTAGCACAGCGGC
	-	CTATGCGAATTCATGGCTGATGATGAGAAAAAG	GCATGAGGTACCTTCTTTTTGGCCTTATTTAG
Troponin T	K43H	GCAAACAGAGATCC**C**A**C**GAGGAGGATGAG	CTCATCCTCCTC**G**T**G**GGATCTCTGTTTGC
	E314@	AGACACCCGAGGGCGAG**T**AGGACGCCAAGGCCGAT	ATCGGCCTTGGCGTCCT**A**CTCGCCCTCGGGTGTCT
Exportin 6	-	GACACCACGGAGAATCAGT	GCTCATGGGCTGGTCG
Capping protein β	-	ACGCAGCCCCTAACATAAACAGTGT	TCAGTTCGATTCGGGCTTGACATTGC
rp49	-	TCCTACCACCTTCAAGATGAC	GTGTATTCCGACCACCTTACA

Appendix II

Legend:

- intron
- GENE FLANKING REGION
- MESSENGER RNA
- TRANSLATION INITIATION CODON
- FORWARD and REVERSE PRIMER

Actin88F (CG5178)

GTCAACAGGAATCGAACGTGCGACTCTATCCAATTTTTCTCCTTTCGTTGACCTAAAAGGt
gtgtgagtgcgacctcaatgtcgaaggatccaaggattattacagaaaaagccaagaggac
taaggatattaaaactctttttaataagttcggattgtttgatggatttttctacaagtca
ctaatcggtcttcgaaagttcaatatctaaatataaagtgaagagtaattgcaacgaaacg
tattttcaattaatttgatacgtttaaattaagttctatgaactattcttttccgatattt
atagagcactgatttagtttcaagtgaataaccatattagcatgagtcaaaaggaaatgga
atataccaattttggcaatttttcatggttttatttactgaaatgtgctcaaatggacaat
agagtttcacttcacttcttcaatatcttaaaaagttaaatattttcttgagacacaaatt
agttttctatgttgtcattaaagtagtagaatttaaagaattgagatgtaggtgggagcta
taaaactttacatatataatcgacagatcgagctaaccgagtgcacttccatctcccttcc
agATAAACAACTGCCAAGATGTGTGACGATGATGCGGGTGCATTAGTTATCGACAACGGAT
CGGGCATGTGCAAAGCCGGCTTCGCCGGTGATGACGCTCCCCGTGCTGTCTTCCCCTCAAT
TGTGGGTCGTCCCCGACACCAGGGTGTGATGGTGGGTATGGGTCAGAAGGACTCGTACGTG
GGCGACGAGGCGCAAAGCAAGCGCGGTATCCTGACGCTGAAGTACCCCATCGAGCACGGCA
TCATCACGAACTGGGACGACATGGAGAAGATCTGGCATCACACCTTCTACAACGAGCTGCG
CGTGGCCCCCGAGGAGCATCCAGTATTATTGACCGAGGCTCCACTGAACCCCAAGGCCAAT
CGCGAGAAGATGACCCAGATCATGTTCGAGACCTTCAACTCGCCGGCCATGTACGTGGCCA
TCCAGGCCGTGCTCTCCCTGTACGCCTCCGGTCGTACCACCGGTATTGTGCTGGACTCCGG
CGATGGTGTCTCCCACACCGTGCCCATCTATGAGGGCTTCGCCCTGCCCCACGCCATTCTG
CGTCTGGATCTGGCTGGTCGCGATCTGACCGATTACCTGATGAAGATCCTGACGGAGCGCG
GCTACAGCTTCACCACCACCGCCGAGCGTGAGATCGTGCGCGACATCAAGGAGAAGCTGTG
CTACGTGGCTCTGGACTTCGAGCAGGAGATGGCCACCGCTGCCGCCTCCACCTCGCTGGAG
AAGTCGTACGAGTTGCCTGACGGCCAGGTGATCACCATTGGCAACGAGCGCTTCCGCTGCC
CCGAGGCTCTGTTCCAGCCCTCGTTCCTGGGCATGGAGTCGTGCGGCATCCACGAGACCGT
CTACAACTCGATCATGAAGTGCGACGTGGACATCCGCAAGGATCTGTATGCCAACTCTGTG
CTGTCCGGCGGTACCACCATGTACCCTGgtaagacaaatcattcgcttcagcagttgcact
tgtgcttaatcctttggtgcactttcagGTATTGCCGATCGTATGCAGAAGGAGATCACTG
CCCTGGCCCCATCGACCATCAAGATCAAGATCATTGCGCCACCCGAGAGGAAGTACTCCGT
CTGGATCGGTGGCTCCATCCTGGCCTCGCTGTCCACCTTCCAGCAGATGTGGATCTCGAAG
CAGGAGTACGACGAGTCCGGCCCCGGAATCGTTCACCGCAAATGCTTTTAAGTCTTTCGCC
CGCCGCGAAAGCTCTTCAAAGGCAGCAACCAGCAGCGACCAACAAGCACCCATCGAGCTAC
CCAACAACCTCGGCTCGGACAGTGATAGACAAAAGCAGCGAACCCATCGCACAACAATTAT
CATCCAACTCAGATTCACAGCAGATAATCAGAGGCAACCTCCGGTTGTCGGTGCTCATCCT

TCATGGCCATTTCATCGGCAGCGGTATAGCGGATTTTTACTTTGAAGAACTAATCGTAAGA
GTCGTGGCTGTGCTCCATGTCGAGTAGCAATCAAATGTATATGAGGAGCTTTTAACCCTAG
TCAGTGAATTGAAAGCCAAATATATCTTCCATTAAAACTATTAAATATTTT

α-actinin ABD (A28450) (1-807 bp coding sequence)

ATGGATCATCACTACGACCCGCAGCAGACCAACGATTACATGCAGCCGGAGGAGGACTGGG
ACCGGGACCTGCTCCTCGACCCGGCTTGGGAGAAGCAGCAGCGGAAGACATTTACAGCATG
GTGTAATTCTCACCTCCGCAAGGCTGGGACACAGATTGAGAACATAGAGGAAGATTTCAGG
GATGGTCTTAAACTCATGTTACTTCTGGAAGTCATTTCAGGTGAACGTTTGGCTAAGCCCG
AAAGAGGCAAAATGCGAGTGCACAAAATATCCAACGTGAACAAGGCCTTGGATTTCATTGC
CAGCAAAGGAGTCAAACTAGTATCAATTGGAGCAGAAGAAATTGTGGATGGCAACGTTAAA
ATGACTCTTGGAATGATCTGGACCATCATCCTTCGTTTTGCCATTCAGGATATCTCAGTTG
AAGAGACATCTGCTAAAGAAGGACTTTTGTTATGGTATCAGAGGAAGACAGCTCCCTACAA
AAATGTAAACATCCAGAACTTCCATATCAGTTGGAAAGATGGCCTTGGTTTCTGCGCTTTA
ATTCACAGACATCGTCCAGAGCTCATTGATTACGGGAAGCTACGAAAGGATGATCCTCTCA
CTAATCTAAACACAGCCTTTGATGTAGCTGAAAAATATCTGGATATCCCCAAGATGCTGGA
TGCAGAAGACATTGTTGGAACTGCCCGTCCTGACGAGAAAGCCATCATGACCTATGTTTCT
AGCTTCTACCACGCCTTCTCAGGAGCCCAGAAGGCGGAGACAGCAGCAAATCGTATTTGCA
AGGTTCTGGCAGTC

Capping protein b (CG17158)

AATAATCGGGCTGTGTTCCAGCTCTAGCACACCATAGCAAAAATAAAAAATCCTAATAATA
AGGAAAAAGAGTCAATTTAGTGCAATCACTTGCAATATAAGCCCGAAATCCTAGCTAGAGT
TTAAGATCGGCCCTGCTCAGCGAACGCAGGCCCCTAACATAAACAGTGTAAAACTATCGAA
ACAAGGGAAAGCAGAAAGTACCAAA**ATG**gtgagtaatactacaatagtaacaagaaaaaaa
agcaggccaacaaacggtgtttttggtcggaaccgcccattctgcaagccaaatattcttg
gcaatcacctaatccaccgagaaaacctccagaggggcggcggcctgtggcctcaaataat
gcccatatatggtaatccctggtttgccgggtggcagtggaaagcggagggatttttttggg
ctctcttatcggcggtggtgcagtgactcaaattcaatttcactggtgtctcttctcctct
cttctcagTCGGAAATGCAGATGGACTGTGCTTTGGATCTGATGCGGAGGCTGCCGCCCCA
GCAGATCGAGAAGAACCTTATTGATCTGATAGACTTGGCACCGGATCTCTGCGAGGACTTG
CTCTCCTCCGTGGACCAGCCGCTGAAGATCGCCAAGGACAAGGAGCACGGCAAGGACTATC
TGCTGTGCGACTATAACCGGGATGGGGACTCCTACAGATCGCCCTGGTCGAACTCCTACTA
TCCGCCGCTGGAGGATGGCCAAATGCCCTCGGAACGACTGCGCAAACTGGAAATCGAGGCG
AACTATGCCTTCGATCAGTACAGGGAGATGTACTACGAGGGAGGCGTCTCCTCCGTCTACC
TATGGGATCTGGATCACGGGTTTGCCGCCGTTATACTGATCAAAAAGGCGGGAGATGGCAG
CAAGATGATCCGCGGCTGCTGGGACTCCATCCATGTGGTCGAGGTACAGGAGAAGACCACC
GGCAGGACGGCCCACTACAAGCTCACCTCCACGGCAATGCTCTGGCTGCAGACCAACAAAC
AGGGTTCGGGAACCATGAATCTGGGCGGATCCCTCACCCGGCAGCAGGAGCAGGACGCCAA
CGTCAGCGAGTCGTCGCCGCACATCGCCAACATTGGCAAGATGGTCGAGGAGATGGAGAAC
AAGATCAGGAACACCCTGAACGAGATCTACTTTGGCAAGACCAAGGACATCGTGAACGGAC
TAAGGAGCACACAATCACTGGCCGATCAGCGCCAGCAGGCGGCCATGAAGCAGGACCTCGC
AGCGGCAATCCTGCGACGCAATGTCAAGCCCGAATCGAACTGGTACTGAGCGGCTGAAGGC
TGAATTTCCACATAAACCAATCCAGTCCAGGGGCGTCCCACAAGCTGGCTGCTCCCAAGAA

GAGCGCAGCAATATTCGAATTGCAAGGCACTGTTGTCACCACTAAATATTGTCATAAATAT
AAATAATTTTCATAATATTTCGGCTGCACCCACCCAATTCGCTGTTACTCGCCCAATTGTG
TTGAGCAGCTCCGTGGAGGACTCCGCTTGGACTGGACTAAAGAGCTGACTAAAAAATATTA
AATACGCATTTCTAGGCAGTAAATTTGTTACATGAGAAAATTGTTACACCACGAGAAGCAC
ATTAATGTAAATTTTGCCCGCCCGTTTCAACTGTCCTCCCACATTGTTGCCGTTTGGAGTC
GCGCTTCATCCAGAGTTCAGCCGAAAATGCCAACTTCGCCGCCCTCAAGACAGTATCCATA
AGTATTTGTATCTTATTTGTAATAATGCATATTTGCACCGAAGTCGAGGCACTTGCGTTTC
GTTCTTAATCCTTCCGCGAATAAATATTGTGTTTATTAATTGTAACTTTGTGTTTGTGTGT
AATCTAACAGTAAGGCGCTCGAAGCAAAATATTAACTGAAATCGCTTTGTGATTGTATTAT
CTGAGGAAATGCACATTACCTTTCTTCTTTACTTAATATTTTTTAACTGAAATTTGGAAGG
CAAGAGAAATTTTATACAAAGAAACTAATAAATATTGAATTACAA

Exportin 6 (CG3923)
(Only part of the gene sequence is shown so as to indicate the amplified regions)

GCCAGCCGTGCGGAATTTGTTCACTTTCCCGGAGTAGATTTTGGCCACCTTTTGTGTAAAG
ACACAAAGAAAACCATGCAATTAATGGACGCCGACTGCTGATGCGATCGGAATTAGAACCG
CGAGCAAGCGGAGCTCACAGTGACCGTAACATCCAGATCACAGATACTCGGAAGGATCGTA
AAGGACACGGAAAATGgtgaggcgggggctccgggccaaacgcactattttgccagtgat
tcagagtgattccacctaaccgggaattggtttccacccacccactgtctgtgcagCACGC
CGCATCTTTGACGACGGTGGAGGGACTGCTGCAGGAGTTTTATCAGCCCAGCACCTCCAAT
GCCCGGAAACGAGAGATCGAGACAAACCTCTTGGCCTTCAAGTCCCAGCCAGAGGCGTGGC
AACTTTGCCTCCGTGTGGCCACCTCTTCCGACACCACGGAGAATCAGTTCCTCTGGTTCTT
CAGCACCTCAACCTTGGAGCACACAATCACGCGGAGATGGACACAGTTGACGTCCACGGAC
AAGACTTTGCTGCGGGAGACCCTTTGGAACTCGTATGCCCAACTGGTAGCCACTCCAAATG
TGGCCAAACGGCACAGGGACACACTGGCCCAGTTGATAGCCCTACTCGGAAAGAGGGAGTT
CCCTGAACAGGACCCCAATTACATGCAACACTGCATGGAACTGACAAAAACACGGTTTCAA
CTTGGCATCAACCTGCTTAAGATCACCTCCGAGGAGGTGGTAAGCAACAGGGGCGACCTGA
CCACCGAATGGAAGCAGTACTTCTACTCCTGgtgggtaaatagagcgaagaggctaaaatc
gtatgtttttaaaaaaggttttgtagtcccatacttttaatgtctgtttaagactacttg
gatttttaactgagtacggcgtatcagatggtcgatgttttcgagcatagcgtatttttat
tattaactttggtgttatttgtttaaatacacgattgcgtcgcacaacatagaataacaca
atcccagaccttgtcagtccgttcttgtttttggtttattaataagtgttatattgagatt
gagtatgtatatggcataacaactaaagtcagctgacctcttaaaactcaactaattgaac
cgttaacccagttatcatattatattgctttgttgagagaaagcactataattactggtca
gttgccacagcactgttcctaacccattttgtgctccctttttgccgtgtgtttctgtagCA
TCTCCATGTGTGTACCCGATGTTCTGGACCTGGTAACCAAGTATCTGCTAATCGCTGTATG
CCACATCAATGGCAAAGACATCCAAACAACCATACCAAACACCCTCATGGACTTTAGTCTA
ACCTCAGCGCTGCCAAATGACAATCAATTAAGgtgggtcatcataacattcaaaagagcat
atgttcattacaacattttgttataacatctctctatatactccgcaGTTCCTCAATTTTG
GACCTGCTAGGATGTGTGCAGCACTTGGTCTCCTGGATACGCACTGAACTGATCTCGGAGT
ACTTCCTTATGAGCATACTTGACCTTTCCCAGTGGCGACCAGCCCATGAGCCCATCTCCTT
GGCGGCTCTCTCTGTGTTGAATGAGCTCCTCTACCTCCAGAAGCCACTGCCCTTCCCAGGA
CCCTTGATGGGCGGCGTTACCAGCCTCCTGGAGCAGCACAATAACAATCGGCGGCAGAGCG
AGATGTACAGCGACAAGTTTCGGGAGCTGCTGCGCCTCTACACCACCAAGTATGCCGCCAA
GCTGATGCAGGAGCCAGACCTGCTGGAGACCTTTCTCAATCTGCTATACAGCTGCACCACT
GAATgtgagtcgcgtgataaaaatattgccttttgagatgctaacttatttttatttttga

gatgatctttttgctgtgtagtcataaaacactcgcaatattaaatgggttatgtgcatct
cgtgatcgagatttcgaaatgtcgttgacaaagatatataacaaaagttattaattttgta
ttccccaaacag

Troponin I (CG7178)

(Only the IFM specific gene coding sequence is shown)

ATGGCTGATGATGAGAAAAAGGCAGCAGCTCCGGCCGCAGCTCCAGCGGCGGCGGCCAAAC
CGGCGGCTCCGGCAGCAGCCCCGGCGGCCAATGGCAAGGCTGCTCCGGCGGCCAATGGAAA
GGCTGCTCCGGCAGCTGCCGCCGCTCCCGCCGGTCCGCCCAAGGATCCCAACGACCCCAAA
GTGAAGGCCGAGGAGGCTAAGAAGGCTAAACAGGCTGAGATCGAGCGCAAGCGTGCTGAGG
TGCGCAAGCGCATGGAGGAAGCCTCCAAGGCCAAGAAGGCCAAGAAGGGTTTCATGACCCC
AGAGAGGAAGAAGAAACTCAGGTTGCTGCTGCGTAAGAAAGCCGCTGAGGAGCTGAAGAAA
GAACAGGAACGCAAAGCGGCTGAACGTAGACGCATCATCGAAGAACGTTGCGGCAGTCCCA
GGAATCTCAGCGATGCCAGCGAAGGCGAATTGCAAGAGATTTGCGAAGAGTATTACGAGCG
TATGTATATTTGTGAAGGCCAGAAATGGGATCTGGAATACGAAGTCAGGAAAAAAGACTGG
GAGATCAACGATCTCAATGCCCAAGTTAACGATCTTCGCGGCAAGTTCGTCAAGCCAGCCC
TGAAGAAGGTCTCCAAATACGAAAACAAATTCGCCAAGCTGCAGAAGAAGGCCGCTGAGTT
CAACTTCCGCAACCAGCTCAAGGTGGTGAAGAAGAAGGAGTTCACGCTGGAGGAGGAGGAG
AAGGAGAAAAAGATAAAAGATGCCGCTGTGCTAAATAAGGCCAAAAAGTAA

Troponin T (CG7107)

(Only the IFM specific gene coding sequence is shown)

ATGTCCGACGATGAAGAGTACACAGGAGAGGGCGATCCAGAGTTCATCAAGCGTCAGGACC
AGAAGCGCTCCGACCTCGATGATCAGCTGAAAGAATACATCACCGAGTGGCGCAAACAGAG
ATCCAAGGAGGAGGATGAGCTGAAGAAGCTGAAGGAGAAGCAGGCCAAGCGCAAGGTCACC
CGCGCCGAGGAGGAGCAAAAGATGGCCCAGCGCAAGAAGGAGGAGGAGGAGCGCCGTGTCC
GTGAGGCTGAGGAGAAGAAGCAGCGCGAGATCGAGGAGAAGCGCATGCGTCTCGAGGAGGC
CGAGAAGAAGCGCCAGGCTATGCTGCAGGCCATGAAGGACAAGGACAAGAAGGGCCCCAAC
TTCACCATTGCCAAGAAGGATGCAGGCGTGTTGGGACTCTCGTCCGCCGCCATGGAACGCA
ACAAGACTAAGGAACAGTTGGAGGAGGAGAAGAAGATCTCGCTGTCGTTCCGCATCAAGCC
CTTGGCCATCGAAGGATTCGGCGAGGCTAAGCTGCGCGAGAAGGCCCAGGAGCTGTGGGAG
CTCATTGTCAAATTGGAAACTGAGAAGTATGACTTGGAAGAAAGGCAGAAACGTCAGGACT
ACGATTTGAAAGAGTTGAAGGAAAGACAGAAGCAACAGCTCAGGCACAAAGCCTTGAAGAA
GGGTCTCGACCCGGAAGCTTTGACTGGCAAATACCCGCCCAAGATCCAAGTCGCCTCCAAG
TATGAGCGACGTGTGGACACCCGCTCTTATGACGACAAGAAGAAGCTCTTCGAGGGTGGCT
ATAATACGGTCTATGCGGAAACCTTAGAAAAGACCTGGCAAGAAAGACAGGAAAGATTCAC
TCAGCGCACAAAATCCAAACTGCCAAAGTGGTTCGGCGAGCGACCAGGCAAGAAGGCCGGT
GAGCCCGAGACACCCGAGGGCGAGGAGGACGCCAAGGCCGATGAGGACATCGTCGAGGATG
ATGAGGAGGTCGAGGAGGAGGTCGTCGAGGAGGAAGATGAGGAGGCCGAGGAGGATGAGGA
GGAGGAGGAGGAGGAAGAGGAGGAAGAAGAGGAAGAGGAGGAGGAAGAGGAGGAGGAGGAA
GAAGAGGAAGAGGAGGAGGAGGAATAG

Appendix III

A typical fluorescent anisotropy setup is shown in figure.

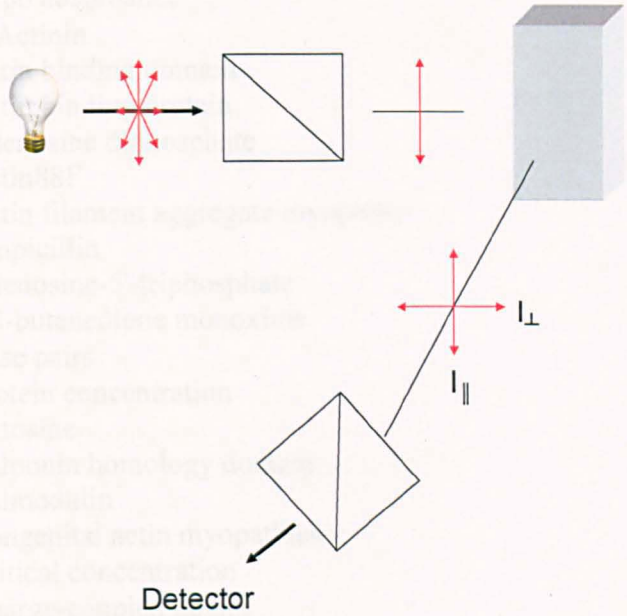

Figure 1. Schematic layout of the fluorescent anisotropy setup.

Fluorescence anisotropy (r) is:

$$r = \frac{I_{\parallel} - I_{\perp}}{I_{\parallel} + 2I_{\perp}}$$

where $I_{\parallel}$ is the fluorescence intensity of vertically polarized emission and $I_{\perp}$ is the intensity of horizontally polarized emission with both symbols referring to emissions when the sample is excited by vertically polarized light.

Abbreviations

Å	Ångstrom
A	Adenosine
A	A280 absorbance
αA	α-Actinin
ABD	Actin binding domain
ABP	Actin binding protein
ADP	Adenosine diphosphate
Act88F	Actin88F
AM	Actin filament aggregate myopathy
Amp	Ampicillin
ATP	Adenosine-5'-triphosphate
BDM	2,3-butanedione monoxime
bp	Base pairs
c	Protein concentration
C	Cytosine
CAL	Calponin homology domain
CaM	Calmodulin
CAM	Congenital actin myopathies
Cc	Critical concentration
CCD	Charge-coupled device
C. elegans	*Caenorhabditis elegans*
CFTD	Congenital fibre type disproportion
CH	Calponin homology
Cm	Chloramphenicol
CP	Capping protein
cpa	Capping protein a
cpb	Capping protein b
cps	Counts per second
CSA	Cross sectional area
c.v.	Column volume
Cy5	Cyanine Dye 5
δ-sg	δ-sarcoglycan
DA	Distal arthrogryposes
Da	Dalton
DAPI	4',6-diamidino-2-phenylindole
Dg	Dystroglycan
DLM	Dorsal longitudinal muscles
DNA	Deoxyribonucleic acid
dSMN	d Spinal muscular atrophy
dNTPs	Deoxyribonucleotide triphosphate
dsRNA	Double stranded ribonucleic acid
DTT	Dithiothreitol
DVM	Dorso ventral muscles
Dys	Dystrophin
ε	molar extinction coefficient

EDTA	Ethylenediaminetetraacetic acid
EGTA	Ethylene glycol tetraacetic acid
EM	Electron microscopy
EMS	Ethyl-methane sulphonate
ENU	ethyl-N-nitrosourea
ERC	Essential light chain
ESI-MS	Electrospray ionisation mass spectrometry
Fab	Fragment antigen binding
FAM	5-carboxyfluorescein
FITC	Fluorescein isothiocyanate
G	Guanine
GFP	Green fluorescent protein
hdp	Held-up
HC	Hypercontraction
HMM	Heavy meromyosin chain
IFM	Indirect flight muscles
Ig	Immunoglobulin-like
IgG	Immunoglobulin G
IPTG	Isopropyl-beta-D-thiogalactopyranoside
IR	Intranuclear rods
kb	Kilo base
kDa	Kilo dalton
K_d	Equilibrium dissociation constant
kPa	Kilopascal
l_0	Myofibril length
L	Litre
LB	Luria-Bertani broth
LMM	Light meromyosin chain
LOM	Larval oblique muscles
M	Molar
μg	Microgram
μl	Microlitre
μM	Micromolar
μm	Micrometre
MALDI-TOF	Matrix-Assisted Laser Desorption Ionisation – Time Of Flight
MS	mass spectrometry
MF	Myofibril
mg	Milligram
MHC	Myosin heavy chain
min	Minute
ml	Millilitre
Mol	Moles
mRNA	Messenger ribonucleic acid
N	Number of
nbr	Number
NEB	Nebulin
NES	Nuclear export signal
NM	Nemaline myopathy

nm	Nanometre
P	Pellet
PAGE	Polyacrylamide gel electrophoresis
PBS	Phosphate buffered saline
PCR	Polymerase chain reaction
pdb	Protein databank
PMSF	Phenylmethylsulphonyl fluoride
R^2	Square of the correlation coefficient
RLC	Regulatory light chain
RE	Regulatory element
RNA	Ribonucleic acid
RT	Reverse transcriptase
SDS	Sodium dodecyl sulfate
Sls	Sallimus
SMA	Spinal muscular atrophy
SMN	Survival motor neurons 1
siRNA	Small interfering RNA
SL	Sarcomere length
SN	Supernatant
T	Thymine
TILLING	Targeting-induced local lesions in genomes
TC	Tendon cells
TCM	Tendon cells and muscle
TDT	Tergal depressor of the trochanter
TEM	Templates
TEMED	N, N, N', N'- tetramethyl ethylenediamide
Tm	Tropomyosin
T_m	Melting temperature
Tmod	Tropomodulin
TnC	Troponin C
TnI	Troponin I
TnT	Troponin T
TRITC	Tetramethylrhodamine isothiocyanate
UAS	Upstream Activating Sequence
up	Upheld

References

Abu-Baker A, Messaed C, Laganiere J, Gaspar C, Brais B, Rouleau GA (2003) Involvement of the ubiquitin-proteasome pathway and molecular chaperones in oculopharyngeal muscular dystrophy. *Hum Mol Genet* **12**(20): 2609-2623

Ackermann MA, Hu LY, Bowman AL, Bloch RJ, Kontrogianni-Konstantopoulos A (2009) Obscurin Interacts with a Novel Isoform of MyBP-C at the Periphery of the Sarcomeric M-Band and Regulates Thick Filament Assembly. *Mol Biol Cell* **20**(12): 2963-2978

Adams MD, Celniker SE, Holt RA, Evans CA, Gocayne JD, Amanatides PG, Scherer SE, Li PW, Hoskins RA, Galle RF, George RA, Lewis SE, Richards S, Ashburner M, Henderson SN, Sutton GG, Wortman JR, Yandell MD, Zhang Q, Chen LX, Brandon RC, Rogers YH, Blazej RG, Champe M, Pfeiffer BD, Wan KH, Doyle C, Baxter EG, Helt G, Nelson CR, Gabor GL, Abril JF, Agbayani A, An HJ, Andrews-Pfannkoch C, Baldwin D, Ballew RM, Basu A, Baxendale J, Bayraktaroglu L, Beasley EM, Beeson KY, Benos PV, Berman BP, Bhandari D, Bolshakov S, Borkova D, Botchan MR, Bouck J, Brokstein P, Brottier P, Burtis KC, Busam DA, Butler H, Cadieu E, Center A, Chandra I, Cherry JM, Cawley S, Dahlke C, Davenport LB, Davies P, de Pablos B, Delcher A, Deng Z, Mays AD, Dew I, Dietz SM, Dodson K, Doup LE, Downes M, Dugan-Rocha S, Dunkov BC, Dunn P, Durbin KJ, Evangelista CC, Ferraz C, Ferriera S, Fleischmann W, Fosler C, Gabrielian AE, Garg NS, Gelbart WM, Glasser K, Glodek A, Gong F, Gorrell JH, Gu Z, Guan P, Harris M, Harris NL, Harvey D, Heiman TJ, Hernandez JR, Houck J, Hostin D, Houston KA, Howland TJ, Wei MH, Ibegwam C, Jalali M, Kalush F, Karpen GH, Ke Z, Kennison JA, Ketchum KA, Kimmel BE, Kodira CD, Kraft C, Kravitz S, Kulp D, Lai Z, Lasko P, Lei Y, Levitsky AA, Li J, Li Z, Liang Y, Lin X, Liu X, Mattei B, McIntosh TC, McLeod MP, McPherson D, Merkulov G, Milshina NV, Mobarry C, Morris J, Moshrefi A, Mount SM, Moy M, Murphy B, Murphy L, Muzny DM, Nelson DL, Nelson DR, Nelson KA, Nixon K, Nusskern DR, Pacleb JM, Palazzolo M, Pittman GS, Pan S, Pollard J, Puri V, Reese MG, Reinert K, Remington K, Saunders RD, Scheeler F, Shen H, Shue BC, Siden-Kiamos I, Simpson M, Skupski MP, Smith T, Spier E, Spradling AC, Stapleton M, Strong R, Sun E, Svirskas R, Tector C, Turner R, Venter E, Wang AH, Wang X, Wang ZY, Wassarman DA, Weinstock GM, Weissenbach J, Williams SM, WoodageT, Worley KC, Wu D, Yang S, Yao QA, Ye J, Yeh RF, Zaveri JS, Zhan M, Zhang G, Zhao Q, Zheng L, Zheng XH, Zhong FN, Zhong W, Zhou X, Zhu S, Zhu X, Smith HO, Gibbs RA, Myers EW, Rubin GM, Venter JC (2000) The genome sequence of Drosophila melanogaster. *Science* **287**(5461): 2185-2195

Agrawal PB, Strickland CD, Midgett C, Morales A, Newburger DE, Poulos MA, Tomczak KK, Ryan MM, Iannaccone ST, Crawford TO, Laing NG, Beggs AH (2004) Heterogeneity of nemaline myopathy cases with skeletal muscle alpha-actin gene mutations. *Ann Neurol* **56**(1): 86-96

Amarasinghe AK, MacDiarmid R, Adams MD, Rio DC (2001) An in vitro-selected RNA-binding site for the KH domain protein PSI acts as a splicing inhibitor element. *RNA* **7**(9): 1239-1253

Amores A, Force A, Yan YL, Joly L, Amemiya C, Fritz A, Ho RK, Langeland J, Prince V, Wang YL, Westerfield M, Ekker M, Postlethwait JH (1998) Zebrafish hox clusters and vertebrate genome evolution. *Science* **282**(5394): 1711-1714

Amsterdam A, Burgess S, Golling G, Chen W, Sun Z, Townsend K, Farrington S, Haldi M, Hopkins N (1999) A large-scale insertional mutagenesis screen in zebrafish. *Genes Dev* **13**(20): 2713-2724

Amsterdam A, Hopkins N (2004) Retroviral-mediated insertional mutagenesis in zebrafish. *Methods Cell Biol* **77**: 3-20

An HS, Mogami K (1996) Isolation of 88F actin mutants of Drosophila melanogaster and possible alterations in the mutant actin structures. *J Mol Biol* **260**(4): 492-505

Ankenbauer T, Kleinschmidt JA, Walsh MJ, Weiner OH, Franke WW (1989) Identification of a widespread nuclear actin binding protein. *Nature* **342**(6251): 822-825

Anson M, Drummond DR, Geeves MA, Hennessey ES, Ritchie MD, Sparrow JC (1995) Actomyosin kinetics and in vitro motility of wild-type Drosophila actin and the effects of two mutations in the Act88F gene. *Biophys J* **68**(5): 1991-2003

Araishi K, Sasaoka T, Imamura M, Noguchi S, Hama H, Wakabayashi E, Yoshida M, Hori T, Ozawa E (1999) Loss of the sarcoglycan complex and sarcospan leads to muscular dystrophy in beta-sarcoglycan-deficient mice. *Hum Mol Genet* **8**(9): 1589-1598

Au Y, Atkinson RA, Guerrini R, Kelly G, Joseph C, Martin SR, Muskett FW, Pallavicini A, Faulkner G, Pastore A (2004) Solution Structure of ZASP PDZ Domain: Implications for Sarcomere Ultrastructure and Enigma Family Redundancy. *Structure* **12**(4): 611-622

Ayme-Southgate A, Saide J, Southgate R, Bounaix C, Cammarato A, Patel S, Wussler C (2005) In indirect flight muscles Drosophila projectin has a short PEVK domain, and its NH2-terminus is embedded at the Z-band. *J Muscle Res Cell Motil* **26**(6-8): 467-477

Balciunas D, Davidson AE, Sivasubbu S, Hermanson SB, Welle Z, Ekker SC (2004) Enhancer trapping in zebrafish using the Sleeping Beauty transposon. *BMC Genomics* **5**(1): 62

Balciunas D, Ekker SC (2005) Trapping fish genes with transposons. *Zebrafish* **1**(4): 335-341

Ball E, Karlik CC, Beall CJ, Saville DL, Sparrow JC, Bullard B, Fyrberg EA (1987) Arthrin, a myofibrillar protein of insect flight muscle, is an actin-ubiquitin conjugate. *Cell* **51**(2): 221-228

Bamshad M, Bohnsack JF, Jorde LB, Carey JC (1996a) Distal arthrogryposis type 1: clinical analysis of a large kindred. *Am J Med Genet* **65**(4): 282-285

Bamshad M, Jorde LB, Carey JC (1996b) A revised and extended classification of the distal arthrogryposes. *Am J Med Genet* **65**(4): 277-281

Barbas JA, Galceran J, Krah-Jentgens I, de la Pompa JL, Canal I, Pongs O, Ferrus A (1991) Troponin I is encoded in the haplolethal region of the Shaker gene complex of Drosophila. *Genes Dev* **5**(1): 132-140

Barbas JA, Galceran J, Torroja L, Prado A, Ferrus A (1993) Abnormal muscle development in the heldup3 mutant of Drosophila melanogaster is caused by a splicing defect affecting selected troponin I isoforms. *Mol Cell Biol* **13**(3): 1433-1439

Barbazuk WB, Korf I, Kadavi C, Heyen J, Tate S, Wun E, Bedell JA, McPherson JD, Johnson SL (2000) The syntenic relationship of the zebrafish and human genomes. *Genome Res* **10**(9): 1351-1358

Barohn RJ, Jackson CE, Kagan-Hallet KS (1994) Neonatal nemaline myopathy with abundant intranuclear rods. *Neuromuscul Disord* **4**(5-6): 513-520

Barth PG, Scholte HR, Berden JA, Van der Klei-Van Moorsel JM, Luyt-Houwen IE, Van 't Veer-Korthof ET, Van der Harten JJ, Sobotka-Plojhar MA (1983) An X-linked mitochondrial disease affecting cardiac muscle, skeletal muscle and neutrophil leucocytes. *J Neurol Sci* **62**(1-3): 327-355

Barth PG, Wanders RJ, Vreken P, Janssen EA, Lam J, Baas F (1999) X-linked cardioskeletal myopathy and neutropenia (Barth syndrome) (MIM 302060). *J Inherit Metab Dis* **22**(4): 555-567

Bassett DI, Currie PD (2003) The zebrafish as a model for muscular dystrophy and congenital myopathy. *Hum Mol Genet* **12 Spec No 2**: R265-R250

Bate M, Rushton E (1993) Myogenesis and muscle patterning in Drosophila. *C R Acad Sci III* **316**(9): 1047-1061

Beall CJ, Fyrberg E (1991) Muscle abnormalities in Drosophila melanogaster heldup mutants are caused by missing or aberrant troponin-I isoforms. *J Cell Biol* **114**(5): 941-951

Beall EL, Rio DC (1997) Drosophila P-element transposase is a novel site-specific endonuclease. *Genes Dev* **11**(16): 2137-21351

Beals RK (2005) The distal arthrogryposes: a new classification of peripheral contractures. *Clin Orthop Relat Res*(435): 203-210

Beattie CE, Carrel TL, McWhorter ML (2007) Fishing for a mechanism: using zebrafish to understand spinal muscular atrophy. *J Child Neurol* **22**(8): 995-1003

Bedell MA, Jenkins NA, Copeland NG (1997a) Mouse models of human disease. Part I: techniques and resources for genetic analysis in mice. *Genes Dev* **11**(1): 1-10

Bedell MA, Largaespada DA, Jenkins NA, Copeland NG (1997b) Mouse models of human disease. Part II: recent progress and future directions. *Genes Dev* **11**(1):11-43.

Bellen HJ, Levis RW, Liao G, He Y, Carlson JW, Tsang G, Evans-Holm M, Hiesinger PR, Schulze KL, Rubin GM, Hoskins RA, Spradling AC (2004) The BDGP gene disruption project: single transposon insertions associated with 40% of Drosophila genes. *Genetics* **167**(2): 761-781

Bellen HJ, O'Kane CJ, Wilson C, Grossniklaus U, Pearson RK, Gehring WJ (1989) P-element-mediated enhancer detection: a versatile method to study development in Drosophila. *Genes Dev* **3**(9): 1288-1300

Benoist P, Mas JA, Marco R, Cervera M (1998) Differential muscle-type expression of the Drosophila troponin T gene. A 3-base pair microexon is involved in visceral and adult hypodermic muscle specification. *J Biol Chem* **273**(13): 7538-7546

Bernstein SI, O'Donnell PT, Cripps RM (1993) Molecular genetic analysis of muscle development, structure, and function in Drosophila. *Int Rev Cytol* **143**: 63-152

Bessereau J-LTCeRC, WormBook 2006. (2006) *Transposons in C. elegans.*

Bessou C, Giugia JB, Franks CJ, Holden-Dye L, Segalat L (1998) Mutations in the Caenorhabditis elegans dystrophin-like gene dys-1 lead to hyperactivity and suggest a link with cholinergic transmission. *Neurogenetics* **2**(1): 61-72

Bier E (2005) Drosophila, the golden bug, emerges as a tool for human genetics. *Nat Rev Genet* **6**(1): 9-23

Bier E, Vaessin H, Shepherd S, Lee K, McCall K, Barbel S, Ackerman L, Carretto R, Uemura T, Grell E, et al. (1989) Searching for pattern and mutation in the Drosophila genome with a P-lacZ vector. *Genes Dev* **3**(9): 1273-1287

Bione S, D'Adamo P, Maestrini E, Gedeon AK, Bolhuis PA, Toniolo D (1996) A novel X-linked gene, G4.5. is responsible for Barth syndrome. *Nat Genet* **12**(4): 385-389

Bissler JJ, Tsoras M, Goring HH, Hug P, Chuck G, Tombragel E, McGraw C, Schlotman J, Ralston MA, Hug G (2002) Infantile dilated X-linked cardiomyopathy, G4.5 mutations, altered lipids, and ultrastructural malformations of mitochondria in heart, liver, and skeletal muscle. *Lab Invest* **82**(3): 335-344

Blanchard A, Ohanian V, Critchley D (1989) The structure and function of alpha-actinin. *J Muscle Res Cell Motil* **10**(4): 280-289

Bloor JW, Kiehart DP (2001) zipper Nonmuscle Myosin-II Functions Downstream of PS2 Integrin in Drosophila Myogenesis and Is Necessary for Myofibril Formation. *Developmental Biology* **239**(2): 215-228

Bodmer R, Venkatesh TV (1998) Heart development in Drosophila and vertebrates: conservation of molecular mechanisms. *Dev Genet* **22**(3): 181-186

Bohnsack MT, Stuven T, Kuhn C, Cordes VC, Gorlich D (2006) A selective block of nuclear actin export stabilizes the giant nuclei of Xenopus oocytes. *Nat Cell Biol* **8**(3): 257-263

Bökel C (2008) *Drosophila : methods and protocols*, Totowa, N.J. London: Humana; Springer

Borrego-Diaz E, Kerff F, Lee SH, Ferron F, Li Y, Dominguez R (2006) Crystal structure of the actin-binding domain of [alpha]-actinin 1: Evaluating two competing actin-binding models. *Journal of Structural Biology* **155**(2): 230-238

Brais B, Bouchard JP, Xie YG, Rochefort DL, Chretien N, Tome FM, Lafreniere RG, Rommens JM, Uyama E, Nohira O, Blumen S, Korczyn AD, Heutink P, Mathieu J, Duranceau A, Codere F, Fardeau M, Rouleau GA (1998) Short GCG expansions in the PABP2 gene cause oculopharyngeal muscular dystrophy. *Nat Genet* **18**(2): 164-167

Bram RJ, Kornberg RD (1985) Specific protein binding to far upstream activating sequences in polymerase II promoters. *Proc Natl Acad Sci U S A* **82**(1): 43-47

Brand AH, Perrimon N (1993) Targeted gene expression as a means of altering cell fates and generating dominant phenotypes. *Development* **118**(2): 401-415.

Braun S, Croizat B, Lagrange MC, Warter JM, Poindron P (1995) Constitutive muscular abnormalities in culture in spinal muscular atrophy. *Lancet* **345**(8951): 694-695

Bresnick AR, Janmey PA, Condeelis J (1991) Evidence that a 27-residue sequence is the actin-binding site of ABP- 120. *J Biol Chem* **266**(20): 12989-12993

Broschat KO (1990) Tropomyosin prevents depolymerization of actin filaments from the pointed end. *J Biol Chem* **265**(34): 21323-21329

Broschat KO, Weber A, Burgess DR (1989) Tropomyosin stabilizes the pointed end of actin filaments by slowing depolymerization. *Biochemistry* **28**(21): 8501-8506

Bubb MR, Govindasamy L, Yarmola EG, Vorobiev SM, Almo SC, Somasundaram T, Chapman MS, Agbandje-McKenna M, McKenna R (2002) Polylysine induces an antiparallel actin dimer that nucleates filament assembly: crystal structure at 3.5-A resolution. *J Biol Chem* **277**(23): 20999-21006

Bullard B, Burkart C, Labeit S, Leonard K (2005) The function of elastic proteins in the oscillatory contraction of insect flight muscle. *J Muscle Res Cell Motil* **26**(6-8): 479-485

Bullard B, Leake MC, Leonard K (2006) Some Functions of Proteins from the Drosophila Sallimus (sls) Gene. In *Nature's Versatile Engine: : Insect Flight Muscle Inside and Out*, Vigoreaux JO (ed), pp 177-186. Georgetown, Texas: Landes Bioscience

Bullard B, Leonard K, Larkins A, Butcher G, Karlik C, Fyrberg E (1988) Troponin of asynchronous flight muscle. *J Mol Biol* **204**(3): 621-637

Bullard B, Linke WA, Leonard K (2002) Varieties of elastic protein in invertebrate muscles. *J Muscle Res Cell Motil* **23**(5-6): 435-447

Burgess S, Walker M, Knight PJ, Sparrow J, Schmitz S, Offer G, Bullard B, Leonard K, Holt J, Trinick J (2004) Structural studies of arthrin: monoubiquitinated actin. *J Mol Biol* **341**(5): 1161-1173

Burkart C, Qiu F, Brendel S, Benes V, Haag P, Labeit S, Leonard K, Bullard B (2007) Modular proteins from the Drosophila sallimus (sls) gene and their expression in muscles with different extensibility. *J Mol Biol* **367**(4): 953-969

Burtnick LD, Urosev D, Irobi E, Narayan K, Robinson RC (2004) Structure of the N-terminal half of gelsolin bound to actin: roles in severing, apoptosis and FAF. *EMBO J* **23**(14): 2713-2722

Calado A, Tome FM, Brais B, Rouleau GA, Kuhn U, Wahle E, Carmo-Fonseca M (2000) Nuclear inclusions in oculopharyngeal muscular dystrophy consist of poly(A) binding protein 2 aggregates which sequester poly(A) RNA. *Hum Mol Genet* **9**(15): 2321-2328

Caldwell JE, Waddle JA, Cooper JA, Hollands JA, Casella SJ, Casella JF (1989) cDNAs encoding the beta subunit of cap Z, the actin-capping protein of the Z line of muscle. *J Biol Chem* **264**(21): 12648-12652

Carlier MF (1991) Actin: protein structure and filament dynamics. *J Biol Chem* **266**(1): 1-4

Carlier MF, Pantaloni D (1986) Direct evidence for ADP-Pi-F-actin as the major intermediate in ATP-actin polymerization. Rate of dissociation of Pi from actin filaments. *Biochemistry* **25**(24): 7789-77892

Carlier MF, Pantaloni D, Evans JA, Lambooy PK, Korn ED, Webb MR (1988) The hydrolysis of ATP that accompanies actin polymerization is essentially irreversible. *FEBS Lett* **235**(1-2): 211-214

Carlier MF, Pantaloni D, Korn ED (1987) The mechanisms of ATP hydrolysis accompanying the polymerization of Mg-actin and Ca-actin. *J Biol Chem* **262**(7): 3052-3059

Carre-Pierrat M, Mariol MC, Chambonnier L, Laugraud A, Heskia F, Giacomotto J, Segalat L (2006) Blocking of striated muscle degeneration by serotonin in C. elegans. *J Muscle Res Cell Motil* **27**(3-4): 253-258

Casella JF, Craig SW, Maack DJ, Brown AE (1987) Cap Z(36/32), a barbed end actin-capping protein, is a component of the Z-line of skeletal muscle. *J Cell Biol* **105**(1): 371-379

Castro JP, Carareto CM (2004) Drosophila melanogaster P transposable elements: mechanisms of transposition and regulation. *Genetica* **121**(2): 107-118

Chambers CA (1994) TKO'ed: lox, stock and barrel. *Bioessays* **16**(12): 865-868

Champagne MB, Edwards KA, Erickson HP, Kiehart DP (2000) Drosophila stretchin-MLCK is a novel member of the Titin/Myosin light chain kinase family. *J Mol Biol* **300**(4): 759-777

Chartier A, Benoit B, Simonelig M (2006) A Drosophila model of oculopharyngeal muscular dystrophy reveals intrinsic toxicity of PABPN1. *EMBO J* **25**(10): 2253-2262

Chen L, Krause M, Sepanski M, Fire A (1994) The Caenorhabditis elegans MYOD homologue HLH-1 is essential for proper muscle function and complete morphogenesis. *Development* **120**(6): 1631-1641

Chen MJ, Shih CL, Wang K (1993) Nebulin as an actin zipper. A two-module nebulin fragment promotes actin nucleation and stabilizes actin filaments. *J Biol Chem* **268**(27): 20327-20334

Chereau D, Boczkowska M, Skwarek-Maruszewska A, Fujiwara I, Hayes DB, Rebowski G, Lappalainen P, Pollard TD, Dominguez R (2008) Leiomodin is an actin filament nucleator in muscle cells. *Science* **320**(5873): 239-243

Clark KA, McElhinny AS, Beckerle MC, Gregorio CC (2002) Striated muscle cytoarchitecture: an intricate web of form and function. *Annu Rev Cell Dev Biol* **18**: 637-706

Clark TG, Merriam RW (1977) Diffusible and bound actin nuclei of Xenopus laevis oocytes. *Cell* **12**(4): 883-891

Clarke NF, Ilkovski B, Cooper S, Valova VA, Robinson PJ, Nonaka I, Feng JJ, Marston S, North K (2007) The pathogenesis of ACTA1-related congenital fiber type disproportion. *Ann Neurol* **61**(6): 552-561

Clyne PJ, Brotman JS, Sweeney ST, Davis G (2003) Green fluorescent protein tagging Drosophila proteins at their native genomic loci with small P elements. *Genetics* **165**(3): 1433-1441

Collins CA, Morgan JE (2003) Duchenne's muscular dystrophy: animal models used to investigate pathogenesis and develop therapeutic strategies. *Int J Exp Pathol* **84**(4): 165-172

consortium Ces (1998) Genome sequence of the nematode C. elegans: a platform for investigating biology. *Science* **282**(5396): 2012-2018

Cooley L, Verheyen E, Ayers K (1992) Chickadee encodes a profilin required for intercellular cytoplasm transport during Drosophila oogenesis. *Cell* **69**(1): 173-184

Cooper JA, Hart MC, Karpova TS, Schafer DA (1999) Capping proteins. In *Guidebook to the Cytoskeletal and Motor Proteins*, Kreis T, Vale R (eds), pp 62-64. New York: Oxford University Press

Costa CF, Rommelaere H, Waterschoot D, Sethi KK, Nowak KJ, Laing NG, Ampe C, Machesky LM (2004) Myopathy mutations in alpha-skeletal-muscle actin cause a range of molecular defects. *J Cell Sci* **117**(Pt 15): 3367-3377

Coue M, Korn ED (1986) ATP hydrolysis by the gelsolin-actin complex and at the pointed ends of gelsolin-capped filaments. *J Biol Chem* **261**(4): 1588-1593

Craig R, Lehman W (2001) Crossbridge and tropomyosin positions observed in native, interacting thick and thin filaments. *J Mol Biol* **311**(5): 1027-1036

Crawford K, Flick R, Close L, Shelly D, Paul R, Bove K, Kumar A, Lessard J (2002) Mice lacking skeletal muscle actin show reduced muscle strength and growth deficits and die during the neonatal period. *Mol Cell Biol* **22**(16): 5887-5896

Critchley DR (2000) Focal adhesions - the cytoskeletal connection. *Curr Opin Cell Biol* **12**(1): 133-139

D'Amico A, Graziano C, Pacileo G, Petrini S, Nowak KJ, Boldrini R, Jacques A, Feng JJ, Porfirio B, Sewry CA, Santorelli FM, Limongelli G, Bertini E, Laing N, Marston SB (2006) Fatal hypertrophic cardiomyopathy and nemaline myopathy associated with ACTA1 K336E mutation. *Neuromuscul Disord* **16**(9-10): 548-552

Dancker P, Low I, Hasselbach W, Wieland T (1975) Interaction of actin with phalloidin: polymerization and stabilization of F-actin. *Biochim Biophys Acta* **400**(2): 407-414

Danowski BA, Imanaka-Yoshida K, Sanger JM, Sanger JW (1992) Costameres are sites of force transmission to the substratum in adult rat cardiomyocytes. *J Cell Biol* **118**(6): 1411-1420

Davis MR, Haan E, Jungbluth H, Sewry C, North K, Muntoni F, Kuntzer T, Lamont P, Bankier A, Tomlinson P, Sanchez A, Walsh P, Nagarajan L, Oley C, Colley A, Gedeon A, Quinlivan R, Dixon J, James D, Muller CR, Laing NG (2003) Principal mutation hotspot for central core disease and related myopathies in the C-terminal transmembrane region of the RYR1 gene. *Neuromuscul Disord* **13**(2): 151-157

Davison MD, Critchley DR (1988) alpha-Actinins and the DMD protein contain spectrin-like repeats. *Cell* **52**(2): 159-160

de Haro M, Al-Ramahi I, De Gouyon B, Ukani L, Rosa A, Faustino NA, Ashizawa T, Cooper TA, Botas J (2006) MBNL1 and CUGBP1 modify expanded CUG-induced toxicity in a Drosophila model of myotonic dystrophy type 1. *Hum Mol Genet* **15**(13): 2138-2145

Deak, II (1977) Mutations of Drosophila melanogaster that affect muscles. *J Embryol Exp Morphol* **40**: 35-63

Deak, II, Bellamy PR, Bienz M, Dubuis Y, Fenner E, Gollin M, Rahmi A, Ramp T, Reinhardt CA, Cotton B (1982) Mutations affecting the indirect flight muscles of Drosophila melanogaster. *J Embryol Exp Morphol* **69**: 61-81

Dekkers LC, van der Plas MC, van Loenen PB, den Dunnen JT, van Ommen GJ, Fradkin LG, Noordermeer JN (2004) Embryonic expression patterns of the Drosophila dystrophin-associated glycoprotein complex orthologs. *Gene Expr Patterns* **4**(2): 153-159

Delalle I, Pfleger CM, Buff E, Lueras P, Hariharan IK (2005) Mutations in the Drosophila orthologs of the F-actin capping protein alpha- and beta-subunits cause actin accumulation and subsequent retinal degeneration. *Genetics* **171**(4): 1757-1765

Demerec M (1950) *Biology of Drosophila*, New York: Wiley.

DesMarais V, Ghosh M, Eddy R, Condeelis J (2005) Cofilin takes the lead. *J Cell Sci* **118**(Pt 1): 19-26

Dickinson MH, Hyatt CJ, Lehmann FO, Moore JR, Reedy MC, Simcox A, Tohtong R, Vigoreaux JO, Yamashita H, Maughan DW (1997) Phosphorylation-dependent power output of transgenic flies: an integrated study. *Biophys J* **73**(6): 3122-3134

Dietzl G, Chen D, Schnorrer F, Su KC, Barinova Y, Fellner M, Gasser B, Kinsey K, Oppel S, Scheiblauer S, Couto A, Marra V, Keleman K, Dickson BJ (2007) A genome-wide transgenic RNAi library for conditional gene inactivation in Drosophila. *Nature* **448**(7150): 151-156

Djinovic-Carugo K (2001) Structural Studies on Cytoskeletal Proteins. *Cell Mol Biol Lett* **6**(2): 199

Djinovic-Carugo K, Young P, Gautel M, Saraste M (1999) Structure of the alpha-actinin rod: molecular basis for cross-linking of actin filaments. *Cell* **98**(4): 537-546

Domazetovska A, Ilkovski B, Cooper ST, Ghoddusi M, Hardeman EC, Minamide LS, Gunning PW, Bamburg JR, North KN (2007a) Mechanisms underlying intranuclear rod formation. *Brain* **130**(Pt 12): 3275-3284

Domazetovska A, Ilkovski B, Kumar V, Valova VA, Vandebrouck A, Hutchinson DO, Robinson PJ, Cooper ST, Sparrow JC, Peckham M, North KN (2007b) Intranuclear rod myopathy: molecular pathogenesis and mechanisms of weakness. *Ann Neurol* **62**(6): 597-608

Domingo A, Gonzalez-Jurado J, Maroto M, Diaz C, Vinos J, Carrasco C, Cervera M, Marco R (1998) Troponin-T is a calcium-binding protein in insect muscle: in vivo phosphorylation, muscle-specific isoforms and developmental profile in Drosophila melanogaster. *J Muscle Res Cell Motil* **19**(4): 393-403

Dominguez R (2004) Actin-binding proteins--a unifying hypothesis. *Trends Biochem Sci* **29**(11): 572-578

Donner K, Ollikainen M, Ridanpaa M, Christen HJ, Goebel HH, de Visser M, Pelin K, Wallgren-Pettersson C (2002) Mutations in the beta-tropomyosin (TPM2) gene--a rare cause of nemaline myopathy. *Neuromuscul Disord* **12**(2): 151-158

dos Remedios CG, Thomas DD (2001) An overview of actin structure and actin-binding proteins. *Results Probl Cell Differ* **32**: 1-7

Drubin DG, Jones HD, Wertman KF (1993) Actin structure and function: roles in mitochondrial organization and morphogenesis in budding yeast and identification of the phalloidin-binding site. *Mol Biol Cell* **4**(12): 1277-1294

Drummond DR, Hennessey ES, Sparrow JC (1991) Characterisation of missense mutations in the Act88F gene of Drosophila melanogaster. *Mol Gen Genet* **226**(1-2): 70-80

Drummond DR, Peckham M, Sparrow JC, White DC (1990) Alteration in crossbridge kinetics caused by mutations in actin. *Nature* **348**(6300): 440-442

Duffy JB (2002) GAL4 system in Drosophila: a fly geneticist's Swiss army knife. *Genesis* **34**(1-2): 1-15

Durbeej M, Campbell KP (2002) Muscular dystrophies involving the dystrophin-glycoprotein complex: an overview of current mouse models. *Curr Opin Genet Dev* **12**(3): 349-361

Durling HJ, Reilich P, Muller-Hocker J, Mendel B, Pongratz D, Wallgren-Pettersson C, Gunning P, Lochmuller H, Laing NG (2002) De novo missense mutation in a constitutively expressed exon of the slow alpha-tropomyosin gene TPM3 associated with an atypical, sporadic case of nemaline myopathy. *Neuromuscul Disord* **12**(10): 947-951

Eisenmann DM (2005) *Wnt signaling. WormBook* **25**:1-17.

Ellingsen S, Laplante MA, Konig M, Kikuta H, Furmanek T, Hoivik EA, Becker TS (2005) Large-scale enhancer detection in the zebrafish genome. *Development* **132**(17): 3799-3811

Engel WK, Cunningham GG (1963) Rapid Examination of Muscle Tissue. An Improved Trichrome Method for Fresh-Frozen Biopsy Sections. *Neurology* **13**: 919-923

Estes JE, Selden LA, Kinosian HJ, Gershman LC (1992) Tightly-bound divalent cation of actin. *J Muscle Res Cell Motil* **13**(3): 272-284

Evangelista M, Zigmond S, Boone C (2003) Formins: signaling effectors for assembly and polarization of actin filaments. *J Cell Sci* **116**(Pt 13): 2603-2611

Fabbrizio E, Bonet-Kerrache A, Leger JJ, Mornet D (1993) Actin-dystrophin interface. *Biochemistry* **32**(39): 10457-10463

Fan L, Moon J, Crodian J, Collodi P (2006) Homologous recombination in zebrafish ES cells. *Transgenic Res* **15**(1): 21-30

Farah CS, Miyamoto CA, Ramos CH, da Silva AC, Quaggio RB, Fujimori K, Smillie LB, Reinach FC (1994) Structural and regulatory functions of the NH2- and COOH-terminal regions of skeletal muscle troponin I. *J Biol Chem* **269**(7): 5230-5240

Farrell ER, Fernandes J, Keshishian H (1996) Muscle organizers in Drosophila: the role of persistent larval fibers in adult flight muscle development. *Dev Biol* **176**(2): 220-229

Faulkner G, Lanfranchi G, Valle G (2001) Telethonin and other new proteins of the Z-disc of skeletal muscle. *IUBMB Life* **51**(5): 275-282

Faulkner G, Pallavicini A, Formentin E, Comelli A, Ievolella C, Trevisan S, Bortoletto G, Scannapieco P, Salamon M, Mouly V, Valle G, Lanfranchi G (1999) ZASP: A New Z-band Alternatively Spliced PDZ-motif Protein. *J Cell Biol* **146**(2): 465-476

Feng JJ, Marston S (2009) Genotype-phenotype correlations in ACTA1 mutations that cause congenital myopathies. *Neuromuscul Disord* **19**(1): 6-16

Fernandes J, Bate M, Vijayraghavan K (1991) Development of the indirect flight muscles of Drosophila. *Development* **113**(1): 67-77

Fire A, Xu S, Montgomery MK, Kostas SA, Driver SE, Mello CC (1998) Potent and specific genetic interference by double-stranded RNA in Caenorhabditis elegans. *Nature* **391**(6669): 806-811

Fischer RS, Fowler VM (2003) Tropomodulins: life at the slow end. *Trends Cell Biol* **13**(11): 593-601

Fowler VM (1996) Regulation of actin filament length in erythrocytes and striated muscle. *Curr Opin Cell Biol* **8**(1): 86-96

Fowler VM (1997) Capping actin filament growth: tropomodulin in muscle and nonmuscle cells. *Soc Gen Physiol Ser* **52**: 79-89

Fowler VM, Greenfield NJ, Moyer J (2003) Tropomodulin contains two actin filament pointed end-capping domains. *J Biol Chem* **278**(41): 40000-40009

Fowler VM, Sussmann MA, Miller PG, Flucher BE, Daniels MP (1993) Tropomodulin is associated with the free (pointed) ends of the thin filaments in rat skeletal muscle. *J Cell Biol* **120**(2): 411-420

Fradelizi J, Noireaux V, Plastino J, Menichi B, Louvard D, Sykes C, Golsteyn RM, Friederich E (2001) ActA and human zyxin harbour Arp2/3-independent actin-polymerization activity. *Nat Cell Biol* **3**(8): 699-707

Frank D, Kuhn C, Katus HA, Frey N (2006) The sarcomeric Z-disc: a nodal point in signalling and disease. *J Mol Med* **84**(6): 446-468

Franzini-Armstrong C (1973) The structure of a simple Z line. *J Cell Biol* **58**(3): 630-642

Franzot G, Sjoblom B, Gautel M, Djinovic Carugo K (2005) The crystal structure of the actin binding domain from alpha-actinin in its closed conformation: structural insight into phospholipid regulation of alpha-actinin. *J Mol Biol* **348**(1): 151-165

Fujime S, Ishiwata S (1971) Dynamic study of F-actin by quasielastic scattering of laser light. *J Mol Biol* **62**(1): 251-265

Fujiwara I, Vavylonis D, Pollard TD (2007) Polymerization kinetics of ADP- and ADP-Pi-actin determined by fluorescence microscopy. *Proc Natl Acad Sci U S A* **104**(21): 8827-8832

Fukui Y (1978) Intranuclear actin bundles induced by dimethyl sulfoxide in interphase nucleus of Dictyostelium. *J Cell Biol* **76**(1): 146-157

Fukui Y, Katsumaru H (1979) Nuclear actin bundles in Amoeba, Dictyostelium and human HeLa cells induced by dimethyl sulfoxide. *Exp Cell Res* **120**(2): 451-455

Fukunaga H, Osame M, Igata A (1980) A case of nemaline myopathy with ophthalmoplegia and mitochondrial abnormalities. *J Neurol Sci* **46**(2): 169-177

Fyrberg EA, Mahaffey JW, Bond BJ, Davidson N (1983) Transcripts of the six Drosophila actin genes accumulate in a stage- and tissue-specific manner. *Cell* **33**(1): 115-123

Gaiano N, Amsterdam A, Kawakami K, Allende M, Becker T, Hopkins N (1996) Insertional mutagenesis and rapid cloning of essential genes in zebrafish. *Nature* **383**(6603): 829-832

Garcia-Lopez A, Monferrer L, Garcia-Alcover I, Vicente-Crespo M, Alvarez-Abril MC, Artero RD (2008) Genetic and chemical modifiers of a CUG toxicity model in Drosophila. *PLoS One* **3**(2): e1595

Gasmi-Seabrook GM, Howarth JW, Finley N, Abusamhadneh E, Gaponenko V, Brito RM, Solaro RJ, Rosevear PR (1999) Solution structures of the C-terminal domain of cardiac troponin C free and bound to the N-terminal domain of cardiac troponin I. *Biochemistry* **38**(26): 8313-8322

Gaud A, Simon JM, Witzel T, Carre-Pierrat M, Wermuth CG, Segalat L (2004) Prednisone reduces muscle degeneration in dystrophin-deficient Caenorhabditis elegans. *Neuromuscul Disord* **14**(6): 365-370

Geeves MA, Holmes KC (2005) The molecular mechanism of muscle contraction. *Adv Protein Chem* **71**: 161-193

Gieseler K, Grisoni K, Segalat L (2000) Genetic suppression of phenotypes arising from mutations in dystrophin-related genes in Caenorhabditis elegans. *Curr Biol* **10**(18): 1092-1097

Gieselmann R, Kwiatkowski DJ, Janmey PA, Witke W (1995) Distinct biochemical characteristics of the two human profilin isoforms. *Eur J Biochem* **229**(3): 621-628

Giniger E, Varnum SM, Ptashne M (1985) Specific DNA binding of GAL4, a positive regulatory protein of yeast. *Cell* **40**(4): 767-774

Goebel HH (2007) Cap disease uncapped. *Neuromuscul Disord* **17**(6): 429-432

Goebel HH, Anderson JR, Hubner C, Oexle K, Warlo I (1997a) Congenital myopathy with excess of thin myofilaments. *Neuromuscul Disord* **7**(3): 160-168

Goebel HH, Piirsoo A, Warlo I, Schofer O, Kehr S, Gaude M (1997b) Infantile intranuclear rod myopathy. *J Child Neurol* **12**(1): 22-30

Goldschmidt-Clermont PJ, Machesky LM, Doberstein SK, Pollard TD (1991) Mechanism of the interaction of human platelet profilin with actin. *J Cell Biol* **113**(5): 1081-1089

Goldstein MA, Schroeter JP, Sass RL (1979) The Z lattice in canine cardiac muscle. *J Cell Biol* **83**(1): 187-204

Golling G, Amsterdam A, Sun Z, Antonelli M, Maldonado E, Chen W, Burgess S, Haldi M, Artzt K, Farrington S, Lin SY, Nissen RM, Hopkins N (2002) Insertional mutagenesis in zebrafish rapidly identifies genes essential for early vertebrate development. *Nat Genet* **31**(2): 135-140

Gonsior SM, Platz S, Buchmeier S, Scheer U, Jockusch BM, Hinssen H (1999) Conformational difference between nuclear and cytoplasmic actin as detected by a monoclonal antibody. *J Cell Sci* **112**: 797-809

Gordon AM, Homsher E, Regnier M (2000) Regulation of contraction in striated muscle. *Physiol Rev* **80**(2): 853-924

Gordon N (1998) Arthrogryposis multiplex congenita. *Brain Dev* **20**(7): 507-511

Granzier HL, Labeit S (2005) Titin and its associated proteins: the third myofilament system of the sarcomere. *Adv Protein Chem* **71**: 89-119

Greenfield NJ, Fowler VM (2002) Tropomyosin requires an intact N-terminal coiled coil to interact with tropomodulin. *Biophys J* **82**(5): 2580-2591

Gregorio CC, Fowler VM (1995) Mechanisms of thin filament assembly in embryonic chick cardiac myocytes: tropomodulin requires tropomyosin for assembly. *J Cell Biol* **129**(3): 683-695

Gregorio CC, Trombitas K, Centner T, Kolmerer B, Stier G, Kunke K, Suzuki K, Obermayr F, Herrmann B, Granzier H, Sorimachi H, Labeit S (1998) The NH2 terminus of titin spans the Z-disc: its interaction with a novel 19-kD ligand (T-cap) is required for sarcomeric integrity. *J Cell Biol* **143**(4): 1013-1027

Gregorio CC, Weber A, Bondad M, Pennise CR, Fowler VM (1995) Requirement of pointed-end capping by tropomodulin to maintain actin filament length in embryonic chick cardiac myocytes. *Nature* **377**(6544): 83-86

Grumbling G, Strelets V (2006) FlyBase: anatomical data, images and queries. *Nucleic Acids Res* **34**(Database issue): 484-488

Gu Z, Valianpour F, Chen S, Vaz FM, Hakkaart GA, Wanders RJ, Greenberg ML (2004) Aberrant cardiolipin metabolism in the yeast taz1 mutant: a model for Barth syndrome. *Mol Microbiol* **51**(1): 149-158

Guarente L, Yocum RR, Gifford P (1982) A GAL10-CYC1 hybrid yeast promoter identifies the GAL4 regulatory region as an upstream site. *Proc Natl Acad Sci U S A* **79**(23): 7410-7414

Guyon JR, Steffen LS, Howell MH, Pusack TJ, Lawrence C. Kunkel LM (2007) Modeling human muscle disease in zebrafish. *Biochim Biophys Acta* **1772**(2): 205-215.

Haarer BK, Corbett A, Kweon Y, Petzold AS, Silver P, Brown SS (1996) SEC3 mutations are synthetically lethal with profilin mutations and cause defects in diploid-specific bud-site selection. *Genetics* **144**(2): 495-510

Haarer BK, Lillie SH, Adams AE, Magdolen V, Bandlow W, Brown SS (1990) Purification of profilin from Saccharomyces cerevisiae and analysis of profilin-deficient cells. *J Cell Biol* **110**(1): 105-114

Haffter P, Granato M, Brand M, Mullins MC, Hammerschmidt M, Kane DA, Odenthal J, van Eeden FJ, Jiang YJ, Heisenberg CP, Kelsh RN, Furutani-Seiki M, Vogelsang E, Beuchle D, Schach U, Fabian C, Nusslein-Volhard C (1996) The identification of genes with unique and essential functions in the development of the zebrafish, Danio rerio. *Development* **123**: 1-36

Haigh S (2003) Drosophila melanogaster actin mutations: suppression of hypercontraction and homologues of human nemaline myopathies. PhD Thesis, Biology, Univeristy of York, York

Hajkova L, Bjorkegren Sjogren C, Korenbaum E, Nordberg P, Karlsson R (1997) Characterization of a mutant profilin with reduced actin-binding capacity: effects in vitro and in vivo. *Exp Cell Res* **234**(1): 66-77

Hall JG (1997) Arthrogryposis multiplex congenita: etiology, genetics, classification, diagnostic approach, and general aspects. *J Pediatr Orthop B* **6**(3): 159-166

Hall JG, Reed SD, Scott CI, Rogers JG, Jones KL, Camarano A (1982) Three distinct types of X-linked arthrogryposis seen in 6 families. *Clin Genet* **21**(2): 81-97

Hamamoto T, Seto H, Beppu T (1983) Leptomycins A and B, new antifungal antibiotics. II. Structure elucidation. *J Antibiot (Tokyo)* **36**(6): 646-650

Hammond SM, Bernstein E, Beach D, Hannon GJ (2000) An RNA-directed nuclease mediates post-transcriptional gene silencing in Drosophila cells. *Nature* **404**(6775): 293-296

Hanauer A, Levin M, Heilig R, Daegelen D, Kahn A, Mandel JL (1983) Isolation and characterization of cDNA clones for human skeletal muscle alpha actin. *Nucleic Acids Res* **11**(11): 3503-3516

Hanson J, Lowy J (1964) The Structure of Actin Filaments and the Origin of the Axial Periodicity in the I-Substance of Vertebrate Striated Muscle. *Proc R Soc Lond B Biol Sci* **160**: 449-460

Hao Y, Bernstein SI, Pollack GH (2004) Passive stiffness of Drosophila IFM myofibrils: a novel, high accuracy measurement method. *J Muscle Res Cell Motil* **25**(4-5): 359-366

Hart MC, Cooper JA (1999) Vertebrate isoforms of actin capping protein beta have distinct functions In vivo. *J Cell Biol* **147**(6): 1287-1298

Hennessey ES, Harrison A, Drummond DR, Sparrow JC (1992) Mutant actin: a dead end? *J Muscle Res Cell Motil* **13**(2): 127-131

Herranz R, Mateos J, Marco R (2005) Diversification and independent evolution of troponin C genes in insects. *J Mol Evol* **60**(1): 31-44

Hertzog M, van Heijenoort C, Didry D, Gaudier M, Coutant J, Gigant B, Didelot G, Preat T, Knossow M, Guittet E, Carlier MF (2004) The beta-thymosin/WH2 domain; structural basis for the switch from inhibition to promotion of actin assembly. *Cell* **117**(5): 611-623

Herzberg O, James MN (1988) Refined crystal structure of troponin C from turkey skeletal muscle at 2.0 A resolution. *J Mol Biol* **203**(3): 761-779

Hitchcock SE (1975) Regulation of muscle contraction: bindings of troponin and its components to actin and tropomyosin. *Eur J Biochem* **52**(2): 255-263

Hitchcock SE, Carisson L, Lindberg U (1976) Depolymerization of F-actin by deoxyribonuclease I. *Cell* **7**(4): 531-542

Hochschild A, Ptashne M (1988) Interaction at a distance between lambda repressors disrupts gene activation. *Nature* **336**(6197): 353-357

Hoffman EP, Brown RH, Jr., Kunkel LM (1987) Dystrophin: the protein product of the Duchenne muscular dystrophy locus. *Cell* **51**(6): 919-928

Hogan B (1994) *Manipulating the mouse embryo : a laboratory manual*, 2nd edn. Plainview, N.Y.: Cold Spring Harbor Laboratory Press.

Hopmann R, Cooper JA, Miller KG (1996) Actin organization, bristle morphology, and viability are affected by actin capping protein mutations in Drosophila. *J Cell Biol* **133**(6): 1293-1305

Hopmann R, Miller KG (2003) A balance of capping protein and profilin functions is required to regulate actin polymerization in Drosophila bristle. *Mol Biol Cell* **14**(1): 118-128

Huang S, Blanchoin L, Kovar DR, Staiger CJ (2003) Arabidopsis capping protein (AtCP) is a heterodimer that regulates assembly at the barbed ends of actin filaments. *J Biol Chem* **278**(45): 44832-44842

Hudson AM, Petrella LN, Tanaka AJ, Cooley L (2008) Mononuclear muscle cells in Drosophila ovaries revealed by GFP protein traps. *Dev Biol* **314**(2): 329-340

Hutchinson DO, Charlton A, Laing NG, Ilkovski B, North KN (2006) Autosomal dominant nemaline myopathy with intranuclear rods due to mutation of the skeletal muscle ACTA1 gene: clinical and pathological variability within a kindred. *Neuromuscul Disord* **16**(2): 113-121

Huxley HE (2004) Recent X-ray diffraction studies of muscle contraction and their implications. *Philos Trans R Soc Lond B Biol Sci* **359**(1452): 1879-1882

Iannaccone ST, Bove KE, Vogler CA, Buchino JJ (1987) Type 1 fiber size disproportion: morphometric data from 37 children with myopathic, neuropathic, or idiopathic hypotonia. *Pediatr Pathol* **7**(4): 395-419

Ilkovski B, Cooper ST, Nowak K, Ryan MM, Yang N, Schnell C, Durling HJ, Roddick LG, Wilkinson I, Kornberg AJ, Collins KJ, Wallace G, Gunning P, Hardeman EC, Laing NG, North KN (2001) Nemaline myopathy caused by mutations in the muscle alpha-skeletal-actin gene. *Am J Hum Genet* **68**(6): 1333-1343

Ilkovski B, Nowak KJ, Domazetovska A, Maxwell AL, Clement S, Davies KE, Laing NG, North KN, Cooper ST (2004) Evidence for a dominant-negative effect in ACTA1 nemaline myopathy caused by abnormal folding, aggregation and altered polymerization of mutant actin isoforms. *Hum Mol Genet* **13**(16): 1727-1743

Isenberg G, Aebi U, Pollard TD (1980) An actin-binding protein from Acanthamoeba regulates actin filament polymerization and interactions. *Nature* **288**(5790): 455-459

Ishikawa R, Yamashiro, S, Matsumura, F (1989) Annealing of Gelsolin-severed Actin Fragments by Tropomyosin in the presence of Ca2+. Potentiation of the annealing process by caldesmon. *J Biol Chem* **264**: 16764-16770

Janmey PA, Lindberg U (2004) Cytoskeletal regulation: rich in lipids. *Nat Rev Mol Cell Biol* **5**(8): 658-666

Janody F, Treisman JE (2006) Actin capping protein {alpha} maintains vestigial-expressing cells within the Drosophila wing disc epithelium. *Development* **133**(17): 3349-3357

Jarrett HW (2000) Temperature dependence of DNA affinity chromatography of transcription factors. *Anal Biochem* 279(2): 209-217

Jiang M, Zhao X, Han W, Bian C, Li X, Wang G, Ao Y, Li Y, Yi D, Zhe Y, Lo WH, Zhang X, Li J (2006) A novel deletion in TNNI2 causes distal arthrogryposis in a large Chinese family with marked variability of expression. *Hum Genet* **120**(2): 238-242

Jin JP, Brotto MA, Hossain MM, Huang QQ, Brotto LS, Nosek TM, Morton DH, Crawford TO (2003) Truncation by Glu180 nonsense mutation results in complete loss of slow skeletal muscle troponin T in a lethal nemaline myopathy. *J Biol Chem* **278**(28): 26159-26165

Jockusch BM, Schoenenberger CA, Stetefeld J, Aebi U (2006) Tracking down the different forms of nuclear actin. *Trends Cell Biol* **16**(8): 391-396

Jockusch BM, Veldman H, Griffiths GW, van Oost BA, Jennekens FG (1980) Immunofluorescence microscopy of a myopathy. alpha-Actinin is a major constituent of nemaline rods. *Exp Cell Res* **127**(2): 409-420

Johnson JD, Collins JH, Robertson SP, Potter JD (1980) A fluorescent probe study of Ca2+ binding to the Ca2+-specific sites of cardiac troponin and troponin C. *J Biol Chem* **255**(20): 9635-9640

Johnston JJ, Kelley RI, Crawford TO, Morton DH, Agarwala R, Koch T, Schaffer AA, Francomano CA, Biesecker LG (2000) A novel nemaline myopathy in the Amish caused by a mutation in troponin T1. *Am J Hum Genet* **67**(4): 814-821

Johnston M, Davis RW (1984) Sequences that regulate the divergent GAL1-GAL10 promoter in Saccharomyces cerevisiae. *Mol Cell Biol* **4**(8): 1440-1448

Josephson RK (2006) *Comparative physiology of insect flight muscle. Nature's versatile engine. Insect Flight Muscle Inside and Out.* Austin, TX: Landes Bioscience.

Jungbluth H, Sewry CA, Brown SC, Nowak KJ, Laing NG, Wallgren-Pettersson C, Pelin K, Manzur AY, Mercuri E, Dubowitz V, Muntoni F (2001) Mild phenotype of nemaline myopathy with sleep hypoventilation due to a mutation in the skeletal muscle alpha-actin (ACTA1) gene. *Neuromuscul Disord* **11**(1): 35-40

Kabsch W, Mannherz HG, Suck D, Pai EF, Holmes KC (1990) Atomic structure of the actin:DNase I complex. *Nature* **347**(6288): 37-44

Kaimaktchiev V, Goebel H, Laing N, Narus M, Weeks D, Nixon R (2006) Intranuclear nemaline rod myopathy. *Muscle Nerve* **34**(3): 369-372

Kakidani H, Ptashne M (1988) GAL4 activates gene expression in mammalian cells. *Cell* **52**(2): 161-167

Karess RE, Rubin GM (1984) Analysis of P transposable element functions in Drosophila. *Cell* **38**(1): 135-146

Kaufman PD, Rio DC (1991) Germline transformation of Drosophila melanogaster by purified P element transposase. *Nucleic Acids Res* **19**(22): 6336

Kawakami K, Takeda H, Kawakami N, Kobayashi M, Matsuda N, Mishina M (2004) A transposon-mediated gene trap approach identifies developmentally regulated genes in zebrafish. *Dev Cell* **7**(1): 133-144

Kerwitz Y, Kuhn U, Lilie H, Knoth A, Scheuermann T, Friedrich H, Schwarz E, Wahle E (2003) Stimulation of poly(A) polymerase through a direct interaction with the nuclear poly(A) binding protein allosterically regulated by RNA. *EMBO J* **22**(14): 3705-3714

Kimber E, Tajsharghi H, Kroksmark AK, Oldfors A, Tulinius M (2006) A mutation in the fast skeletal muscle troponin I gene causes myopathy and distal arthrogryposis. *Neurology* **67**(4): 597-601

Kimmel CB (1989) Genetics and early development of zebrafish. *Trends Genet* **5**(8): 283-288

Klaavuniemi T, Kelloniemi A, Ylanne J (2004) The ZASP-like Motif in Actinin-associated LIM Protein Is Required for Interaction with the {alpha}-Actinin Rod and for Targeting to the Muscle Z-line. *J Biol Chem* **279**(25): 26402-26410

Klenchin VA, Allingham JS, King R, Tanaka J, Marriott G, Rayment I (2003) Trisoxazole macrolide toxins mimic the binding of actin-capping proteins to actin. *Nat Struct Biol* **10**(12): 1058-1063

Kobayashi T, Tao T, Gergely J, Collins JH (1994) Structure of the troponin complex. Implications of photocross-linking of troponin I to troponin C thiol mutants. *J Biol Chem* **269**(8): 5725-5729

Kobayashi T, Tao T, Grabarek Z, Gergely J, Collins JH (1991) Cross-linking of residue 57 in the regulatory domain of a mutant rabbit skeletal muscle troponin C to the inhibitory region of troponin I. *J Biol Chem* **266**(21): 13746-13751

Kong KY, Kedes L (2004) Cytoplasmic nuclear transfer of the actin-capping protein tropomodulin. *J Biol Chem* **279**(29): 30856-30864

Korenbaum E, Nordberg P, Bjorkegren-Sjogren C, Schutt CE, Lindberg U, Karlsson R (1998) The role of profilin in actin polymerization and nucleotide exchange. *Biochemistry* **37**(26): 9274-9283

Kostyukova AS, Choy A, Rapp BA (2006) Tropomodulin binds two tropomyosins: a novel model for actin filament capping. *Biochemistry* **45**(39): 12068-12075

Kotani T, Nagayoshi S, Urasaki A, Kawakami K (2006) Transposon-mediated gene trapping in zebrafish. *Methods* **39**(3): 199-206

Krakowiak PA, Bohnsack JF, Carey JC, Bamshad M (1998) Clinical analysis of a variant of Freeman-Sheldon syndrome (DA2B). *Am J Med Genet* **76**(1): 93-98

Kreuz AJ, Simcox A, Maughan D (1996) Alterations in flight muscle ultrastructure and function in Drosophila tropomyosin mutants. *J Cell Biol* **135**(3): 673-687

Kronert WA, Acebes A, Ferrus A, Bernstein SI (1999) Specific myosin heavy chain mutations suppress troponin I defects in Drosophila muscles. *J Cell Biol* **144**(5): 989-1000

Kronert WA, O'Donnell PT, Fieck A, Lawn A, Vigoreaux JO, Sparrow JC, Bernstein SI (1995) Defects in the Drosophila myosin rod permit sarcomere assembly but cause flight muscle degeneration. *J Mol Biol* **249**(1): 111-125

Kueh HY, Charras GT, Mitchison TJ, Brieher WM (2008) Actin disassembly by cofilin, coronin, and Aip1 occurs in bursts and is inhibited by barbed-end cappers. *J Cell Biol* **182**(2): 341-353

Kuhlman PA, Ellis J, Critchley DR, Bagshaw CR (1994) The kinetics of the interaction between the actin-binding domain of alpha-actinin and F-actin. *FEBS Lett* **339**(3): 297-301

Kuhlman PA, Hemmings L, Critchley DR (1992) The identification and characterisation of an actin-binding site in [alpha]-actinin by mutagenesis. *FEBS Letters* **304**(2-3): 201-206

Kuhn U, Nemeth A, Meyer S, Wahle E (2003) The RNA binding domains of the nuclear poly(A)-binding protein. *J Biol Chem* **278**(19): 16916-16925

Kulke M, Neagoe C, Kolmerer B, Minajeva A, Hinssen H, Bullard B, Linke WA (2001) Kettin, a major source of myofibrillar stiffness in Drosophila indirect flight muscle. *J Cell Biol* **154**(5): 1045-1057

Kumar A, Crawford K, Close L, Madison M, Lorenz J, Doetschman T, Pawlowski S, Duffy J, Neumann J, Robbins J, Boivin GP, O'Toole BA, Lessard JL (1997) Rescue of cardiac alpha-actin-deficient mice by enteric smooth muscle gamma-actin. *Proc Natl Acad Sci U S A* **94**(9): 4406-4411

Kunkel LM, Bachrach E, Bennett RR, Guyon J, Steffen L (2006) Diagnosis and cell-based therapy for Duchenne muscular dystrophy in humans, mice, and zebrafish. *J Hum Genet* **51**(5): 397-406

Kwak IH, Kim HS, Choi OR, Ryu MS, Lim IK (2004) Nuclear accumulation of globular actin as a cellular senescence marker. *Cancer Res* **64**(2): 572-580

Labeit S, Gibson T, Lakey A, Leonard K, Zeviani M, Knight P, Wardale J, Trinick J (1991) Evidence that nebulin is a protein-ruler in muscle thin filaments. *FEBS Lett* **282**(2): 313-316

Labeit S, Kolmerer B (1995) Titins: giant proteins in charge of muscle ultrastructure and elasticity. *Science* **270**(5234): 293-296

Laing NG, Clarke NF, Dye DE, Liyanage K, Walker KR, Kobayashi Y, Shimakawa S, Hagiwara T, Ouvrier R, Sparrow JC, Nishino I, North KN, Nonaka I (2004) Actin mutations are one cause of congenital fibre type disproportion. *Ann Neurol* **56**(5): 689-694

Laing NG, Dye, D. E., Wallgren-Pettersson, C., Richard, G., Monnier, N., Lillis, S., , Winder T, Lochmueller, H., Graziano, C., Mitrani-Rosenbaum, S., Sparrow, J., Beggs, A., Nowak, K. (2009) Mutations and polymorphisms of the skeletal muscle α-actin gene. *Hum Mut* **humu-2009-0072.R1.**

Laing NG, Nowak KJ (2005) When contractile proteins go bad: the sarcomere and skeletal muscle disease. *Bioessays* **27**(8): 809-822

Laing NG, Wilton SD, Akkari PA, Dorosz S, Boundy K, Kneebone C, Blumbergs P, White S, Watkins H, Love DR, et al. (1995) A mutation in the alpha tropomyosin gene TPM3 associated with autosomal dominant nemaline myopathy. *Nat Genet* **9**(1): 75-79

Lakey A, Ferguson C, Labeit S, Reedy M, Larkins A, Butcher G, Leonard K, Bullard B (1990) Identification and localization of high molecular weight proteins in insect flight and leg muscle. *EMBO J* **9**(11): 3459-3467

Lammens M, Moerman P, Fryns JP, Lemmens F, van de Kamp GM, Goemans N, Dom R (1997) Fetal akinesia sequence caused by nemaline myopathy. *Neuropediatrics* **28**(2): 116-119

Laughon A, Driscoll R, Wills N, Gesteland RF (1984) Identification of two proteins encoded by the Saccharomyces cerevisiae GAL4 gene. *Mol Cell Biol* **4**(2): 268-275

Laughon A, Gesteland RF (1984) Primary structure of the Saccharomyces cerevisiae GAL4 gene. *Mol Cell Biol* **4**(2): 260-267

Lazarides E, Nelson WJ (1985) Expression and assembly of the erythroid membrane-skeletal proteins ankyrin (goblin) and spectrin in the morphogenesis of chicken neurons. *J Cell Biochem* **27**(4): 423-441

Lebart MC, Mejean C, Roustan C, Benyamin Y (1993) Further characterization of the alpha-actinin-actin interface and comparison with filamin-binding sites on actin. *J Biol Chem* **268**(8): 5642-5648

Lecroisey C, Segalat L, Gieseler K (2007) The C. elegans dense body: anchoring and signaling structure of the muscle. *J Muscle Res Cell Motil* **28**(1): 79-87

Lee SH, Weins A, Hayes DB, Pollak MR, Dominguez R (2008) Crystal structure of the actin-binding domain of alpha-actinin-4 Lys255Glu mutant implicated in focal segmental glomerulosclerosis. *J Mol Biol* **376**(2): 317-324

Lee YS, Carthew RW (2003) Making a better RNAi vector for Drosophila: use of intron spacers. *Methods* **30**(4): 322-329

Lefebvre S, Burglen L, Reboullet S, Clermont O, Burlet P, Viollet L, Benichou B, Cruaud C, Millasseau P, Zeviani M, et al. (1995) Identification and characterization of a spinal muscular atrophy-determining gene. *Cell* **80**(1): 155-165

Lehman W, Craig R, Vibert P (1994) Ca(2+)-induced tropomyosin movement in Limulus thin filaments revealed by three-dimensional reconstruction. *Nature* **368**(6466): 65-67

Lehman W, Vibert P, Uman P, Craig R (1995) Steric-blocking by tropomyosin visualized in relaxed vertebrate muscle thin filaments. *J Mol Biol* **251**(2): 191-196

Lehninger AL, Nelson DL, Cox MM (2005) *Lehninger principles of biochemistry*, 4th edn. New York: W.H. Freeman.

Li MX, Spyracopoulos L, Sykes BD (1999) Binding of cardiac troponin-I147-163 induces a structural opening in human cardiac troponin-C. *Biochemistry* **38**(26): 8289-8298

Lieschke GJ, Currie PD (2007) Animal models of human disease: zebrafish swim into view. *Nat Rev Genet* **8**(5): 353-367

Lin Z, Hijikata T, Zhang Z, Choi J, Holtzer S, Sweeney HL, Holtzer H (1998) Dispensability of the actin-binding site and spectrin repeats for targeting sarcomeric alpha-actinin into maturing Z bands in vivo: implications for in vitro binding studies. *Dev Biol* **199**(2): 291-308

Littlefield R, Almenar-Queralt A, Fowler VM (2001) Actin dynamics at pointed ends regulates thin filament length in striated muscle. *Nat Cell Biol* **3**(6): 544-551

Littlefield R, Fowler VM (1998) Defining actin filament length in striated muscle: rulers and caps or dynamic stability? *Annu Rev Cell Dev Biol* **14**: 487-525

Liu TX, Zhou Y, Kanki JP, Deng M, Rhodes J, Yang HW, Sheng XM, Zon LI, Look AT (2002) Evolutionary conservation of zebrafish linkage group 14 with frequently deleted regions of human chromosome 5 in myeloid malignancies. *Proc Natl Acad Sci U S A* **99**(9): 6136-6141

Lodish HF (2004) *Molecular cell biology*, 5th edn. New York: W.H. Freeman and Company.

Lohr D, Venkov P, Zlatanova J. (1995) Transcriptional regulation in the yeast GAL gene family: a complex genetic network. *FASEB J* 9(9):777 -787.

Lorenzi M, Gimona M (2008) Synthetic actin-binding domains reveal compositional constraints for function. *The International Journal of Biochemistry & Cell Biology* **40**(9): 1806-1816

Lowey S, Waller GS, Trybus KM (1993) Skeletal muscle myosin light chains are essential for physiological speeds of shortening. *Nature* **365**(6445): 454-456

Luther PK (2000) Three-dimensional structure of a vertebrate muscle Z-band: implications for titin and alpha-actinin binding. *J Struct Biol* **129**(1): 1-16

Luther PK, Barry JS, Squire JM (2002) The three-dimensional structure of a vertebrate wide (slow muscle) Z-band: lessons on Z-band assembly. *J Mol Biol* **315**(1): 9-20

Luther PK, Squire JM (2002) Muscle Z-band ultrastructure: titin Z-repeats and Z-band periodicities do not match. *J Mol Biol* **319**(5): 1157-1164

Ma XZ, Cai LJ, Wu XH, Zhao SY, Li CB, Deng KJ (2003) Overexpression of human genes in Drosophila melanogaster by using GAL4 UAS system. *Sheng Wu Hua Xue Yu Sheng Wu Wu Li Xue Bao (Shanghai)* **35**(7): 597-600

Machado C, Sunkel CE, Andrew DJ (1998) Human autoantibodies reveal titin as a chromosomal protein. *J Cell Biol* **141**(2): 321-333

Marco-Ferreres R, Arredondo JJ, Fraile B, Cervera M (2005) Overexpression of troponin T in Drosophila muscles causes a decrease in the levels of thin-filament proteins. *Biochem J* **386**(Pt 1): 145-152

Mardahl-Dumesnil M, Fowler VM (2001) Thin filaments elongate from their pointed ends during myofibril assembly in Drosophila indirect flight muscle. *J Cell Biol* **155**(6): 1043-1053

Marin MC, Rodriguez JR, Ferrus A (2004) Transcription of Drosophila troponin I gene is regulated by two conserved, functionally identical, synergistic elements. *Mol Biol Cell* **15**(3): 1185-1196

Mas JA, Garcia-Zaragoza E, Cervera M (2004) Two functionally identical modular enhancers in Drosophila troponin T gene establish the correct protein levels in different muscle types. *Mol Biol Cell* **15**(4): 1931-1945

Masaki T, Endo M, Ebashi S (1967) Localization of 6S component of a alpha-actinin at Z-band. *J Biochem* **62**(5): 630-632

McArdle K, Allen TS, Bucher EA (1998) Ca2+-dependent muscle dysfunction caused by mutation of the Caenorhabditis elegans troponin T-1 gene. *J Cell Biol* **143**(5): 1201-1213

McDonald D, Carrero G, Andrin C, de Vries G, Hendzel MJ (2006) Nucleoplasmic beta-actin exists in a dynamic equilibrium between low-mobility polymeric species and rapidly diffusing populations. *J Cell Biol* **172**(4): 541-552

McElhinny AS, Kazmierski ST, Labeit S, Gregorio CC (2003) Nebulin: the nebulous, multifunctional giant of striated muscle. *Trends Cardiovasc Med* **13**(5): 195-201

McGough A, Way M, DeRosier D (1994) Determination of the alpha-actinin-binding site on actin filaments by cryoelectron microscopy and image analysis. *J Cell Biol* **126**(2): 433-443

McGregor A, Blanchard AD, Rowe AJ, Critchley DR (1994) Identification of the vinculin-binding site in the cytoskeletal protein alpha-actinin. *Biochem J* **301 (Pt 1)**: 225-233

McKane M, Wen KK, Boldogh IR, Ramcharan S, Pon LA, Rubenstein PA (2005) A mammalian actin substitution in yeast actin (H372R) causes a suppressible mitochondria/vacuole phenotype. *J Biol Chem* **280**(43): 36494-36501

McKillop DF, Geeves MA (1993) Regulation of the interaction between actin and myosin subfragment 1: evidence for three states of the thin filament. *Biophys J* **65**(2): 693-701

McLaughlin PJ, Gooch JT, Mannherz HG, Weeds AG (1993) Structure of gelsolin segment 1-actin complex and the mechanism of filament severing. *Nature* **364**(6439): 685-692

Melki R, Fievez S, Carlier MF (1996) Continuous monitoring of Pi release following nucleotide hydrolysis in actin or tubulin assembly using 2-amino-6-mercapto-7-methylpurine ribonucleoside and purine-nucleoside phosphorylase as an enzyme-linked assay. *Biochemistry* **35**(37): 12038-12045

Menkel AR, Kroemker M, Bubeck P, Ronsiek M, Nikolai G, Jockusch BM (1994) Characterization of an F-actin-binding domain in the cytoskeletal protein vinculin. *J Cell Biol* **126**(5): 1231-1240

Meyer RK, Aebi U (1990) Bundling of actin filaments by alpha-actinin depends on its molecular length. *J Cell Biol* **110**(6): 2013-2024

Michele DE, Metzger JM (2000) Physiological consequences of tropomyosin mutations associated with cardiac and skeletal myopathies. *J Mol Med* **78**(10): 543-553

Miike T, Ohtani Y, Tamari H, Ishitsu T, Une Y (1986) Muscle fiber type transformation in nemaline myopathy and congenital fiber type disproportion. *Brain Dev* **8**(5): 526-532

Miller A (1950) The internal anatomy and histology of the imago of Drosophila melanogaster. In *Biology of Drosophila*, Demerec M (ed), 6, pp 420-534. Cold Spring Harbor: Cold Spring Harbor Laboratory Press

Milligan RA (1996) Protein-protein interactions in the rigor actomyosin complex. *Proc Natl Acad Sci U S A* **93**(1): 21-26

Mimura N, Asano A (1986) Isolation and characterization of a conserved actin-binding domain from rat hepatic actinogelin, rat skeletal muscle, and chicken gizzard alpha-actinins. *J Biol Chem* **261**(23): 10680-10687

Mimura N, Asano A (1987) Further characterization of a conserved actin-binding 27-kDa fragment of actinogelin and alpha-actinins and mapping of their binding sites on the actin molecule by chemical cross-linking. *J Biol Chem* **262**(10): 4717-4723

Miralles F, Posern G, Zaromytidou AI, Treisman R (2003) Actin dynamics control SRF activity by regulation of its coactivator MAL. *Cell* **113**(3): 329-342

Mockrin SC, Korn ED (1980) Acanthamoeba profilin interacts with G-actin to increase the rate of exchange of actin-bound adenosine 5'-triphosphate. *Biochemistry* **19**(23): 5359-5362

Moerman DG, Williams BD (2006) Sarcomere assembly in C. elegans muscle. *WormBook*: 1-16

Mogami K, Hotta Y (1981) Isolation of Drosophila flightless mutants which affect myofibrillar proteins of indirect flight muscle. *Mol Gen Genet* **183**(3): 409-417

Molloy J, Kreuz A, Miller R, Tansey T, Maughan D (1993) Effects of tropomyosin deficiency in flight muscle of Drosophila melanogaster. *Adv Exp Med Biol* **332**: 165-171; discussion 172

Molloy JE, Kyrtatas, V., Sparrow, J. C. and White D. C. S. (1987) Kinetics of flight muscles from insects with different wingbeat frequencies. *Nature* **328**: 429-451

Monani UR (2005) Spinal muscular atrophy: a deficiency in a ubiquitous protein; a motor neuron-specific disease. *Neuron* **48**(6): 885-896

Morin X, Daneman R, Zavortink M, Chia W (2001) A protein trap strategy to detect GFP-tagged proteins expressed from their endogenous loci in Drosophila. *Proc Natl Acad Sci U S A* **98**(26): 15050-15055

Morris EP, Nneji G, Squire JM (1990) The three-dimensional structure of the nemaline rod Z-band. *J Cell Biol* **111**(6 Pt 2): 2961-2978

Myers CD, Goh PY, Allen TS, Bucher EA, Bogaert T (1996) Developmental genetic analysis of troponin T mutations in striated and nonstriated muscle cells of Caenorhabditis elegans. *J Cell Biol* **132**(6): 1061-1077

Naimi B, Harrison A, Cummins M, Nongthomba U, Clark S, Canal I, Ferrus A, Sparrow JC (2001) A tropomyosin-2 mutation suppresses a troponin I myopathy in Drosophila. *Mol Biol Cell* **12**(5): 1529-1539

Nakajima H, Kunioka Y, Nakano K, Shimizu K, Seto M, Ando T (1997) Scanning force microscopy of the interaction events between a single molecule of heavy meromyosin and actin. *Biochem Biophys Res Commun* **234**(1): 178-182

Narita A, Takeda S, Yamashita A, Maeda Y (2006) Structural basis of actin filament capping at the barbed-end: a cryo-electron microscopy study. *EMBO J* **25**(23): 5626-5633

Nasevicius A, Ekker SC (2000) Effective targeted gene 'knockdown' in zebrafish. *Nat Genet* **26**(2): 216-220

Netter FH, Brueckner JK, Granger N (2006) *Atlas of human anatomy*, 4th edn. Edinburgh: Elsevier Saunders.

Neuman S, Kaban A, Volk T, Yaffe D, Nudel U (2001) The dystrophin / utrophin homologues in Drosophila and in sea urchin. *Gene* **263**(1-2): 17-29

Ngai SM, Sonnichsen FD, Hodges RS (1994) Photochemical cross-linking between native rabbit skeletal troponin C and benzoylbenzoyl-troponin I inhibitory peptide, residues 104-115. *J Biol Chem* **269**(3): 2165-2172

Nguyen MA, Hardeman EC (2008) Mouse models for thin filament disease. *Adv Exp Med Biol* **642**: 66-77

Nienhuis AW, Coleman RF, Brown WJ, Munsat TL, Pearson CM (1967) Nemaline myopathy. A histopathologic and histochemical study. *Am J Clin Pathol* **48**(1): 1-13

Nishida E (1985) Opposite effects of cofilin and profilin from porcine brain on rate of exchange of actin-bound adenosine 5'-triphosphate. *Biochemistry* **24**(5): 1160-1164

Nishida E, Iida K, Yonezawa N, Koyasu S, Yahara I, Sakai H (1987) Cofilin is a component of intranuclear and cytoplasmic actin rods induced in cultured cells. *Proc Natl Acad Sci U S A* **84**(15): 5262-5266

Nix DA, Beckerle MC (1997) Nuclear-cytoplasmic shuttling of the focal contact protein, zyxin: a potential mechanism for communication between sites of cell adhesion and the nucleus. *J Cell Biol* **138**(5): 1139-1147

Nongthomba U, Ansari M, Thimmaiya D, Stark M, Sparrow J (2007) Aberrant splicing of an alternative exon in the Drosophila troponin-T gene affects flight muscle development. *Genetics* **177**(1): 295-306

Nongthomba U, Clark S, Cummins M, Ansari M, Stark M, Sparrow JC (2004) Troponin I is required for myofibrillogenesis and sarcomere formation in Drosophila flight muscle. *J Cell Sci* **117**(Pt 9): 1795-1805

Nongthomba U, Cummins M, Clark S, Vigoreaux JO, Sparrow JC (2003) Suppression of muscle hypercontraction by mutations in the myosin heavy chain gene of Drosophila melanogaster. *Genetics* **164**(1): 209-222

Nongthomba U, Pasalodos-Sanchez S, Clark S, Clayton JD, Sparrow JC (2001) Expression and function of the Drosophila ACT88F actin isoform is not restricted to the indirect flight muscles. *J Muscle Res Cell Motil* **22**(2): 111-119

Nongthomba U, Ramachandra NB (1999) A direct screen identifies new flight muscle mutants on the Drosophila second chromosome. *Genetics* **153**(1): 261-274

North KN, Laing NG (2008) Skeletal muscle alpha-actin diseases. *Adv Exp Med Biol* **642**: 15-27

North KN, Laing NG, Wallgren-Pettersson C (1997) Nemaline myopathy: current concepts. The ENMC International Consortium and Nemaline Myopathy. *J Med Genet* **34**(9): 705-713

Nowak KJ (2008) Therapeutic approaches for the sarcomeric protein diseases. *Adv Exp Med Biol* **642**: 207-223

Nowak KJ, Sewry CA, Navarro C, Squier W, Reina C, Ricoy JR, Jayawant SS, Childs AM, Dobbie JA, Appleton RE, Mountford RC, Walker KR, Clement S, Barois A, Muntoni F, Romero NB, Laing NG (2007) Nemaline myopathy caused by absence of alpha-skeletal muscle actin. *Ann Neurol* **61**(2): 175-184

Nowak KJ, Wattanasirichaigoon D, Goebel HH, Wilce M, Pelin K, Donner K, Jacob RL, Hubner C, Oexle K, Anderson JR, Verity CM, North KN, Iannaccone ST, Muller CR, Nurnberg P, Muntoni F, Sewry C, Hughes I, Sutphen R, Lacson AG, Swoboda KJ, Vigneron J, Wallgren-Pettersson C, Beggs AH, Laing NG (1999) Mutations in the skeletal muscle alpha-actin gene in patients with actin myopathy and nemaline myopathy. *Nat Genet* **23**(2): 208-212

O'Donnell PT, Bernstein SI (1988) Molecular and ultrastructural defects in a Drosophila myosin heavy chain mutant: differential effects on muscle function produced by similar thick filament abnormalities. *J Cell Biol* **107**(6 Pt 2): 2601-2612

O'Hare K, Rubin GM (1983) Structures of P transposable elements and their sites of insertion and excision in the Drosophila melanogaster genome. *Cell* **34**(1): 25-35

Oda T, Iwasa M, Aihara T, Maeda Y, Narita A (2009) The nature of the globular- to fibrous-actin transition. *Nature* **457**(7228): 441-445

Ogino S, Wilson RB (2004) Spinal muscular atrophy: molecular genetics and diagnostics. *Expert Rev Mol Diagn* **4**(1): 15-29

Ohta Y, Nishida E, Sakai H, Miyamoto E (1989) Dephosphorylation of cofilin accompanies heat shock-induced nuclear accumulation of cofilin. *J Biol Chem* **264**(27): 16143-16148

Ohtsuki I, Nagano K (1982) Molecular arrangement of troponin-tropomyosin in the thin filament. *Adv Biophys* **15**: 93-130

Ono S, Abe H, Nagaoka R, Obinata T (1993) Colocalization of ADF and cofilin in intranuclear actin rods of cultured muscle cells. *J Muscle Res Cell Motil* **14**(2): 195-204

Ono S, Abe H, Obinata T (1996) Stimulus-dependent disorganization of actin filaments induced by overexpression of cofilin in C2 myoblasts. *Cell Struct Funct* **21**(6): 491-499

Ono S, Ono K (2002) Tropomyosin inhibits ADF/cofilin-dependent actin filament dynamics. *J Cell Biol* **156**(6): 1065-1076

Onoda K, Yu FX, Yin HL (1993) gCap39 is a nuclear and cytoplasmic protein. *Cell Motil Cytoskeleton* **26**(3): 227-238

Oosawa F (1970) Size distribution of protein polymers. *J Theor Biol* **27**(1): 69-86

Oosawa F (1972) Dynamic properties of F-actin and the thin filament. *Nippon Seirigaku Zasshi* **34**(2): 96-97

Ordahl CP (1986) The skeletal and cardiac alpha-actin genes are coexpressed in early embryonic striated muscle. *Dev Biol* **117**(2): 488-492

Osborn M, Weber K (1980) Dimethylsulfoxide and the ionophore A23187 affect the arrangement of actin and induce nuclear actin paracrystals in PtK2 cells. *Exp Cell Res* **129**(1): 103-114

Ottenheijm CA, Witt CC, Stienen GJ, Labeit S, Beggs AH, Granzier H (2009) Thin filament length dysregulation contributes to muscle weakness in nemaline myopathy patients with nebulin deficiency. *Hum Mol Genet* **18**(13): 2359-2369

Otterbein LR, Graceffa P, Dominguez R (2001) The crystal structure of uncomplexed actin in the ADP state. *Science* **293**(5530): 708-711

Papa I, Astier C, Kwiatek O, Raynaud F, Bonnal C, Lebart MC, Roustan C, Benyamin Y (1999) Alpha actinin-CapZ, an anchoring complex for thin filaments in Z-line. *J Muscle Res Cell Motil* **20**(2): 187-197

Pappas CT, Bhattacharya N, Cooper JA, Gregorio CC (2008) Nebulin interacts with CapZ and regulates thin filament architecture within the Z-disc. *Mol Biol Cell* **19**(5): 1837-1847

Pardo JV, Siliciano JD, Craig SW (1983) A vinculin-containing cortical lattice in skeletal muscle: transverse lattice elements ("costameres") mark sites of attachment between myofibrils and sarcolemma. *Proc Natl Acad Sci U S A* **80**(4): 1008-1012

Parinov S, Kondrichin I, Korzh V, Emelyanov A (2004) Tol2 transposon-mediated enhancer trap to identify developmentally regulated zebrafish genes in vivo. *Dev Dyn* **231**(2): 449-459

Park S, Raines RT (2004) Fluorescence Polarization Assay to Quantify Protein-Protein Interactions. *Methods Mol Biol* **261**; 161-165.

Parks AL, Cook KR, Belvin M, Dompe NA, Fawcett R, Huppert K, Tan LR, Winter CG, Bogart KP, Deal JE, Deal-Herr ME, Grant D, Marcinko M, Miyazaki WY, Robertson S, Shaw KJ, Tabios M, Vysotskaia V, Zhao L, Andrade RS, Edgar KA, Howie E, Killpack K, Milash B, Norton A, Thao D, Whittaker K, Winner MA, Friedman L, Margolis J, Singer MA, Kopczynski C, Curtis D, Kaufman TC, Plowman GD, Duyk G, Francis-Lang HL (2004) Systematic generation of high-resolution deletion coverage of the Drosophila melanogaster genome. *Nat Genet* **36**(3): 288-292

Parry DA, Squire JM (1973) Structural role of tropomyosin in muscle regulation: analysis of the x-ray diffraction patterns from relaxed and contracting muscles. *J Mol Biol* **75**(1): 33-55

Pascual J, Castresana J, Saraste M (1997) Evolution of the spectrin repeat. *Bioessays* **19**(9): 811-817

Patton EE, Zon LI (2001) The art and design of genetic screens: zebrafish. *Nat Rev Genet* **2**(12): 956-966

Peckham M, Molloy JE, Sparrow JC, White DC (1990) Physiological properties of the dorsal longitudinal flight muscle and the tergal depressor of the trochanter muscle of Drosophila melanogaster. *J Muscle Res Cell Motil* **11**(3): 203-215

Pederson T, Aebi U (2002) Actin in the nucleus: what form and what for? *J Struct Biol* **140**(1-3): 3-9

Pederson T, Aebi U (2005) Nuclear actin extends, with no contraction in sight. *Mol Biol Cell* **16**(11): 5055-5060

Pelin K, Hilpela P, Donner K, Sewry C, Akkari PA, Wilton SD, Wattanasirichaigoon D, Bang ML, Centner T, Hanefeld F, Odent S, Fardeau M, Urtizberea JA, Muntoni F, Dubowitz V, Beggs AH, Laing NG, Labeit S, de la Chapelle A, Wallgren-Pettersson C (1999) Mutations in the nebulin gene associated with autosomal recessive nemaline myopathy. *Proc Natl Acad Sci U S A* **96**(5): 2305-2310

Pendleton A, Pope B, Weeds A, Koffer A (2003) Latrunculin B or ATP depletion induces cofilin-dependent translocation of actin into nuclei of mast cells. *J Biol Chem* **278**(16): 14394-14400

Perelroizen I, Carlier MF, Pantaloni D (1995) Binding of divalent cation and nucleotide to G-actin in the presence of profilin. *J Biol Chem* **270**(4): 1501-1508

Perrimon N, Engstrom L, Mahowald AP (1989) Zygotic lethals with specific maternal effect phenotypes in Drosophila melanogaster. I. Loci on the X chromosome. *Genetics* **121**(2): 333-352

Perry SV (2001) Vertebrate tropomyosin: distribution, properties and function. *J Muscle Res Cell Motil* **22**(1): 45-49

Pollard TD (1983) Measurement of rate constants for actin filament elongation in solution. *Anal Biochem* **134**(2): 406-412

Pollard TD (1986) Rate constants for the reactions of ATP- and ADP-actin with the ends of actin filaments. *J Cell Biol* **103**(6 Pt 2): 2747-2754

Pollard TD (1990) Actin. *Curr Opin Cell Biol* **2**(1): 33-40

Pollard TD, Blanchoin L, Mullins RD (2000) Molecular mechanisms controlling actin filament dynamics in nonmuscle cells. *Annu Rev Biophys Biomol Struct* **29**: 545-576

Pollard TD, Borisy GG (2003) Cellular motility driven by assembly and disassembly of actin filaments. *Cell* **112**(4): 453-465

Pollard TD, Cooper JA (1984) Quantitative analysis of the effect of Acanthamoeba profilin on actin filament nucleation and elongation. *Biochemistry* **23**(26): 6631-6641

Postlethwait JH, Woods IG, Ngo-Hazelett P, Yan YL, Kelly PD, Chu F, Huang H, Hill-Force A, Talbot WS (2000) Zebrafish comparative genomics and the origins of vertebrate chromosomes. *Genome Res* **10**(12): 1890-1902

Postlethwait JH, Yan YL, Gates MA, Horne S, Amores A, Brownlie A, Donovan A, Egan ES, Force A, Gong Z, Goutel C, Fritz A, Kelsh R, Knapik E, Liao E, Paw B, Ransom D, Singer A, Thomson M, Abduljabbar TS, Yelick P, Beier D, Joly JS, Larhammar D, Rosa F, Westerfield M, Zon LI, Johnson SL, Talbot WS (1998) Vertebrate genome evolution and the zebrafish gene map. *Nat Genet* **18**(4): 345-349

Potter JD, Gergely J (1974) Troponin, tropomyosin, and actin interactions in the Ca2+ regulation of muscle contraction. *Biochemistry* **13**(13): 2697-2703

Potter JD, Gergely J (1975) The calcium and magnesium binding sites on troponin and their role in the regulation of myofibrillar adenosine triphosphatase. *J Biol Chem* **250** 4628-4633

Prado A, Canal I, Barbas JA, Molloy J, Ferrus A (1995) Functional recovery of troponin I in a Drosophila heldup mutant after a second site mutation. *Mol Biol Cell* **6**(11): 1433-1441

Prado A, Canal I, Ferrus A (1999) The haplolethal region at the 16F gene cluster of Drosophila melanogaster: structure and function. *Genetics* **151**(1): 163-175

Pring M, Weber A, Bubb MR (1992) Profilin-actin complexes directly elongate actin filaments at the barbed end. *Biochemistry* **31**(6): 1827-1836

Ptashne M (1988) How eukaryotic transcriptional activators work. *Nature* **335**(6192): 683-689

Rajendra TK, Gonsalvez GB, Walker MP, Shpargel KB, Salz HK, Matera AG (2007) A Drosophila melanogaster model of spinal muscular atrophy reveals a function for SMN in striated muscle. *J Cell Biol* **176**(6): 831-841

Ranganayakulu G, Schulz RA, Olson EN (1996) Wingless Signaling InducesnautilusExpression in the Ventral Mesoderm of theDrosophilaEmbryo. *Developmental Biology* **176**(1): 143-148

Rayment I, Holden HM, Whittaker M, Yohn CB, Lorenz M, Holmes KC, Milligan RA (1993) Structure of the actin-myosin complex and its implications for muscle contraction. *Science* **261**(5117): 58-65

Raz E, van Luenen HG, Schaerringer B, Plasterk RH, Driever W (1998) Transposition of the nematode Caenorhabditis elegans Tc3 element in the zebrafish Danio rerio. *Curr Biol* **8**(2): 82-88

Razumova MV, Bukatina AE, Campbell KB (2000) Different myofilament nearest-neighbor interactions have distinctive effects on contractile behavior. *Biophys J* **78**(6): 3120-3137

Reedy MC, Beall C (1993) Ultrastructure of developing flight muscle in Drosophila. I. Assembly of myofibrils. *Dev Biol* **160**(2): 443-465

Reedy MC, Bullard B, Vigoreaux JO (2000) Flightin is essential for thick filament assembly and sarcomere stability in Drosophila flight muscles. *J Cell Biol* **151**(7): 1483-1500

Rickard JE, Sheterline P (1986) Cytoplasmic concentrations of inorganic phosphate affect the critical concentration for assembly of actin in the presence of cytochalasin D or ADP. *J Mol Biol* **191**(2): 273-280

Rieckher M, Kourtis N, Pasparaki A, Tavernarakis N (2009) Transgenesis in Caenorhabditis elegans. *Methods Mol Biol* **561**: 21-39

Roberts RG, Bobrow M (1998) Dystrophins in vertebrates and invertebrates. *Hum Mol Genet* 7(4): 589-595

Robinson P, Lipscomb S, Preston LC, Altin E, Watkins H, Ashley CC, Redwood CS (2007) Mutations in fast skeletal troponin I, troponin T, and beta-tropomyosin that cause distal arthrogryposis all increase contractile function. *FASEB J* **21**(3): 896-905

Romero N, Fardeau, M. (1996) Congenital onset nemaline myopathy. Case presentation at the 33rd ENMC International Workshop on Nemaline Myopathy, Naarden, The Netherlands.

Rould MA, Wan Q, Joel PB, Lowey S, Trybus KM (2006) Crystal Structures of Expressed Non-polymerizable Monomeric Actin in the ADP and ATP States. *J Biol Chem* **281**(42): 31909-31919

Roulier EM, Fyrberg C, Fyrberg E (1992) Perturbations of Drosophila alpha-actinin cause muscle paralysis, weakness, and atrophy but do not confer obvious nonmuscle phenotypes. *J Cell Biol* **116**(4): 911-922

Rubin GM, Yandell MD, Wortman JR, Gabor Miklos GL, Nelson CR, Hariharan IK, Fortini ME, Li PW, Apweiler R, Fleischmann W, Cherry JM, Henikoff S, Skupski MP, Misra S, Ashburner M, Birney E, Boguski MS, Brody T, Brokstein P, Celniker SE, Chervitz SA, Coates D, Cravchik A, Gabrielian A, Galle RF, Gelbart WM, George RA, Goldstein LS, Gong F, Guan P, Harris NL, Hay BA, Hoskins RA, Li J, Li Z, Hynes RO, Jones SJ, Kuehl PM, Lemaitre B, Littleton JT, Morrison DK, Mungall C, O'Farrell PH, Pickeral OK, Shue C, Vosshall LB, Zhang J, Zhao Q, Zheng XH, Lewis S (2000) Comparative genomics of the eukaryotes. *Science* **287**(5461): 2204-2215

Russell WL, Kelly EM, Hunsicker PR, Bangham JW, Maddux SC, Phipps EL (1979) Specific-locus test shows ethylnitrosourea to be the most potent mutagen in the mouse. *Proc Natl Acad Sci U S A* **76**(11): 5818-5819

Ryan MM, Ilkovski B, Strickland CD, Schnell C, Sanoudou D, Midgett C, Houston R, Muirhead D, Dennett X, Shield LK, De Girolami U, Iannaccone ST, Laing NG, North KN, Beggs AH (2003) Clinical course correlates poorly with muscle pathology in nemaline myopathy. *Neurology* **60**(4): 665-673

Ryan MM, Sy C, Rudge S, Ellaway C, Ketteridge D, Roddick LG, Iannaccone ST, Kornberg AJ, North KN (2008) Dietary L-tyrosine supplementation in nemaline myopathy. *J Child Neurol* **23**(6): 609-613

Rzadzinska AK, Schneider ME, Davies C, Riordan GP, Kachar B (2004) An actin molecular treadmill and myosins maintain stereocilia functional architecture and self-renewal. *J Cell Biol* **164**(6): 887-897

Saide JD, Chin-Bow S, Hogan-Sheldon J, Busquets-Turner L, Vigoreaux JO, Valgeirsdottir K, Pardue ML (1989) Characterization of components of Z-bands in the fibrillar flight muscle of Drosophila melanogaster. *J Cell Biol* **109**(5): 2157-2167

Sameshima M, Chijiiwa Y, Kishi Y, Hashimoto Y (1994) Novel actin rods appeared in spores of Dictyostelium discoideum. *Cell Struct Funct* **19**(4): 189-194

Sanger JW, Gwinn J, Sanger JM (1980) Dissolution of cytoplasmic actin bundles and the induction of nuclear actin bundles by dimethyl sulfoxide. *J Exp Zool* **213**(2): 227-230

Sanger JW, Sanger JM, Jockusch BM (1983) Differential response of three types of actin filament bundles to depletion of cellular ATP levels. *Eur J Cell Biol* **31**(2): 197-204

Sanoudou D, Haslett JN, Kho AT, Guo S, Gazda HT, Greenberg SA, Lidov HG, Kohane IS, Kunkel LM, Beggs AH (2003) Expression profiling reveals altered satellite cell numbers and glycolytic enzyme transcription in nemaline myopathy muscle. *Proc Natl Acad Sci U S A* **100**(8): 4666-4671

Satyshur KA, Rao ST, Pyzalska D, Drendel W, Greaser M, Sundaralingam M (1988) Refined structure of chicken skeletal muscle troponin C in the two-calcium state at 2-A resolution. *J Biol Chem* **263**(4): 1628-1647

Schachat FH, Canine AC, Briggs MM, Reedy MC (1985) The presence of two skeletal muscle alpha-actinins correlates with troponin-tropomyosin expression and Z-line width. *J Cell Biol* **101**(3): 1001-1008

Schafer B, Perriard JC, Eppenberger HM (1985) Appearance of M-band attached MM-creatine kinase in differentiating chicken heart cells after injection of M-type isoprotein or poly (A+)-RNA enriched for M-type creatine kinase message. *Basic Res Cardiol* **80 Suppl 2**: 129-133

Schafer DA, Waddle JA, Cooper JA (1993) Localization of CapZ during myofibrillogenesis in cultured chicken muscle. *Cell Motil Cytoskeleton* **25**(4): 317-335

Schlame M, Rua D, Greenberg ML (2000) The biosynthesis and functional role of cardiolipin. *Prog Lipid Res* **39**(3): 257-288

Schlame M, Towbin JA, Heerdt PM, Jehle R, DiMauro S, Blanck TJ (2002) Deficiency of tetralinoleoyl-cardiolipin in Barth syndrome. *Ann Neurol* **51**(5): 634-637

Schmitz S, Schankin CJ, Prinz H, Curwen RS, Ashton PD, Caves LS, Fink RH, Sparrow JC, Mayhew PJ, Veigel C (2003) Molecular evolutionary convergence of the flight muscle protein arthrin in Diptera and hemiptera. *Mol Biol Evol* **20**(12): 2019-2033

Schoenenberger CA, Bischler N, Fahrenkrog B, Aebi U (2002) Actin's propensity for dynamic filament patterning. *FEBS Lett* **529**(1): 27-33

Schroder R, Reimann J, Salmikangas P, Clemen CS, Hayashi YK, Nonaka I, Arahata K, Carpen O (2003) Beyond LGMD1A: myotilin is a component of central core lesions and nemaline rods. *Neuromuscul Disord* **13**(6): 451-455

Schroeter JP, Bretaudiere JP, Sass RL, Goldstein MA (1996) Three-dimensional structure of the Z band in a normal mammalian skeletal muscle. *J Cell Biol* **133**(3): 571-583

Schultheiss T, Choi J, Lin ZX, DiLullo C, Cohen-Gould L, Fischman D, Holtzer H (1992) A sarcomeric alpha-actinin truncated at the carboxyl end induces the breakdown of stress fibers in PtK2 cells and the formation of nemaline-like bodies and breakdown of myofibrils in myotubes. *Proc Natl Acad Sci U S A* **89**(19): 9282-9286

Schutt CE, Myslik JC, Rozycki MD, Goonesekere NC, Lindberg U (1993) The structure of crystalline profilin-beta-actin. *Nature* **365**(6449): 810-816

Sewry CA, Brown SC, Pelin K, Jungbluth H, Wallgren-Pettersson C, Labeit S, Manzur A, Muntoni F (2001) Abnormalities in the expression of nebulin in chromosome-2 linked nemaline myopathy. *Neuromuscul Disord* **11**(2): 146-153

Shcherbata HR, Yatsenko AS, Patterson L, Sood VD, Nudel U, Yaffe D, Baker D, Ruohola-Baker H (2007) Dissecting muscle and neuronal disorders in a Drosophila model of muscular dystrophy. *EMBO J* **26**(2): 481-493

Shelton GD, Engvall E (2005) Canine and feline models of human inherited muscle diseases. *Neuromuscul Disord* **15**(2): 127-138

Sheterline P (1988) Actin dynamics in cells. Actin on the more. *J Muscle Res Cell Motil* **9**(3): 291-292

Sheterline P, Clayton J, Sparrow JC (1998) *Actin*, 4th edn. New York: Oxford University Press.

Shimomura C, Nonaka I (1989) Nemaline myopathy: comparative muscle histochemistry in the severe neonatal, moderate congenital, and adult-onset forms. *Pediatr Neurol* **5**(1): 25-31

Sicinski P, Geng Y, Ryder-Cook AS, Barnard EA, Darlison MG, Barnard PJ (1989) The molecular basis of muscular dystrophy in the mdx mouse: a point mutation. *Science* **244**(4912): 1578-1580

Silva R, Sparrow JC, Geeves MA (2003) Isolation and kinetic characterisation of myosin and myosin S1 from the Drosophila indirect flight muscles. *J Muscle Res Cell Motil* **24**(8): 489-498

Siripala AD, Welch MD (2007a) SnapShot: actin regulators I. *Cell* **128**(3): 626

Siripala AD, Welch MD (2007b) SnapShot: actin regulators II. *Cell* **128**(5): 1014

Sivasubbu S, Balciunas D, Amsterdam A, Ekker SC (2007) Insertional mutagenesis strategies in zebrafish. *Genome Biol* **8 Suppl 1**: S9

Skare P, Kreivi JP, Bergstrom A, Karlsson R (2003) Profilin I colocalizes with speckles and Cajal bodies: a possible role in pre-mRNA splicing. *Exp Cell Res* **286**(1): 12-21

Slupsky CM, Sykes BD (1995) NMR solution structure of calcium-saturated skeletal muscle troponin C. *Biochemistry* **34**(49): 15953-15964

Smith JM, Bozcuk AN, Tebbutt S (1970) Protein turnover in adult Drosophila. *J Insect Physiol* **16**(4): 601-613

Sorimachi H, Freiburg A, Kolmerer B, Ishiura S, Stier G, Gregorio CC, Labeit D, Linke WA, Suzuki K, Labeit S (1997) Tissue-specific expression and alpha-actinin binding properties of the Z-disc titin: implications for the nature of vertebrate Z-discs. *J Mol Biol* **270**(5): 688-695

Southgate R, Ayme-Southgate A (2001) Alternative splicing of an amino-terminal PEVK-like region generates multiple isoforms of Drosophila projectin. *J Mol Biol* **313**(5): 1035-1043

Sparrow J, Hughes SM, Ségalat L (2008) Other model organisms for sarcomeric muscle diseases in The sarcomere and skeletal muscle disease (ed. N.G. Laing). *Advances in Experimental Medicine and Biology* **642**: 192-206

Sparrow JC, Nowak KJ, Durling HJ, Beggs AH, Wallgren-Pettersson C, Romero N, Nonaka I, Laing NG (2003) Muscle disease caused by mutations in the skeletal muscle alpha-actin gene (ACTA1). *Neuromuscul Disord* **13**(7-8): 519-531

Spradling AC, Rubin GM (1982) Transposition of cloned P elements into Drosophila germ line chromosomes. *Science* **218**(4570): 341-347

Spradling AC, Stern D, Beaton A, Rhem EJ, Laverty T, Mozden N, Misra S, Rubin GM (1999) The Berkeley Drosophila Genome Project gene disruption project: Single P-element insertions mutating 25% of vital Drosophila genes. *Genetics* **153**(1): 135-177

Squire J, Vibert PJ, Elliott A (1987) *Fibrous protein structure : a volume dedicated to Dr. Arthur Elliott*, London ; San Diego CA: Academic Press.

Squire JM, Morris EP (1998) A new look at thin filament regulation in vertebrate skeletal muscle. *FASEB J* **12**(10): 761-771

Steffen LS GJ, Vogel ED, Beltre, R., Pusack, T.J., Zhou, Y., Zon, LI. and Kunkel, L.M. (2007) Zebrafish orthologs of human muscular dystrophy genes. *BMC Genomics* **8**: Art 79.

Stehle R, Kruger M, Pfitzer G (2002a) Force kinetics and individual sarcomere dynamics in cardiac myofibrils after rapid ca(2+) changes. *Biophys J* **83**(4): 2152-2161

Stehle R, Kruger M, Scherer P, Brixius K, Schwinger RH, Pfitzer G (2002b) Isometric force kinetics upon rapid activation and relaxation of mouse, guinea pig and human heart

muscle studied on the subcellular myofibrillar level. *Basic Res Cardiol* **97 Suppl 1:** I127-I135

Stossel TP, Chaponnier C, Ezzell RM, Hartwig JH, Janmey PA, Kwiatkowski DJ, Lind SE, Smith DB, Southwick FS, Yin HL, et al. (1985) Nonmuscle actin-binding proteins. *Annu Rev Cell Biol* **1:** 353-402

Stuven T, Hartmann E, Gorlich D (2003) Exportin 6: a novel nuclear export receptor that is specific for profilin.actin complexes. *EMBO J* **22**(21): 5928-5940

Sung LA, Lin JJ (1994) Erythrocyte tropomodulin binds to the N-terminus of hTM5, a tropomyosin isoform encoded by the gamma-tropomyosin gene. *Biochem Biophys Res Commun* **201**(2): 627-634

Sung SS, Brassington AM, Grannatt K, Rutherford A, Whitby FG, Krakowiak PA, Jorde LB, Carey JC, Bamshad M (2003a) Mutations in genes encoding fast-twitch contractile proteins cause distal arthrogryposis syndromes. *Am J Hum Genet* **72**(3): 681-690

Sung SS, Brassington AM, Krakowiak PA, Carey JC, Jorde LB, Bamshad M (2003b) Mutations in TNNT3 cause multiple congenital contractures: a second locus for distal arthrogryposis type 2B. *Am J Hum Genet* **73**(1): 212-214

Suyama R, Jenny A, Curado S, Pellis-van Berkel W, Ephrussi A (2009) The actin-binding protein Lasp promotes Oskar accumulation at the posterior pole of the Drosophila embryo. *Development* **136**(1): 95-105

Syska H, Wilkinson JM, Grand RJ, Perry SV (1976) The relationship between biological activity and primary structure of troponin I from white skeletal muscle of the rabbit. *Biochem J* **153**(2): 375-387

Szliwowski HB, Drochmans P (1975) Ultrastructural aspects of muscle and nerve in Werdnig-Hoffmann disease. *Acta Neuropathol* **31**(4): 281-296

Tajsharghi H (2008) Thick and thin filament gene mutations in striated muscle diseases. *Int J Mol Sci* **9**(7): 1259-1275

Tajsharghi H, Ohlsson M, Lindberg C, Oldfors A (2007) Congenital myopathy with nemaline rods and cap structures caused by a mutation in the beta-tropomyosin gene (TPM2). *Arch Neurol* **64**(9): 1334-1338

Takeda S, Yamashita A, Maeda K, Maeda Y (2003) Structure of the core domain of human cardiac troponin in the Ca(2+)-saturated form. *Nature* **424**(6944): 35-41

Talbot JA, Hodges RS (1981) Synthetic studies on the inhibitory region of rabbit skeletal troponin I. Relationship of amino acid sequence to biological activity. *J Biol Chem* **256**(6): 2798-2802

Talbot WS, Hopkins N (2000) Zebrafish mutations and functional analysis of the vertebrate genome. *Genes Dev* **14**(7): 755-762

Tan P, Briner J, Boltshauser E, Davis MR, Wilton SD, North K, Wallgren-Pettersson C, Laing NG (1999) Homozygosity for a nonsense mutation in the alpha-tropomyosin slow gene TPM3 in a patient with severe infantile nemaline myopathy. *Neuromuscul Disord* **9**(8): 573-579

Tang J, Taylor DW, Taylor KA (2001) The three-dimensional structure of alpha-actinin obtained by cryoelectron microscopy suggests a model for Ca(2+)-dependent actin binding. *J Mol Biol* **310**(4): 845-858

Taylor MV (2006) *Comparison of muscle development in Drosophila and vertebrates* in Muscle Development in Drosophila Sink H (ed.), pp. 169-203. Georgetown, TX, Eurekah,

Thibault ST, Singer MA, Miyazaki WY, Milash B, Dompe NA, Singh CM, Buchholz R, Demsky M, Fawcett R, Francis-Lang HL, Ryner L, Cheung LM, Chong A, Erickson C, Fisher WW, Greer K, Hartouni SR, Howie E, Jakkula L, Joo D, Killpack K, Laufer A, Mazzotta J, Smith RD, Stevens LM, Stuber C, Tan LR, Ventura R, Woo A, Zakrajsek I, Zhao L, Chen F, Swimmer C, Kopczynski C, Duyk G, Winberg ML, Margolis J (2004) A complementary transposon tool kit for Drosophila melanogaster using P and piggyBac. *Nat Genet* **36**(3): 283-287

Tilney LG, Bonder EM, Coluccio LM, Mooseker MS (1983) Actin from Thyone sperm assembles on only one end of an actin filament: a behavior regulated by profilin. *J Cell Biol* **97**(1): 112-124

Tobacman LS, Lin D, Butters C, Landis C, Back N, Pavlov D, Homsher E (1999) Functional consequences of troponin T mutations found in hypertrophic cardiomyopathy. *J Biol Chem* **274**(40): 28363-28370

Trave G, Pastore A, Hyvonen M, Saraste M (1995) The C-terminal domain of alpha-spectrin is structurally related to calmodulin. *Eur J Biochem* **227**(1-2): 35-42

Tskhovrebova L, Trinick J (2003) Titin: properties and family relationships. *Nat Rev Mol Cell Biol* **4**(9): 679-689

Valentine BA, Cooper BJ, de Lahunta A, O'Quinn R, Blue JT (1988) Canine X-linked muscular dystrophy. An animal model of Duchenne muscular dystrophy: clinical studies. *J Neurol Sci* **88**(1-3): 69-81

Valianpour F, Wanders RJ, Overmars H, Vreken P, Van Gennip AH, Baas F, Plecko B, Santer R, Becker K, Barth PG (2002) Cardiolipin deficiency in X-linked cardioskeletal myopathy and neutropenia (Barth syndrome, MIM 302060): a study in cultured skin fibroblasts. *J Pediatr* **141**(5): 729-733

van der Plas MC, Pilgram GS, de Jong AW, Bansraj MR, Fradkin LG, Noordermeer JN (2007) Drosophila Dystrophin is required for integrity of the musculature. *Mech Dev* **124**(7-8): 617-630

van Straaten M, Goulding D, Kolmerer B, Labeit S, Clayton J, Leonard K, Bullard B (1999) Association of kettin with actin in the Z-disc of insect flight muscle. *J Mol Biol* **285**(4): 1549-1562

Vassylyev DG, Takeda S, Wakatsuki S, Maeda K, Maeda Y (1998) The crystal structure of troponin C in complex with N-terminal fragment of troponin I. The mechanism of how the inhibitory action of troponin I is released by Ca(2+)-binding to troponin C. *Adv Exp Med Biol* **453**: 157-167

Venken KJ, Bellen HJ (2007) Transgenesis upgrades for Drosophila melanogaster. *Development* **134**(20): 3571-3584

Vera C, Sood A, Gao KM, Yee LJ, Lin JJ, Sung LA (2000) Tropomodulin-binding site mapped to residues 7-14 at the N-terminal heptad repeats of tropomyosin isoform 5. *Arch Biochem Biophys* **378**(1): 16-24

Verheyen EM, Cooley L (1994) Profilin mutations disrupt multiple actin-dependent processes during Drosophila development. *Development* **120**(4): 717-728

Vibert P, Craig R, Lehman W (1997) Steric-model for activation of muscle thin filaments. *J Mol Biol* **266**(1): 8-14

Vidal M, Cagan RL (2006) Drosophila models for cancer research. *Curr Opin Genet Dev* **16**(1): 10-16

Vigoreaux JO (1994) The muscle Z band: lessons in stress management. *J Muscle Res Cell Motil* **15**(3): 237-255

Vigoreaux JO (2001) Genetics of the Drosophila flight muscle myofibril: a window into the biology of complex systems. *Bioessays* **23**(11): 1047-1063

Vigoreaux JO (2005) *Nature's versatile engine: Insect Flight Muscle Inside and Out. New York/Georgetown*: Springer.

Vigoreaux JO, Hernandez C, Moore J, Ayer G, Maughan D (1998) A genetic deficiency that spans the flightin gene of Drosophila melanogaster affects the ultrastructure and function of the flight muscles. *J Exp Biol* **201**(Pt 13): 2033-2044

Vigoreaux JO, Saide JD, Pardue ML (1991) Structurally different Drosophila striated muscles utilize distinct variants of Z-band-associated proteins. *J Muscle Res Cell Motil* **12**(4): 340-354

Vigoreaux JO, Saide JD, Valgeirsdottir K, Pardue ML (1993) Flightin, a novel myofibrillar protein of Drosophila stretch-activated muscles. *J Cell Biol* **121**(3): 587-598

Vinogradova MV, Stone DB, Malanina GG, Karatzaferi C, Cooke R, Mendelson RA, Fletterick RJ (2005) Ca(2+)-regulated structural changes in troponin. *Proc Natl Acad Sci U S A* **102**(14): 5038-5043

Vreken P, Valianpour F, Nijtmans LG, Grivell LA, Plecko B, Wanders RJ, Barth PG (2000) Defective remodeling of cardiolipin and phosphatidylglycerol in Barth syndrome. *Biochem Biophys Res Commun* **279**(2): 378-382

Wada A, Fukuda M, Mishima M, Nishida E (1998) Nuclear export of actin: a novel mechanism regulating the subcellular localization of a major cytoskeletal protein. *EMBO J* **17**(6): 1635-1641

Wadman SA, Clark KJ, Hackett PB (2005) Fishing for answers with transposons. *Mar Biotechnol (NY)* 7(3): 135-141

Wallgren-Pettersson C (1990) Congenital nemaline myopathy: a longitudinal study. University of Helsinki,

Wallgren-Pettersson C, Pelin K, Hilpela P, Donner K, Porfirio B, Graziano C, Swoboda KJ, Fardeau M, Urtizberea JA, Muntoni F, Sewry C, Dubowitz V, Iannaccone S, Minetti C, Pedemonte M, Seri M, Cusano R, Lammens M, Castagna-Sloane A, Beggs AH, Laing NG, de la Chapelle A (1999) Clinical and genetic heterogeneity in autosomal recessive nemaline myopathy. *Neuromuscul Disord* **9**(8): 564-572

Wallgren-Pettersson C, Pelin K, Nowak KJ, Muntoni F, Romero NB, Goebel HH, North KN, Beggs AH, Laing NG (2004) Genotype-phenotype correlations in nemaline myopathy caused by mutations in the genes for nebulin and skeletal muscle alpha-actin. *Neuromuscul Disord* **14**(8-9): 461-470

Wang K, Williamson CL (1980) Identification of an N2 line protein of striated muscle. *Proc Natl Acad Sci U S A* 77(6): 3254-3258

Waterston RH, Lindblad-Toh K, Birney E, Rogers J, Abril JF, Agarwal P, Agarwala R, Ainscough R, Alexandersson M, An P, Antonarakis SE, Attwood J, Baertsch R, Bailey J, Barlow K, Beck S, Berry E, Birren B, Bloom T, Bork P, Botcherby M, Bray N, Brent MR, Brown DG, Brown SD, Bult C, Burton J, Butler J, Campbell RD, Carninci P, Cawley S, Chiaromonte F, Chinwalla AT, Church DM, Clamp M, Clee C, Collins FS, Cook LL, Copley RR, Coulson A, Couronne O, Cuff J, Curwen V, Cutts T, Daly M, David R, Davies J, Delehaunty KD, Deri J, Dermitzakis ET, Dewey C, Dickens NJ, Diekhans M, Dodge S, Dubchak I, Dunn DM, Eddy SR, Elnitski L, Emes RD, Eswara P, Eyras E, Felsenfeld A, Fewell GA, Flicek P, Foley K, Frankel WN, Fulton LA, Fulton RS, Furey TS, Gage D, Gibbs RA, Glusman G, Gnerre S, Goldman N, Goodstadt L, Grafham D, Graves TA, Green ED, Gregory S, Guigo R, Guyer M, Hardison RC, Haussler D, Hayashizaki Y, Hillier LW, Hinrichs A, Hlavina W, Holzer T, Hsu F, Hua A, Hubbard T, Hunt A, Jackson I, Jaffe DB, Johnson LS, Jones M, Jones TA, Joy A, Kamal M, Karlsson EK, Karolchik D, Kasprzyk A, Kawai J, Keibler E, Kells C, Kent WJ, Kirby A, Kolbe DL, Korf I, Kucherlapati RS, Kulbokas EJ, Kulp D, Landers T, Leger JP, Leonard S, Letunic I, Levine R, Li J, Li M,

Lloyd C, Lucas S, Ma B, Maglott DR, Mardis ER, Matthews L, Mauceli E, Mayer JH, McCarthy M, McCombie WR, McLaren S, McLay K, McPherson JD, Meldrim J, Meredith B, Mesirov JP, Miller W, Miner TL, Mongin E, Montgomery KT, Morgan M, Mott R, Mullikin JC, Muzny DM, Nash WE, Nelson JO, Nhan MN, Nicol R, Ning Z, Nusbaum C, O'Connor MJ, Okazaki Y, Oliver K, Overton-Larty E, Pachter L, Parra G, Pepin KH, Peterson J, Pevzner P, Plumb R, Pohl CS, Poliakov A, Ponce TC, Ponting CP, Potter S, Quail M, Reymond A, Roe BA, Roskin KM, Rubin EM, Rust AG, Santos R, Sapojnikov V, Schultz B, Schultz J, Schwartz MS, Schwartz S, Scott C, Seaman S, Searle S, Sharpe T, Sheridan A, Shownkeen R, Sims S, Singer JB, Slater G, Smit A, Smith DR, Spencer B, Stabenau A, Stange-Thomann N, Sugnet C, Suyama M, Tesler G, Thompson J, Torrents D, Trevaskis E, Tromp J, Ucla C, Ureta-Vidal A, Vinson JP, Von Niederhausern AC, Wade CM, Wall M, Weber RJ, Weiss RB, Wendl MC, West AP, Wetterstrand K, Wheeler R, Whelan S, Wierzbowski J, Willey D, Williams S, Wilson RK, Winter E, Worley KC, Wyman D, Yang S, Yang SP, Zdobnov EM, Zody MC, Lander ES (2002) Initial sequencing and comparative analysis of the mouse genome. *Nature* **420**(6915): 520-562

Wattanasirichaigoon D, Swoboda KJ, Takada F, Tong HQ, Lip V, Iannaccone ST, Wallgren-Pettersson C, Laing NG, Beggs AH (2002) Mutations of the slow muscle alpha-tropomyosin gene, TPM3, are a rare cause of nemaline myopathy. *Neurology* **59**(4): 613-617

Way M, Pope B, Weeds AG (1992) Evidence for functional homology in the F-actin binding domains of gelsolin and alpha-actinin: implications for the requirements of severing and capping. *J Cell Biol* **119**(4): 835-842

Wear MA, Yamashita A, Kim K, Maeda Y, Cooper JA (2003) How capping protein binds the barbed end of the actin filament. *Curr Biol* **13**(17): 1531-1537

Webster N, Jin JR, Green S, Hollis M, Chambon P (1988) The yeast UASG is a transcriptional enhancer in human HeLa cells in the presence of the GAL4 trans-activator. *Cell* **52**(2): 169-178

Weeks DA, Nixon RR, Kaimaktchiev V, Mierau GW (2003) Intranuclear rod myopathy, a rare and morphologically striking variant of nemaline rod myopathy. *Ultrastruct Pathol* **27**(3): 151-154

Wegner A (1976) Head to tail polymerization of actin. *J Mol Biol* **108**(1): 139-150

Weinberg ES (1998) Zebrafish genetics: harnessing horizontal gene transfer. *Curr Biol* **8**(7): R244-247

Weins A, Schlondorff JS, Nakamura F, Denker BM, Hartwig JH, Stossel TP, Pollak MR (2007) Disease-associated mutant {alpha}-actinin-4 reveals a mechanism for regulating its F-actin-binding affinity. *Proceedings of the National Academy of Sciences* **104**(41): 16080-16085

Welch WJ, Suhan JP (1985) Morphological study of the mammalian stress response: characterization of changes in cytoplasmic organelles, cytoskeleton, and nucleoli, and

appearance of intranuclear actin filaments in rat fibroblasts after heat-shock treatment. *J Cell Biol* **101**(4): 1198-1211

West RW, Jr., Yocum RR, Ptashne M (1984) Saccharomyces cerevisiae GAL1-GAL10 divergent promoter region: location and function of the upstream activating sequence UASG. *Mol Cell Biol* **4**(11): 2467-2478

Wienholds E, Plasterk RH (2004) Target-selected gene inactivation in zebrafish. *Methods Cell Biol* **77**: 69-90

Wilson C, Pearson RK, Bellen HJ, O'Kane CJ, Grossniklaus U, Gehring WJ (1989) P-element-mediated enhancer detection: an efficient method for isolating and characterizing developmentally regulated genes in Drosophila. *Genes Dev* **3**(9): 1301-1313

Witke W (2004) The role of profilin complexes in cell motility and other cellular processes. *Trends Cell Biol* **14**(8): 461-469

Wood WB (1988) *The Nematode Caenorhabditis elegans*, Cold Spring Harbor, N.Y.: Cold Spring Harbor Laboratory.

Xia X-G, Zhou H, Xu Z (2006) Transgenic RNAi: Accelerating and Expanding Reverse Genetics in Mammals. *Transgenic Research* **15**(3): 271-275

Xu Y, Kelley RI, Blanck TJ, Schlame M (2003) Remodeling of cardiolipin by phospholipid transacylation. *J Biol Chem* **278**(51): 51380-51385

Yamaguchi M, Izumimoto M, Robson RM, Stromer MH (1985) Fine structure of wide and narrow vertebrate muscle Z-lines. A proposed model and computer simulation of Z-line architecture. *J Mol Biol* **184**(4): 621-643

Yamaguchi M, Robson RM, Stromer MH, Dahl DS, Oda T (1982) Nemaline myopathy rod bodies. Structure and composition. *J Neurol Sci* **56**(1): 35-56

Yamashita A, Maeda K, Maeda Y (2003) Crystal structure of CapZ: structural basis for actin filament barbed end capping. *EMBO J* **22**(7): 1529-1538

Yang D, Lu H, Erickson JW (2000) Evidence that processed small dsRNAs may mediate sequence-specific mRNA degradation during RNAi in Drosophila embryos. *Curr Biol* **10**(19): 1191-1200

Yocum RR, Hanley S, West R, Jr., Ptashne M (1984) Use of lacZ fusions to delimit regulatory elements of the inducible divergent GAL1-GAL10 promoter in Saccharomyces cerevisiae. *Mol Cell Biol* **4**(10): 1985-1998

Young P, Ehler E, Gautel M (2001) Obscurin, a giant sarcomeric Rho guanine nucleotide exchange factor protein involved in sarcomere assembly. *J Cell Biol* **154**(1): 123-136

Young P, Ferguson C, Banuelos S, Gautel M (1998) Molecular structure of the sarcomeric Z-disk: two types of titin interactions lead to an asymmetrical sorting of alpha-actinin. *EMBO J* **17**(6): 1614-1624

Young P, Gautel M (2000) The interaction of titin and alpha-actinin is controlled by a phospholipid-regulated intramolecular pseudoligand mechanism. *EMBO J* **19**(23): 6331-6340

Zhang S, Buder K, Burkhardt C, Schlott B, Gorlach M, Grosse F (2002) Nuclear DNA helicase II/RNA helicase A binds to filamentous actin. *J Biol Chem* **277**(1): 843-853

Zhang ZQ, Bish LT, Holtzer H, Sweeney HL (2009) Sarcomeric-alpha-actinin defective in vinculin-binding causes Z-line expansion and nemaline-like body formation in cultured chick myotubes. *Exp Cell Res* **315**(5): 748-759

Zot AS, Potter JD (1987) The effect of [Mg2+] on the Ca2+ dependence of ATPase and tension development of fast skeletal muscle. The role of the Ca2+-specific sites of troponin C. *J Biol Chem* **262**(5): 1966-1969